



Politecnico di Milano

MASTER OF SCIENCE IN

CIVIL ENGINEERING FOR RISK MITIGATION

**COMPARATIVE STUDY OF DIFFERENT SCENARIOS FOR
THE MORPHOLOGICAL EVOLUTION
IN A RIVER STREAM**

Saber Mohamed ELSAYED

780671

Supervisor

Dr. Alessio RADICE

October 2013

Table of Contents

Table of Contents	i
List of Figures	vi
List of Tables	xv
Abstract (English)	1
Abstract (Italian)	2
Introduction	3
1 Sediment Transport: Properties and Modelling	8
1.1 Introduction	8
1.2 Sedimentation Sources and Destination.....	9
1.3 The environmental effects of sediment transport.....	10
1.4 Sediments Properties and Terminology.....	14
1.4.1 Properties of a single particle	14
1.4.2 Median sediment size	16
1.4.3 Sediment Mixture density.....	16
1.4.4 Settling (falling) velocity.....	17
1.4.5 Angle of Repose	18
1.5 Inception of motion	19
1.6 Effective bed roughness.....	21
1.7 The transport capacity	24
1.7.1 Meyer Peter and Müller formula.....	24
1.7.2 Wong and Parker	25
1.7.3 Parker fit to Einstein equation	25
1.7.4 Power law.....	26
1.8 Morphological evolution.....	26
1.8.1 The governing equations in 1D	26
1.8.2 Non-dimensionalization of the governing equations	29
1.8.3 Effect of porosity.....	30
1.8.4 Sediment / water flow ratio.....	31
1.8.5 Effect of higher slopes.....	32
1.9 Characteristic form of governing equations	32
1.10 Boundary Conditions and initial conditions	35
1.11 Dealing with non-uniform gradation	36
1.12 Numerical Scheme for the governing equations	38

1.13	Stability of numerical codes.....	44
1.14	Objective of the work.....	45
2	Strategies for Numerical Analysis	47
2.1	Introduction	47
2.2	Modelling the morphological evolution by HEC-RAS.....	47
2.2.1	The numerical scheme for HEC-RAS.	49
2.2.2	Effective Friction in HEC-RAS	50
2.2.3	Quasi-unsteady flow in HEC-RAS	51
2.2.4	Sorting method in HEC-RAS	52
2.2.5	Mini user guide for sediment transport modelling by HEC-RAS.....	53
2.3	Modelling morphological evolution by Basement.....	64
2.3.1	The numerical scheme for Basement	66
2.3.2	Effective bed roughness in Basement.....	70
2.3.2.1	Manning-Strickler approach (manual approach).....	71
2.3.2.2	Equivalent Sand Roughness	72
2.3.3	Influence of Bed Forms on Bottom Shear Stress	73
2.3.4	Mini user guide for sediment transport modelling by Basement.....	74
2.3.4.1	The pre-processing phase	77
2.3.4.2	Phase for Preparing an auxiliary input files	80
2.3.4.3	Phase of Building the command file	81
2.3.4.4	Phase of Running the command file and extracting the results:.....	85
2.4	Modeling the morphological evolution by ISIS.....	88
2.4.1	Numerical scheme with ISIS.....	90
2.4.2	Mini user guide for sediment transport modelling by ISIS	91
2.4.2.1	Building ISIS geometry file	91
2.4.2.2	Importing the initial conditions.....	92
2.4.2.3	Building the sediment properties and boundaries file	93
2.4.2.4	Running the sediment transport analysis	99
2.4.2.5	Extracting the outputs.	100
2.5	Comparative hydraulic analysis by ISIS, Basement, and HEC-RAS.....	101
3	Modelling and Analysis of Synthetic Channel Cases.....	110
3.1	Introduction	110
3.2	Properties of the synthetic cases.....	110
3.3	Comparative morphological analysis by HEC-RAS, Basement and ISIS.....	114

3.3.1	Comparison between HEC-RAS and Basement.....	115
3.3.2	Comparison between ISIS and Basement	117
3.4	behavior of morphology in channels have uniform bed gradation	117
3.4.1	Case of upstream feeding by uniform sediment	118
3.4.1.1	Mild channels	118
3.4.1.2	Steep channels	120
3.4.1.3	Effect of skin friction	121
3.4.2	Case of lateral feeding by uniform sediment.....	122
3.4.2.1	Mild channels	123
3.4.2.2	Steep channels	124
3.4.2.3	Sensitivity to spatial discretization	125
3.4.3	Case of sequent fixed and mobile beds	126
3.4.3.1	Mild channels	126
3.4.3.2	Steep channels	127
3.5	Behavior of morphology in channels have non-uniform bed gradation.....	128
3.5.1	Basement treatment for multiple grain sizes	129
3.5.2	Upstream feeding by non-uniform sediment	133
3.5.3	Lateral feeding by non-uniform sediment	137
3.5.4	Sensitivity to control volume thickness	142
3.6	Conclusions	146
4	The Case of Mallero: Mallero Description	148
4.1	Introduction	148
4.2	The Mallero basin	150
4.3	Grain sizes and bed slopes	152
4.4	Measuring the precipitation on Valmalenco	155
4.5	Measuring the discharge in Mallero	156
4.6	The 1987 floods in Sondrio	158
4.7	Spriana landslide	161
5	The Case of Mallero: 1987 Flood	163
5.1	Introduction	163
5.2	The model cross sections	163
5.3	Models granulometry	166
5.4	Model boundary and initial conditions.....	168
5.5	Model results and comparison with previous analyses.....	169

5.6	Model sensitivity to bed granulometry	175
5.7	Model sensitivity to bed friction	178
5.8	Model sensitivity to control volume thickness	180
5.9	Numerical Issues	182
5.10	Final considerations and conclusions	183
6	The Case of Mallero: Integrated Scenario for Spriana Landslide.....	186
6.1	The scenario of lateral feeding from Spriana.....	186
6.1.1	The model description	188
6.1.2	Results of scenario (1).....	190
6.1.3	Results of scenario (2).....	193
6.2	Integrated scenario for the sequent landslide and dam- break in Spriana.	194
6.2.1	The sub model for the landslide distribution.....	196
6.2.2	The sub model for estimating the discharge in Mallero.....	198
6.2.3	The sub model for lake formation	199
6.2.4	Dam failure causes, modelling and consequences	208
	Common causes of earthen dam failure.....	210
	• Failure of dams due to overtopping	210
	• Failure by piping or internal erosion.....	212
	• Failure due to foundation and structural defects.....	213
	Dam failure modelling.....	214
	• Modelling the seepage process	214
	➤ Seepage analysis for scenario 80	216
	➤ Sensitivity of the seepage model to the hydraulic conductivity.....	221
	• Models for overtopping breach	224
	➤ Breaching model by Macchione.....	225
	▪ Model assumptions.....	225
	▪ Model description	226
	▪ Sensitivity to dam height	231
	▪ Sensitivity to crest width.....	232
	▪ Sensitivity to dam's side slopes	234
	➤ Breaching model by Weiming Wu	235
	▪ The model assumptions	235
	▪ Model description	236
6.2.5	Dam breaching effect on Mallero morphology.....	241

6.3	Influence of Morphological evolution on flood risk and emergency cost	251
6.4	Conclusions and recommendations.....	255
7	The Millennium Dam.....	257
7.1	Introduction	257
7.2	The Nile catchments	258
7.3	Physiography in the Nile Basin.....	262
7.4	Nile River Sediment.....	264
7.5	The ecological and morphological effects of blue Nile	266
7.5.1	Bank erosion in the Nile	266
7.5.2	Sand encroachment on the Nile River	267
7.5.3	Reservoir sedimentation.....	268
7.6	Statement of the Millennium dam problem.....	270
7.7	Effects of the Millennium Dam	271
7.7.1	Ecological effects.....	272
7.7.2	Morphological effects	273
7.7.3	Effects on the risk management	274
7.8	Proposal for solving the problem.....	275
	Final Conclusions.....	277
	List of Symbols	B
	Bibliography	D

List of Figures

Chapter 1

Fig. 1. 1: Bed load and suspended load.	8
Fig. 1. 2: Sources of sedimentation.....	9
Fig. 1. 3: Bed degradation in Arno river at Empoli-Italy.....	10
Fig. 1. 4: Functional failure of Dam due to sedimentation.	11
Fig. 1. 5 : Roads collapse in Sinai-Egypt due to erosion and sediment transport.....	11
Fig. 1. 6: Choluteca Bridge, Honduras after Hurricane Mitch. 1998.....	12
Fig. 1. 7: Bank erosion as a source of sediment.....	12
Fig. 1. 8: Ripples in the Rum River, Minnesota USA at very low flow (Parker, 2004).	13
Fig. 1. 9: Dune bed forms in a small stream, flow from right to left (Chanson, 2004).	13
Fig. 1. 10: Nile’s delta formed by sediment transport.	14
Fig. 1. 11: Particle-size distribution curve.....	16
Fig. 1. 12: Sediments porosity definition.	17
Fig. 1. 13: Drag coefficient of single particle in still fluid (Chanson, 2004).	18
Fig. 1. 14 : Examples of angle of repose (Chanson, 2004).	19
Fig. 1. 15: Particle movement; a) Bed load; b) Suspended load (Parker, 2004).	19
Fig. 1. 16: Threshold of sediment motion (bed-load and suspension), Shield’s parameter as a function of the dimensionless particle parameter d^* (Chanson, 2004).	20
Fig. 1. 17: Bed shear stress as a function of the mean flow velocity (Chanson, 2004).	22
Fig. 1. 18: Fluid pressure and shear stresses distribution along a dune (Van Rijn, 1993).	23
Fig. 1. 19: Bed evolution and terms of Exner equation (Parker, 2004).....	27
Fig. 1. 20: Mass conservation at the river bed (Chaudhry, 2008).	29
Fig. 1. 21: Definition sketch of the forward and backward characteristics: (a) subcritical flow conditions and (b) supercritical flow conditions (Chanson, 2004).	34
Fig. 1. 22:Computational domain for a one-dimensional system (Chaudhry, 2008).	35
Fig. 1. 23: Characteristics at the limits of computational domain (Dingman, 2009).	36
Fig. 1. 24: Illustration of the active layer concept (Chaudhry, 2008).	37
Fig. 1. 25: Finite-difference grid.....	40

Chapter 2

Fig. 2. 1: HEC-RAS Main Window Button Bar (Brunner, et al., 2010).	48
Fig. 2. 2: Schematic of the control volume used by HEC-RAS for sediment (Brunner, 2010).	50
Fig. 2. 3: A Quasi-Unsteady Flow Series with time step (Brunner, 2010).	52

Fig. 2. 4: Schematic of the mixing layers in HEC-RAS' sorting and armouring methods (Brunner, 2010).	53
Fig. 2. 5: Cross section definition by HEC-RAS.	54
Fig. 2. 6: Downstream B.C. definition for quasi unsteady flow.....	55
Fig. 2. 7: Assigning the upstream BC as a Qausi Unsteady flow.	56
Fig. 2. 8: Assigning the temperature value for each flow duration.	56
Fig. 2. 9: Sediment properties options.....	57
Fig. 2. 10:Bed change options.	58
Fig. 2. 11: Calibration transportation functions option.	58
Fig. 2. 12: User defined grain classes dialog.	59
Fig. 2. 13: Assigning the initial conditions & transport parameters with HEC-RAS.	60
Fig. 2. 14: Defining the bed gradation in HEC-RAS (Brunner, et al., 2010).	60
Fig. 2. 15: Sediment BC definition in HEC-RAS.	61
Fig. 2. 16: load specification editor for entering the coupled sediment (water-sediment rating curve) (Brunner, et al., 2010).....	62
Fig. 2. 17: Sediment load series editor (Brunner, et al., 2010).	62
Fig. 2.18: Sediment analysis perform by HEC-RAS.....	63
Fig. 2. 19: Result visualization and extraction by HEC-RAS.....	64
Fig. 2. 20 : Basement Modules and their Components (Faeh, et al., 2012).....	65
Fig. 2. 21: Definition for finite volume discretization for the spatial derivatives (Faeh, et al., 2012). .	66
Fig. 2. 22: Soil Discretisation in a cross section in Basement (Faeh, et al., 2012).....	68
Fig. 2. 23: Effect of bed load on cross section geometry (Faeh, et al., 2012).....	69
Fig. 2. 24: Distribution of sediment area change over the cross section (Faeh, et al., 2012).....	70
Fig. 2. 25: Graphical user interface (GUI) for Basement software.	75
Fig. 2. 27: Opening a new geometry file in Basement.	77
Fig. 2. 28: Assigning the sections properties in Basement.....	78
Fig. 2. 29: Inserting soil definition block and the corresponding tags.	79
Fig. 2. 30: Specimen of the flow boundary text file.	80
Fig. 2. 31: Preparing the initial condition file from the restart file.	81
Fig. 2. 32: Starting a new command file.....	82
Fig. 2. 33: The domain block and it's sub blocks.....	83
Fig. 2. 34: Defining the output file type and output time step.	85
Fig. 2. 35: Running the Basement command line.	86
Fig. 2. 36: Component of MATLAB output matrix.....	86

Fig. 2. 37: Matrix of sediment fluxes.....	87
Fig. 2. 38: ISIS main user interface.....	90
Fig. 2. 39 : Building the Geometry file by ISIS.....	92
Fig. 2. 40: Importing the initial conditions in ISIS.....	93
Fig. 2. 41: Comparison of bed updating methods (ISIS, 2012).....	95
Fig. 2. 42: Example of the General System Parameters data file section (ISIS, 2012).....	95
Fig. 2. 43: The Sediment Boundary Conditions data files section (ISIS, 2012).....	98
Fig. 2. 44: The Hard Bed Option data file section (ISIS, 2012).....	99
Fig. 2. 45: Running sediment transport model by ISIS (ISIS, 2012).....	100
Fig. 2. 46: Opening the mobile bed results binary file 'filename.zze' using the ISIS TabularCSV output (ISIS, 2012).....	100
Fig. 2. 47: TabularCSV window and available results Mobile Bed Module results.....	101
Fig. 2. 48: Synthetic case study with sudden enlargement and bed drop.....	102
Fig. 2. 49: Steady water profile using 250 m spatial discretization.....	103
Fig. 2. 50: Steady water profile using 50 m spatial discretization.....	104
Fig. 2. 51: Considered flow hydrograph for unsteady analysis.....	105
Fig. 2. 52: Comparison between MAX. WSE by ISIS and WSE by HEC-RAS with steady peak discharge.....	107
Fig. 2. 53: Comparison between MAX. WSE by ISIS and HEC-RAS with WSE by Basement with steady peak discharge.....	108

Chapter 3

Fig. 3. 1: The locations and symbology of sediment feeding.....	113
Fig. 3. 2 : Comparison between HEC-RAS and Basement in mild channel with 2‰ bed slope.....	115
Fig. 3. 3: Bed skin shear friction calculated by HEC-RAS and Basement.....	116
Fig. 3. 4: Transport capacity (MPM) calculated by HEC and Basement.....	116
Fig. 3. 5: Degradation at upstream due to low feeding of sediment (Mild channel M1, $k_s=0.5$).....	119
Fig. 3. 6:Aggradation at upstream due to high feeding of sediment (Mild channel M1, $k_s=3$).....	119
Fig. 3. 7: Degradation at upstream due to low feeding of sediment (steep channel S1, $k_s=0.5$).....	120
Fig. 3. 8: Aggradation at upstream due to high feeding of sediment (steep channel S1, $k_s=3$).....	121
Fig. 3. 9: Effect of using skin friction and total friction in representing the bed shear stress.....	122
Fig. 3. 10: Dam formation in mild channel due to the lateral feeding of sediment.....	123
Fig. 3. 11: Sediment distribution in the cross section.....	124
Fig. 3. 12:Dam and lake formation in steep channel due to the lateral feeding of sediment.....	124
Fig. 3. 13: Effect of the spatial discretization in the results precision (mild channel - model #9).....	125

Fig. 3. 14: Effect of the spatial discretization in the results precision (steel channel - model #10). ...	126
Fig. 3. 15: The bed erosion in sequent hard and mobile bed for model # 11.....	127
Fig. 3. 16: The sediment aggradation in sequent hard and mobile bed for model # 12.....	127
Fig. 3. 17:The bed erosion in sequent hard and mobile bed for model # 13.....	128
Fig. 3. 18:The sediment aggradation in sequent hard and mobile bed for model # 14.	128
Fig. 3. 19: Assigning of multiple grain sizes in Basement.....	130
Fig. 3. 20: The sediment mixing in the control volume.....	131
Fig. 3. 21:The change in the gradation curve due to sorting effect at specific cross section.	132
Fig. 3. 22: Bed evolution for case#1 of non-uniform granulometry.	134
Fig. 3. 23: Case #1; the mixing between the in-flow diameter and the bed diameter in the cvt	134
Fig. 3. 24:Case #1; the mixing between the in-flow diameter and the bed diameter in the sub layer.	135
Fig. 3. 25: Bed evolution for case#2 of non-uniform granulometry.	135
Fig. 3. 26:Case #2; the mixing between the in-flow diameter and the bed diameter in the cvt	136
Fig. 3. 27:Bed evolution for case#3 of non-uniform granulometry.	136
Fig. 3. 28: Case #3; the mixing between the in-flow diameter and the bed diameter in the cvt	137
Fig. 3. 29: Bed evolution for case#4 of non-uniform granulometry.	138
Fig. 3. 30: Case #4; the mixing between the in-flow diameter and the bed diameter in the cvt	138
Fig. 3. 31: Bed evolution for case #5 of non-uniform granulometry.	139
Fig. 3. 32: Case #5; the mixing between the in-flow diameter and the bed diameter in the cvt	139
Fig. 3. 33:Bed evolution for case #6 of non-uniform granulometry.	140
Fig. 3. 34: Case #6; the mixing between the in-flow diameter and the bed diameter in the cvt	140
Fig. 3. 35: Bed evolution for case #7 of non-uniform granulometry.	141
Fig. 3. 36:Case #7; the mixing between the in-flow diameter and the bed diameter in the cvt.....	141
Fig. 3. 37: Sensitivity to cvt for case#2.....	143
Fig. 3. 38: Sensitivity to cvt for case#3.....	143
Fig. 3. 39: Sensitivity to cvt for case#4.....	144
Fig. 3. 40: Sensitivity to cvt for case#5.....	145
Fig. 3. 41:Sensitivity to cvt for case#7.....	145

Chapter 4

Fig. 4. 1: The Mallero basin (water courses underlined and towns in normal font) (Radice, et al., 2013).	148
Fig. 4. 2: Mallero River, it's tributaries, it's catchment and it's confluence with Adda River.....	151
Fig. 4. 3: The topography of Valmalenco valley.	151

Fig. 4. 4:Slopes in the basin expressed in percentage.	152
Fig. 4. 5: Traits of Mallero - profile & photo (Mauri, et al., 2009).	153
Fig. 4. 6: Photo for the Mallero in Sondrio.....	154
Fig. 4. 7: Locations of rainfall stations.....	156
Fig. 4. 8: The rating curve at Sondrio, ponte Eiffel station.	157
Fig. 4. 9: Annual flow curves from 1992 to 1998 at Sondrio ponte Eiffelin station.....	157
Fig. 4. 10: Level reached by the water due to the flood in Mallero at 1987.....	159
Fig. 4. 11: Dredging operations after 1987 flood.	159
Fig. 4. 12: The hydrograph for 1987 flood.	160
Fig. 4. 13:Google Earth view of Sondrio with indication of bridges location;taken from (Radice, et al., 2013).	160
Fig. 4. 14: The location of Spriana.....	161
Fig. 4. 15: The body of Spriana landslide.	162

Chapter 5

Fig. 5. 1:Simplification for section 39 (4585 m from Adda River).	164
Fig. 5. 2: Simplification for section 89 (389 m from Adda River).	164
Fig. 5. 3: The bed profile of Mallero and the zones of hard bed.	165
Fig. 5. 4: The distances among the sections used in the numerical modeling.	165
Fig. 5. 5: The bed profile in the zone contains the check dams (Mauri, et al., 2009).	166
Fig. 5. 6: The feeding discharge corresponding to 1987 hydrograph.	168
Fig. 5. 7: The feeding sediment discharge corresponding to 1987 event.....	169
Fig. 5. 8: The bed evolution for 1987 event.	170
Fig. 5. 9: Bed differences for 1987 event.	170
Fig. 5. 10: The migration of the 10 mm diameter in the active layer.	172
Fig. 5. 11:The migration of the 80 mm diameter in the active layer.	172
Fig. 5. 12:The migration of the 800 mm diameter in the active layer.	173
Fig. 5. 13: Bed differences for 1987 event by (Filippetti, et al., 2012).	174
Fig. 5. 14:Comparison between measured values and calculated values by (Filippetti, et al., 2012) for the Mallero in the city section.	174
Fig. 5. 15: Comparison between measured values and calculated values in the in-town part.	175
Fig. 5. 16: The bed evolution due to 1987 event using different granulometry.....	176
Fig. 5. 17: The bed differences using different granulometry.	176
Fig. 5. 18: Granulometry distribution along Mallero at the end of simulation time using 4 sizes model.	177

Fig. 5. 19: Granulometry distribution along Mallero at the end of simulation time using 10 sizes model.	177
Fig. 5. 20: The sorting effect in open channels.	178
Fig. 5. 21: Effect of the skin friction on the morphological evolution for bed consist of 3 diameters.	179
Fig. 5. 22: Effect of skin friction on the morphological evolution for bed consist of 4 diameters.	179
Fig. 5. 23: Effect of skin friction on the morphological evolution for bed consist of 10 diameters. ..	180
Fig. 5. 24: Influence of changing the control volume thickness on the bed evolution for 3 grain sizes model.	181
Fig. 5. 25: Influence of changing the control volume thickness on the bed evolution for 4 grain sizes model.	181
Fig. 5. 26: Influence of changing the control volume thickness on the bed evolution for 10 grain sizes model.	181

Chapter 6

Fig. 6. 1: : Location map of the 1987 Val Pola rock avalanche (Central Alps, Northern Italy).	188
Fig. 6. 2: Time histories of the local maximum velocity and footprint area for 1987 val pola landslide (Crosta, et al., 2004).	188
Fig. 6. 3: Scenario(1) for lateral feeding (sudden feeding).	189
Fig. 6. 4: Scenario(2) for lateral feeding (distributed feeding).	190
Fig. 6. 5: The bed and the WSE profiles at intermediate times of the simulation.	190
Fig. 6. 6: Bed differences in case of lateral feeding according scenario (1) and using model of 3 grain sizes.	191
Fig. 6. 7: Bed differences in case of lateral feeding according scenario (1) and using model of 10 grain sizes.	192
Fig. 6. 8: Bed differences in case of lateral feeding according scenario (2) and using model of 3 grain sizes.	193
Fig. 6. 9: Relation among the sub-models relating dam failure in Spriana.	195
Fig. 6. 10: Instantaneous velocity field at the indicated instant (110 s) with fully 3D features (Crosta, et al., 2004).	196
Fig. 6. 11: Debris profiles in Val Pola extracted along the longitudinal section $y = 1280$ m (Crosta, et al., 2004).	197
Fig. 6. 12: The parameters of the lake formation model.	200
Fig. 6. 13: Location of the lake will be formed in Spriana.	201
Fig. 6. 14: Effect of the feeding discharge on the lake filling time with different dam heights.	201

Fig. 6. 15: The surface area curves for different dam height scenarios.....	202
Fig. 6. 16: The lake volume curves for different dam height scenarios.	203
Fig. 6. 17: Effect of feeding discharge on the relation between dam height and filling time (scenario 80).	204
Fig. 6. 18: Relation among the feeding discharge, the filling time and the storage volume.	205
Fig. 6. 19: The calculated filling time and stored volume for scenario 80.	206
Fig. 6. 20:Level reservoir volume curve.	208
Fig. 6. 21:Flowchart for dam failure types.	210
Fig. 6. 22: Phases of cohesive dam breaching by overtopping.	212
Fig. 6. 23: Dam breaching attributable to piping.	213
Fig. 6. 24: The soil stratification at Spriana slide.	215
Fig. 6. 25:The assumed hydraulic conductivity function.....	216
Fig. 6. 26: Seepage analysis at water depth in the lake = 20 m.	217
Fig. 6. 27: Downstream fluxes from seepage face due to 20 m water height at upstream.	218
Fig. 6. 28: Seepage analysis at water depth in the lake = 40 m.	218
Fig. 6. 29: Downstream fluxes from seepage face due to 40 m water height at upstream.	219
Fig. 6. 30: Seepage analysis at water depth in the lake = 60 m.	219
Fig. 6. 31: Downstream fluxes from seepage face due to 60 m water height at upstream.	220
Fig. 6. 32: Seepage analysis at water depth in the lake = 80 m.	220
Fig. 6. 33: Downstream fluxes from seepage face due to 80 m water height at upstream.	221
Fig. 6. 34: Different hydraulic conductivity functions (case 2= 10*case 1).	222
Fig. 6. 35: Seepage analysis at water depth in the lake = 60 m (case 2).....	223
Fig. 6. 36:Downstream fluxes from seepage face due to 60 m water height at upstream with different permeability($K_2=10.K_1$).	223
Fig. 6. 37: Definition sketch of breach section by Macchione.	227
Fig. 6. 38 : The produced hydrograph for scenario 80 according Macchione breaching model 2008.	230
Fig. 6. 39: The produced sediment hydrograph for scenario 80 according Macchione breaching model 2008.	230
Fig. 6. 40: Macchione model sensitivity to dam height (water hydrograph).....	231
Fig. 6. 41: Macchione model sensitivity to dam height (sediment hydrograph).	232
Fig. 6. 42: Macchione model sensitivity to crest width (water hydrograph for scenario 80).	233
Fig. 6. 43: Macchione model sensitivity to crest width (sediment hydrograph for scenario 80)	233

Fig. 6. 44:Macchione model sensitivity to dam slopes (water hydrograph for scenario 80 with different slopes).....	234
Fig. 6. 45: Macchione model sensitivity to dam slopes (sediment hydrograph for scenario 80 with different slopes).....	235
Fig. 6. 46: Noncohesive embankment breach by overtopping: (a) longitudinal;(b) cross section.	236
Fig. 6. 47: Breach side slope stability analysis.	239
Fig. 6. 48: In, mid and out-flow hydrographs for scenario 80.....	243
Fig. 6. 49:Water depths in some section due to scenario 80.....	243
Fig. 6. 50: In, mid and out-flow of sediment hydrographs for scenario 80.	244
Fig. 6. 51:Bed level before and after the wave for 3,4,and 10 diameters model (tf=216000 s).....	245
Fig. 6. 52: Bed differences before and after the wave for 3,4,and 10 diameters models and its comparison with 1987 results (3 diameters).	245
Fig. 6. 53: Bed evolution for scenario 80 using model with 3 grain sizes.	246
Fig. 6. 54: The migration of the 10 mm diameter after the dam break (3 diameters model).....	247
Fig. 6. 55: The migration of the 80 mm diameter after the dam break (3 diameters model).....	247
Fig. 6. 56: The migration of the 800 mm diameter after the dam break (3 diameters model).....	247
Fig. 6. 57: Bed evolution for scenario 80 using model with 4 grain sizes.	249
Fig. 6. 58: The migration of the 10 mm diameter after the dam breach (4 diameters model).....	249
Fig. 6. 59: The migration of the 50 mm diameter after the dam breach (4 diameters model).....	250
Fig. 6. 60: The migration of the 80 mm diameter after the dam breach (4 diameters model).....	250
Fig. 6. 61: the propagation of the 800 mm diameter after the dam breach (4 diameters model). ...	250
Fig. 6. 62: Bed evolution for scenario 80 using model with 10 grain sizes.	251
Fig. 6. 63: Sondrio during 1987 flood.....	252
Fig. 6. 64: Physical model represents the scour under bridges.	253
Fig. 6. 65: The scenario for emergency planning corresponding to Spriana landslide.	254

Chapter 7

Fig 7. 1: Location of the Millennium dam.	257
Fig 7. 2: Nile River Basin (Ahmed, et al., 2008).	258
Fig 7. 3:The three main watersheds of the Nile.....	260
Fig 7. 4: Average flow at Aswan High Dam reservoir.....	261
Fig 7. 5 : Hydrograph of the Blue Nile, White Nile and Atbara Rivers (Klaassen, et al., 2005).	262
Fig 7. 6: Nile basin topography and profile from the Kagera measure station (Tanzania) to the sea (Karyabwite, 2000).....	263
Fig 7. 7 : Sediment load in different tributaries of the Nile river (Ahmed, et al., 2008).	265

Fig 7. 8: Suspended sediment concentration in AHD reservoir (Ahmed, et al., 2008).	265
Fig 7. 9: Bank erosion in the main Nile.	267
Fig 7. 10: Sand Nile River bank in the Sudan Northern State.	268
Fig 7. 11: Monthly average discharge (million m ³) downstream AHD reservoir before and after construction.....	269
Fig 7. 12: Longitudinal bed profile in AHD reservoir & sediment distribution.	269

List of Tables

Chapter 2

Table 2. 1: The transport capacity equations in Basement (ISIS, 2012). 94

Table 2. 2: Properties of the synthetic case study. 103

Chapter 3

Table 3. 1: The geometric properties of the synthetic cases. 111

Table 3. 2: Sediment and water properties. 112

Table 3. 3: The combination of sediment feeding. 118

Table 3. 4: The combination of non-uniform sediment feeding. 133

Chapter 4

Table 4. 1: Grain sizes and slopes in different sections of Mallero. 153

Table 4. 2 : List of the rainfall stations. 155

Table 4. 3: List of hydrometric stations. 156

Chapter 5

Table 5. 1: Basement models according to actual and assumed granulometry 167

Chapter 6

Table 6. 1: Different scenarios for the dam features. 198

Table 6. 2: The results of the lake formation model for different scenarios. 206

Table 6. 3: Expressions for Macchione model's parameters. 227

Chapter 7

Table 7. 1: Areas and rainfall by country in the Nile Basin. 260

Abstract (English)

The sediment transport phenomenon and the resulting morphological evolution of a river streams may have significant implications for flood hazard and related emergency planning, especially in case of mountain floods, during which very large volumes of sediments may be involved. Capability of developing mathematical and numerical models for river morphologic processes is crucial towards making reliable territorial analyses.

This work first addresses an assessment of the suitability of some numerical codes to model the morphological evolution in river streams. The features and the capabilities of each code are introduced. Then, some synthetic test cases are generated in order to choose the potentially best code for the following purposes, and to quantify the importance of the user-defined parameters for the obtained results. The generated tests refer to the most typical situations that may be encountered in mountain environments (such as upstream or lateral sediment feeding, presence of rocky beds, non-uniform grain-size distribution).

The core of the work refers to the Mallero River in northern Italy, for which two hazardous scenarios are considered. First, an ordinary flood is modeled, and in particular that of 1987 for which some data are available. Second, the landslide collapse at Spriana is considered as an external source of sediment feeding that creates an earthen dam with a huge lake behind. An Integrated scenario is introduced involving the landslide and the dam formation, the lake formation, the dam breaching either due to piping or overtopping, the dam-break wave propagation and its influence on the morphological evolution of the Mallero. The relevance of hydro-morphologic modelling for territorial risk and planning is discussed.

A second case-study, relevant for the country of the writer, is construction of the Millennium dam in the Blue Nile, with potential effects on the morphological changes in Nile River.

Keywords: Sediment transport; River morphology; External sediment source; Non-uniform granulometry; Wave propagation; Earthen dam; Lake formation; Breaching; Piping; Overtopping; Flood risk; Emergency planning; Millennium dam.

Abstract (Italian)

I fenomeni di trasporto solido e la conseguente evoluzione morfologica dei corsi d'acqua rivestono notevole importanza nella valutazione della pericolosità alluvionale e delle relative procedure di emergenza, in particolare nel caso degli ambiti montani dove spesso le piene trasportano ingenti quantità di sedimenti. Poter condurre affidabili modellazioni matematico/numeriche dei processi in atto è quindi di grande importanza per produrre analisi territoriali significative.

In questo lavoro si affronta per prima cosa un'analisi comparativa delle potenzialità di differenti codici numerici per la modellazione della morfologia fluviale. Dopo una presentazione delle funzionalità dei codici, sono introdotti alcuni casi test con riferimento ai quali verificare le possibilità dei software. Viene identificato il codice più promettente e si valuta l'effetto della scelta dei parametri sul risultato finale. I casi sintetici si riferiscono alle situazioni più tipiche dei torrenti montani, quali l'apporto solido di monte e laterale, la presenza di tratti inerodibili e di sedimenti con granulometria non uniforme.

Il cuore del lavoro è rappresentato dall'analisi del torrente Mallero in Valmalenco, con riferimento a due scenari di pericolo particolarmente rilevanti per il corso d'acqua. Si analizza lo scenario di piena ordinaria, per il quale si considerano i dati disponibili per l'evento del 1987. In secondo luogo, si considera uno scenario relativo al collasso della frana di Spriana con formazione di uno sbarramento di materiale incoerente. Viene presentato uno scenario modellistico integrato, comprendente la formazione dello sbarramento e il riempimento di un lago a monte, la formazione di una breccia con conseguente onda di crollo e l'evoluzione morfologica del torrente a seguito di questo evento. Si discute infine la valenza dei risultati per la gestione territoriale.

Un secondo caso studio si riferisce alla costruzione della Millennium dam sul Nilo (realità di interesse per il Paese dell'autore), con le potenziali implicazioni per il fiume.

Parole chiave: Trasporto solido; Morfologia fluviale; Apporto di sedimenti; Granulometria non uniforme; Propagazione di onde; Diga in terra; Lago artificiale; Breccia; Sorgente sospesa; Tracimazione; Rischio alluvionale; Gestione delle emergenze; Millennium dam.

Introduction

The phenomenon of the sediment transport is a sequent step of the soil erosion due to the friction with movable fluid like water or wind. The movement of such fluids above the unbridled soil urges its particles to transport from an original location to another. This transportation has harmful consequences; from agricultural point of view the sediment transport from onsite removes, by time, the suitable soil layer for agriculture and finally causes desertification, while from hydraulic point of view the offsite transport of sediment reduces the capacity of the bifurcation, effluent and the rivers.

On the other hand, the sedimentation reduces the capacity of reservoirs and lakes behind dams causing the so-called reservoir siltation. Hence the storage height behind the constructed dams reduces, also the lateral loads on such structures increase by more sedimentation. In total; sediment transport leads to reduction of the storage and/or shortage of design life either because of sediment deposition behind the hydraulic structures or scouring under it, that lead to failure of these structures either from objective point of view (loss in capacity implies less stored water and implies hydropower generation interruption or curtailment) or from structural point of view. Avoiding such effects can be done, for example, by retrieving the capacity from time to time either by excavation or by enlargement of reservoirs which affects the land use on the banks of these waterways and reservoirs.

Nowadays, due to the climate change, catastrophic flood, hurricanes and landslides, as an induced effect for intensive precipitation or severe earthquake, become likely. All these disasters are mainly accompanied or followed by huge amount of sediment. The sediment in these conditions may

even amplify these disasters, so, for management for such crisis, the sources, the evolution, the amount transported and the redistribution of sediment must be assessed by suitable modelling for the sediment transportation.

These harmful fallouts of sediment transport motivate to study this phenomenon and its mathematical and numerical modelling to find a way to evaluate its consequences. In this work, the features of the sediment transport phenomenon and especially its numerical modelling are introduced by three different numerical tools such as: BASEMENT v.2.2.1 (Basic Simulation Environment for Computation of Environmental Flow and Natural Hazard Simulations) by ETH Zurich (Switzerland), HEC-RAS v 4.1 by U.S. Army Corps of Engineers and ISIS v. 3.6.1 by Halcrow group Ltd. Some synthetic cases with typical conditions of river systems (such as variable inflow of sediment, lateral feeding of sediment, sequences of fixed and mobile beds, presence of significant granulometric variability) have been designed and solved with all the codes (whenever possible), with the aim of assessing the capabilities and the weak points of each code and thus determining the most suitable code for modelling the phenomenon in both steep and mild channels.

The above investigative study is followed by implementation to the flooding problem in the town of Sondrio as a case study, chosen because of relatively good availability of data. The analysis was focused on two calamitous scenarios for the Mallero river and Sondrio: a scenario related with the 1987 flood wave in the river, which produced huge amount of sedimentation, and a scenario related with occurrence of a landslide in Spriana (some km upstream of Sondrio), with formation and consequent collapse of an earth dam resulting in a dam-break wave.

As a second case study, that is relevant for the country of the writer, a discussion is introduced about the influences of constructing the Millennium dam in the Blue Nile valley in Ethiopia on the environmental and morphological changes in Nile River.

The following gives a brief description of the contents of the work:

- **Chapter 1 – Sediment transport: Properties and Modelling;** gives a broad overview about sediment transport causes, effects, properties, mathematical representation and the numerical modelling. Some related terms and strategies are discussed like: the effective shear stress, the inception of sediment motion, the formulas used for calculating sediment transport capacity in this work, the laws governing unsteady flow in open channels and it's coupling with both the formulas that quantify the sediment capacity and those governing the morphological evaluation, the effect of non-uniform sediment gradation and finally the numerical modelling of the morphological evolution and it's stability.
- **Chapter 2 - Strategies for numerical analysis;** a brief description of the three numerical codes (HEC-RAS, Basement and ISIS) used in the analysis is given, together with a so-called "Mini User Guide" for each software (useful for the reader who wants to reproduce the results obtained in this work). An aid is provided for entering all the input data needed to recreate the same models conditions and interpreting the output data. In the tail of the chapter there is a preliminary comparison among the results from the three codes, based on clear-water synthetic cases.
- **Chapter 3 - Modelling and analysis of synthetic channel cases;** the synthetic cases considered in this part are: (1) upstream feeding of sediment in mild and steep channels by sediment rates lower or higher than

the transport capacity, with unique and multiple sediment sizes, (2) analysis of lateral sediment feeding representing, for example, a debris flow (landslide) at an intermediate section of the channel and (3) sequent reaches with mobile and fixed beds, with scouring of the bed in the mobile reaches and aggradation to be simulated above hard beds. Through these synthetic cases, the sensitivity of sediment transport to some parameters like the thickness of the active layer, bed friction and spatial discretization, is discussed. Within this chapter, the code Basement is chosen for following analyses.

- **Chapter 4 - The case of Mallero: Mallero description;** introduces the case of Mallero river in the north of Italy, describes the catchments and its topography, the Mallero bed slope, the bed granulometry, the rain gauges location, the flow in the Mallero and the landslide in Spriana.
- **Chapter 5 - The case of Mallero: 1987 flood;** introduces the description for the 1987 flood and presents the numerical modelling of the morphological evolution in the Mallero due to this event. Different scenarios of bed granulometry are used to analyze the contribution of each grain size to the bed variation. A comparison among the obtained results, those of previous studies and some field measurements is presented in a final discussion.
- **Chapter 6 - The case of Mallero: Integrated scenario for Spriana landslide;** introduces the lateral feeding of sediment due to the Spriana landslide and its effects, presents multiple scenarios for dam creation and formation of a lake due to the land slide, discusses the simulation of the seepage process and the probability of dam breaching due to piping, shows application of some models for the breaching process due to dam overtopping and final computation of the morphological evolution of Mallero due to the sediment

produced by the breaching process. Finally, the role played by sediment in flood risk in the town of Sondrio and its management is discussed.

- **Chapter 7 - The Millennium dam;** introduces the influences of constructing the Millennium dam in the Blue Nile on the morphological and environmental changes in Nile River.

The results achieved in the various analyses of the work are summarized in the final conclusions.

1 Sediment Transport: Properties and Modelling

1.1 Introduction

Sediment transport is essentially a two-phase flow problem in which the fluid phase is air or water and the solid phase is the sediment particles. The processes of erosion, transport, and deposition of sediment, collectively termed as sedimentation, are natural processes and have been occurring throughout the geologic time. The landscape as well as the continental margin that includes the shelf, slope and canyons are continuously shaped by the process of sedimentation. Sediment transport occurs due to water, wind, and gravity. Interest in sediment transport stems from practical engineering importance of flood control, erosion control, and river basin management as well as economic interest associated with the extraction of petroleum and other mineral resources.

The study of the movement of sediment particles constitutes a fascinating field. The most common modes of sediment transport in rivers are bedload and suspended load (Fig 1.1). As bed load, sediment particles saltate, roll, and slide, but always staying close to the bed. As suspended load, sediment is carried by the fluid turbulence up in the water column.

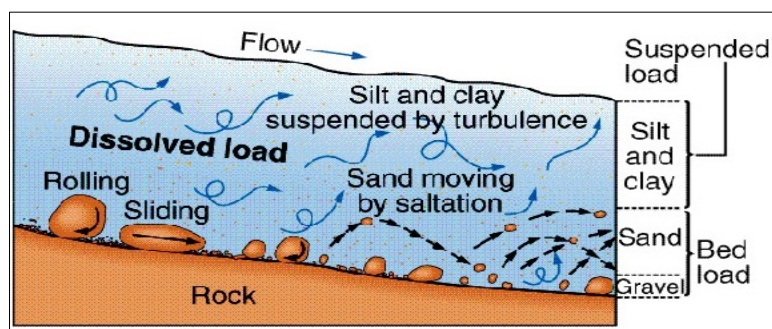


Fig. 1. 1: Bed load and suspended load.

In this chapter, focus primarily is given to the importance and properties of the sediment transport in rivers. Later, complete views about mathematical and numerical models governing the sedimentation are developed.

1.2 Sedimentation Sources and Destination

Removal of vegetation (as from agricultural, logging and construction operations) promotes erosion and increases the sediment loads of rivers and creeks. Runoff from rains and snowmelt carry sediments into nearby streams. As rivers and creeks flow seaward, they carry with them sediments from the land then sediments entering and settling in the estuary (lake, sea or ocean) as in Fig 1.2.

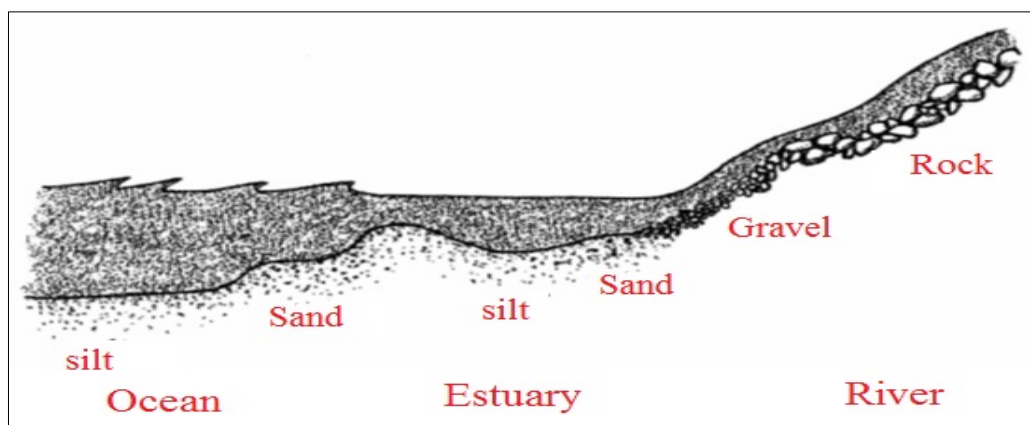


Fig. 1. 2: Sources of sedimentation.

Sediments ranging in size from small rocks and coarse gravel to silt and clay particles as fine as talcum powder enter the water where currents carry them downstream. The faster the current, the greater the size of sediment particles a stream can move.

As a river or creek moves from the mountains or inland areas toward the ocean, its course broadens and velocity gradually slackens. During this process, smaller and smaller particles of sediment drop out and settle toward the bottom, so that the larger rocks and coarser gravel are found farther upstream

and finer sediments downstream, creating what is known as a sediment gradient. In the slower currents of river's lower reaches, only the finest sediments will remain suspended in the water. In the tidewater portion (confluence point with the estuary) of the river, fine sediments begin settling out and deposit in several ways.

Sediments are deposited wherever currents are slowed i.e. turning from steep slopes to the mild one. Also on the bend of a stream, for example, sediments will settle and create shallows along the inside of the curve, because the current is slower there. Currents are also slowed as they flow over plants and algal mats, causing nutrient-bearing sediments to sink to the bottom where they nourish the vegetation.

1.3 The environmental effects of sediment transport

Waters flowing in natural streams and rivers have the ability to scour channel beds, to carry particles (heavier than water) and to deposit materials, hence changing the bed topography. The degradation in a river stream may lead to bridge collapse due to the erosion under the foundations (pier erosion) as in figure 1.3, while the aggregation of sediment in a river stream leads to reduction in river capacity which leads to more exposure to flooding.



Fig. 1. 3: Bed degradation in Arno river at Empoli-Italy.

Comparative study of different scenarios for the morphological evolution in a river stream

Sediment transport phenomenon is of great economic importance to estimate the siltation of a reservoir upstream of a dam wall, since the sedimentation, with time, reduces the storage capacity and finally the functional failure of the reservoir and the dam (Fig 1.4).



Fig. 1. 4: Functional failure of Dam due to sedimentation.

Numerous failures resulted from the inability of engineers to predict sediment motion: e.g., formation of sand bars in estuaries and navigable rivers, destruction of banks, levees, and roads as usually happen in Sinai in Egypt (fig 1.5).



Fig. 1. 5 : Roads collapse in Sinai-Egypt due to erosion and sediment transport.

The most famous sediment transport example: A road to the Honduran town of Choluteca needed to cross a river, so a bridge (Fig 1.6) was built that fulfilled it's purpose for many years. But in 1998 Hurricane Mitch dropped 36 inches of rain on Choluteca (18 inches in one day alone), swelling the river to six times it's normal width, destroying the road and moving the river. When the storm was over, the bridge was standing in perfect condition, but with no reason to exist because it connected no roads and spanned only dry land.



Fig. 1. 6: Choluteca Bridge, Honduras after Hurricane Mitch. 1998.

Another side effect of the sediment transport is the bank erosion which affects the land use on the banks of the waterways and lead to the failure of the roads.



Fig. 1. 7: Bank erosion as a source of sediment.

The rivers are constructed and deformed by it's own content. Depending on the flow conditions and sediment size distribution, bed forms (e.g. Ripples Fig 1.3 and Dunes Fig 1.4) of various scale and shape can appear. These bed forms cause extra resistance to the flow and thus can alter the flow depth significantly.



Fig. 1. 8: Ripples in the Rum River, Minnesota USA at very low flow (Parker, 2004).



Fig. 1. 9: Dune bed forms in a small stream, flow from right to left (Chanson, 2004).

Indeed, not all the effects of sediment transport are harmful. As the situation In Egypt; the sediment transported from it's origin in Ethiopia through the Nile led to the creation of the delta in Egypt (Fig 1.10) which is a fertile land suitable for agriculture. The sediment transport with the floods in Nile was a good source for soil fertility renewal in the Nile Valley and it's Delta. After building the high dam in Aswan at 1970 all the sediment deposit behind

the dam in Nasser Lake, while the farmers invoked to use organic and chemical fertilizers.



Fig. 1. 10: Nile's delta formed by sediment transport.

1.4 Sediments Properties and Terminology

There are specific properties for the single particle and for the mixture of sediment. In the following, there is a discussion about the important properties of sediments and their effects on the sediment transportation.

1.4.1 Properties of a single particle

Perhaps the most basic hydraulic property of sediment is particle size d_s . For noncohesive sediments the size can be measured in several ways: (1) **Equivalent diameter**: the diameter of a sphere having the same volume as the

particle, (2) **Sieve diameter**: the minimum sieve size opening that passes the particle, (3) **Sedimentation diameter**: the diameter of a solid sphere having the same density and fall velocity and (4) **Surface diameter**: the diameter of a sphere having the same surface area. Sieve diameter is the simplest one to measure experimentally of these different measures.

Another hydraulic property of interest is the particle shape. There are several ways of characterizing this value. Traditionally, the particle shape has been defined in terms either of sphericity, which is the ratio of surface area of a sphere of equal volume to that of the particle or of roundness, which is the ratio of the average radius of curvature of the edges of the particle to the radius of the largest circle that can be inscribed within the particle cross section.

The specific gravity S or average density ρ_s of a particle also is important in determining its hydraulic characteristics. Specific gravity is defined as the ratio of the solid weight of a particle to the weight of an equal volume of water under standard conditions. (Rubin, et al., 2001) Stated that for Quartz or silicon-based particles such as sands have a specific gravity of around 2.65, but aggregates of smaller materials typically have much lower specific gravities, sometimes approaching 1.0.

The heavier particle is more stable, so the transport capacity inversely proportional with the sediment density or, by accurate speaking, with the difference between the sediment density and fluid density, so $q_s \propto \frac{1}{\rho_s}$ or $q_s \propto \frac{1}{\rho_s - \rho} = \frac{1}{\rho(s-1)}$ where ρ is the water density. By another way it is possible to say that the sediment capacity is affected by the difference between sediment weight and the applied buoyancy force acting on the sediment from fluid.

1.4.2 Median sediment size

For a sediment mixture; the sediment size is not unique, but it differs from very fine to coarse which is known by particle size distribution (fig 1.11). Usually it is better to express the sediment mixture by the median diameter (d_m or d_{50}) i.e. the size for which 50% by weight of the material is finer.

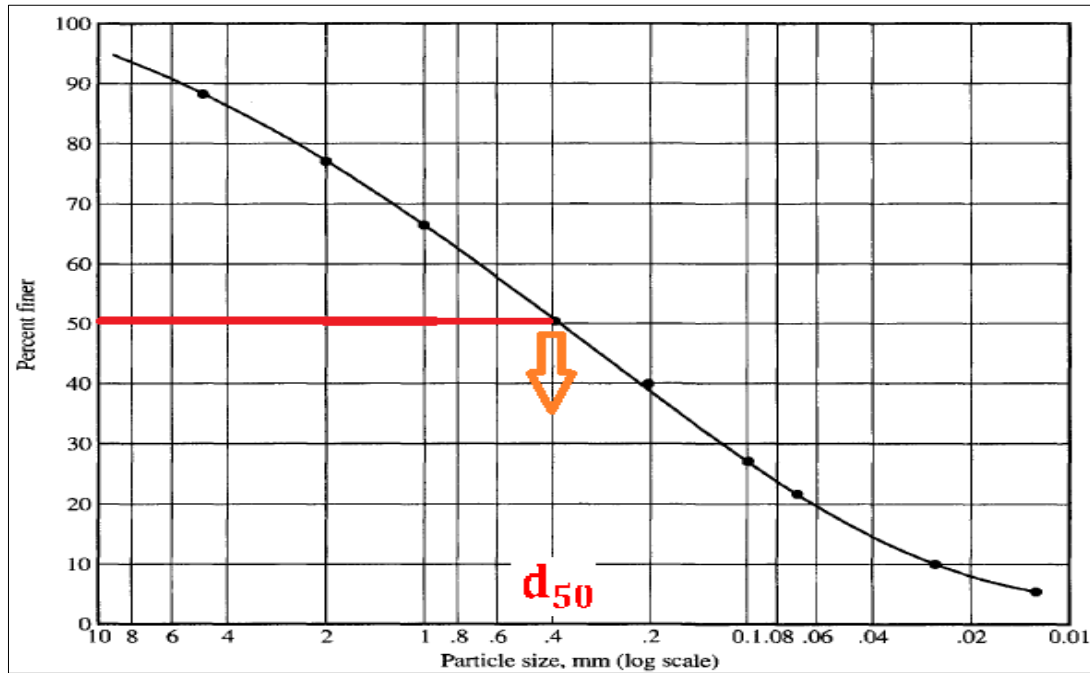


Fig. 1. 11: Particle-size distribution curve.

For low values of median diameter; the transport capacity is inversely proportional with the median diameter of sediment. The coarse sediments are the more stable, so it needs higher dragging force for transportation from its position i.e. for a single size $q_s \propto \frac{1}{d_s}$ while for multiple size mixture $q_s \propto \frac{1}{d_m}$ where q_s is the transport capacity, d_s is the single sediment size, and d_m is the median diameter for multiple sizes mixture.

1.4.3 Sediment Mixture density

The sediment mixture has the same soil properties such as the void ratio, which means that the mixture is unbridged (Fig 1.12), this is the reason why the

particles move once any sufficient shearing force urges it. If there are no voids, the sediment will be one unit and it can't be moved whatever the values of the shearing force. The void ratio can be expressed also by the so called sediment porosity factor p_0 . So the dry sediment mixture has density expressed in terms of porosity by the Eq 1.1, while the wet density where the water occupies the voids is given by Eq 1.2.

$$(\rho_{\text{sed}})_{\text{dry}} = (1 - p_0)\rho_s \quad 1.1$$

$$(\rho_{\text{sed}})_{\text{wet}} = p_0 \rho + (1 - p_0)\rho_s \quad 1.2$$

According to (Chanson, 2004); the porosity factor ranges basically from 0.26 to 0.48. In practice, p_0 is typically about 0.36–0.40.

Eq 1.2 gives two useful notes; the first that the voids will be filled by the fluid, the second is that the sediment particle will not absorb any part of the fluid.

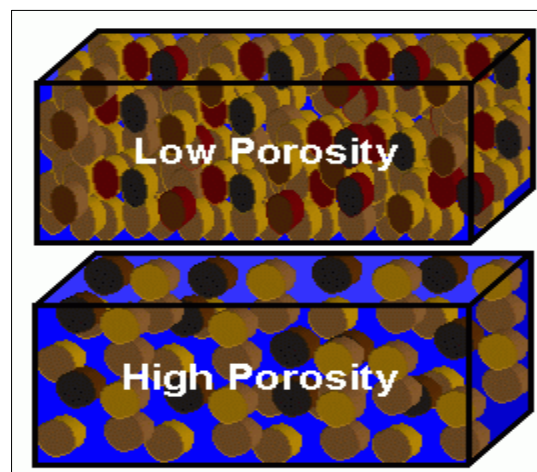


Fig. 1. 12: Sediments porosity definition.

1.4.4 Settling (falling) velocity

In a fluid at rest, a suspended particle heavier than water has a downward motion. The terminal fall velocity of the particle equals it's velocity when the

sum of the gravity force, buoyancy force and fluid drag force equals zero. For a spherical particle, settling in a still fluid, the terminal fall velocity w_0 equals:

$$w_0 = -\sqrt{\frac{4gd_s}{3c_d}(s-1)} \quad 1.3$$

Where d_s is the particle diameter, S is the specific gravity and C_d is the drag coefficient which is function of Reynolds number and particle shape (C_d estimated experimentally Fig 1.13). The negative sign indicates a downward motion for $s > 1$.

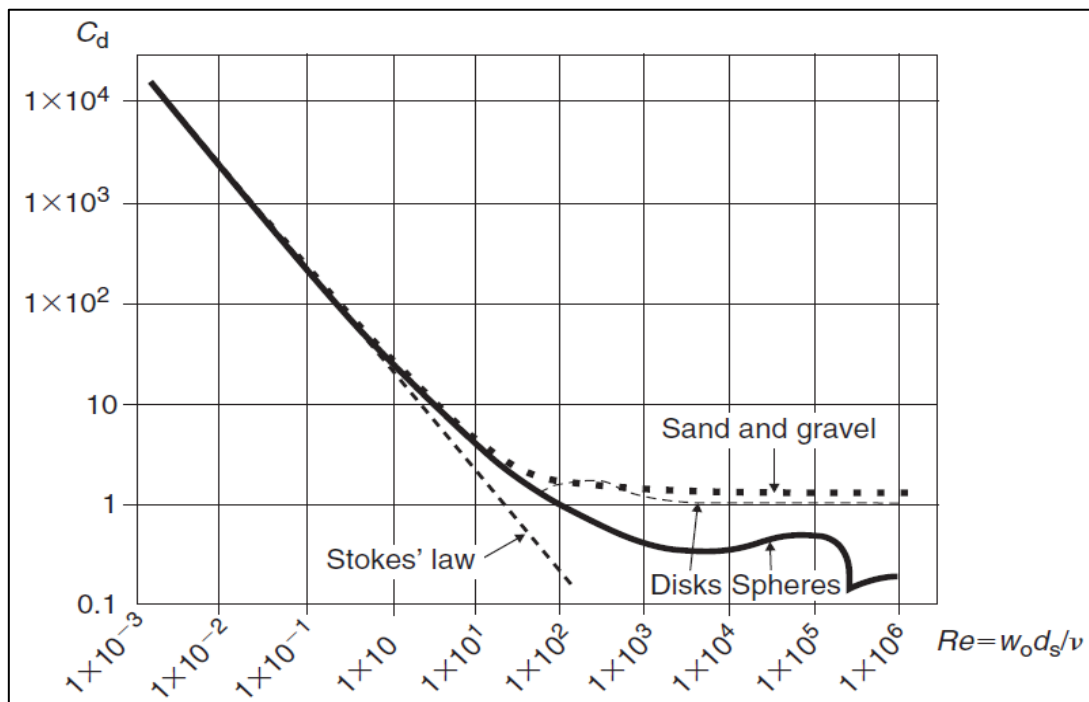


Fig. 1. 13: Drag coefficient of single particle in still fluid (Chanson, 2004).

1.4.5 Angle of Repose

Considering the stability of a single particle in a horizontal plane, the threshold condition (for motion) is achieved when the center of gravity of the particle is vertically above the point of contact. The critical angle at which motion occurs is called the angle of repose ϕ_s .

According to (Chanson, 2004) ; the angle of repose is a function of the particle shape and, on a flat surface, it increases with angularity. Typical examples are shown in Fig. 1.14. For sediment particles, the angle of repose ranges usually from 26° to 42°. For sands, ϕ_s is typically between 26° and 34°.

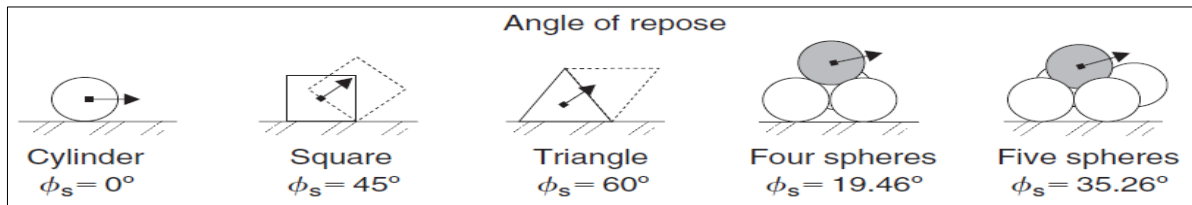


Fig. 1. 14 : Examples of angle of repose (Chanson, 2004).

1.5 Inception of motion

The onset of particle motion depends on the bed shear stress. If it exceeded the limit value called critical shear stresses, the particles will start to move just above the bed which called "bed load". As a second step; once the water velocity increases and exceed a specific velocity limit, the fluid turbulence carry the lighter sediment up in the water column and the so called suspended load starts. In the suspended load the water moves the small particles in it's eddies upward, hence the concentration of the sediment increases in a zone higher than the bed zone Fig 1.15. Once the severity of turbulence decreases (i.e. velocity decreases) this sediment settles down. The limits of both bed load and suspended load are shown in Fig 1.16.

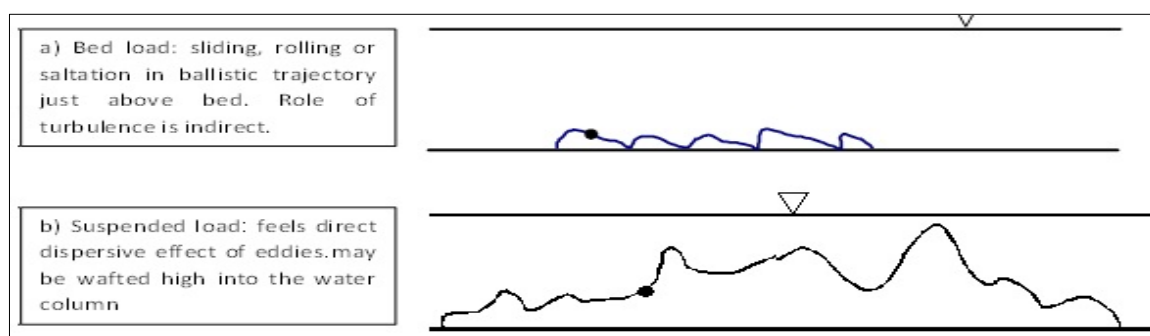


Fig. 1. 15: Particle movement; a) Bed load; b) Suspended load (Parker, 2004).

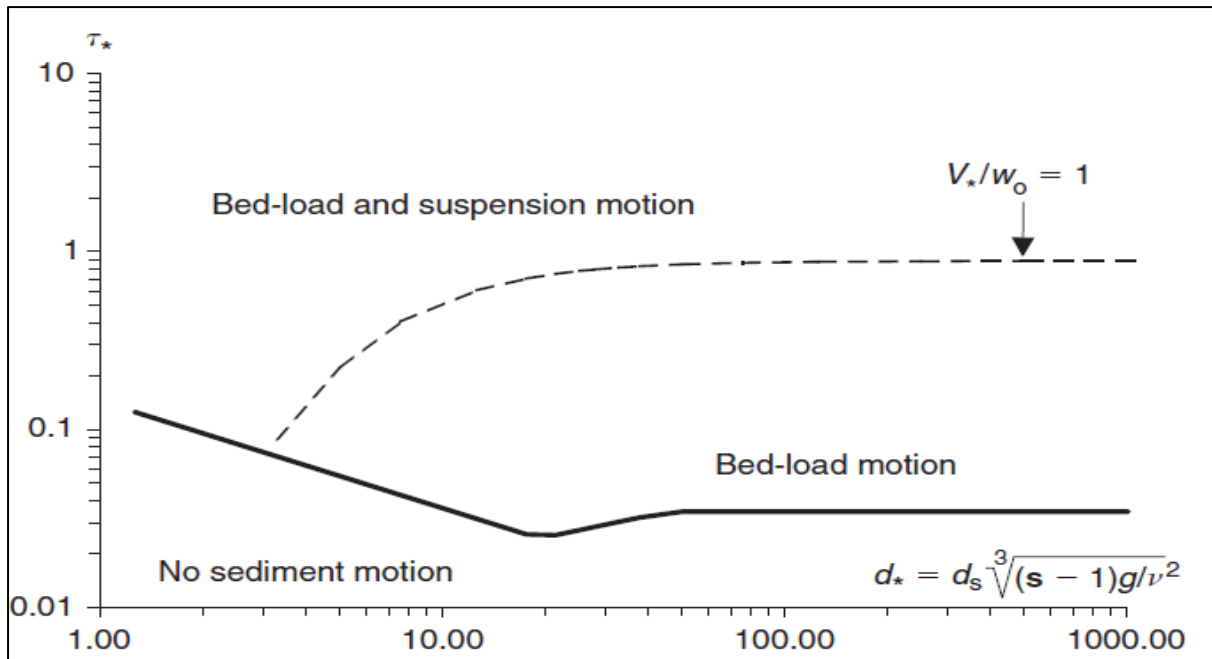


Fig. 1. 16: Threshold of sediment motion (bed-load and suspension), Shield's parameter as a function of the dimensionless particle parameter d^* (Chanson, 2004).

So as shown in Fig 1.16; two dimensionless quantities must be determined for knowing that there is no sediment motion as a bed load motion only or together bed load and suspended load motion take place; the first is the dimensionless particle diameter given by Eq 1.4 and the second is the ratio between the driving shear stress to the critical shear stress, this ratio is known as "shield's number τ_* " given by Eq 1.5.

$$d_* = d_s \sqrt[3]{\frac{(s-1)g}{\nu^3}} \quad 1.4$$

$$\tau_* = \frac{\tau_0}{\rho(s-1)gd_s} = \frac{u_*^2}{(s-1)gd_s} \quad 1.5$$

Where ν is the kinematic viscosity of the fluid, τ_0 is the average shear stress on the wetted surface, $\tau_0 = \rho g R_H \sin \theta$, g is the gravity acceleration =9.81 m/s², R_H is the hydraulic radius, θ is the bed slope, u_* is the shear velocity

$u_* = \sqrt{\frac{\tau_0}{\rho}}$ which is a measure of shear stress and velocity gradient near the

boundary. The relation between the mean velocity of the fluid and shear velocity is given by Eq 1.6.

$$\frac{u_*}{V} = \sqrt{\frac{f}{8}} = \sqrt{\frac{g}{c_{chezy}^2}} \quad 1.6$$

Where f is the friction coefficient estimated by Moody; c_{chezy} is the friction coefficient by Chezy. So once the mean water velocity increases (turbulence), the shear velocity increases as well with respect to the settling velocity and the water forces the small particles to move up forming the suspended load, so when $\frac{u_*}{w_0} \approx 0.2 - 2$ there is a bed load and suspended starts (Fig 1.16).

The inception of bed motion happen when the bed shear stress just equal the critical one i.e. $(\tau_0)_c = \rho(s - 1)gd_s(\tau_*)_c$, $(\tau_*)_c$ is the critical shield number represented by the solid bold line in Fig 1.3, while the onset of suspended load is given by the dotted line. The summation of the bed load and suspended load is the total load transported from section to another one through the channel.

1.6 Effective bed roughness

The movement of water in open channel is withstood usually by many sources of friction, so the estimation of the bed roughness must consider these sources of friction like the grains roughness (also called Nikaradse roughness), bed form, and vegetation e.g. the total Manning coefficient ($n_T = n_{grains} + n_{bedforms} + n_{vegetation} + n_{other\ frictions}$) and the same for Strickler or Chezy coefficients.

As discussed in item 1.3; movable hydraulics is characterized by a dual interaction between bed forms and flow resistance. The type of bed form and

the sediment transport rate are both related to the discharge which is, in turn, a function of the bed-form resistance.

The boundary friction is related, mainly after regardless the vegetation effect, to the skin friction (or grain-related friction) and to the form losses caused by the bed forms. Figure 1.17 presents a typical relationship between the mean boundary shear stress τ_0 and the flow velocity. It indicates that the effect of bed forms is particularly substantial with ripples and dunes.

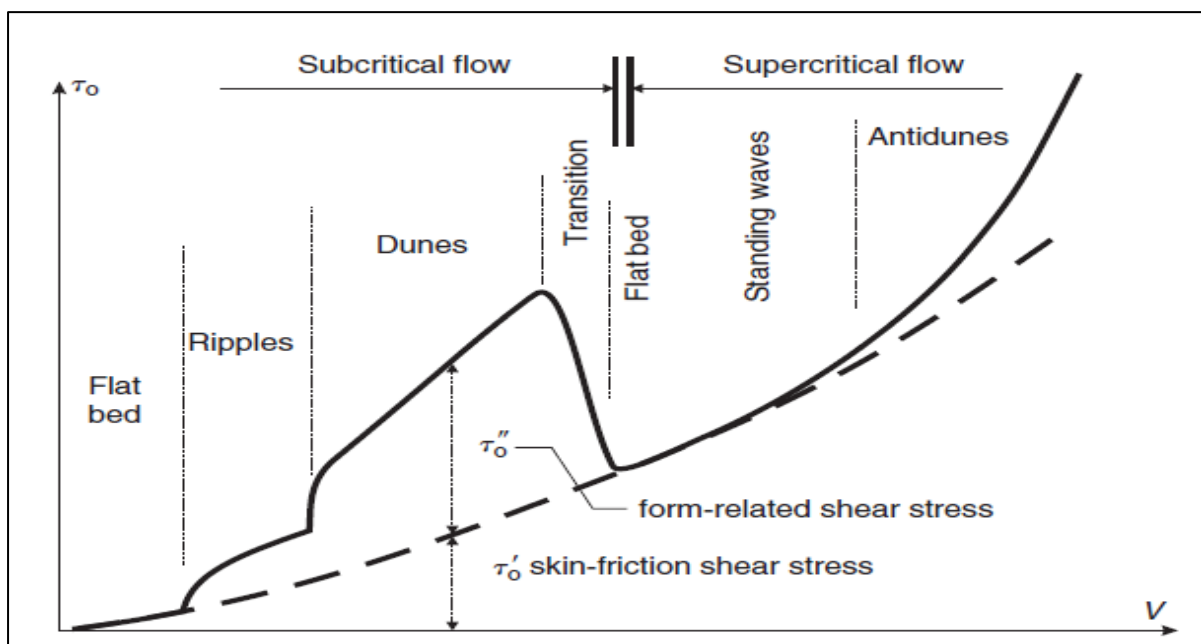


Fig. 1. 17: Bed shear stress as a function of the mean flow velocity (Chanson, 2004).

So as shown the mean boundary shear stress τ_0 may be expressed as:

$$\tau_0 = \tau'_0 + \tau''_0 \quad 1.7$$

Where τ'_0 is the skin friction shear stress and τ''_0 is the form-related shear stress. The skin friction shear stress equals:

$$\tau'_0 = \frac{f}{8} \rho V^2 \quad 1.8$$

Where ρ is the fluid density, V is the mean flow velocity and f is the Darcy–Weisbach friction factor. The bed-form shear stress τ_0'' is related to the fluid pressure distribution on the bed form and to the form loss (fig.1.18).

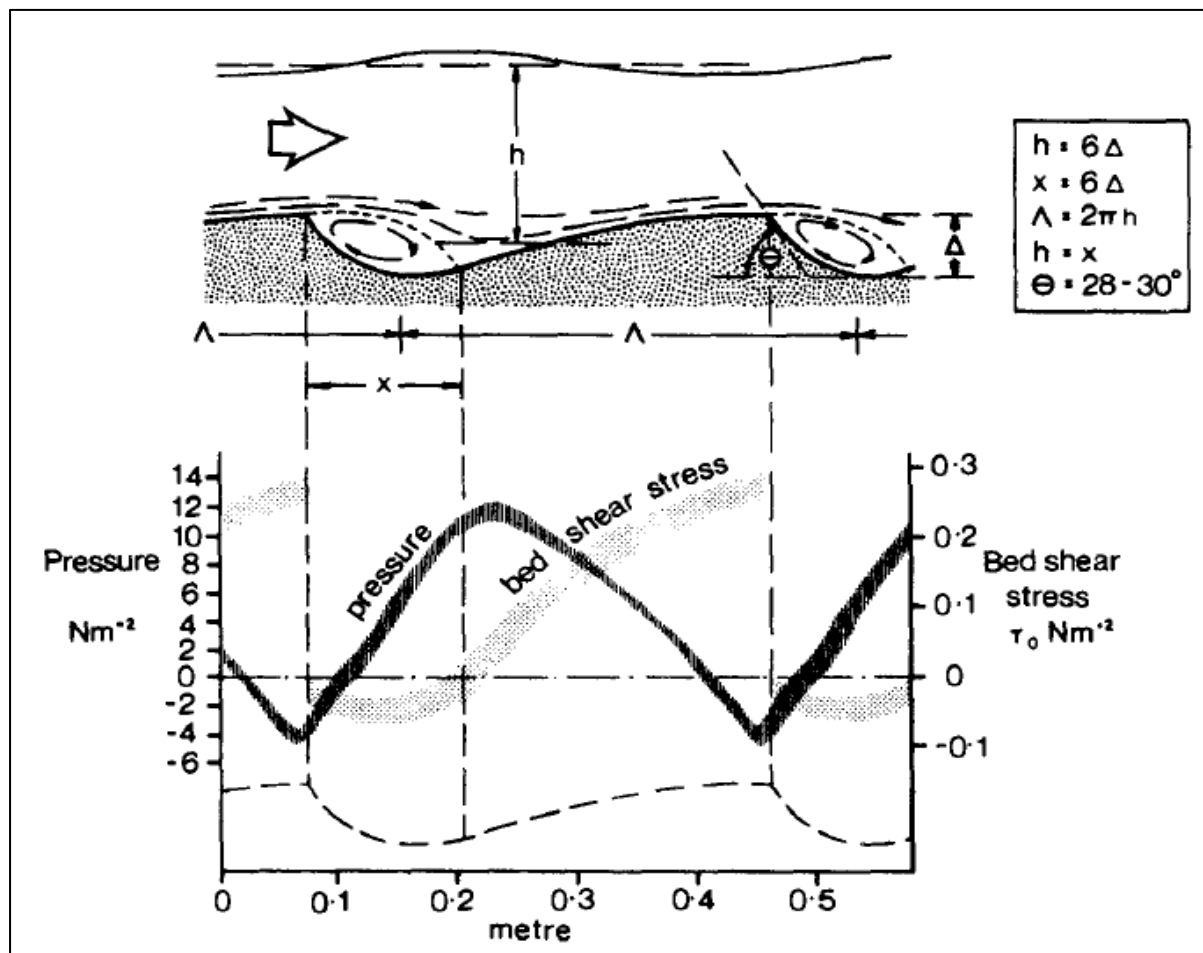


Fig. 1. 18: Fluid pressure and shear stresses distribution along a dune (Van Rijn, 1993).

The form loss may be crudely analyzed as a sudden expansion downstream of the bed-form crest. According to (Chanson, 2004); for a two-dimensional bed-form element, it yields:

$$\tau_0'' = \frac{1}{2} \rho V^2 \frac{h^2}{ld} \quad 1.9$$

Where h & l are the bed-form height and length respectively.

According to (Chanson, 2004); importantly the bed-load transport must be related to the effective shear stress (skin friction shear stress) **only** and not to

the form roughness. In natural rivers, the Shields parameter and bed-load layer characteristics must be calculated using the skin friction bed shear stress. The onset of sediment motion and bed-load transport rate is predicted using the Shields parameter defined as:

$$\tau_* = \frac{\tau'_0}{\rho(s-1)gd_s} \quad 1.10$$

1.7 The transport capacity

The workers in the field of morphodynamics have developed numerous relationships for estimating the total load transport rate. When the Shield's number become higher than the critical value, but still less than the threshold for suspended load e.g. in figure 1.16 $\tau_{*c} < \tau_* < \left(\frac{u_*}{w_0} = 1\right)$, then the total load equals to the bed load only, since the suspended load in this case is negligible. Once the velocity exceeds the limit value $\left(\frac{V}{w_0} = 0.2 \sim 2\right)$, the transport capacity must be calculated based on both the bed load and the suspended load.

The bed load formulae generally relate the transport capacity with the difference between applied Shield's number and the critical one ($\tau_* - \tau_{*c}$) and sediment properties like the median diameter and the specific gravity. In the following some formulas that estimate the transport capacity are presented.

1.7.1 Meyer Peter and Müller formula.

- For single size

The formula for Meyer-Peter and Müller can be written in the form given in Eq. 1.11.a.

$$Q_s = B * \sqrt{g(s-1)d_s^3} * 8(\tau_* - \tau_{*c})^{\frac{3}{2}} \quad 1.11.a$$

Where Q_s is the bed load capacity, B is channel width, τ_{*c} is critical Shield's number (MPM proposed the value of 0.047) and τ_* is the applied Shield's number calculated using Eq 1.10. According to (Faeh, et al., 2012); the formula of Meyer-Peter and Müller is applicable in particular for coarse sand and gravel with grain diameters above 1 mm.

- For multiple sizes

The formula for single size is extended by using correction factor for the inception of motion ξ_g then the Shield's number for each grain size g is given by ($\tau_{*c,g} = \xi_g * 0.047$). Where ξ_g is estimated by equation 1.11.b proposed by (Ashida, et al., 1971).

$$\xi_g = \left\{ \begin{array}{ll} \left[\frac{\log(19)}{\log\left(\frac{19d_g}{d_m}\right)} \right]^2 & \text{for } \frac{d_g}{d_m} \geq 0.4 \\ \frac{d_m}{d_g} & \text{for } \frac{d_g}{d_m} < 0.4 \end{array} \right\} \quad 1.11. b$$

It is clear that this type of equations for multi sizes consider the sorting effect where the smallest grain size is the faster in transporting, then the coarse sediment remain forming the so called armoring layer. The armoring layer prevents more erosion, since it defend the small grain under it.

1.7.2 Wong and Parker

Wong and Parker [2006] proposed a correction of the Meyer-Peter and Muller relation. There sediment transport capacity given by Eq 1.11.c, while the applicability still with sediment diameter $d_s \geq 1$ mm:

$$Q_s = B * \sqrt{g(s-1)d_s^3} * 4.93(\tau_* - \tau_{*c})^{\frac{8}{5}} ; \tau_{*c} = 0.047 \quad 1.11. c$$

1.7.3 Parker fit to Einstein equation

Parker [1979] fit to Einstein [1950] equation and proposed the equation 1.11.d applicable for sizes smaller than 1mm, $\tau_{*c} = 0.03$.

$$Q_s = B * \sqrt{g(s-1)d_s^3} * 11.2 * \tau_*^{\frac{3}{2}} \left(1 - \frac{\tau_{*c}}{\tau_*}\right)^{\frac{9}{2}} \quad 1.11.d$$

1.7.4 Power law

According to (Faeh, et al., 2012); the sediment discharge may be estimated by an empirical power function of the flow velocity Eq 1.11.d, in which no critical shear stress is regarded in this approach and the transport only depends on the empirical constants a & b whose values depend upon the flow velocity.

$$Q_s = a \left(\frac{Q}{h}\right)^b \quad 1.11.e$$

1.8 Morphological evolution

The morphological evolution means: the change in bed levels by aggradation or degradation from the bed due to the phenomenon of sedimentation.

1.8.1 The governing equations in 1D

The field of morphodynamics consists of the class of problems for which the flow over a bed interacts strongly with the shape of the bed, both of which evolve in time. That is, the flow and the bed talk to each other. The flow field over the bed determines a pattern of variation of sediment transport rate. This variation changes the bed by erosion or deposition of sediment. The changed bed now induces a changed flow field.

"Felix Exner" was the first researcher to state a morphodynamic problem in quantitative terms. The term "morphodynamics" itself evolved many decades

afterward. This notwithstanding, Exner deserves recognition as the founder of morphodynamics.

Recall that Q_s denotes the volume sediment transport rate and p_0 denotes bed porosity. The mass sediment transport rate per unit width is then $\rho_s Q_s$, where ρ_s is the material density of sediment. Mass conservation within the control volume with a unit width requires that:

$$\frac{\partial}{\partial t} (\text{sediment mass in bed}) = \text{mass sediment inflow rate} - \text{mass sediment outflow rate} \quad 1.12. a$$

$$\frac{\partial}{\partial t} [\rho_s(1 - p_0)\eta] \cdot \Delta x \cdot B = \rho_s \cdot [Q_s|_x - Q_s|_{x+\Delta x}] \cdot B \quad 1.12. b$$

$$(1 - p_0) \frac{\partial \eta}{\partial t} = - \frac{\partial Q_s}{\partial x} \quad 1.12. c$$

The terms of Exner formula [1.12.c] described in Fig 1.19 which represents the continuity equation for sediment, where $\partial \eta$ represents the change in bed level, B is the channel width and Δx is the spatial step.

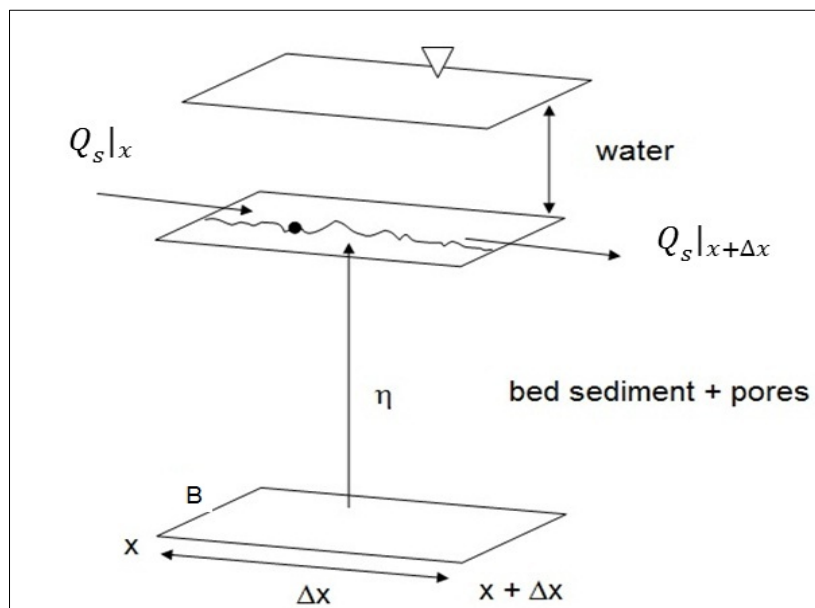


Fig. 1. 19: Bed evolution and terms of Exner equation (Parker, 2004).

The governing equations, for one dimensional morphological evolution, are the De Saint Venant equations [1.13] plus Exner equation [1.12.c] beside one suitable equation for calculating the sediment transport capacity [1.11].

$$\frac{\partial A}{\partial t} + \frac{\partial Q}{\partial x} - q_l = 0 \quad \text{Continuity equation for water} \quad 1.13.a$$

$$\frac{\partial V}{\partial t} + V \frac{\partial V}{\partial x} + \frac{\partial h}{\partial x} = g(s_0 - s_f) \quad \text{Momentum equation for water} \quad 1.13.b$$

The following system of equations [1.14] describes unsteady flow in a wide rectangular channel with deformable bed take into account both bed load and suspended load.

$$\frac{\partial h}{\partial t} + \frac{\partial Vh}{\partial x} - q_l = 0 \quad \text{Continuity equation for water} \quad 1.14.a$$

$$\frac{\partial V}{\partial t} + V \frac{\partial V}{\partial x} + \frac{\partial h}{\partial x} = g(s_0 - s_f) \quad \text{Momentum equation for water} \quad 1.14.b$$

$$\frac{\partial q_s}{\partial x} + \frac{\partial C \cdot h}{\partial t} = -(1 - p_0) \frac{\partial \eta}{\partial t} \quad \text{Continuity equation for sediment} \quad 1.14.c$$

$$q_s = f(Q, d_s, \rho_s, \dots \dots \dots) \quad \text{transport capacity formula} \quad 1.14.d$$

$$c = f(V, d_s, \dots \dots \dots) \quad \text{local concentration formula} \quad 1.14.e$$

While C is the concentration of suspended sediment averaged over the cross section $C = \int_A c \, dh$.

In case of internal feeding/erosion of sediment from/to external source like in Fig 1.20 the continuity equation for sediment (Exner Eq [1.14.c]) takes the form given in Eq 1.15.

$$(1 - p_0) \frac{\partial \eta}{\partial t} * B = - \frac{\partial q_s}{\partial x} * B + D_s + E_s \quad 1.15$$

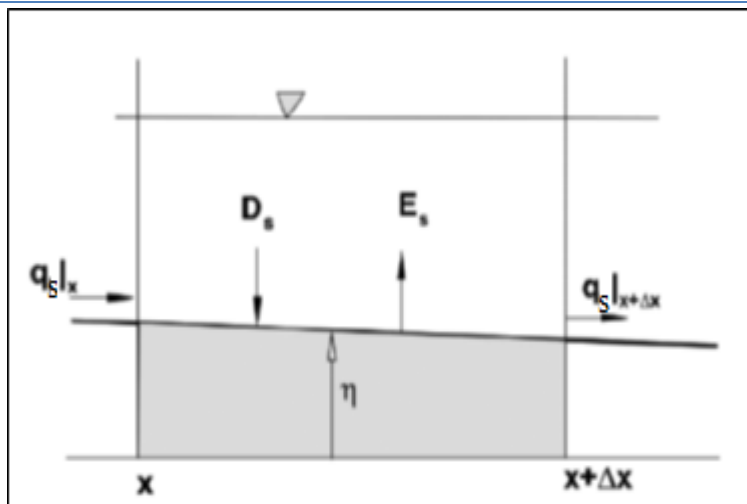


Fig. 1. 20: Mass conservation at the river bed (Chaudhry, 2008).

Where x denotes the stream wise direction, η denotes the bed elevation, q_b denotes the volume transport rate of bed load per unit width per unit time, D_s is the feeding rate from the external source and E_s is the erosion rate both expressed as volume per unit area per unit time. The bed of the river exchanges sediment with the flow at the upper surface of the control volume indicated by the shaded area.

1.8.2 Non-dimensionalization of the governing equations

The essence of morphodynamics is in the interaction between the flow and the bed. The flow changes the bed, which in turn changes the flow. By considering a reference mobile-bed equilibrium state with constant flow velocity V_0 flow depth h_0 , bed slope S_0 and total volume bed material transport rate Q_{s0} . For the sake of simplicity the bed friction coefficient S_f is assumed to be constant. The analysis easily generalizes, however, to the case of varying friction coefficient. Then the following non-dimensionalizations are introduced:

$$h = h_0 \tilde{h}, V = V_0 \tilde{V}, \eta = h_0 \tilde{\eta}, Q_s = Q_{s0} \tilde{Q}_s, x = h_0 \tilde{x}, \text{ and } t = \frac{h_0}{V_0} \tilde{t} \quad 1.16$$

The non-dimensionalization of time involves the “hydraulic” time scale $\frac{h_0}{V_0}$, which physically corresponds to the time required for the flow to move a distance equal to one depth in the downstream direction. Substituting the non-dimensional variables into the balance equations [1.12.c and 1.13] yields the results in [1.17].

$$\frac{\partial \check{h}}{\partial \check{t}} + \frac{\partial \check{V}\check{h}}{\partial \check{x}} = 0 \quad 1.17.a$$

$$\frac{\partial \check{V}}{\partial \check{t}} + \check{V} \frac{\partial \check{V}}{\partial \check{x}} = -Fr_0^{-2} \left(\frac{\partial \check{h}}{\partial \check{x}} + \frac{\partial \check{\eta}}{\partial \check{x}} \right) + \frac{gh_0 S_0}{V_0^2} \left(1 - \frac{\check{V}^2}{\check{h}} \right) \quad 1.17.b$$

$$\frac{\partial \check{\eta}}{\partial \check{t}} = -\varepsilon \frac{\partial \check{q}_s}{\partial \check{x}} \quad 1.17.c$$

$$\text{where } Fr_0 = \frac{V_0}{\sqrt{gh_0}} \quad 1.17.d$$

$$\varepsilon = \frac{1}{(1-P_0)} \frac{Q_{s0}}{h_0 V_0} = \frac{1}{(1-P_0)} \frac{Q_{s0}}{Q_{w0}} \cong \frac{1}{(1-P_0)} \left(\frac{Q_s}{Q_w} \right)_{\max} \quad 1.17.e$$

Where, Fr is the Froude number; which represents the ratio between the dynamic forces moves the fluid and the inertial force withstanding this movement, so it is the distinction number between the supercritical and the subcritical flows. The ratio ε given by equation [1.17.e] represents the ratio between the sediment flow and the water flow.

1.8.3 Effect of porosity

As shown in equation [1.17.e] the porosity has influence of the ratio ε between the sediment discharge Q_s and water discharge Q_w . Bed porosity P_0 is typically in the range $0.25 \sim 0.45$ for beds of non-cohesive sediment.

Theoretically, if the porosity reached the unity, which is the maximum theoretical value for it, the ratio ε will reach to infinity. This means that once the bed soil become looser, the transport capacity increases. In the other hand; if the bed material is hard and it's porosity nears to zero, the ratio ε will be reduced i.e. the sediment transport will not happen whatever the value of the water discharge. So for rocky beds no erosion can happen, but only deposition can occur.

As a learnt lesson; to prevent the erosion for the channels bed, the compaction of these beds is needed. Otherwise; the lining of this bed is proposed by material has no void ratio like concrete and by this way sediment/water flow ratio ε will be minimized.

1.8.4 Sediment / water flow ratio

The sediment / water flow ratio ε is just a scale ratio, which scales the ratio of the volume transport of solids to the volume transport of water by a river. For the great majority of cases of interest this ratio is exceedingly small, even during floods. Practically; the value of the ratio ε is very small and the largest values of ε attained in the great majority of rivers is much less than unity ($\varepsilon \approx 0.4\%$ according (Parker, 2004) for mild slope river). This is the reason why, in short time hydraulic models for mild channels, the morphological evolution is not so important to consider it, because the evolution in bed level is very small and can be neglected. While for long time models, the morphological evolution must be considered.

Indeed the value of the ratio ε is mainly controlled by the transport capacity Q_s which increases by decreasing of the gradation sizes or the median size, so for finer soils more erosion is expected hence more bed evolution.

1.8.5 Effect of higher slopes

The bed slope is directly proportional to the driving bed shear stress, $\tau_0 = \rho g R_H \sin \theta$, hence the Shield's number calculated by equation [1.10] is higher than the Shield's number for similar case with lower slope. This means that the transport capacity increases with more increasing of bed slope.

Mountain streams not only convey water, but also transport large amounts of bed sediment, including sand and gravel, and in some cases cobbles and boulders. The transport of gravel and coarser material is primarily in the form of bed load, with particles sliding, rolling or saltation within a thin layer nears the stream bed. Another characteristic of these streams is that bed load transport events are sporadic and associated with floods. Thus in a perennial stream, significant bed load transport may occur.

So for the case of mountain floods; the value of the sediment/water flow ratio ϵ is higher than the usual value for flat rivers. This is the reason why the morphological evolution in mountain floods must be considered whatever the flood duration, because in mountains the flash floods can produce huge amount of sedimentation.

1.9 Characteristic form of governing equations

According to (Chaudhry, 2008); the concept of characteristic curves is helpful in understanding the propagation of waves and the development of boundary conditions for the explicit finite difference methods.

The governing equations for morphological evolution [1.14] form a set of nonlinear partial differential equations. A closed form solution of these equations is not available except for very simplified cases. Therefore, numerical methods are used for their integration. To select a numerical

scheme, it is helpful to know the type of these equations i.e. whether they are hyperbolic, parabolic or elliptic.

For this aim; the governing equation [1.14] will be transformed to a system composed of 3 equations in 3 unknowns (V, h, η). This 3 equation are obtained by finding the eigenvalues for the governing equation, which had been done by (De Vries). The obtained eigenvalues are shown in Eqs 1.18 in the following table.

Flow type Eigenvalue	subcritical flow ($F_r < 1$)	subcritical flow ($F_r > 1$)	1.18
$\lambda_1 =$	$V + \sqrt{gd}$	$V + \sqrt{gd}$	a
$\lambda_2 =$	$V - \sqrt{gd}$	$V - \sqrt{gd}$	b
$\lambda_3 =$	$\frac{V}{1 - F_r^2} \left(\frac{V}{Q} \frac{\partial Q_s}{\partial V} - \frac{h}{Q} \frac{\partial Q_s}{\partial h} \right)$	$\frac{V}{1 - F_r^2} \left(\frac{V}{Q} \frac{\partial Q_s}{\partial V} - \frac{h}{Q} \frac{\partial Q_s}{\partial h} \right)$	c

Hence, the eigenvalues λ_1, λ_2 represent absolute wave velocities, $V + \sqrt{gd}$ and $V - \sqrt{gd}$, the expressions for the eigenvalues λ_1, λ_2 show that both of them are real and distinct for subcritical and supercritical flows. Therefore, Eqs [1.14. a] and [1.14.b] are a set of hyperbolic partial differential equations. These types of equation represent the propagation of waves in different media. Hence the characteristic form of Eqs. [1.14.a, 1.14.b] takes the form given in Eqs 1.19.

$$\frac{d}{dt}(V + 2C) = -g(s_0 - s_f) \quad , C = \sqrt{gh} \quad 1.19.a$$

$$\frac{d}{dt}(V - 2C) = -g(s_0 - s_f) \quad , C = \sqrt{gh} \quad 1.19.b$$

Along their respective characteristic trajectories given by Eqs [1.20]:

$$\frac{dx}{dt} = v + c \quad \text{Forward characteristic C1} \quad 1.20.a$$

$$\frac{dx}{dt} = v - c \quad \text{Forward characteristic C2} \quad 1.20.b$$

These trajectories are called characteristic directions or characteristics of the system. For an observer travelling along the forward characteristics (Fig. 1.21, equation (1.19a)), equation (1.20a) is valid at any point. For an observer travelling on the backward characteristics (equation 1.19b), equation (1.20b) is satisfied everywhere.

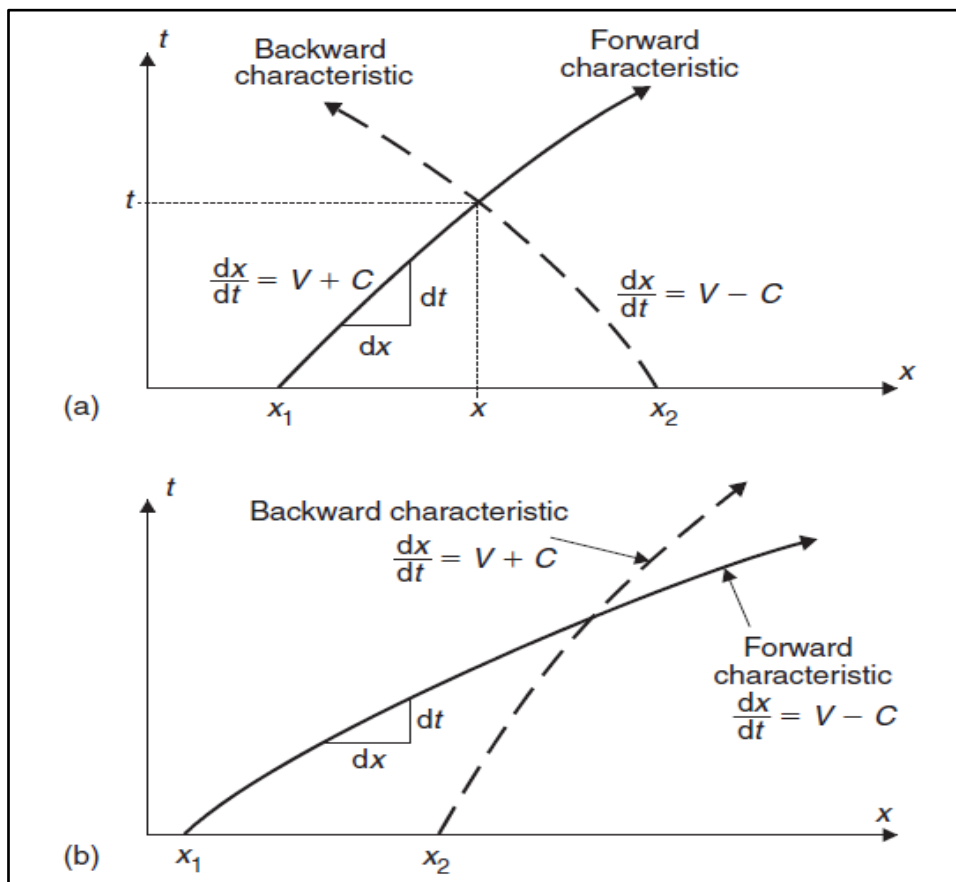


Fig. 1. 21: Definition sketch of the forward and backward characteristics: (a) subcritical flow conditions and (b) supercritical flow conditions (Chanson, 2004).

According to (Lyn, et al., 2001); the third characteristic line C3 is variable through the (x-t) domain depend on the value of Froude's number. The needed

boundary conditions for solving the governing equations [1.14] depend on the direction of characteristics (C1, C2 and C3) in (x-t) domain.

1.10 Boundary Conditions and initial conditions

In the analysis of unsteady flow or steady with movable bed in open channels, the calculations start at a specified time. The flow conditions at this starting time are referred to the initial conditions. Since the boundaries of all physical systems are located at finite distances, some particular conditions at the limits or boundaries of the physical system must be specified. These conditions are called the boundary conditions. The location where these boundaries are needed depend on the flow type and the sign of the characteristics curves (C1, C2 and C3). By building computational domain (x-t) the location where the initial and boundary conditions needed is shown in Fig 1.22.

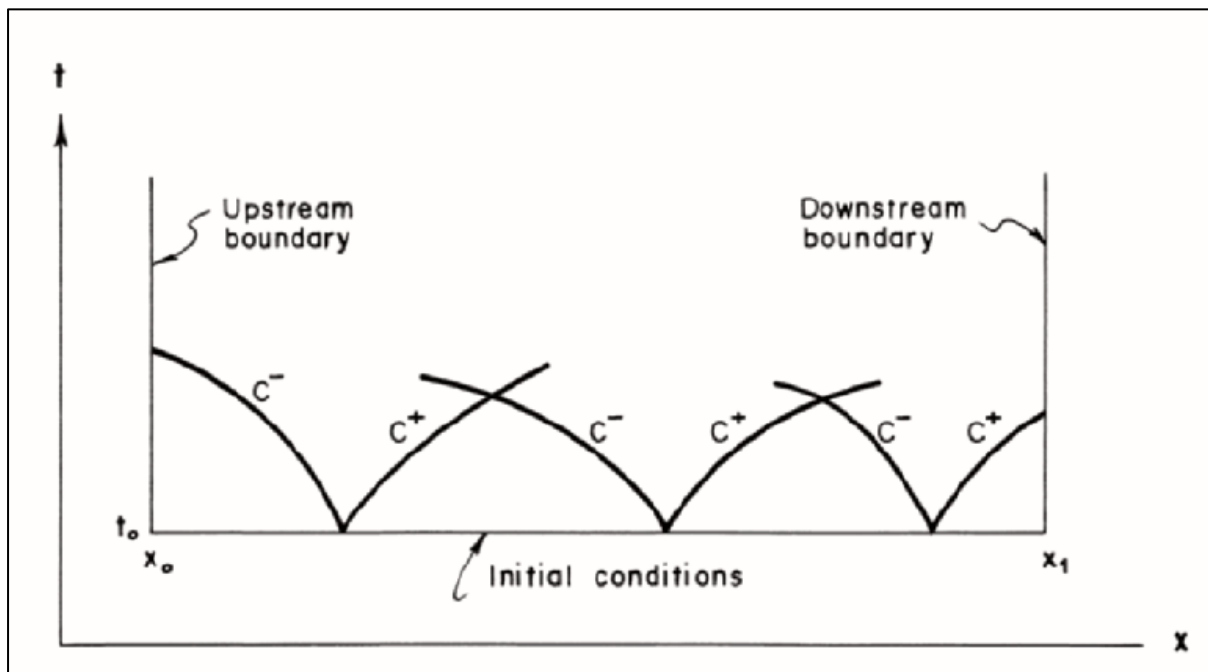


Fig. 1. 22:Computational domain for a one-dimensional system (Chaudhry, 2008).

Figure 1-23 shows the characteristics at the limits of the computational domain for the subcritical and supercritical flows. The following rule may be

followed for specifying the conditions at the boundaries (the initial conditions may be considered as a special case of the boundary condition in time): One condition has to be specified for each characteristic entering the computational domain at its limits. For example, two characteristics enter the computational domain at time $t = t_0$. Thus, two conditions have to be given as the initial conditions. At the upstream boundary, one condition is needed for subcritical flows and two conditions are needed for the supercritical flow. At the downstream boundary, one condition must be specified for the subcritical flow and non for the supercritical flows. In addition, all conditions, specified, have to be independent from one another.

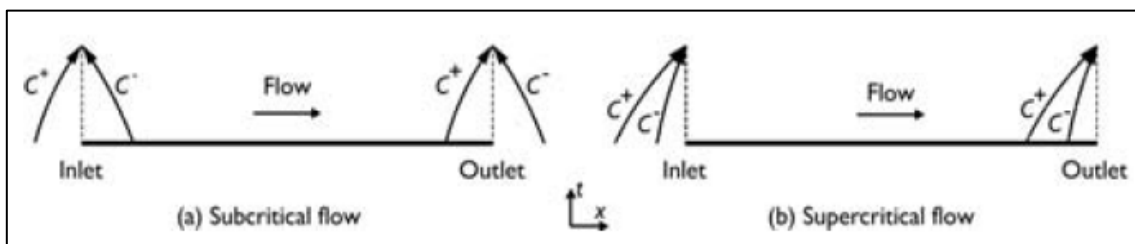


Fig. 1. 23: Characteristics at the limits of computational domain (Dingman, 2009).

In addition to the flow boundaries; at least one boundary for sediment must be defined either the bed level at specific point or the sediment discharge at any point. If any additional boundaries are known like the sediment feeding from external source at an intermediate section, it can be defined as a boundary.

1.11 Dealing with non-uniform gradation

There are two ways for the dealing with non-uniform gradation; either to use capacity formula takes into account the multiple sizes of the bed sediment like (Meyer-Peter and Müller for multiple sizes) Eq [1.11.a, 1.11.b] or to modify Exner equation [1.14.c] to deal with multiple sizes, then the transport capacity is calculated as the summation of the sediment discharge for size by size

instead of using the mean size d_m or d_{50} in the formula used for calculating the capacity. This modification for Exner equation is discussed in below.

Under most circumstances, sediment exchange between the flow and the river bed remains limited to a thin layer near the water-sediment interface. It is possible to define a rather thin active or exchange layer with thickness L_a which is typically taken to correspond to some multiple of characteristic surface grain size or dune height. The active layer concept (also called control volume) was proposed by (Hirano, 1971) and later advanced and utilized by others like (Parker, 2004) for modelling the morphodynamics of gravel-bed rivers, including downstream fining and armoring. Consider Fig. 1.24 showing an illustration of bed load transport, the active layer and the substrate in 1-D.

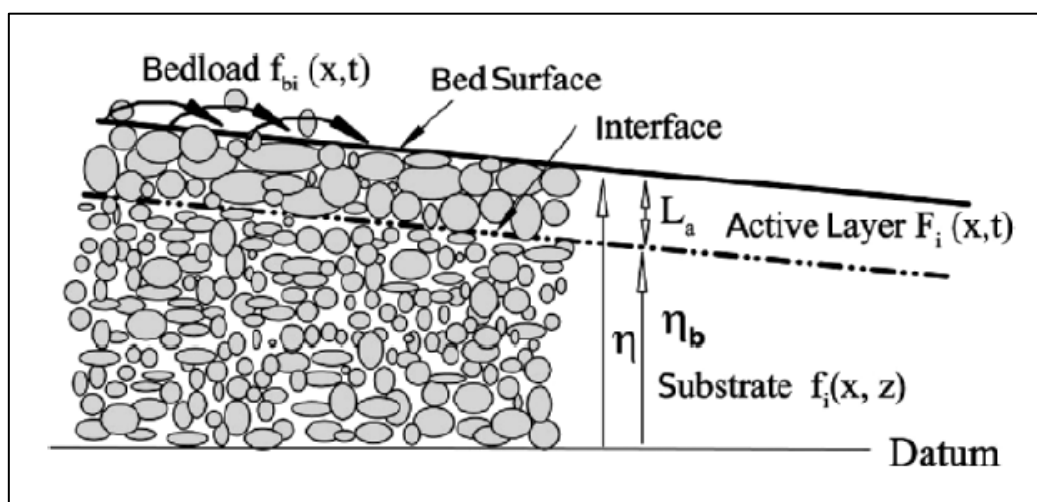


Fig. 1. 24: Illustration of the active layer concept (Chaudhry, 2008).

Let f_{bi} , F_i and f_i respectively denote the fraction of the i^{th} size class in the bed load, the active layer and the substrate (sub layer). According to the active layer concept, F_i does not have a vertical structure while f_i does not generally vary with time. Under these conditions, considering bed load transport alone, the mass conservation equation for an individual size fraction in the river bed may be written as:

$$(1 - p_0) \left(f_{li} \frac{\partial \eta}{\partial t} + \frac{\partial}{\partial t} L_a F_i \right) = - \frac{\partial q_{si}}{\partial x} \quad 1.21$$

Where f_{li} denotes the fraction of the i -th size class at the interface between the substrate and the active layer and q_{bi} is the volume transport rate of the same size class in the bed load. Summing Eq. 1.21 over all grain-size classes, the following equation is obtained:

$$(1 - p_0) \frac{\partial \eta}{\partial t} = - \frac{\partial}{\partial x} \sum_1^N q_{si} \quad 1.22$$

With the aid of Eq. 1.21, η can be eliminated from Eq. 1.22 leading to:

$$(1 - p_0) \left(\frac{\partial}{\partial t} L_a F_i - f_{li} \frac{\partial L_a}{\partial t} \right) = - \frac{\partial q_{si}}{\partial x} + f_{li} \frac{\partial}{\partial x} \sum_1^N q_{si} \quad 1.23$$

By solving this equation, the change in the active layer can be calculated. It is clear from equation 1.23 that the control volume thickness ($cvt = L_a$) plays a role in the morphological evolution, so later the sensitivity to this parameter will be discussed intensively.

1.12 Numerical Scheme for the governing equations

The complete unsteady water flow equations along with the sediment continuity equation are a set of nonlinear hyperbolic equations. Closed form solutions for them are available only for idealized cases, so these equations are solved by numerical techniques (the finite difference method (FD), the finite volume method (FV) or the finite element method (FE)). The aim of this item is to present a simple discretized form for the governing equations[1.14], to know how the computation can be done inside any numerical code, what are the precautions needed to enhance the numerical solution and to capture the use of flow conditions (boundary and initial condation0 inside the code.

In FD methods; the partial derivations of equations are approximated by using Taylor series. This method is particularly appropriate for an equidistant Cartesian mesh (Fig 1.25). In FV methods; the partial derivations of equations are not directly approximated like in FD methods. Instead of that, the equations are integrated over a volume, which is defined by nodes of grids on the mesh. The volume integral terms will be replaced by surface integrals using the Gauss formula. These surface integrals define the convective and diffusive fluxes through the surfaces. Due to the integration over the volume, the method is fully conservative. This is an important property of FV methods. It is known that in order to simulate discontinuous transition phenomena such as flood propagation, one must use conservative numerical methods. In FE method; the problem domain is ideally subdivided into a collection of small regions, of finite dimensions, called finite elements. The elements have either a triangular or a quadrilateral form and can be rectilinear or curved. After subdivision of the domain, the solution of discrete problem is assumed to have a prescribed form. This representation of the solution is strongly linked to the geometric division of sub domains and characterized by the prescribed nodal values of the mesh. These prescribed nodal values must be determined in such way that the partial differential equations are satisfied. The FD and FV methods have been used in this study; therefore it is explained in more detailed.

In case of using finite difference in the solution of the governing equations [1.14] there are several possibilities for approximating the partial derivatives. The spatial partial derivatives replaced in terms of the variables at the known time level are referred to the explicit finite differences, whereas those in terms of the variables at the unknown time level are called implicit finite differences. To know the use of the finite differences, the (x-t) domain is divided into many

cells as shown in fig 1.25, while Eqs. 1.24 and Eqs 1.25 gives the explicit finite differences and the implicit finite differences respectively that use to calculate the joints value for this grid, in which f refers to V , η and h in the partial derivatives form.

$$\frac{\partial f}{\partial x} = \frac{f_i^n - f_{i-1}^n}{\Delta x} \quad \text{Explicit backward} \quad 1.24.a$$

$$\frac{\partial f}{\partial x} = \frac{f_{i+1}^n - f_i^n}{\Delta x} \quad \text{Explicit forward} \quad 1.24.b$$

$$\frac{\partial f}{\partial x} = \frac{f_{i+1}^n - f_{i-1}^n}{2\Delta x} \quad \text{Explicit central} \quad 1.24.c$$

$$\frac{\partial f}{\partial x} = \frac{f_i^{n+1} - f_{i-1}^{n+1}}{\Delta x} \quad \text{Implicit backward} \quad 1.25.a$$

$$\frac{\partial f}{\partial x} = \frac{f_{i+1}^{n+1} - f_i^{n+1}}{\Delta x} \quad \text{Implicit forward} \quad 1.25.b$$

$$\frac{\partial f}{\partial x} = \frac{f_{i+1}^{n+1} - f_{i-1}^{n+1}}{2\Delta x} \quad \text{Implicit central} \quad 1.25.c$$

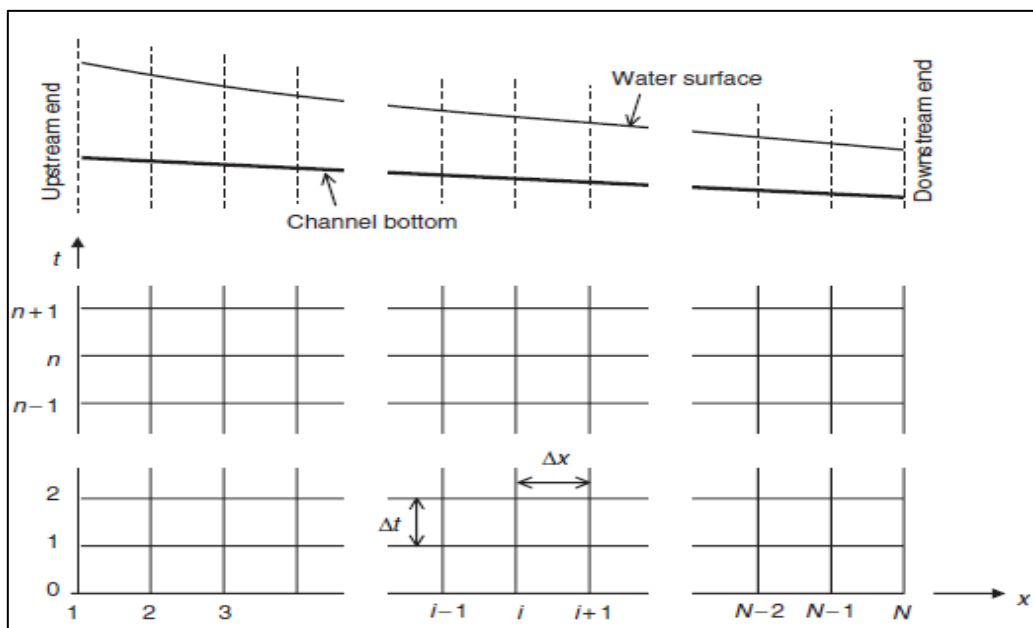


Fig. 1. 25: Finite-difference grid.

The Explicit finite difference scheme is inherently unstable i.e. computations become unstable irrespective of the size of grid spacing. To prevent the instability, some precautions must be followed as in the stability analysis procedure presented in next item. In the implicit finite-difference schemes, the spatial partial derivatives and/or the coefficients are replaced in terms of the values at the unknown time level. The unknown variables, therefore, appear implicitly in the algebraic equations and the methods are called implicit methods. The algebraic equations for the entire system have to be solved simultaneously in these methods.

Finite-volume schemes can be applied to irregular flow domains and at the same time they are as easy to implement as finite-difference schemes. The main advantages of this scheme are simplicity and ease of implementation. It can also handle sharp gradients in the water surface profile, if they are present. The derivation of the finite volume form of the governing equation is shown in chapter 2.

According to (Zhixian, et al., 2002); one-dimensional unsteady sediment transport models may be classified into two categories: the uncoupled models, in which the water-flow equations and sediment continuity equation are uncoupled during a given time step and the coupled models, in which the energy equation is solved along with the sediment continuity equation.

As an example for the use of FD in solving the governing equations; a one-dimensional, unsteady, coupled deformable bed model by (Bhallamudi, et al., 1991) is presented by the predictor and corrector method. The complete Saint-Venant equations for water flow and the sediment continuity equation are solved simultaneously.

- Predictor

In the following equations, a superscript * indicates value of the variable computed at the end of the predictor part, where Eq 1.26.d is the formula used to calculate the sediment capacity known as power law Eq 1.11.e .

$$h_i^* = h_i^n - \frac{\Delta t}{\Delta x} (Q_{i+1}^n - Q_i^n) \quad 1.26.a$$

$$Q_i^* = Q_i^n - \frac{\Delta t}{\Delta x} \left[\frac{(Q_{i+1}^n)^2}{h_{i+1}^n} - \frac{(Q_i^n)^2}{h_i^n} + \frac{g}{2} \{ (h_{i+1}^n)^2 - (h_i^n)^2 \} \right] \\ - gh_i^n \frac{\Delta t}{\Delta x} (\eta_{i+1}^n - \eta_i^n) - gh_i^n \Delta t \frac{(Q_i^n n)^2}{(h_i^n)^{3.33}} \quad 1.26.b$$

$$\eta_i^* = \eta_i^n - \frac{1}{1 - P_0} \left[\left(\frac{Q_s h}{Q} \right)_i^n - \left(\frac{Q_s h}{Q} \right)_i^* \right] - \frac{\Delta t}{(1 - P_0) \Delta x} [(Q_s)_{i+1}^n - (Q_s)_i^n] \quad 1.26.c$$

$$(Q_s)_i^* = a \left(\frac{Q_i^*}{h_i^*} \right)^b \quad 1.26.d$$

- Corrector

$$h_i^{**} = h_i^* - \frac{\Delta t}{\Delta x} (Q_{i+1}^* - Q_i^*) \quad 1.27.a$$

$$Q_i^{**} = Q_i^* - \frac{\Delta t}{\Delta x} \left[\frac{(Q_i^*)^2}{h_i^*} - \frac{(Q_{i-1}^*)^2}{h_{i-1}^*} + \frac{g}{2} \{ (h_i^*)^2 - (h_{i-1}^*)^2 \} \right] \\ - gh_i^* \frac{\Delta t}{\Delta x} (\eta_i^* - \eta_{i-1}^*) - gh_i^* \Delta t \frac{(Q_i^* n)^2}{(h_i^*)^{3.33}} \quad 1.27.b$$

$$\eta_i^{**} = \eta_i^* - \frac{1}{1 - P_0} \left[\left(\frac{Q_s h}{Q} \right)_i^* - \left(\frac{Q_s h}{Q} \right)_i^{**} \right] - \frac{\Delta t}{(1 - P_0) \Delta x} [(Q_s)_i^* - (Q_s)_{i-1}^*] \quad 1.27.c$$

$$(Q_s)_i^{**} = a \left(\frac{Q_i^{**}}{h_i^{**}} \right)^b \quad 1.27.d$$

In which the superscript ** denotes the value of the variable after the corrector step. Now, the values of the unknowns at $n + 1$ time level (i.e. at the end of time) are given by interval Δt are given by Eqs 1.28:

$$h_i^{n+1} = \frac{1}{2}(h_i^n + h_i^{**}) \quad 1.28.a$$

$$Q_i^{n+1} = \frac{1}{2}(Q_i^n + Q_i^{**}) \quad 1.28.b$$

$$\eta_i^{n+1} = \frac{1}{2}(\eta_i^n + \eta_i^{**}) \quad 1.28.c$$

By using the preceding algorithm, the values of h , q and η at the new time level $n + 1$ are determined at every interior node ($i = 2, \dots, N$). The values of the dependent variables h , q and η at the boundary nodes 1 and $N + 1$ are determined by using the boundary conditions. For subcritical flow, it can be shown by using the characteristic theory that: two boundary conditions at the upstream boundary and one condition at the downstream boundary have to be specified. The values of the dependent variables which are not specified through boundary conditions may be determined from the characteristic equations. Their values may also be determined by interpolation from the known values at the interior nodes.

The flow equations and the sediment continuity equation are coupled in this procedure because it uses a two-level predictor-corrector approach. In this sense, this procedure may be called coupled. On the other hand, coupling is not achieved, if Eq [1.26.c] is solved after completely solving Eqs. [1.26.a] and [1.24.6].

1.13 Stability of numerical codes.

Investigating the stability of a numerical scheme will be done by studying whether an error grows or decays as the solution progresses in a marching procedure.

Mainly the implicit finite difference schemes are unconditionally stable, while for the explicit schemes; the Courant-Friedrichs-Lewy condition (CFL for short) has to be satisfied for any scheme to be stable. For the stability of the schemes, it is necessary that the Courant number C_n is less than or equal to 1, where:

$$C_n = \frac{\text{Actual wave velocity}}{\text{Numerical wave velocity}} = \frac{|V| + \sqrt{gd}}{\frac{\Delta x}{\Delta t}} \quad 1.29$$

Thus, the computational time interval depends upon the spatial grid spacing, flow velocity and celerity \sqrt{gd} , which are functions of the flow depth. Since the flow depth and the flow velocity may change significantly during the computations, it may be necessary to reduce the size of computational time interval for stability. The time interval should be such that C_n is as close to 1 as possible. If it is substantially less than unity, then the interval size should be increased to improve accuracy and to prevent the smearing of bores and steep waves. To overcome the instability; most of the finite differences based numerical codes uses Preissmann Scheme.

- Preissmann Scheme

The Preissmann scheme has been extensively used since the early 1960s. It has the advantages that a variable spatial grid may be used, steep wave fronts may be properly simulated by varying the weighting coefficient θ , and the scheme yields exact solution of linearized form of the governing equations for a

particular value of Δx and Δt . The partial derivatives and other coefficients are approximated as follows:

$$\frac{\partial f}{\partial t} = \frac{(f_{i+1}^{n+1} + f_i^{n+1}) - (f_i^n + f_{i+1}^n)}{2\Delta t} \quad 1.30.a$$

$$\frac{\partial f}{\partial x} = \frac{\theta(f_{i+1}^{n+1} - f_i^{n+1})}{\Delta x} + \frac{(1 - \theta)(f_{i+1}^n - f_i^n)}{\Delta x} \quad 1.30.b$$

$$f = \theta \left(\frac{f_{i+1}^{n+1} - f_i^{n+1}}{2} \right) + (1 - \theta) \left(\frac{f_{i+1}^n - f_i^n}{2} \right) \quad 1.30.c$$

In which θ is a weighting coefficient; f refers to V , η and h in the partial derivatives. By selecting a suitable value for θ , the scheme may be made totally explicit ($\theta = 0$) or implicit ($\theta = 1$). The scheme is stable, if $0.55 < \theta \leq 1$. Steep wave fronts are properly simulated for low values of θ , but there are oscillations behind the wave front. These oscillations are eliminated for θ close to unity, for typical applications, $\theta = 0.6- 0.7$ may be used.

1.14 Objective of the work

The objective of this work is to start from previous studies on the sediment transport carried by the Politecnico di Milano to introduce comparative analysis among different numerical codes to estimate which one is able to simulate the phenomenon of sediment transport by accurate way through some steps and tests such as:

- Giving brief description for the usage of these numerical codes, the conditions for numerical stability, how these codes simulate the bed friction and effect of using different formulas for sediment capacity in the morphological evolution.
- Studying the aggradation and the degradation due to upstream feeding with rates lower or higher than the transport capacity.

- Studying the aggradation and the degradation due to lateral feeding with rates lower or higher than the transport capacity, studying the effect of the dam formed in the water profile and discussing the ability of these codes to simulate the breaching of the created dams.
- Studying the effect of sequent mobile and hard beds in the morphological evolution.
- Studying the effect of feeding by non-uniform sediments either from upstream or by lateral feeding and how will be the interaction between the multi sizes used, then studying sensitivity of the control volume thickness.
- Simulation of a real event such as the 1987 flood happened in Sondrio.
- Studying the effect of the landslide may be happen in front of Mallero valley at Spriana and the expected morphological evolution expected in this case.
- Studying the seepage process through an earthen dam likely to form in Mallero due to Spriana landslide and how much the likelihood of breaching due to the seepage process (piping).
- Studying the effect of the wave generated due to the breaching of the created dam resulted from water overtopping.
- Studying the effect of Spriana landslide collapse on the emergency planning in Sondrio.
- Finally, discussion about the expected morphological changes in Nile River due to constructing the Millennium dam in the Blue Nile.

2 Strategies for Numerical Analysis

2.1 Introduction

In this chapter the mathematical representation discussed in the first chapter will be transformed to numerical schemes through numerical codes (software). The numerical codes used are: BASEMENT¹ v.2.2.1 (Basic Simulation Environment for Computation of Environmental Flow and Natural Hazard Simulations) by ETH Zurich (Switzerland), HEC-RAS² v 4.1 by U.S. Army Corps of Engineers, and ISIS³ v. 3.6.1 by Halcrow group Ltd. So this chapter is divided into four parts, under each part there are presentation for each code, the numerical scheme, a mini user guide that can be used for creating the same cases which have been analyzed in this work and a hydraulic comparison among these three codes.

2.2 Modelling the morphological evolution by HEC-RAS

HEC-RAS as a word is the first letters of “the Hydrologic Engineering Centers River Analysis System”. It is one of the products of the U.S. Army Corps of Engineers (USACE). It allows performing one-dimensional steady flow, unsteady flow, sediment transport/mobile bed computations and water quality modelling.

The HEC-RAS system contains four one-dimensional river analysis components: (1) steady flow water surface profile computations, (2) unsteady flow simulation, (3) movable boundary sediment transport computations and (4) water quality analysis. A key element is that all four components use a common geometric data representation and common geometric and hydraulic

¹ <http://www.basement.ethz.ch/>

² <http://www.hec.usace.army.mil/software/hecras/>

³ <http://www.halcrow.com/isis/>

computation routines. In addition to the four river analysis components; the system contains several hydraulic design features that can be invoked once the basic water surface profiles are computed.

The version 4.1 of the River Analysis System (HEC-RAS) is that one used during this work. This version supersedes version 4.0, which was released in March of 2008 to the general public and all previous versions. Several new simulation features have been added to the software since that time such as Sediment Transport Modelling Enhancements.

The main user interface is a button bar. This button bar provides quick access to the most frequently used options under the HEC-RAS menu bar. A description of each button is shown in Fig 2.1.

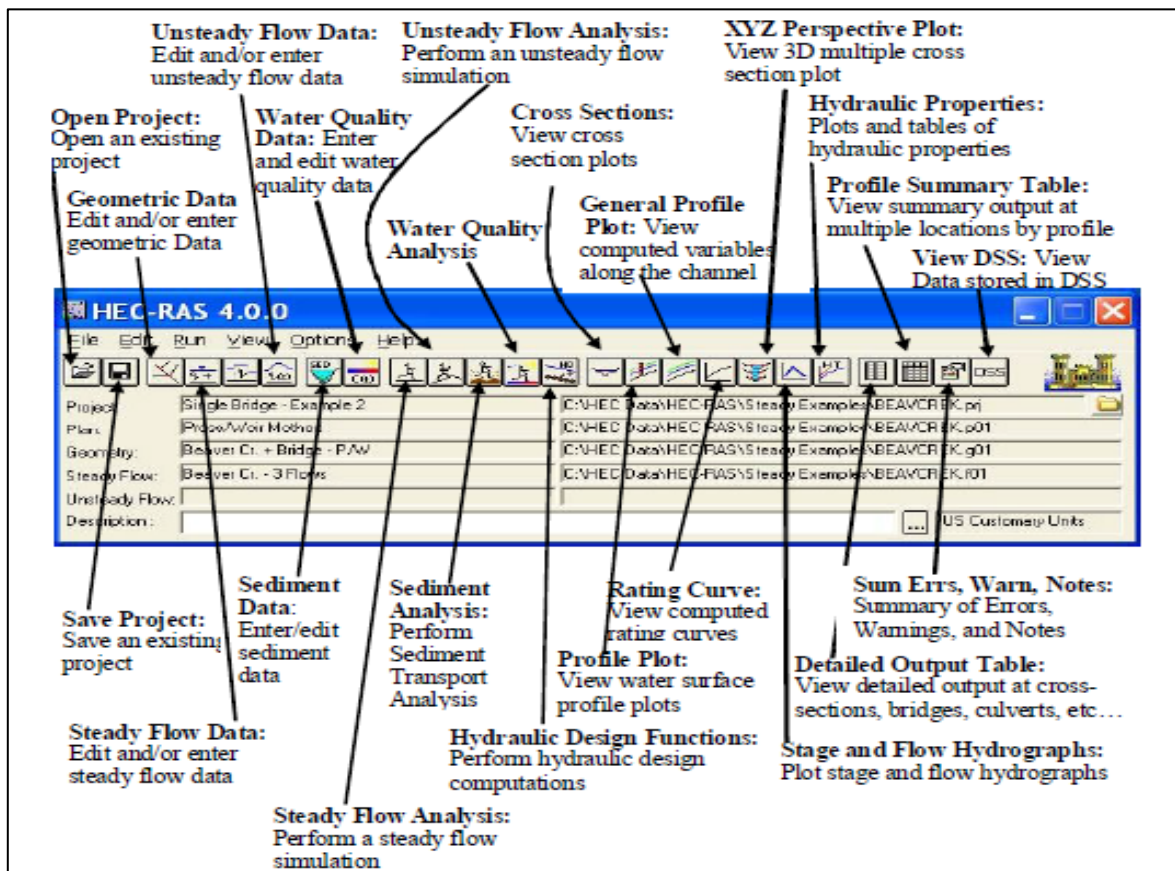


Fig. 2. 1: HEC-RAS main window button bar (Brunner, et al., 2010).

2.2.1 The numerical scheme for HEC-RAS.

HEC-RAS uses an implicit finite difference scheme for the governing equation (Preissmann Scheme Eqs.1.30). This scheme, which called the four-point implicit scheme, is presented in Eqs.2.1 which taken from (Brunner, 2010). Where f represent the value of the required variables such as water velocity V , water depth h or the bed elevation η .

$$f_j = f_j^n \quad 2.1. a$$

$$\Delta f_j = f_j^{n+1} - f_j^n \quad 2.1. b$$

$$\frac{\partial f}{\partial t} \approx \frac{\Delta f}{\Delta t} = \frac{1}{\Delta t} \left(\frac{\Delta f_{j+1} + \Delta f_j}{2} \right) \quad \text{Time derivative} \quad 2.1. c$$

$$\frac{\partial f}{\partial x} \approx \frac{\Delta f}{\Delta x} = \left(\frac{(f_{j+1} - f_j) + \theta(\Delta f_{j+1} - \Delta f_j)}{\Delta x} \right) \quad \text{spatial derivative} \quad 2.1. d$$

$$f = 0.5(f_{j+1} + f_j) + 0.5\theta(\Delta f_{j+1} + \Delta f_j) \quad \text{Function value} \quad 2.1. e$$

This scheme means that any time derivatives in the governing equations [1.14] will be transformed to the form [2.1.c], while any spatial derivatives will be transformed to the form [2.1.d]. Then the value of the variable will be calculated using [2.1.e] after calculating Δf_{j+1} and f_{j+1} from 2.1.c and 2.1.d respectively, while Eq 2.1.a represent the first value of the variable which called the boundary condition.

This scheme [2.1] is an implicit numerical scheme has a weighting factor θ . Consequently; the time step can be significantly larger than with explicit numerical schemes. The implicit scheme is unconditionally stable (theoretically) for $0.5 < \theta < 1$, conditionally stable for $\theta = 0.5$ and unstable

for $\theta < 0.5$. The numerical damping increased as the ratio $\lambda/\Delta x$ decreased, where λ is the length of a wave in the hydraulic system.

The sediment continuity equation is solved by computing a sediment transport capacity through the control volume (Fig 2.2) associated with each cross section. This capacity is compared to the sediment supply entering the control volume. If the capacity is greater than sediment supply, there is a sediment deficit which is satisfied by eroding bed sediments. If supply exceeds capacity there is a sediment surplus causing material to deposit.

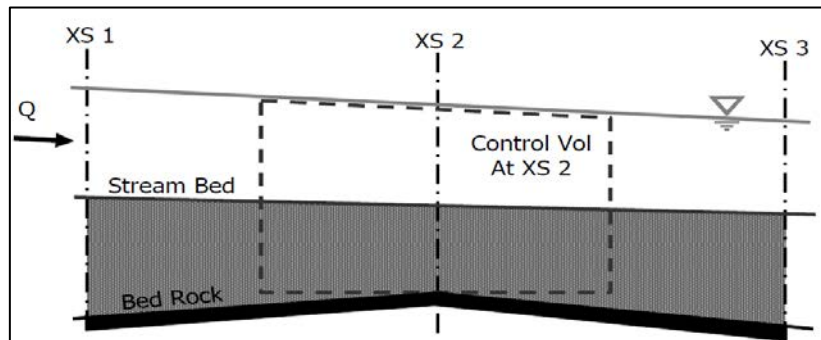


Fig. 2. 2: Schematic of the control volume used by HEC-RAS for sediment (Brunner, 2010).

2.2.2 Effective Friction in HEC-RAS

In the geometric description of an open channel with HEC-RAS; the value estimated for total bed friction must be entered. Although of that; HEC-RAS, in the sediment transport calculation considers only the skin friction from the bed grains τ' which depend on the bed grain sizes i.e. it doesn't take the friction due to bed forms and vegetation into account. Hence in HEC - RAS the driving bed shear stress $\tau_0 = \tau'$ only, whereas Eq 2.2 present the formula used for calculating the skin bed friction τ' and f is Darcy-Weisbach friction factor, which will be calculated automatically within HEC-RAS based on the bed gradation.

$$\tau' = \frac{f}{8} \rho V^2 \quad 2.2$$

2.2.3 Quasi-unsteady flow in HEC-RAS

HEC-RAS uses a hydrodynamic simplification, a common approach used by many sediment transport models, called Quasi-unsteady approximation. The quasi-unsteady flow assumption approximates a continuous hydrograph with a series of discrete steady flow profiles. For each record in the flow series, flow remains constant over a specified time window for transport. The steady flow profiles are easier to develop than a fully unsteady model and program execution is faster (An unsteady version of sediment transport is not released yet up to version 4.1.).

Each discrete steady flow profile is divided and further subdivided into shorter blocks of time for sediment transport computations. HEC-RAS utilizes three different time steps each a subdivision of another. The three time steps are the flow duration, the computation increment and the mixing time step. The definitions of flow duration and computation increment are shown in Fig 2.3. Finally; computational increments are further subdivided into the bed mixing time step. During each mixing time step in a computation increment, bathymetry, hydraulic parameters and transport potential for each grain size remains constant. However, the computations for sediment erosion and deposition take place during this time step and this can cause changes to the composition of the bed mixing layers (e.g. the active, cover and/or inactive layers). The vertical gradational profile is rearranged in response to the removal or addition of material. Since the active layer gradation changes during the bed mixing time step, the sediment transport capacity changes even when the hydrodynamics and, therefore, the transport potential remains constant.

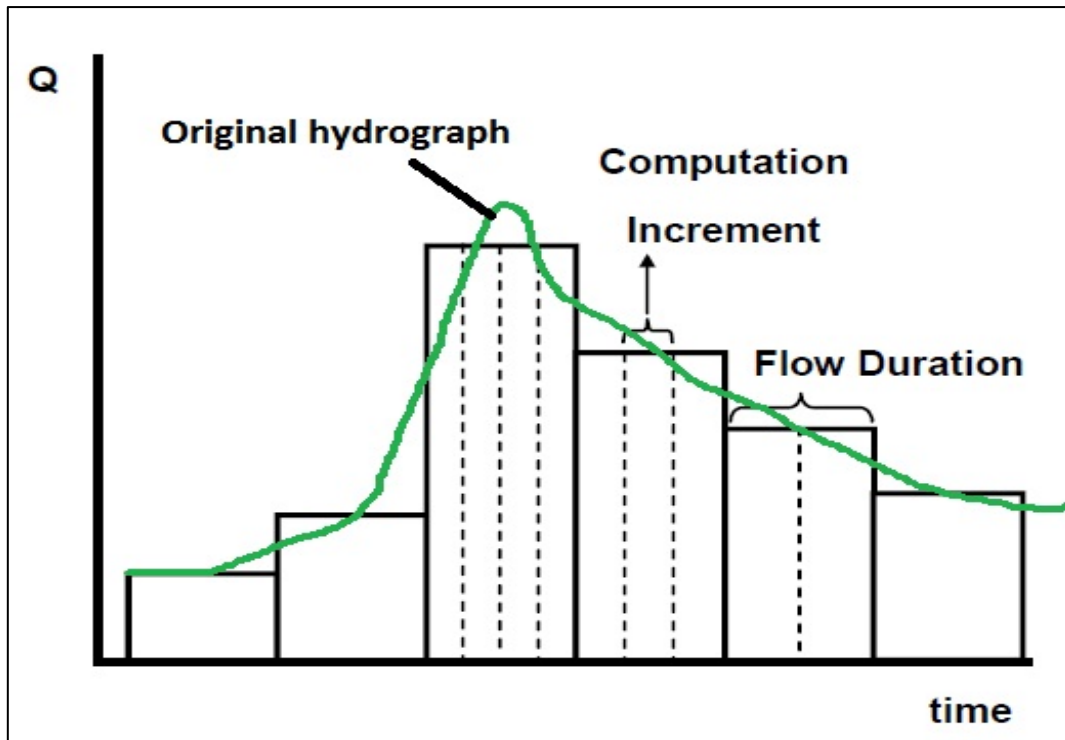


Fig. 2. 3: A quasi-unsteady flow series with time step (Brunner, 2010).

2.2.4 Sorting method in HEC-RAS

In many well graded rivers, the full bed gradation is covered by a layer of coarse material called an armor layer. This layer can be formed by static armoring or the differential transport of finer materials. Most of the flows mobilize fine particles, while the coarse material is static and collects on the surface shielding the deeper material from transport. The formation of an armor layer tends to decrease total transport because of the surface particles. The only particles available for transport tend to be coarser and harder to move. Also, this is a physical limiter on the transport capacity.

In order to model this armor layer, two algorithms have been included in HEC-RAS to simulate bed sorting and armoring. Both are based on dividing the bed into an active layer and an inactive layer. The key difference between the active layer and the inactive layer is: when computing transport capacity by multiplying transport potential with grain size percentage, the grain size

percentage based only on the particle distribution in the active layer. The two available algorithms (Fig. 2.4) are:

- Exner 5: A three layer active bed model that includes the capability of forming a coarse surface layer that will limit erosion of deeper material thereby simulating bed armoring (default method).
- Active Layer: This is a simplified two layer active bed approach. The active layer thickness is set equal to the d_{90} of the layer. This assumption is only appropriate for gravel beds.

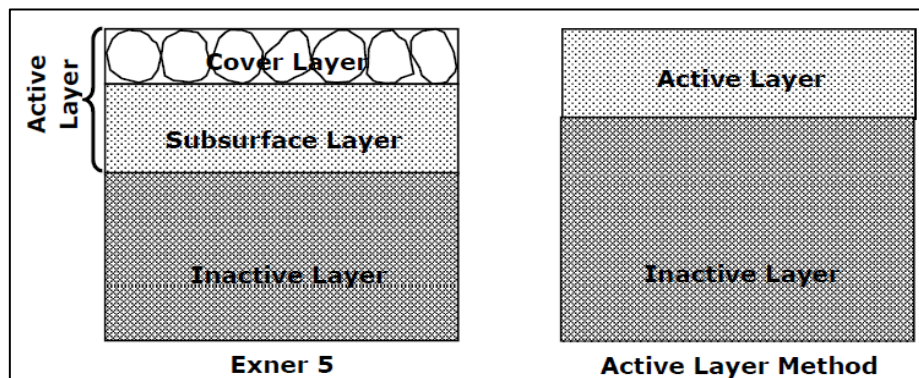


Fig. 2. 4: Schematic of the mixing layers in HEC-RAS' sorting and armoring methods (Brunner, 2010).

Theoretically when the bed gradation is only one size either Exner 5 or active layer algorithm can be used instead of each other, and the result will be the same. But with multi grain sizes Exner 5 is preferred because it simulates the real sorting.

2.2.5 Mini user guide for sediment transport modelling by HEC-RAS


For building a sediment transport model by HEC-RAS; six main steps must be followed. These steps are: (1) project definition, (2) geometry data definition, (3) quasi-unsteady analysis definition, (4) sediment data definition, (5)


sediment analyses perform and finally (6) results visualization. In the following; brief description for each step bit by bit.

1. Project definition.

Starting from main menu showed in Fig 2.1; from file menu select NEW to open new project then define the project name and the location where it wanted to save this model in the pc.

2. Geometry data definition 

- Once clicking on the geometry data definition button new window will open. In this window; by clicking on river reach button , the river reach can be drawn in the GUI shown.

- By using cross section editor ; the upstream, intermediate and downstream sections can be defined as in Fig 2.5.

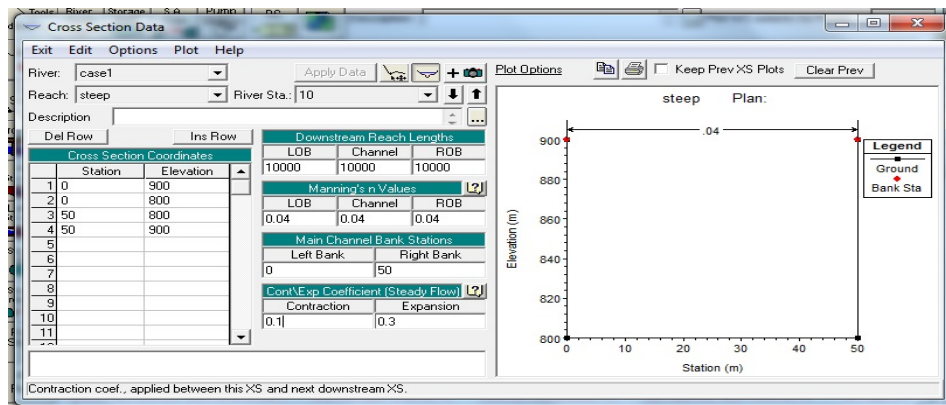


Fig. 2. 5: Cross section definition by HEC-RAS.

- For finite spatial discretization; interpolation of sections ,between any two section or between all the sections, can be done from the same window by using tools menu, then enter the spatial step between section and another i.e. divide the river reach to a discretized distances Δx (to reduce the instability of the numerical solution and to improve the accuracy).

- Save the geometry data from file menu in the geometry window.



3. Quasi-unsteady analysis definition

- It uses to enter the flow boundary conditions.
- The downstream boundary condition can be normal depth, flow stage, or rating curve. Mainly the down stream BC is the normal depth during this work Fig 2.6.

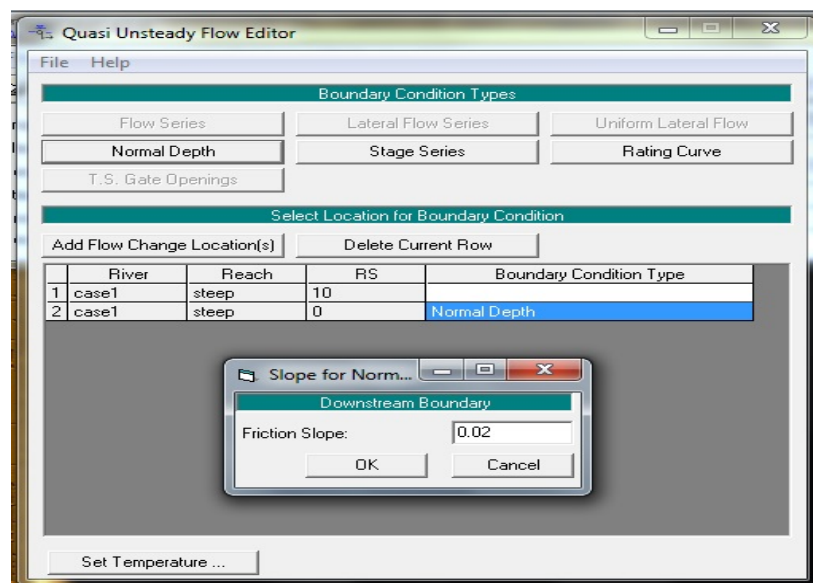


Fig. 2. 6: Downstream B.C. definition for quasi unsteady flow.

- For the upstream BC; select the upstream section, the flow series will be activated as in Fig 2.7.
- Assign the flow duration, computation increment, and the flow corresponding to each flow duration according to the definitions in Fig 2.3.
- Define the temperature of the fluid:

Because of several aspects of sediment transport mechanics, particularly fall velocity, are sensitive to water temperature, HEC-RAS requires temperature information. Currently, only one temperature per flow duration can be specified.

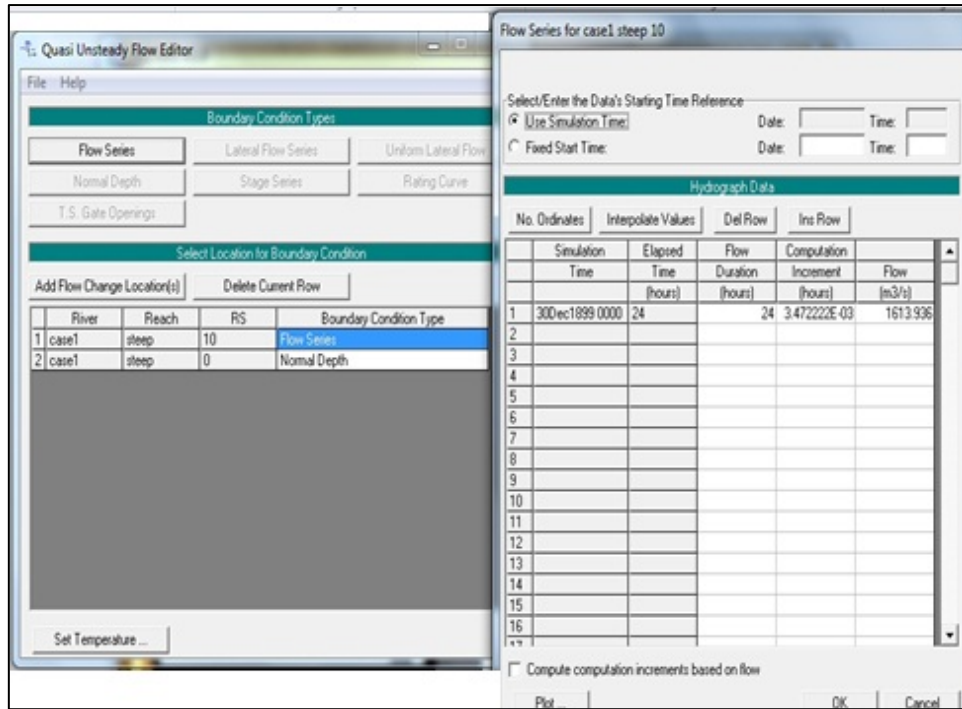


Fig. 2. 7: Assigning the upstream BC as a Quasi Unsteady flow.

- As in figure 2.8; by clicking the button (set temperature), the temperature can be defined for each flow duration, then by clicking ok the temperature window will close. Then save all the quasi unsteady data by clicking file menu then save quasi unsteady data for saving.

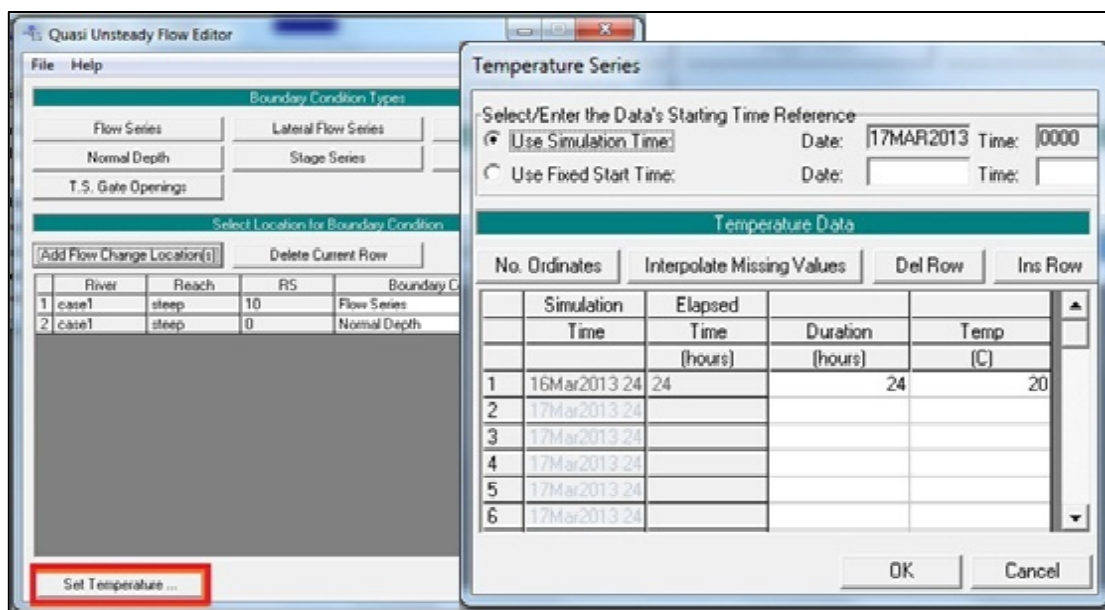


Fig. 2. 8: Assigning the temperature value for each flow duration.



4. Sediment data definition

There are two tabs and one important menu: initial conditions & transport parameters tab, boundary condition tab, and option menu.

A. Option menu

Under option menu there are some options, the most important are:

- Set sediment properties.
- The Specific gravity for the single particle must be entered e.g. $S = 2.6$ as in Fig2.9.
- Also shape factor for the particle e.g. for circular particles $= y/x = 1$, where x and y are the particle dimensions.
- Define densities of sediment divisions, where Sediment unit weights or densities are used to convert deposited or eroded masses into volumes that translate into bed elevation changes. It also give present the mixture porosity.

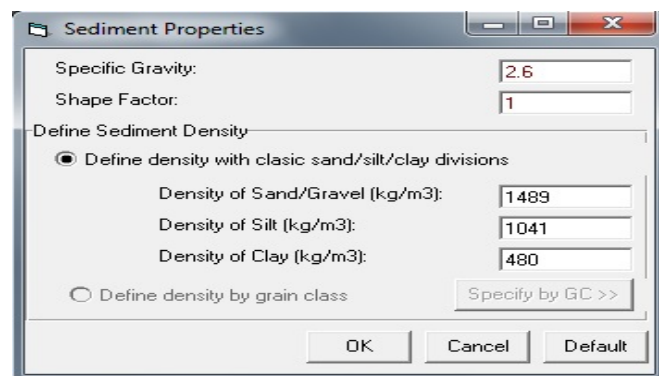


Fig. 2. 9: Sediment properties options.

- Bed change option.
- It used to allow aggradation outside the mobile layer limits defined before Fig 2.10.

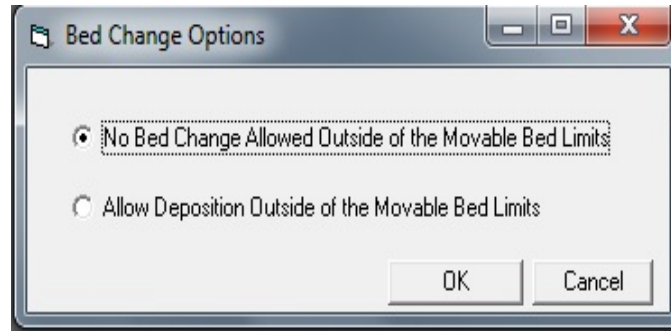


Fig. 2. 10:Bed change options.

- Calibrate transform functions.
- It used to modify the factors of the transport formulas like MPM Fig 2.11.

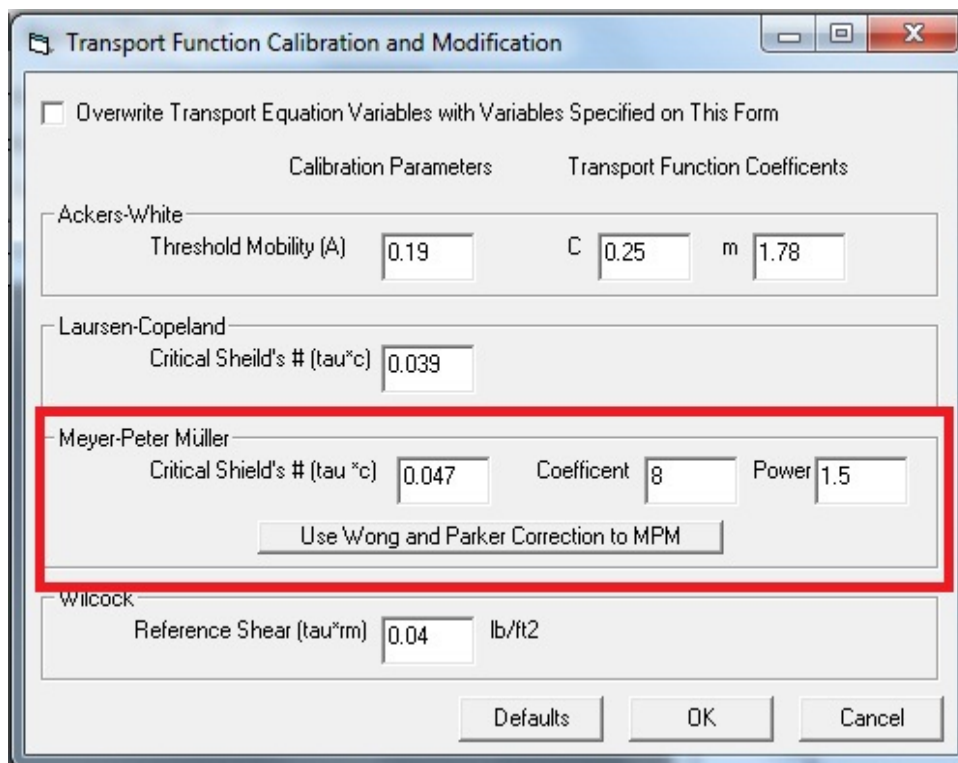


Fig. 2. 11: Calibration transportation functions option.

- User defined grain classes.
- HEC-RAS defaults to twenty grain classes, the user can define a customized set of grain classes in order to focus more detail in a particular size range or model specific grain sizes. This can be done by changing in the table in Fig 2.12.



Fig. 2. 12: User defined grain classes dialog.

B. Initial conditions & transport parameters tab.

- After clicking this tab assign the river name defined before in the geometry data, also assign the reach name as in Fig 2.13.
- Assign the transport capacity formula e.g. Meyer Peter Muller as in Fig 2.13.
- In the sorting method select either Exner 5 or Active layer method discussed in item 2.2.4.
- Assign the formula for calculating the falling velocity (settling velocity w_0) e.g. Van Rijn as in Fig 2.13.
- In the table define at each section either the maximum depth of the mobile soil layer or the minimum elevation of the bed after erosion e.g. Max depth = 5 m as in Fig 2.13.
- Define the limits of the mobile layer (width) by defining the station left and station right.

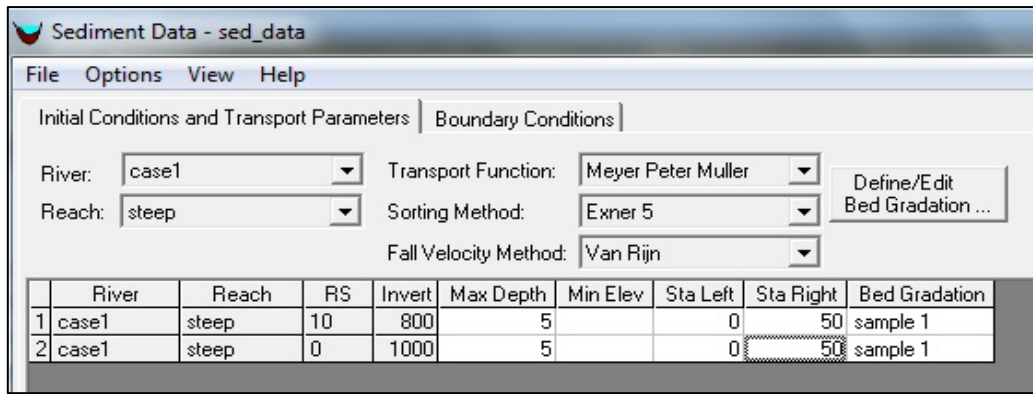


Fig. 2. 13: Assigning the initial conditions & transport parameters with HEC-RAS.

- By clicking the button (define /Edit bed gradation), soil gradation can be defined for the bed.
- The bed gradation window appears as in Fig 2.14 , clicking (1) for defining the sample name , then in (2)select between % finer or grain class fraction per weight, then enter the fraction of each size in (3) . The curve will be plotted automatically, and then by clicking ok it will be saved.

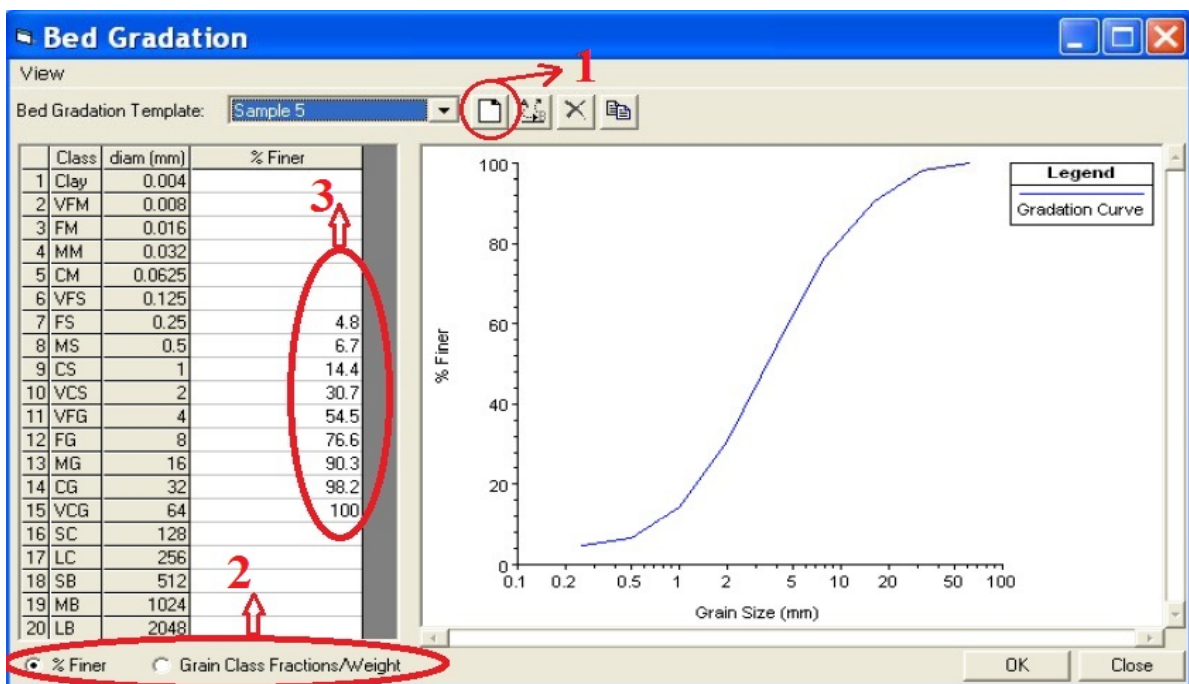


Fig. 2. 14: Defining the bed gradation in HEC-RAS (Brunner, et al., 2010).

- After defining the bed gradation, assign the sample name for each section in the table under the bed gradation as in Fig 2.14.

C. Boundary condition tab

- In this tab the sediment boundary conditions are assigned. By clicking the button (add sediment boundary location), it will be able to select the sections where the BC is known as shown in Fig 2.15. (1)

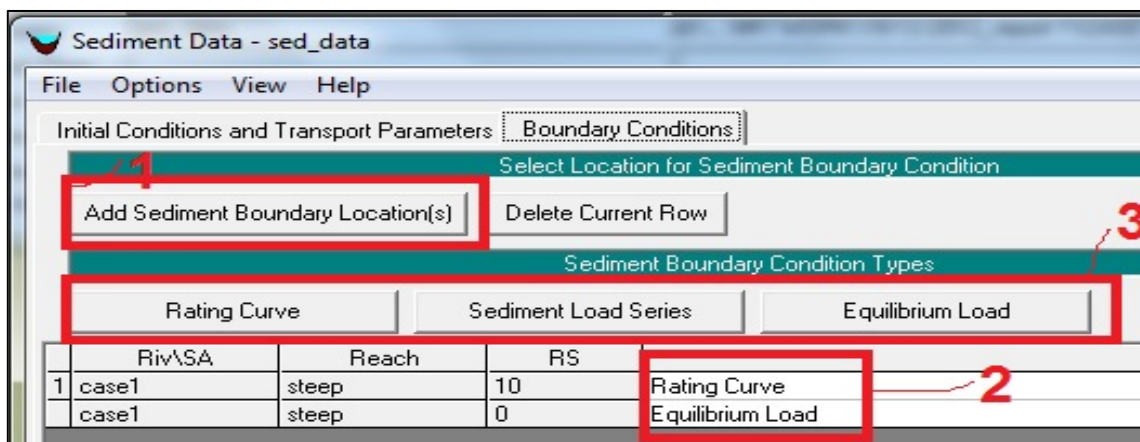


Fig. 2. 15: Sediment BC definition in HEC-RAS.

- In the table click in the cell, to enter the sediment B.C (2).
- Select the boundary condition (3).

There are three types of boundaries in HEC-RAS:

- Equilibrium load: means that the incoming sediment equals the transport capacity at this section. Hence, the bed at this section is fixed, although the bed layer is movable there.
- Rating curve: Since HEC-RAS works with steady flow not unsteady, so the unsteady hydrograph will transform to quasi-steady as a sets (steps), so the discharge sets are defined and the coupled inflow sediment for each set. Percentages (or decimal fractions) can be entered for each grain class for each load. If the summation of the percentages (decimal fractions) does not equal 100 (or 1.0), HEC-RAS will normalize the summation during computations (so that a given flow will produce the entered total load based on the ratios of the grain sizes).

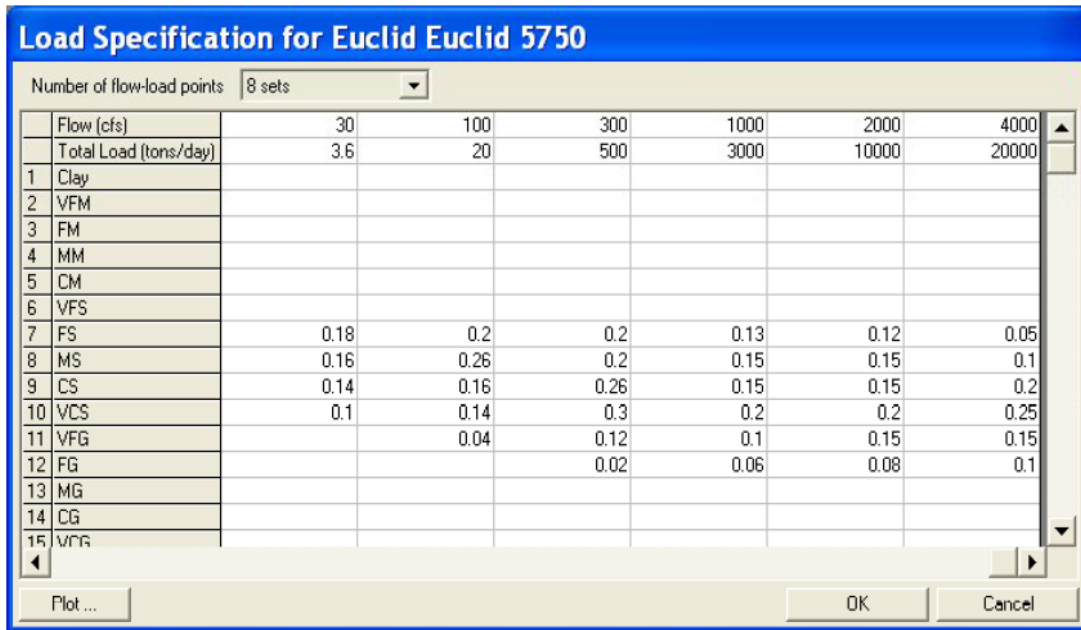


Fig. 2. 16: load specification editor for entering the coupled sediment (water-sediment rating curve) (Brunner, et al., 2010).

- Sediment load series: It is used when the sediment flow only income without water e.g. Landslide or debris flow i.e. boundary condition is not dependent on a flow boundary. As in Fig 2.17; the flow duration is defined (time step in quasi-unsteady hydrograph), and the total sediment inflow during this flow duration.

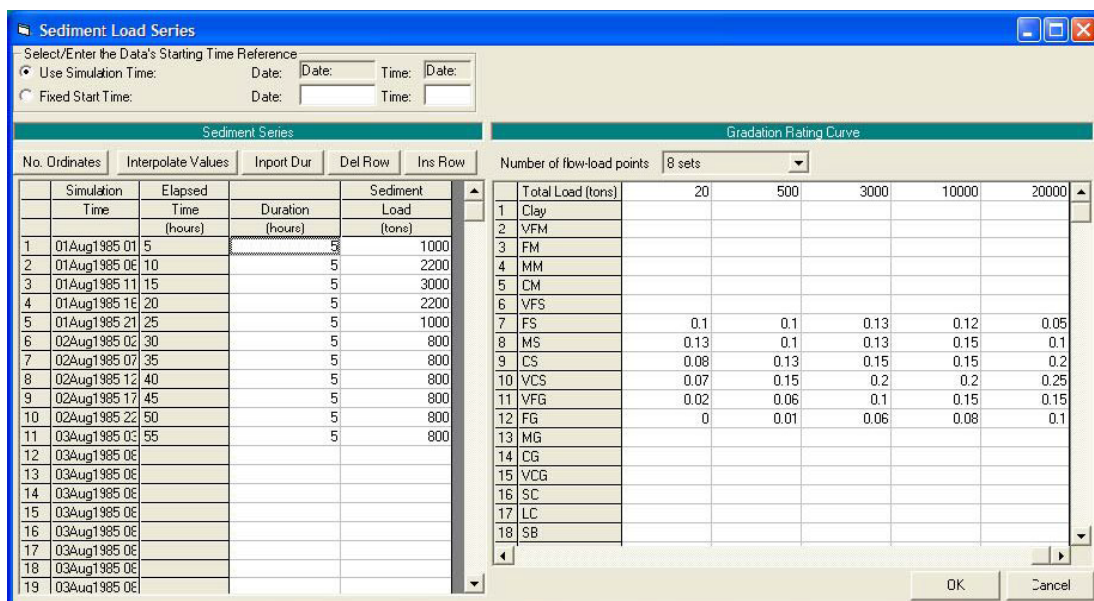


Fig. 2. 17: Sediment load series editor (Brunner, et al., 2010).

Comparative study of different scenarios for the morphological evolution in a river stream

In the right table; sets of sediment load and the fractions of inflow sediment must be entered, also HEC-RAS will normalize the total during computations.



5. Sediment analysis perform

- By clicking the sediment analysis button, the window for computation will appear. The simulation time must be specified, also the level of output details must be specified from sediment output options as in Fig 2.18 (level 6 gives all the available output details), then by clicking compute; the analysis will start.

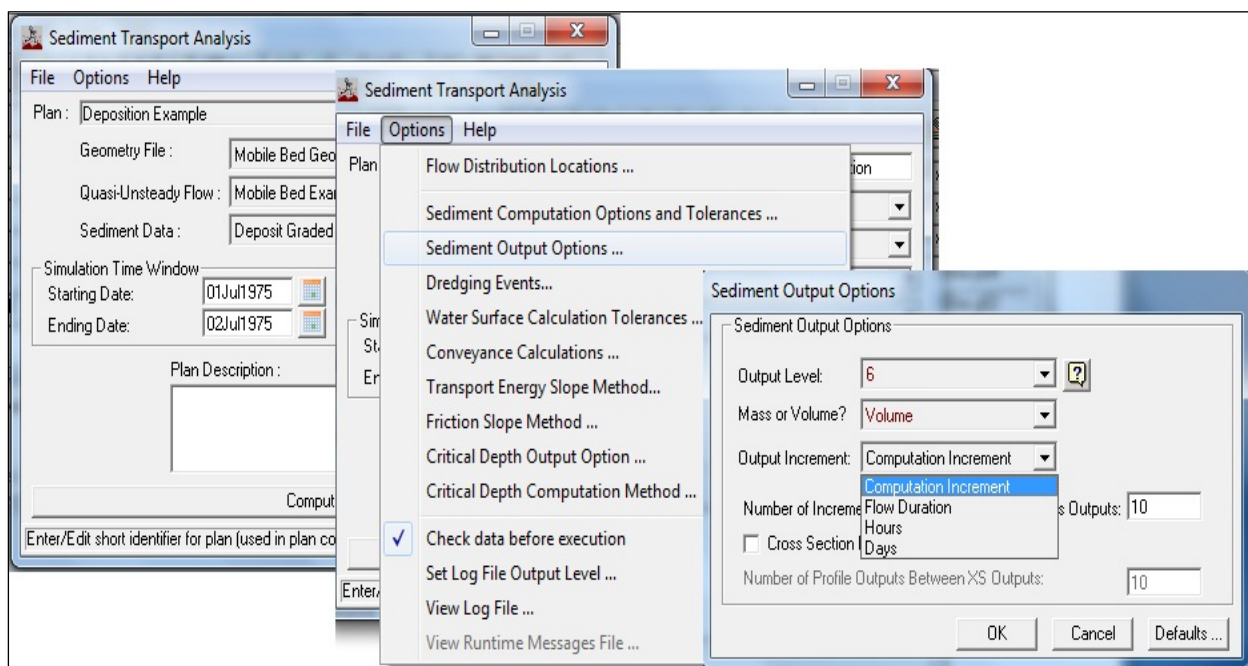


Fig. 2.18: Sediment analysis perform by HEC-RAS.

6. Results visualization

- For profiles visualization and the corresponding tables use step number (1) in Fig 2.19 by starting from view menu.
- For cross sections visualization and the corresponding tables use (2).

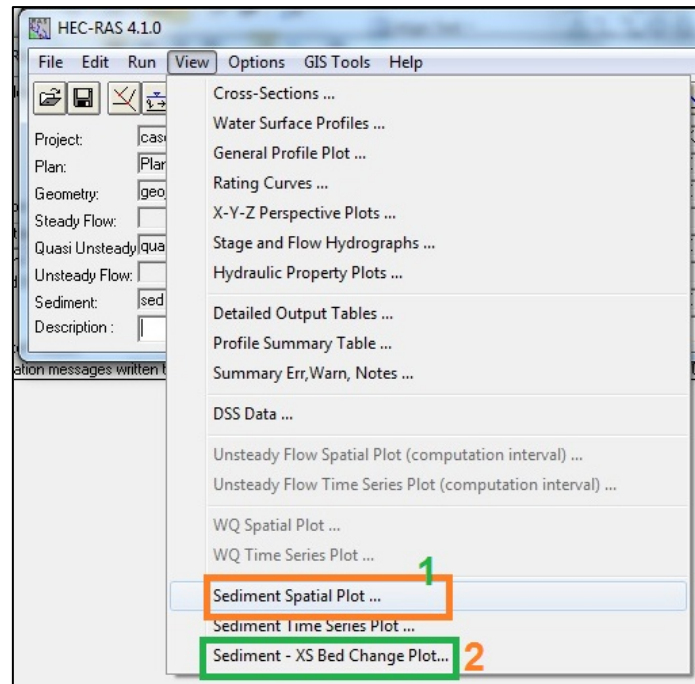


Fig. 2. 19: Result visualization and extraction by HEC-RAS.

2.3 Modelling morphological evolution by Basement.

Basement is numerical simulation software developed at the Laboratory of Hydraulics, Hydrology and Glaciology (VAW) of the Swiss Federal Institute of Technology (ETH) at Zurich, Switzerland. The purpose of the software is to provide a software tool for numerical modelling of environmental flow and natural hazard events, the simulation of water flow, and sediment and pollutant transport.

The software system “BASEMENT” (**BAS**ic-simulation-**Environ**MENT) shall provide a flexible and functional environment for numerical simulation of rivers and sediment transport involved. The numerical models for the computation of one and two dimensional flows with moving boundaries and appropriate models for bed load as well as suspended load are forming the core of the software system.

The core of the software system consists of the numerical subsystems, which actually are:

- BASEchain: one dimensional numerical tool enables the simulation of river reaches (based on cross sections) with respect to sediment transport.
- BASEplane: two dimensional numerical tool enables the simulation of river reaches as well as flood plains (bases on a digital terrain model) with respect to sediment transport.

The simulation tools of BASEMENT can be subdivided, as in Fig 2.20, into three different parts:

- The mathematical-physical modules consisting of the governing flow equations.
- The computational grid representing the discrete form of the topography.
- The numerical modules with their methods for solving the equations.

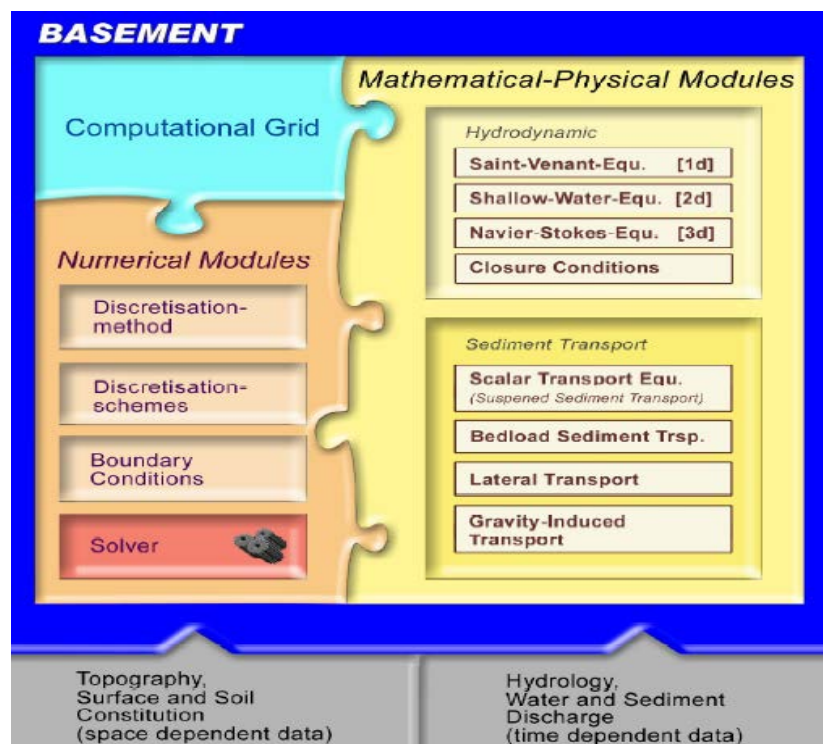


Fig. 2. 20 : Basement Modules and their Components (Faeh, et al., 2012).

The version used during this work in the analysis is v2.2.1. This version supersedes version 2.1 and all previous versions.

2.3.1 The numerical scheme for Basement

The time discretization is based on the explicit Euler scheme, where the new values are calculated considering only values from the precedent time step. The spatial discretization of the Saint Venant equations is carried out as in Fig 2.21 by the finite volume method, where the differential equations are integrated over the single elements. It is assumed that values, which are known at the cross section location, are constant within the element throughout this section, therefore it can be stated that:

$$\int_{x_{iw}}^{x_{ie}} f(x)dx \approx f(x_i)(x_{ie} - x_{iw}) = f_i \Delta x_i \quad 2.3$$

Where x_{ie} and x_{iw} are the positions of the edges at the east and the west sides of element (i).

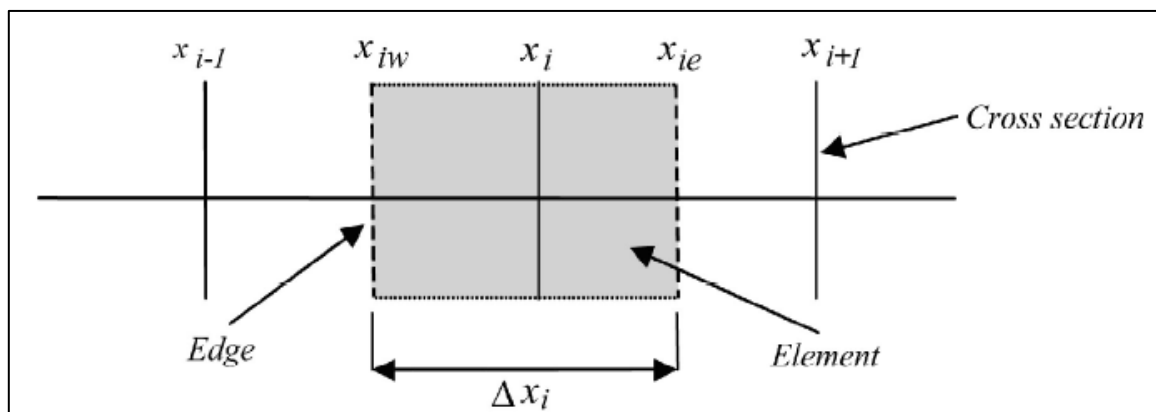


Fig. 2. 21: Definition for finite volume discretization for the spatial derivatives (Faeh, et al., 2012).

Continuity equation discretization

The discretization of continuity equation, based on explicit Euler discretization for time derivatives and finite volume integrals for the spatial derivatives, takes the following form:

$$\int_{x_{iw}}^{x_{ie}} \left(\frac{\partial A}{\partial t} + \frac{\partial Q}{\partial x} - q_l \right) dx = 0 \quad 2.4. a$$

$$\frac{A_i^{t+1} - A_i^t}{\Delta t} \Delta x_i + (Q(x_{ie}) - Q(x_{iw})) - (q_{ie}(x_{ie} - x_i) + q_{iw}(x_i - x_{iw})) = 0 \quad 2.4. b$$

Where $Q(x_{ie})$ and $Q(x_{iw})$ are the continuity fluxes, q_{ie} and q_{iw} are the lateral water sources in the corresponding river segments. So for the explicit time discretization, the new value of A will be:

$$A_i^{t+1} = A_i^t - \frac{\Delta t}{\Delta x_i} (Q(x_{ie}) - Q(x_{iw})) - \frac{\Delta t}{\Delta x_i} (q_{ie}(x_{ie} - x_i) + q_{iw}(x_i - x_{iw})) \quad 2.4. c$$

Momentum equation Discretization

The momentum equation discretize under assuming that the lateral in and outflows do not contribute to the momentum balance, thus neglecting the last term of equation (1.13.b), and integrating over the element; the momentum equation becomes:

$$\int_{x_{iw}}^{x_{ie}} \left(\frac{\partial Q}{\partial t} + \frac{\partial}{\partial x} \left(\frac{Q^2}{A_{red}} \right) + \sum Sources \right) dx = 0 \quad 2.5. a$$

$$\frac{Q_i^{t+1} - Q_i^t}{\Delta t} \Delta x_i + \left(\left(\frac{Q^2}{A_{red}} \right) \Big|_{@x_{ie}} - \left(\frac{Q^2}{A_{red}} \right) \Big|_{@x_{iw}} \right) + \sum Sources \quad 2.5. b$$

Where A_{red} is the reduced area i.e. the part of the cross section area where water flows. Hence, for the explicit time discretization the new value of Q will be:

$$Q_i^{t+1} = Q_i^t - \frac{\Delta t}{\Delta x_i} \left(\left(\frac{Q^2}{A_{red}} \right) \Big|_{@x_{ie}} - \left(\frac{Q^2}{A_{red}} \right) \Big|_{@x_{iw}} \right) + \sum Sources \quad 2.5.c$$

Where the summation of the sources also calculated by integral, it's result is:

$$\sum Sources = -\Delta t g (A_{red})_i \left(\frac{(h + \eta)_{i+1} - (h + \eta)_{i-1}}{x_{i+1} - x_{i-1}} \right) \quad 2.5.d$$

Where Δt is the time step, g acceleration gravity, h is the water depth, and η is the bed elevation above reference datum.

Discretization of Exner equation

For each cross section slice; a different composition of the soil can be specified. A variable number of sediment layers can be defined.as in Fig 2.22.

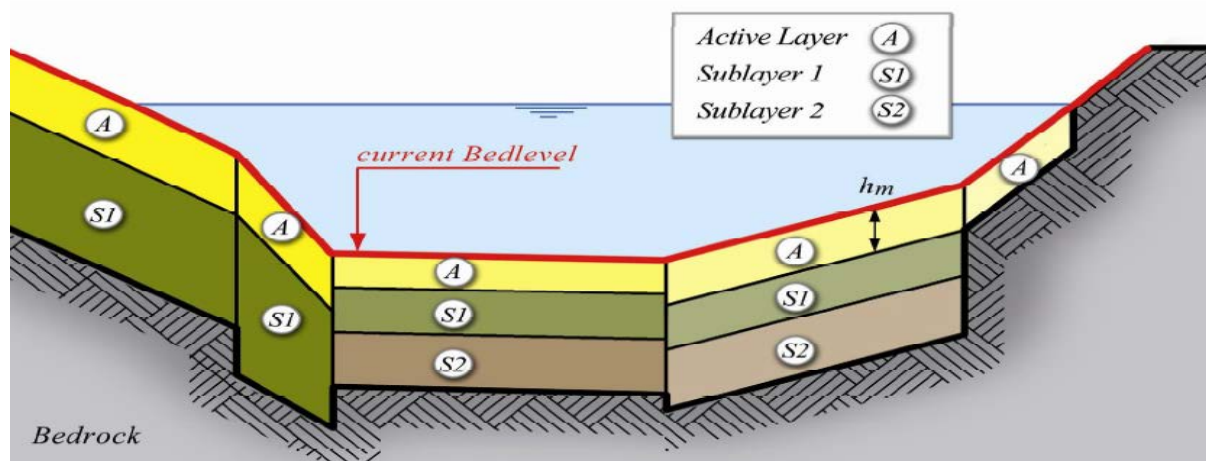


Fig. 2. 22: Soil Discretisation in a cross section in Basement (Faeh, et al., 2012).

This figure illustrates, by example, a possible distribution of soil types in a cross section. Each color represents a different grain class mixture. Usually however one soil type will cover several cross sectional slices.

The modification of the geometry of the cross section due to sediment transport is illustrated in Fig. 2.23. This can lead to the elimination of layers or creation of new ones. The grain class mixture of deposition will be the same over the whole wetted width.

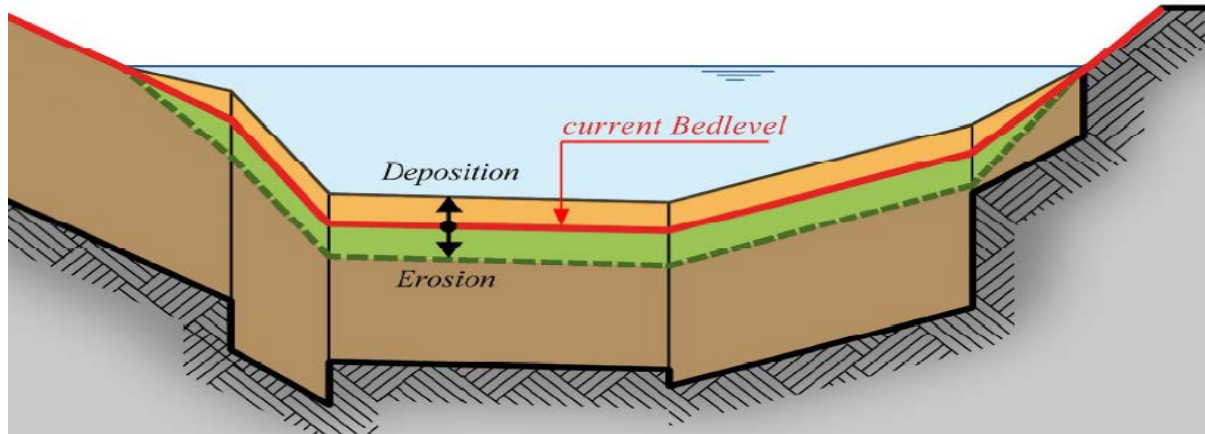


Fig. 2. 23: Effect of bed load on cross section geometry (Faeh, et al., 2012).

The global bed material conservation equation Eq. 1.15 will be integrated by the same way, it will take the following form.

$$\int_{x_{iw}}^{x_{ie}} \left((1 - p_0) \frac{\partial A_{sed}}{\partial t} + \frac{\partial Q_s}{\partial x} + D_s + E_s \right) dx = 0 \quad 2.6. a$$

$$(1 - p_0) \frac{A_{sed_i}^{t+1} - A_{sed_i}^t}{\Delta t} \Delta x_i + ((Q_s|@x_{ie}) - (Q_s|@x_{iw})) +$$

$$\sum_{x_i}^{x_{i+1}} D_s + \sum_{x_i}^{x_{i+1}} E_s = 0 \quad 2.6. b$$

Where D_s is the deposition rate and E_s is the erosion rate both expressed as volume per unit area per unit time, then the change of the sediment area is thus calculated by:

$$\begin{aligned}\Delta A_{sed} &= A_{sed_i}^{t+1} - A_{sed_i}^t \\ &= \frac{\Delta t}{\Delta x_i} \left((Q_s|@x_{ie}) - (Q_s|@x_{iw}) + \sum_{x_i}^{x_{i+1}} D_s + \sum_{x_i}^{x_{i+1}} E_s \right) \quad 2.6.c\end{aligned}$$

As the result of the sediment balance is an area, the deposition or erosion height $\Delta\eta$ has not yet determined. The erosion or deposition is distributed over the wetted part of the cross section. If a bed bottom is defined, the deposition height is equal and constant for all wetted slices. Only in the exterior slices the bed level difference is zero where the cross section becomes dry. The repartition of the soil level change is illustrated in Fig 2.24, then $\Delta\eta$ calculated using Eq. 2.7.

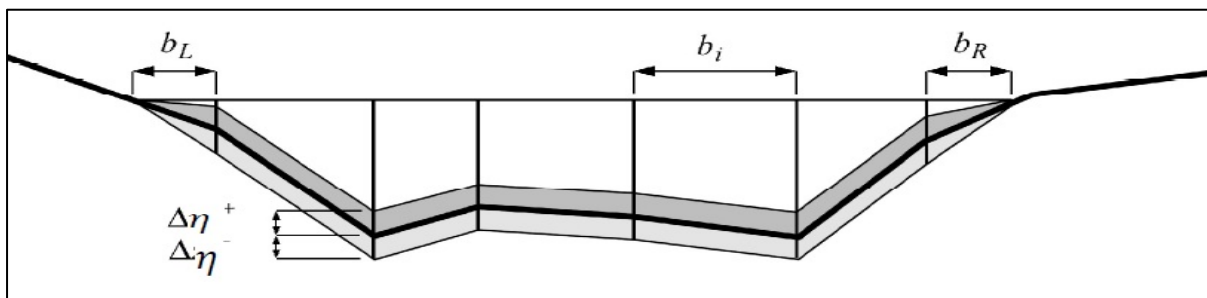


Fig. 2. 24: Distribution of sediment area change over the cross section (Faeh, et al., 2012).

$$\Delta\eta = \frac{\Delta A_{sed}}{\frac{b_r}{2} + \frac{b_l}{2} + \sum b_i} \quad 2.7$$

2.3.2 Effective bed roughness in Basement

For calculating the bed shear stress in Basement; there are two ways. The first way is evaluating the friction coefficient (Manning, Strickler, or Chezy) based on the bed granulometry, the dunes and bed forms, and the vegetation. Then Basement will calculate the bed shear stress depend on the assigned value for friction coefficient. The second way uses Basement to calculate the bed shear stress automatically without assigning value for friction coefficient,

but it will calculate the skin friction effect only in this case. The first way called “the approach by Manning-Strickler”; the second way called “the equivalent sand roughness approach” which depends on the equivalent sand roughness k_s of Nikaradse (The smallest form of roughness is that of the sediment grains themselves, called “grain roughness” or “Nikaradse roughness”).

2.3.2.1 Manning-Strickler approach (manual approach)

To define the channel roughness, either notation k_{str} , n , or C_{chezy} can be used (for conversion $n = \frac{1}{k_{str}}$). By introducing the factor c_f relates the total bed stress with the mean velocity. c_f can be calculated based on the Manning or Strickler coefficient, assigned manually to the software by the user, as in Eq 2.8.

$$c_f = \frac{k_{str} R_H^{1/6}}{\sqrt{g}} \quad 2.8$$

The relation between τ_0 and c_f can be presented as in Eq 2.9 ,then the value of the bed shear stress will be given by Eq 2.10.

$$u_* = \frac{V}{c_f} = \sqrt{\frac{\tau_0}{\rho}} \quad 2.9$$

$$\tau_0 = \rho u_*^2 = c_f^{-2} \rho V^2 \quad 2.10$$

So the Strickler coefficient or Manning coefficient entered here must take into account all the possible sources of friction e.g. skin friction, bed form, or vegetation. If it took into account only the skin friction the result will be $\tau_0 = \tau'_0$, where τ'_0 is the bed shear stress based on skin friction only. This

means that in this approach the result of the shear stress depends on the assigned value for Manning or Strickler coefficients.

2.3.2.2 Equivalent Sand Roughness

The Darcy-Weisbach approach is implemented to determine automatically the coefficient c_f which represent the coefficient used to calculate the skin friction only. The relation between the factor c_f and Darcy-Weisbach friction factor is given in Eq 2.11 then the skin friction is introduced in Eq 2.12:

$$\sqrt{\frac{f}{8}} = \frac{1}{c_f} \quad f = \frac{0.24}{\log\left(\frac{12R_H}{k_s}\right)} \quad 2.11$$

$$\tau'_0 = c_f^{-2} \rho V^2 \quad 2.12$$

Where R_H is the hydraulic radius, f is Darcy-Weisbach friction factor, and k_s in case of a defined soil can be determined as $k_s = \text{factor} * d_{90}$ where the default value for the factor = 3 correspond to a soil with various grain sizes and exposed coarse components. Also c_f can be calculated using Eq 2.8 considering the skin friction only where $k'_{str} = \frac{\text{factor}}{\sqrt[6]{d_{90}}}$, but skin friction only (τ'_0) is the calculated in this case where the default value of this factor = 21.1.

Finally; bed shear stresses can be calculated in Basement either (1) manually by assigning value for Strickler, Manning, or Chezy coefficient, this value for coefficient must include all sources of friction (Nikaradse (grain roughness), bed form, vegetation, and any other sources of friction) or (2) automatically where Basement calculates the skin friction based on the assigned granulometry, then this skin friction amplified by a ratio to take the bed form effect into account. This ratio and its calculations is presented in the following item (2.3.3).

2.3.3 Influence of Bed Forms on Bottom Shear Stress

In presence of bed forms, like ripples, sand dunes or gravel banks, additional friction losses can occur due to complex flow conditions around these bed forms and the formation of turbulent eddies. In such cases the dimensionless bottom shear stress τ_* determined from the present flow conditions can differ from the effective dimensionless bottom shear stress τ'_* , which is relevant for the transport of the sediment particles. It is usually assumed that the determination of the effective shear stress should be based upon the grain friction losses **only** and should exclude additional form losses, to prevent too large sediment transport rates. Therefore a reduction factor Ω is introduced for the determination of the effective bottom shear stress τ'_* from the bottom shear stress as τ_* .

$$\Omega = \frac{\tau'_0}{\tau_0} = \frac{\tau'_*}{\tau_*} \quad \text{or} \quad \tau_0 = \frac{\tau'_0}{\Omega} \quad \text{with} \begin{cases} \Omega = 1 & \text{no bed form} \\ \Omega < 1 & \text{bed form} \end{cases} \quad 2.13$$

This reduction factor (also called ripple factor) can be given a constant value if the bed forms are distributed uniformly over the simulation domain. After (Jäggi, 1995) this factor should be set between 0.8 and 0.85. If there are no bed forms present, one can consider that $\tau_0 = \tau'_0$ i.e. $\Omega = 1.0$. Generally can be said, the larger the form resistance, the smaller the reduction factor Ω becomes.

Another approach to calculate the reduction factor Ω by introducing a reduced energy slope j' , compared to the energy slope j , due to the presence of the bed forms as done by Meyer-Peter and Müller. This approach is in particular suitable if ripples are present at the river bed and finally leads to the following estimation of the reduction factor.

$$\Omega = \left(\frac{k_{str}}{k'_{str}} \right)^{3/2} \quad 2.14$$

Here, k'_{str} corresponds to the definition of the Strickler coefficient for experiments with Nikaradse-roughness (Jäggi, 1995) and can be calculated from the grain sizes using the d90 diameter $k'_{str} = \frac{\text{factor}}{\sqrt[6]{d_{90}}}$, while k_{str} is the calibrated Strickler coefficient used in the hydraulic calculations which includes the form friction effects.

Hint: HEC-RAS always uses the bed form factor with any bed load calculation like Meyer-Peter and Müller formula (1.11.a), so the formula usually takes the form in Eq 2.15.

$$Q_s = B * \sqrt{g(s-1)d_s^3} * 8(\Omega * \tau_* - \tau_{*c})^{\frac{3}{2}} \quad \text{and} \quad \Omega = (RKR)^{\frac{3}{2}} \quad 2.15$$

Where RKR is Nikaradse roughness ratio depends on the grain sizes, so HEC-RAS takes only the skin friction effect in sediment transport calculations and regardless the other sources of bed friction(see page E-13 in (Brunner, 2010)).

Finally; according to (Chanson, 2004) the skin friction must be considered only in the calculations of bed load (this is the followed way by HEC-RAS), while basement gives two options to assign the friction; the first one (item 2.3.2.1) is preferred in the calculations of water profile and the second (item 2.3.2.2) is preferred in the bed load calculations. However the manual approach (item 2.3.2.1) can be used in bed load calculations if the assigned value for friction is the skin friction only, otherwise the reduction factor Ω must be assigned if the assigned value for friction is the total value.

2.3.4 Mini user guide for sediment transport modelling by Basement

Basement v 2.2.1 has a graphical user interface Fig. 2.25. It is clear that it has three drop main menu and four buttons (Edit command, Edit 1-D Grid, run, and

Comparative study of different scenarios for the morphological evolution in a river stream

stop buttons). The file menu is responsible for opening an existing command line or grid file (geometry file). Hence all the discussion below will focus on the use of this four buttons, which can be summarized in a few words as below.

Edit 1-D grid: uses either to open an existing geometry file and then to edit on it or to build a new one.

Edit command line: uses to open an existing command file then to edit on it or to build a new command file.

Run button: is uses to run the command file, it will be activated once the command file has been built.

Stop button: uses to stop the analysis once it started, so it will be active only during the running.

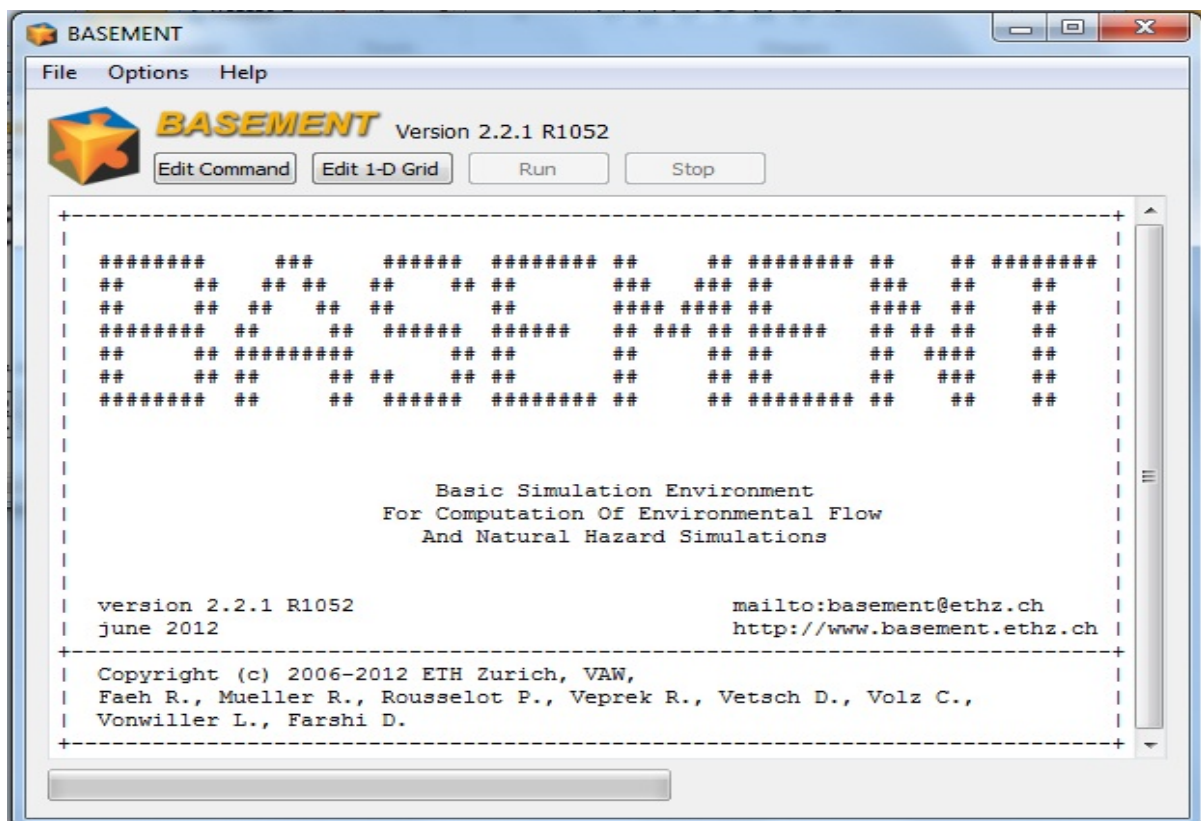


Fig. 2. 25: Graphical user interface (GUI) for Basement software.

Working with Basement pass through four main sequential phases. (1) The pre-processing phase: the purpose from this phase is preparing the geometric input file in the format needed. (2) Preparing an auxiliary input files: the purpose is building an auxiliary files that will be asked by Basement during building the command line file. These files must be built by specific format; mainly these auxiliary files for the flow boundaries. It is used to reduce the effort by the user. (3) Building the command file: for gathering the geometry file and the flow conditions together in commands file, these commands are subdivided to blocks under the main block called Basement as in Fig 2.26. The last phase; (4) Running the command file and extracting the results. In the following detailed description for each phase.

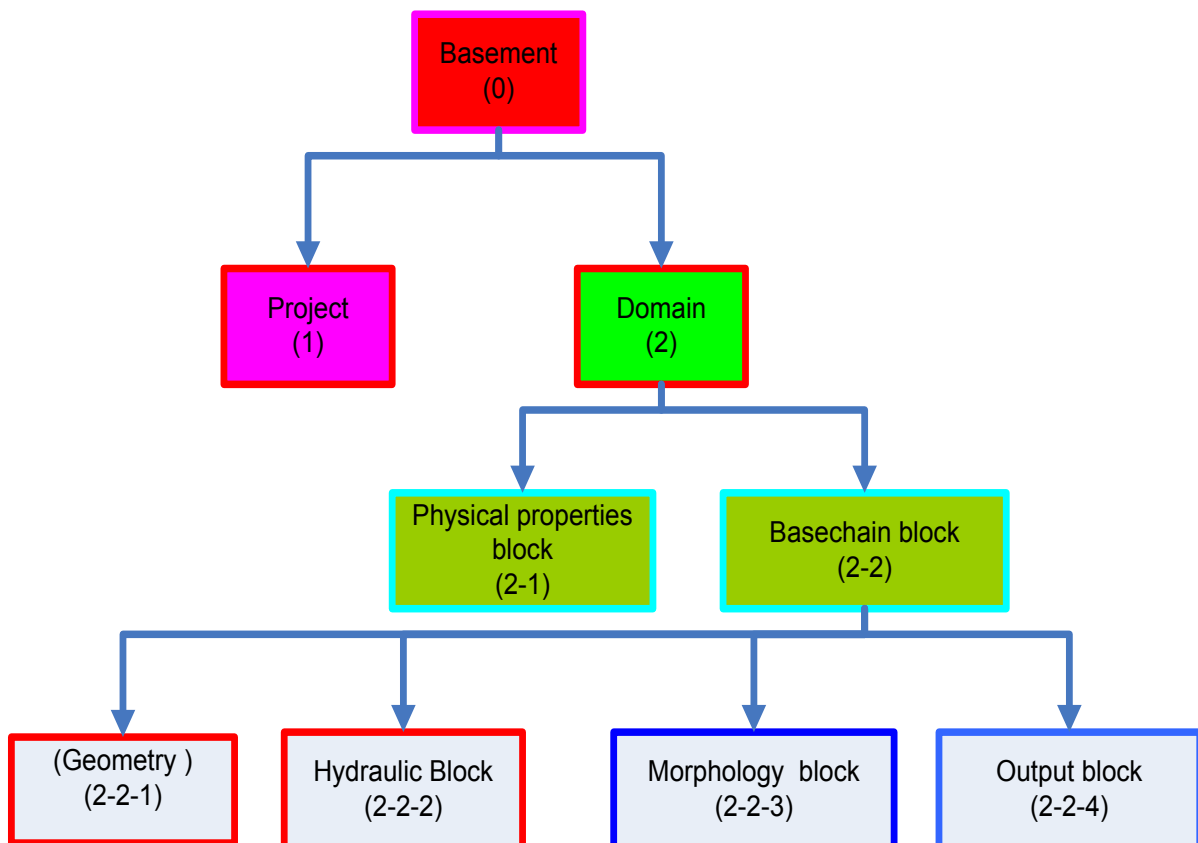


Fig. 2. 26: Flow chart describes the sub-blocks in the command file.

2.3.4.1 The pre-processing phase

The aim from this phase is building the geometry file, which contains all the cross sections, soil definition for each cross section, the friction for each segment (slice) from the cross section, and the water flow range.

- To start this phase open Basement, then click the button edit 1-D Grid. A new window will appear as in Fig 2-26, and from file menu open a new geometry file as in window (2).

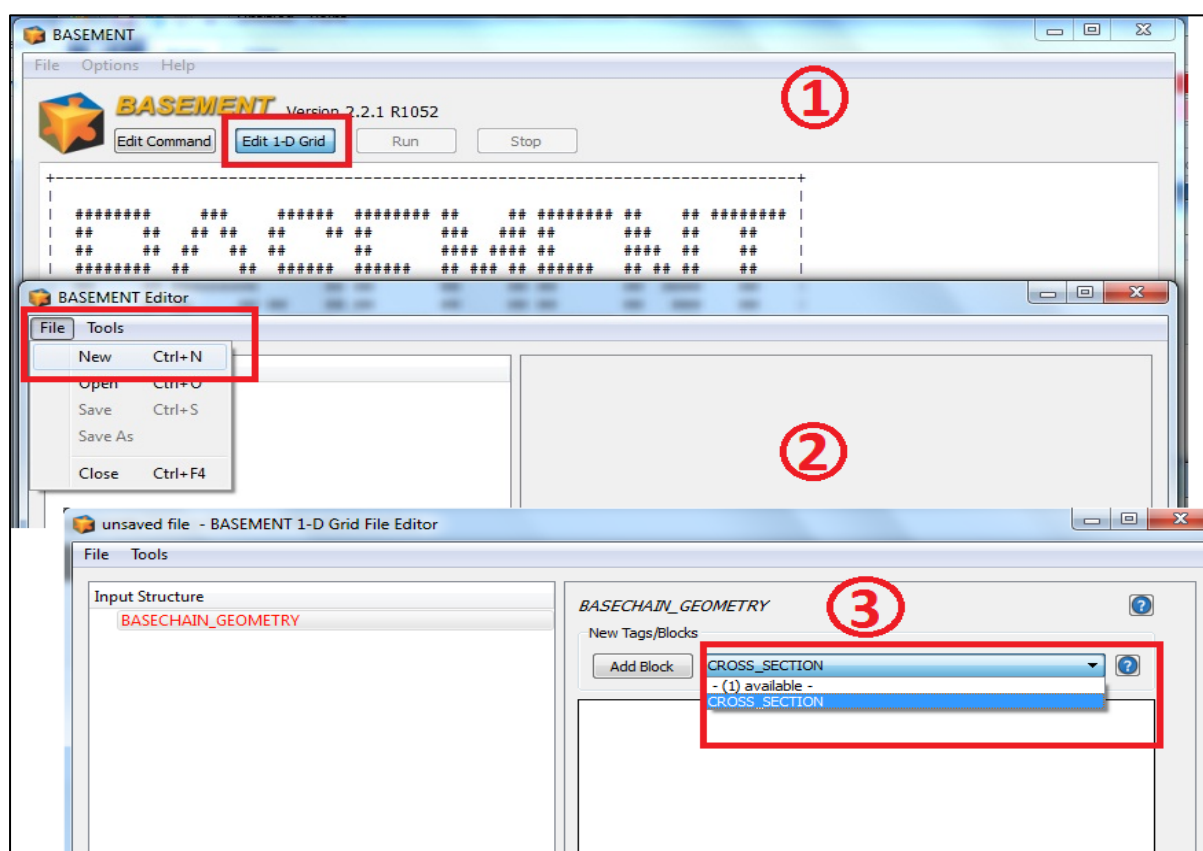


Fig. 2. 27: Opening a new geometry file in Basement.

- In the BASEMENT 1-D Grid file editor window (3); section by section will be added as a sequent blocks , so in the right hand side from window (3) by clicking the button labelled (– (1) available) the cross section selection will appear as in the Fig 2.27. Then by clicking the button labelled (Add Block) the first section will be added under the red title (BASECHAIN_GEOMETRY) and this will be the same procedure to add the next cross sections.

- For entering the cross sections properties like name, distance coordinates, and node coordinates; the modeller must click the button labelled `-(26) available` as window (4) in Fig 2.28, then by selecting name and clicking the button labelled `Add Tag`. The cell name will be added under the drawing zone as in window (5) in Fig 2.28, then type the section name e.g. section 1.

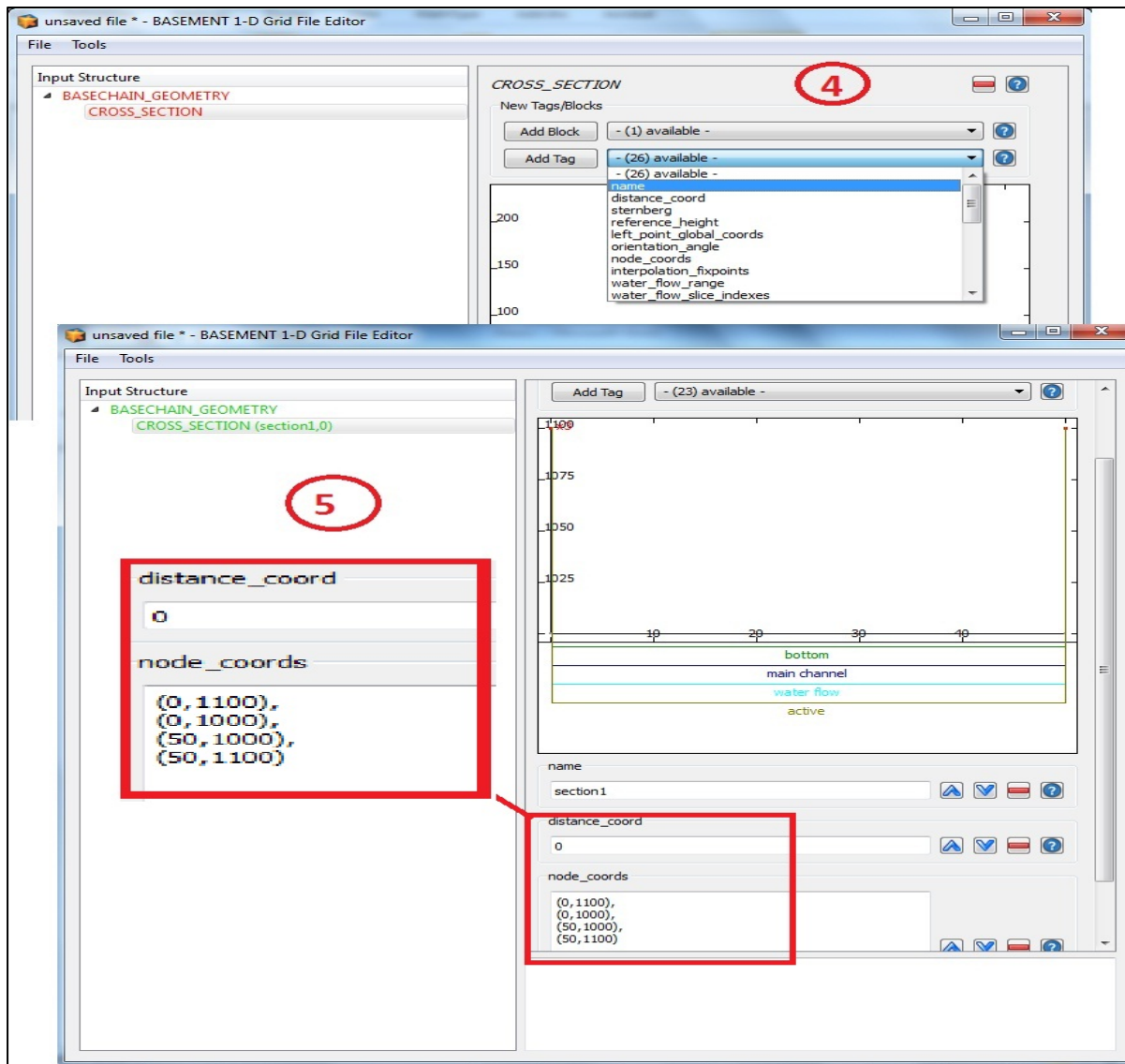


Fig. 2. 28: Assigning the sections properties in Basement.

- After adding the tag of section name ; the distance of this section measured from upstream must be added by adding the tag called `(distance_coord)` as in the zoomed part in window (5) e.g. type 0 under this tag for the first section.

Comparative study of different scenarios for the morphological evolution in a river stream

- The next step; adding the tag for section points called (node_coords), then adding the point's coordinates as in window (5) in Fig 2.28.
- Other tags can be added by the same manner like the bottom range tag, or the bottom slices to define the bottom segment. All the 26 tags will not be added, but according the data available or section shape.
- There is a tag for the bed form effect Ω , to assign the value corresponding to this effect discussed in item 2.3.3; the default value for this tag is 1.
- Once the definition of all section properties done, the soil at the cross section must be defined as in Fig 2.29.
- As in window (6); another block under each cross section must be added called soil_def, so by clicking in soil_def block, then add block. It will be added as in window (8), also it's properties must be added like the soil index and either slice where this soil must be assigned or the range.
- By finishing soil definition; the first cross section definition finished, and the other section shall be defined by the same way.
- After finishing all the cross section, the geometry file must be saved as 1-D grid file .bmg in a specific known location in the pc.

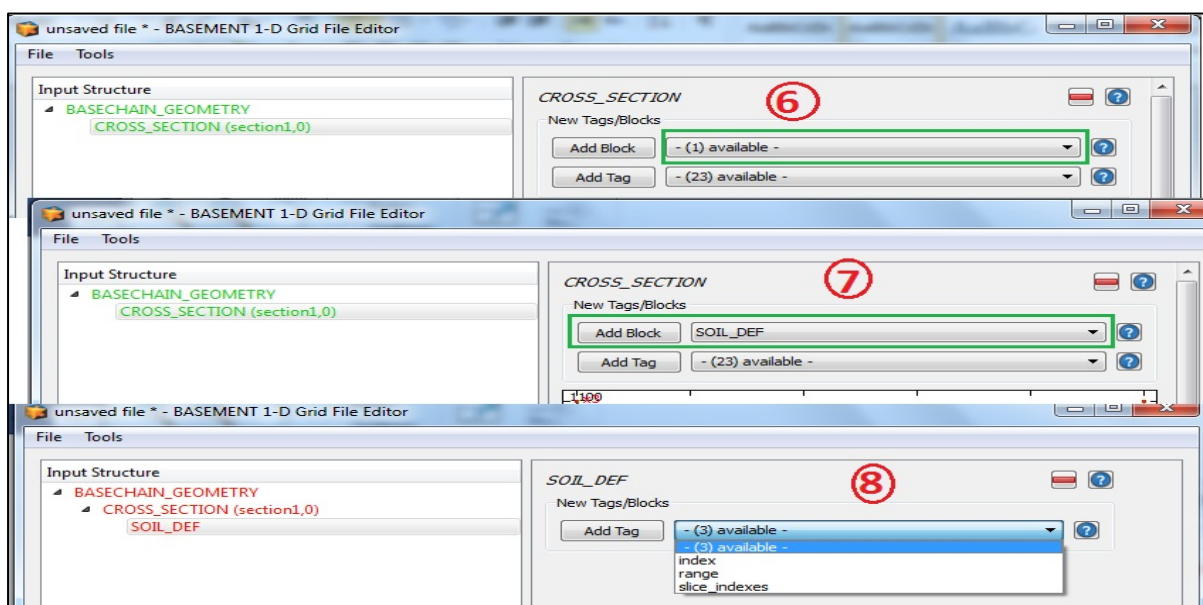


Fig. 2. 29: Inserting soil definition block and the corresponding tags.

2.3.4.2 Phase for Preparing an auxiliary input files

In the next phase before building the command line; some auxiliary files needed. It will be asked by Basement during building the command line coming later. These files are mainly as the following:

- A) Geometry file: prepared before in the previous phase. It has the extension .bmg
- B) Flow boundary (hydrograph) file: it is a text file contains two columns; the first for time by second and the other column is the discharge by m^3/s . specimen of this text file is given in Fig 2.30. The first line contains information about the listed parameters. This line is not read by Basement.

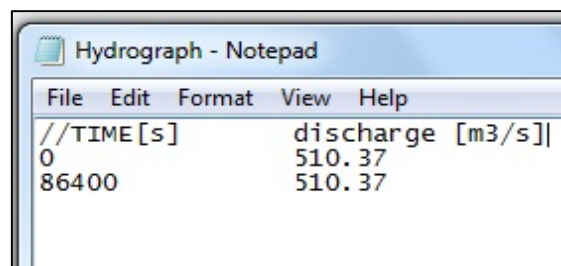


Fig. 2. 30: Specimen of the flow boundary text file.

- C) Initial condition file (restart file): it is a file contains the initial condition at each cross section like wetted cross sectional area and discharge. This text file is easily generated by Basement after each run at the last time for the simulation. By modifying the time to 0; this file will be the new restart file. Fig 2.31 shows where is the value will be changed to zero in the restart file to represent the initial condition file.

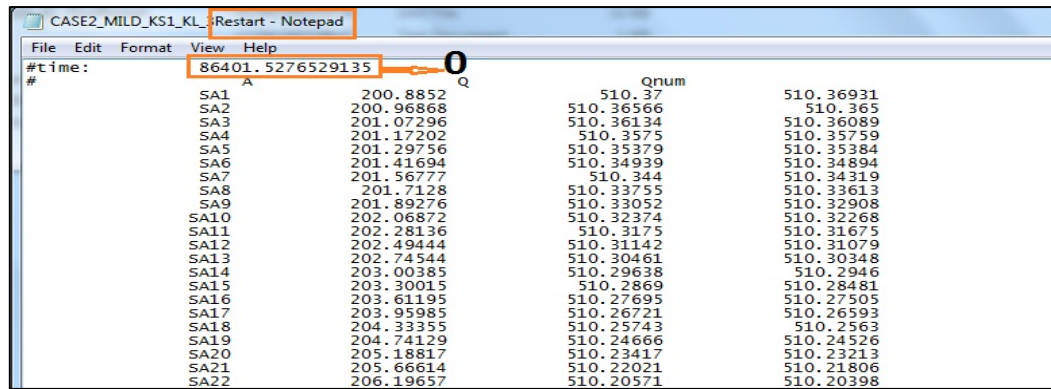


Fig. 2. 31: Preparing the initial condition file from the restart file.

D) Sediment boundary (sediment hydrograph) file: it is also a text file has the same shape of the discharge file in Fig 2.30, but the second column is the sediment discharge [m^3/s]. This sediment boundary can be added either at the upstream SA10 section or at any middle section i.e. lateral sediment feeding (source).

2.3.4.3 Phase of Building the command file

As described in the flow chart in Fig 2.25, the command file is mainly divided to two blocks: the project block uses only to label the project, while the second is the domain block as in Fig 2.32. Under the domain block sub blocks will be added. The steps needed to build the command file summarized in the following points:

- To create a new command file for a new project ; the starting will be by clicking the Edit command button as in window (1) in Fig.2.31, a new window will open called BASEMENT Editor window (2), by clicking file menu then new , a command file editor will open as in window (3) .
- By selecting project and clicking add block button; the project block will be added. On the R.H.S under the tag add the tag for project title, author, and date.

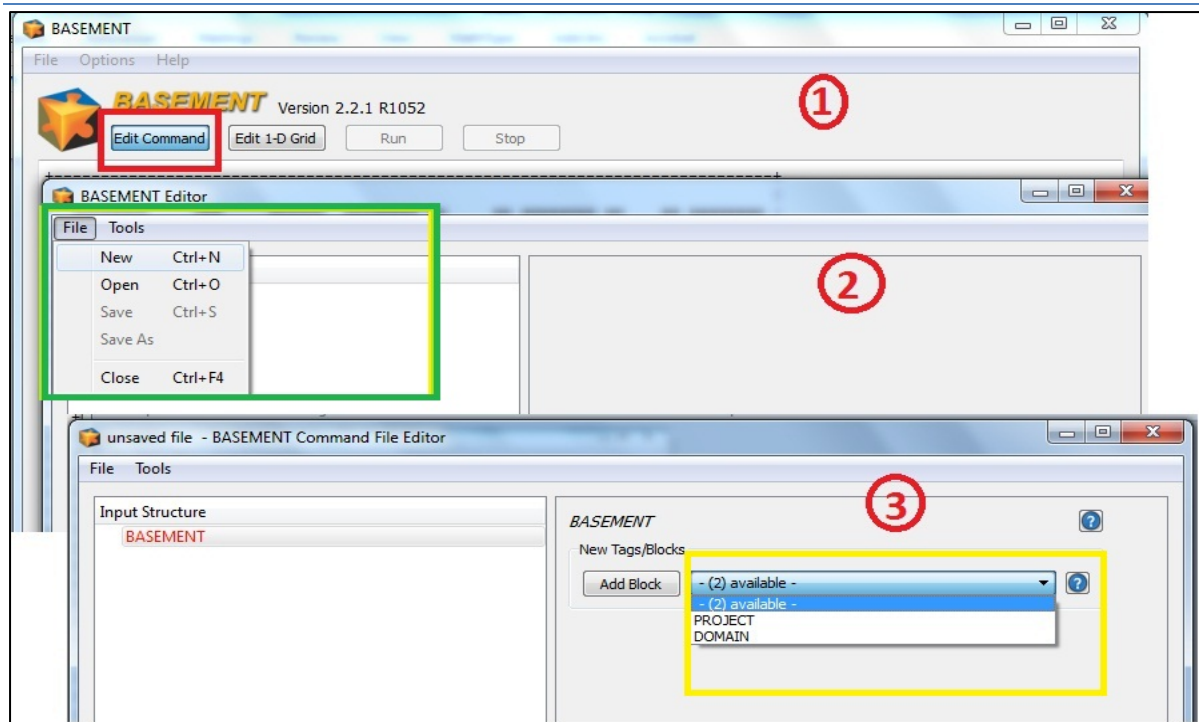


Fig. 2. 32: Starting a new command file.

- To add the domain block; by clicking on basement word just above the project, one new available block is active in R.H.S for adding which is the domain block.
- Under the domain block there are 7 available blocks as in Fig 2.33 window (4). Two blocks only are needed for the 1-D modeling; the physical properties and the BASECHAIN_1D. Under the physical properties add the physical property tags e.g. gravity, viscosity, water density and sediment particle density as in window (5) in Fig 2.33.

Comparative study of different scenarios for the morphological evolution in a river stream

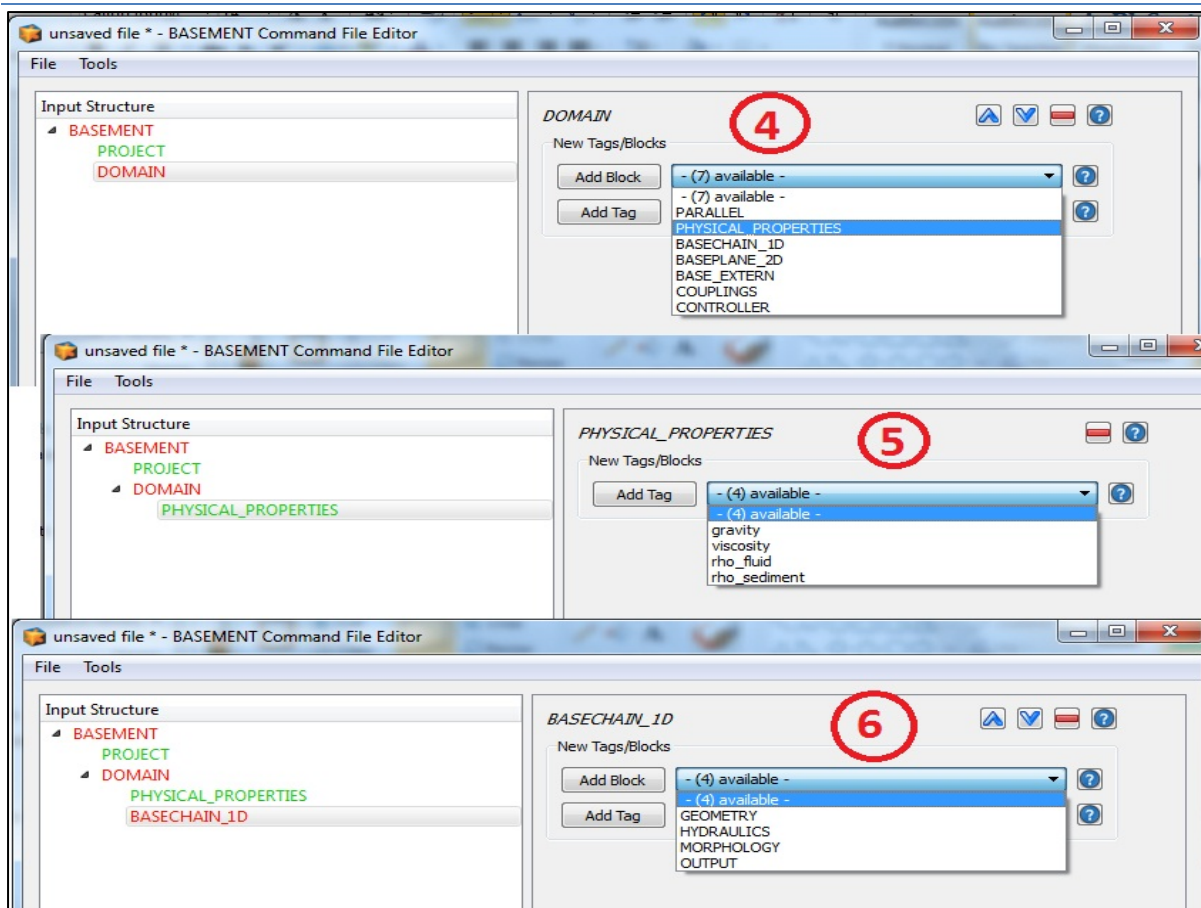


Fig. 2. 33: The domain block and it's sub blocks.

- As in Fig 2.33 window (6) there are four sub blocks; geometry block, hydraulic block, morphology block, and output block.
- Under the geometry block, there are tags for name of the geometry file, type, and cross section order. Under the type, the geometry file prepared in phase 1 will be asked. Under the cross section order the arranging of cross section by name must be entered.
- In the hydraulic block all the hydraulic data will be added, so there are 7 available blocks under hydraulic block; parameter, friction, initial, boundary, sources, and inner boundary blocks.
 - Parameter block: contain some numerical parameter like CFL (Courant-Friedrichs-Lewy condition) which is the stability condition, also the

weighting parameter theta which control the numerical scheme (Explicit or implicit for the time discretization).

- Friction block: uses to define the default value for friction either as manning, Strickler, or Chezy coefficient or the skin friction for the soil particles.
- Initial block: uses to enter the initial conditions either dry or it will ask about the modified restart file.
- Boundary: to assign the flow condition, it will ask about the text file prepared for the hydrograph.
- Source is used when lateral feeding by fluid from a channel cross the reach under study.
- By adding the block called morphology; four sub blocks will be available to define the sediment transport which are parameter, bed material, bed load, and suspended load blocks.
 - Parameter block: uses to define the sediment like porosity, density, also the control volume thickness (c.v.t).
 - Bed material: it is for defining the grain class and the soil mixtures, soil type (mobile or fixed), and assigning the soil type with the index defined in the first phase in the geometry file.
 - Bed load block: it is for assigning the formula for calculating the transport capacity and the boundaries for sediment through three sub blocks:
 - Parameters: to select the transport capacity formula, the angle of repose, and the critical shear stress.
 - Boundary : to enter the file prepared for the sediment hydrograph
 - Source: to enter the file prepared for the lateral sediment feeding.
 - Suspended load block: it looks like the block for the bed load but it is for entering the properties and the boundaries for the suspended load.

Comparative study of different scenarios for the morphological evolution in a river stream

- Finally the output block: it is used to define the format for the output files and the time step for the output. So after adding the output block a special_ output block must be added, after adding it; tags for the type and the output time step must be added as in Fig 2.34.
- The type of the output used is MATLAB and MATLAB flux as (tables can be handled by MATLAB) in Fig 2.34.

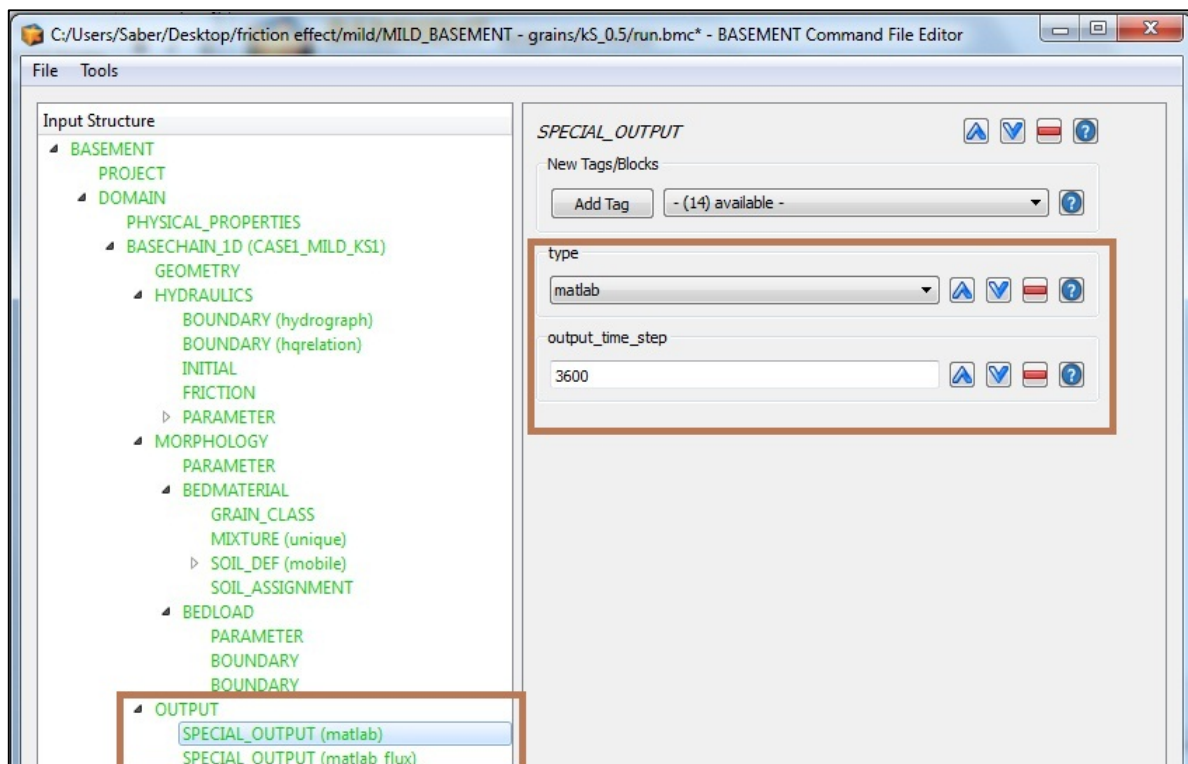


Fig. 2. 34: Defining the output file type and output time step.

2.3.4.4 Phase of Running the command file and extracting the results:

- After finishing the command line; by clicking the RUN button, the analysis will start as in Fig 2.35.

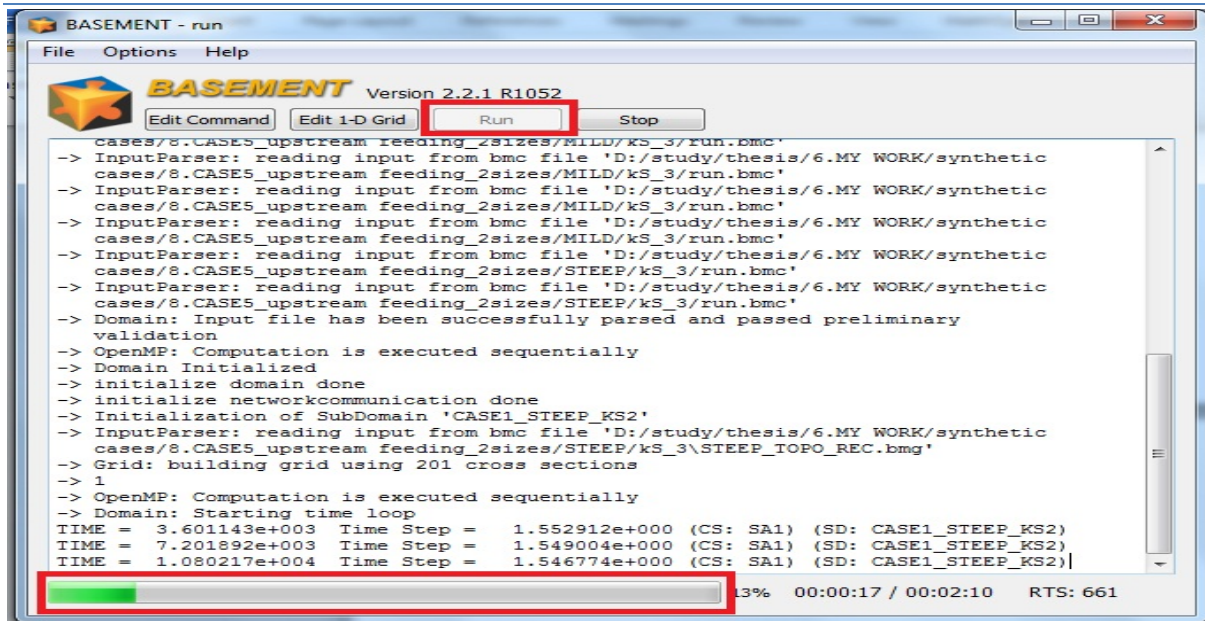


Fig. 2. 35: Running the Basement command line.

- After running; by opening the MATLAB output file by MATLAB software, the matrix contains the result can be opened like in figure 2.36.

	1	2	3	4	5	6	7	8	9	10	11	12	13	14	15	16	17	18	19
1	0	0	1000	1100	1100	1000	1004	1007.319	1613.93	1613.93	0	0	0	0	1	0	1	4.9	1
2	0	50	999	1099	1099	999	1003	1006.319	1613.93	1613.93	0	0	0	0	1	0	1	4.9	1
3	0	100	998	1098	1098	998	1002	1005.319	1613.93	1613.93	0	0	0	0	1	0	1	4.9	1
4	0	150	997	1097	1097	997	1001	1004.319	1613.93	1613.93	0	0	0	0	1	0	1	4.9	1
5	0	200	996	1096	1096	996	999.99999	1003.319	1613.93	1613.93	0	0	0	0	1	0	1	4.9	1
6	0	250	995	1095	1095	995	998.99999	1002.319	1613.93	1613.93	0	0	0	0	1	0	1	4.9	1
7	0	300	994	1094	1094	994	997.99999	1001.319	1613.93	1613.93	0	0	0	0	1	0	1	4.9	1
8	0	350	993	1093	1093	993	996.99999	1000.319	1613.93	1613.93	0	0	0	0	1	0	1	4.9	1
9	0	400	992	1092	1092	992	995.99999	999.31903	1613.93	1613.93	0	0	0	0	1	0	1	4.9	1
10	0	450	991	1091	1091	991	994.99999	998.31903	1613.93	1613.93	0	0	0	0	1	0	1	4.9	1
11	0	500	990	1090	1090	990	993.99999	997.31903	1613.93	1613.93	0	0	0	0	1	0	1	4.9	1
12	10803.713	0	1016.596	1100	1100	1016.596	1019.5423	1025.3902	1613.93	1611.2154	0	34.93613	1308.98	1	4.9406565e-324	0.73826006	0.26173994	21.496031	1
13	10803.713	50	1008.3963	1099	1099	1008.3963	1011.4156	1017.2138	1611.7364	1611.1612	0	33.48884	1284.02	1	1.9762626e-323	0.65500471	0.34499529	14.296269	1
14	10803.713	100	1011.7593	1098	1098	1011.7593	1014.836	1020.3578	1614.9154	1616.6016	0	31.47902	1212.29	1	2.9643939e-323	0.7066292	0.2933708	18.659326	1
15	10803.713	150	1004.3069	1097	1097	1004.3069	1007.3577	1012.8688	1613.2958	1612.1902	0	30.16838	1217.54	1	4.9406565e-323	0.63306879	0.36693121	12.206947	1
16	10803.713	200	1007.323	1096	1096	1007.323	1010.4951	1015.7429	1611.1114	1610.6063	0	28.80997	1145.07	1	5.9287878e-323	0.68248536	0.31751464	16.222988	1
17	10803.713	250	1000.5839	1095	1095	1000.5839	1003.7222	1008.947	1613.6514	1615.1267	0	27.34852	1141.22	1	1.62E-284	0.56159268	0.43840732	10.483924	1
18	10803.713	300	1003.2693	1094	1094	1003.2693	1006.4402	1011.4166	1614.8561	1615.2479	0	26.16505	1084.73	1	6.69E-283	0.63739937	0.36260063	14.169334	1
19	10803.713	350	997.17847	1093	1093	997.17847	1000.4186	1005.2996	1613.4836	1613.5612	0	24.61701	1057.52	1	6.11E-237	0.48785758	0.51214242	9.0784724	1
20	10803.713	400	999.59274	1092	1092	999.59274	1002.9104	1007.6071	1613.2444	1610.8773	0	23.2318	1010.89	1	4.48E-212	0.58771106	0.41228894	12.492741	1
21	10803.713	450	994.01354	1091	1091	994.01354	997.38414	1002.0562	1613.8751	1613.8422	0	22.22401	1000.98	1	3.69E-151	0.4140431	0.5859569	7.9135383	1
22	10803.713	500	996.21437	1090	1090	996.21437	999.60587	1004.0167	1614.5102	1617.0708	0	20.99917	943.255	1	1.33E-149	0.53636131	0.46363869	11.114366	1

Fig. 2. 36: Component of MATLAB output matrix.

Each column refers to specific characteristics:

- 1, 2: time step [s] and distance from upstream [m];
- 3, 4, 5: min. bed level, the right bank, and the left bank elevations [m];
- 6, 7, 8: the mean bed level, water surface elevation, and the total energy line [m];

- 9,10: the discharge [$Q \text{ m}^3/\text{s}$];
- 11: the concentration of sediment as a suspended load;
- 12 : the sediment discharge [$Q_s \text{ m}^3/\text{s}$];
- 13 : the bed shear stress [pa];
- 14,15: percentage of smaller diameter in the control volume, percentage of larger diameter in the control volume;
- 16, 17: percentage of smaller diameter in the lower (sub) layer; percentage of larger diameter in the lower layer;
- 18: thickness of the sub layer;
- 19: number of sub layers.

In case of single grain size the columns 15 and 17 will be eliminated.

- Also the MATLAB flux file can be extracted using MATLAB, it include the data for fluxes as shown in Fig 2.37.

	1	2	3	4	5	6	7	8	9
1	1.744124	0	1613.93	13023.9	35.21	35.21	0	0	0
2	1.744124	1	1613.93	13023.9	0	0	0	0	0
3	1.744124	2	1613.93	13023.9	0	0	0	0	0
4	1.744124	3	1613.93	13023.9	0	0	0	0	0
5	1.744124	4	1613.93	13023.9	0	0	0	0	0
6	1.744124	5	1613.93	13023.9	0	0	0	0	0
7	1.744124	6	1613.93	13023.9	0	0	0	0	0
8	1.744124	7	1613.93	13023.9	0	0	0	0	0
9	1.744124	8	1613.93	13023.9	0	0	0	0	0
10	1.744124	9	1613.93	13023.9	0	0	0	0	0
11	1.744124	10	1613.93	13023.9	0	0	0	0	0
12	86400.16	0	1613.93	13026	35.21	35.21	0	0	0
13	86400.16	1	1613.93	17356.1	34.8888	34.8888	1.4822e-322	0	0
14	86400.16	2	1613.93	17397.4	33.9666	33.9666	5.2371e-322	0	0
15	86400.16	3	1613.93	17227.2	33.6125	33.6125	8.36752E-36	0	0
16	86400.16	4	1613.93	17264.6	33.4361	33.4361	3.4464E-07	0	0
17	86400.16	5	1613.93	17044.7	32.4164	32.4164	2.8997E-06	0	0
18	86400.16	6	1613.93	17086.2	32.2489	32.2489	0.000024142	0	0
19	86400.16	7	1613.93	16833.8	31.2634	31.2633	9.18168E-05	0	0
20	86400.16	8	1613.93	16821.3	29.9982	29.9979	0.000309196	0	0
21	86400.16	9	1613.92	16688.8	29.77	29.7692	0.000756847	0	0
22	86400.16	10	1613.91	16724.4	29.6764	29.6748	0.00160557	0	0

Fig. 2. 37: Matrix of sediment fluxes.

The meanings of the columns in the MATLAB flux Matrix are the following:

- 1, 2: time step [s], section number;
- 3, 4: the discharge [$Q \text{ m}^3/\text{s}$], and Q^2/A ;

5, 6: total Sediment discharge, bed load, and suspended load.

7, 8: Suspended Flux total advective and suspended Flux total diffusive.

- By using these two matrixes, the relation between the distance and the bed level and the contribution of each grain size in the control volume and the sub layer by using either MATLAB or Excel can be drawn.

2.4 Modeling the morphological evolution by ISIS.

ISIS is a software package which is used for river modeling. It developed by Halcrow Group Limited, which is one of the UK's largest consultancies. ISIS is a full hydrodynamic simulator for modeling flows and levels in open channels and estuaries. ISIS is able to model complex looped and branched networks. It is designed to provide a comprehensive range of methods for simulating floodplain flows. ISIS incorporates both unsteady and steady flow solvers with options that include simple backwaters flow routing and full unsteady simulation. The simulation engine provides a direct steady-state solver and adaptive time-stepping methods to optimize run-time and enhance model stability.

ISIS provides full interactive views of the model data and results using plan views, long sections, form based editing tools and time series plots. Results can also be reported in text and tabular formats. The software includes a wide range of diagnostic error checks and a comprehensive on-line help system.

A key strength of ISIS is the ability to model a wide range of hydraulic structures including all common types of bridges, sluices, culverts, pumps and weirs. Wherever possible, standard equations or methods are incorporated into the software so that the calculation of level and discharge relationships is

fully handled by the software. For structures with automatic operation such as pumps and sluices, ISIS allows the user to incorporate logical control rules.

ISIS Sediment is the mobile bed sediment transport module used with ISIS for studying the morphology of rivers and alluvial canals. It has been applied to engineering problems and for studying sedimentation problems in rivers and canals, including a number of the world's major irrigation systems. The software predicts sediment transport rates, changes in bed elevation and amounts of erosion and deposition throughout the channel system. A range of sediment transport predictors are included and additional formulae are easily incorporated. The conveyance properties of the river sections are updated throughout the simulation based on the predictions of the module. ISIS sediment also includes the ability to simulate dredging of the channel at periodic intervals during a simulation.

There are many types of ISIS like ISIS professional, ISIS 2D, and ISIS FAST, but the used copy is the free copy version 3.6.1. Halcrow have developed ISIS Free so that it offers an integrated 1D and 2D modeling software package. ISIS free provides the same core features as ISIS 1D with water quality and sediment transport add-ons, ISIS 2D with ADI Solver, ISIS FAST and ISIS MAPPER which enable you to confidently apply it to smaller river modeling projects and to tackle different types of hydraulic conditions including flood risk assessments, flood mapping and flood alleviation scheme design. The software can seamlessly be upgraded to ISIS 1D, ISIS 2D or ISIS FAST, if the project grows beyond the 250 1D nodes, 2,500 2D cells or DEM grid size of 2,500 cells limits. Fig 2.37 shows the interface of ISIS and the components of the GUI.

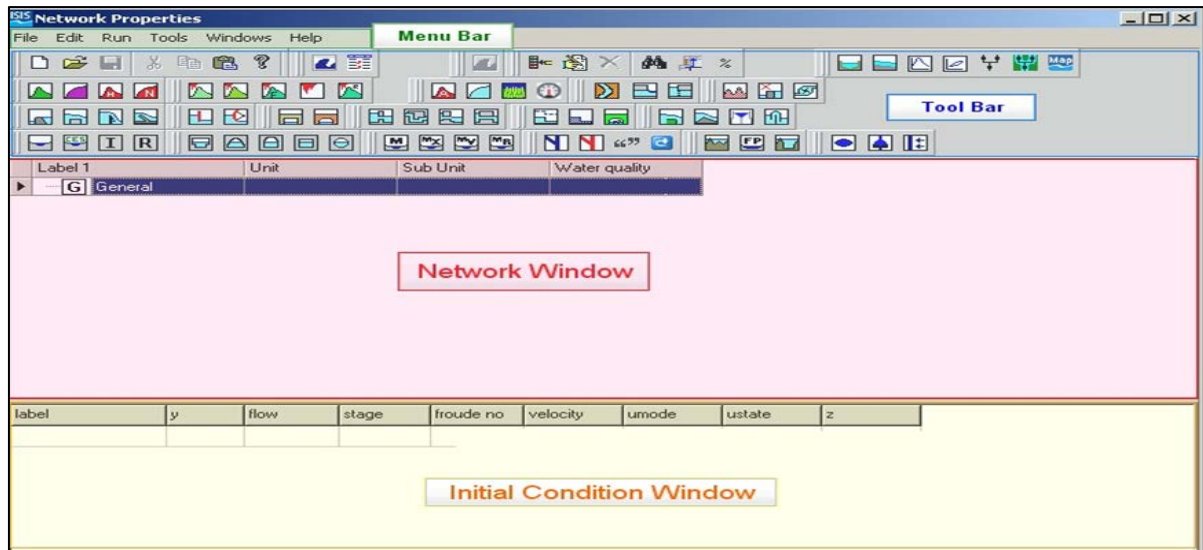


Fig. 2. 38: ISIS main user interface.

Halcrow introduces an e-learning for ISIS in their web site for simulating steady flow, unsteady flow, and simulating some structures. The link of the video tutorial e-learning is embedded in the help of the software. By clicking the title e-learning it will open the learning web page⁴, while in the following a discussion about the ISIS sediment transport module.

2.4.1 Numerical scheme with ISIS

ISIS like HEC-RAS uses the finite differences for both time and spatial derivatives for the governing equations [1.14]. It also employs the Preissmann implicit scheme, which is popularly referred to as the 4 points Box scheme. The numerical scheme outlined in item 1.12 uses for discretizing saint Venant equations [1.14.a, 1.14.b], While the discretization of Exner equation takes the form

$$(1 - p_0) \frac{\Delta \eta_{k+1}}{\Delta t} * B_{k+1} + \frac{Q_{sk+1}^{i+1} - Q_{sk}^{i+1}}{\Delta x} = 0 \quad 2.16$$

Where k = position (spatial) index, which increases in the downstream direction i = time index, and $\Delta \eta$ = change in bed elevation over time step Δt .

⁴ http://www.isisuser.com/docs/manuals/elearning_riverhydraulics/Teaching_Hydraulics_Using_ISIS.htm

Equation 2.16 can be solved explicitly for $\Delta\eta$, where $Q_{s_{k+1}}^{i+1}$ is calculated by the sediment transport capacity equations [1.11] and $Q_{s_k}^{i+1}$ is the sediment capacity determined previously.

2.4.2 Mini user guide for sediment transport modelling by ISIS

The working with ISIS is near to the modelling by Basement and it pass by the steps: (A) building the geometry of the model, (B) running the model under steady case to get the initial condition, (C) building a text file include the sediment properties and boundaries with the extension (filename.sed), (D) running the sediment transport analysis (unsteady analysis), and finally (E) extracting the output.

It is important before starting the modelling to know the limitation of ISIS in sediment transport modelling which are:

- Dunes and ripples are not explicitly modeled and therefore the effects of changes in form roughness on the hydraulic resistance is not simulated;
- The following ISIS units are currently not permitted in a mobile bed module run: inline RESERVOIRs, INTERPOLATE, REPLICATE, LDPUMP, MUSKINGUM, ABSTRACTION, QH CONTROL, LATERAL and Q RATING;
- Reaches with zero flows are not permitted at present;
- Essentially one-dimensional representations are used (e.g. cross section averaged velocities) which are not sufficiently accurate for some situations, e.g. 'local' effects such as scour at bridge piers.

In the following; how to build the model as step by step is discussed?

2.4.2.1 Building ISIS geometry file

Building the geometry starts with adding the flow boundary condition with a label has the same label for the first cross section, then the cross sections one

by one until the last section, then the flow downstream boundary. The following Figure 2.39 shows the Network built in ISIS. While the schematic visualizer window that shows the diagram for sections arranging.

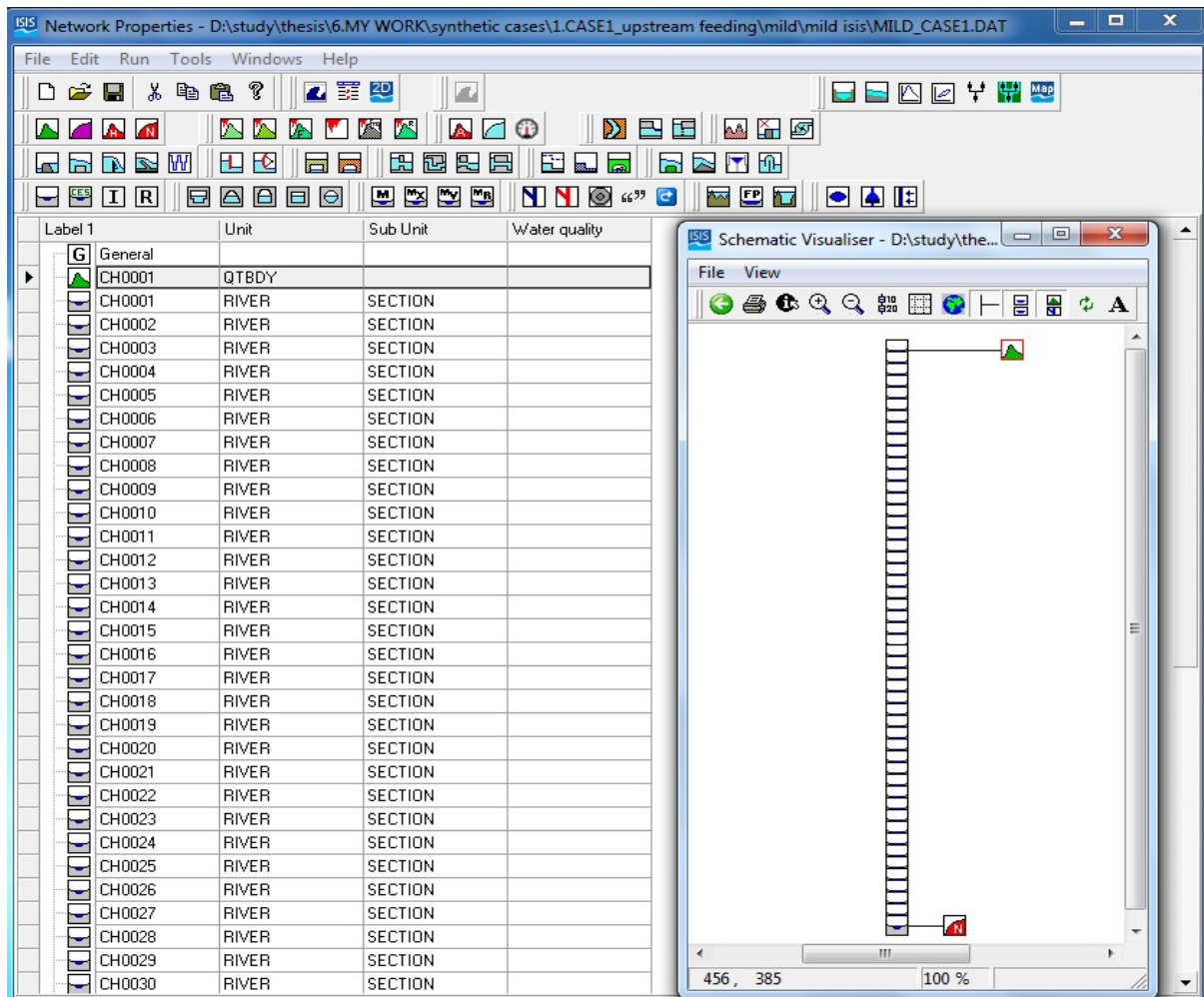


Fig. 2. 39 : Building the Geometry file by ISIS.

2.4.2.2 Importing the initial conditions

After building the geometry file; the model must run as a steady flow to find the initial water depth and discharge at each cross section. These values will be used as initial values in the discretized equations for the unsteady simulation.

After running; from file menu import the initial condition as shown in Fig 2.40, then the initial conditions will be imported in the initial condition window.

Comparative study of different scenarios for the morphological evolution in a river stream

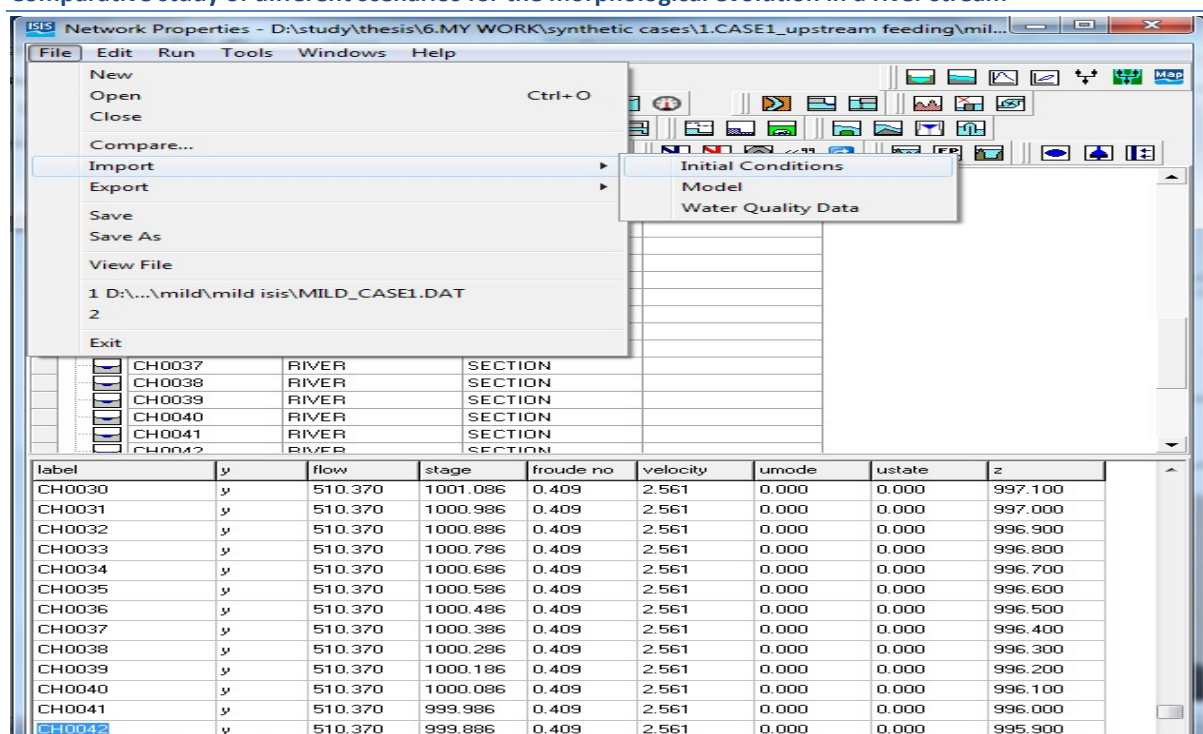


Fig. 2. 40: Importing the initial conditions in ISIS.

2.4.2.3 Building the sediment properties and boundaries file

The extension of the sediment file must take the extension .SED, and the same name for the model i.e. after modelling the network; ISIS saves the data in a file has a name (filename.dat) also the sediment file must be named by the same name filename.sed, which is a file created by the modeler and filename is any name selected by the modeler. Filename.dat and filename.sed must be in the same folder before running the simulation.

Before speaking about creating the sediment file, a discussion must be opened about the sediment capacity equations used with ISIS, sorting and armoring in ISIS, and how to update channel geometry.

- Sediment transport equation

The following sediment transport equations are available in ISIS and all include a calibration factor which has the default value of unity to give the

published form of the equations. The number in the following table will be used to indicate the equation within the sediment file.

No.	Equation	Applicability
1	Engelund-Hansen (1967)	uniform sand - total load
2	Ackers-White (1973)	uniform sand and gravel - total load
3	Revised Ackers-White (1993)	uniform sand and gravel - total load
4	Westrich-Jurashek (1985)	fine sediment - total load
7	Parker (1990)	uniform/graded coarse sand and gravel - bed load
10	Modified Parker (1990)	uniform/graded coarse sand and gravel - bed load

Table 2. 1: The transport capacity equations in Basement (ISIS, 2012).

- Graded Sediments & sorting:

There are two approaches for the sediment sorting. The first approach is termed the 'COMPOSITE' algorithm, as a single 'composite' grading represents the channel bed material. The latter approach is termed the 'SORTED' algorithm because sediment sorting effects are modeled. So 'COMPOSITE' algorithm uses for single size or when sorting is not needed. While 'SORTED' algorithm uses for sorting the small sediment sizes from the bed first.

- Updating Channel Geometry with ISIS

A range of methods for updating the channel geometry are available as in Fig 2.41 : (0) no change in channel geometry, (1) move all section points uniformly by the Δz calculated for the particular section, (2) move only those points at a section below water level uniformly by the Δz calculated for the particular section, and (3) move those points below water level by a Δz distributed according to shear stress (scaling Δz at every data point). The following figure describes each updating method.

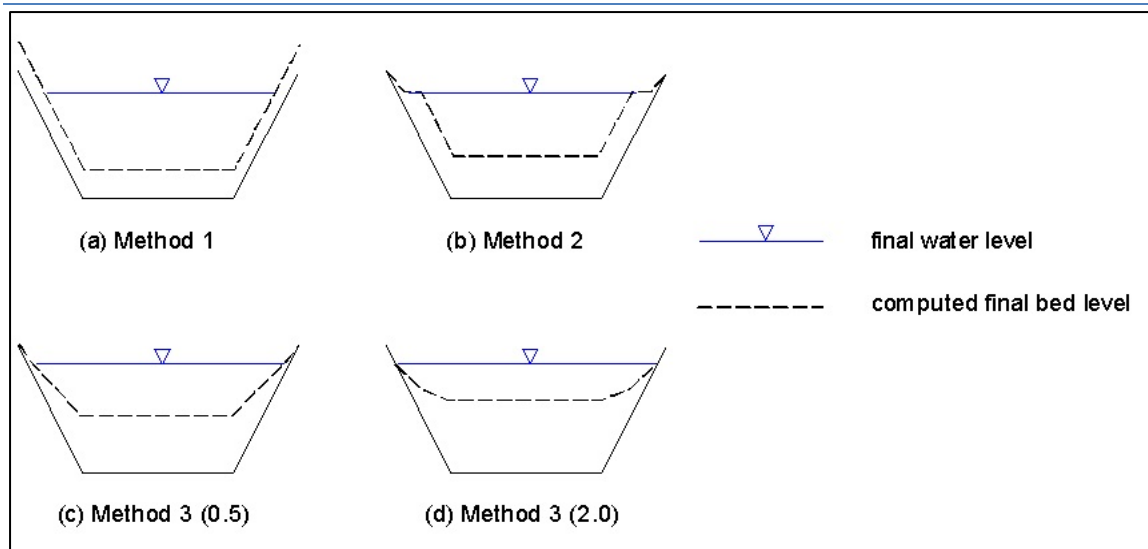


Fig. 2. 41: Comparison of bed updating methods (ISIS, 2012).

The first data block in the mobile bed model data file should be the general system parameters. These data are followed by boundary units and other data blocks in any order. The end of the data file is denoted by the keyword 'END' on it's own line. Real numbers should not be given as integers and integers should not be given as real numbers. In the following; a description for each block.

- Block (1) General System Parameters

The system parameters are specified at the top of the data file, an example of the structure of this section of the file shown in Figure 2.42.

Line	
1	MOBILE BED MODEL C
2	1.0 1.0 0.4 0.010 1
3	3 COMPOSITE
4	0.1 2650. 1 0.2
	0.35 2650. 1 0.5
3 + n1	0.50 2650. 1 0.3

Datafile Format (initial data block)	
Line 1	Title
Line 2	$\alpha, K, \lambda, \Delta z_c, \text{method}, m$
Line 3	n_1, type
Line 4 to Line 3 + n_1	$d_i, \rho_i, \text{stequ}, P_i$

Fig. 2. 42: Example of the General System Parameters data file section (ISIS, 2012).

Where

- Title = data file title of up to 40 characters. The first character must not be blank (i.e. not a space).
- α = active layer thickness factor. The maximum active layer thickness is calculated as D95 multiplied by α .
- K = sediment transport equation calibration coefficient (set to 1 to get original equation).
- λ = bed porosity (e.g. 0.4).
- Δz_c = erosion/deposition depth change criteria to cause updating of channel geometry (m).
- Method = integer defining the method to update the channel geometry (Fig 2.41). Entering 0 will not update section points, 1 to move all section points at a node by a uniform Δz , 2 to move all section points at a node below the water surface by a uniform Δz , 3 to move those section points at a node below the water surface by a Δz distributed according to local shear stress (water depth).
- m (only required to be present if method=3): exponent used in method 3 to distribute changes in bed elevation around the cross section. Likely range is 0 to 2. A value of 0 will give a uniform distribution and 1 will weight erosion/deposition to the larger water depths.
- n1 = number of sediment sizes in the size distribution (between 1 and 10).
- Type = sediment transport calculation methodology. Enter:

COMPOSITE for no sediment sorting

SORTED for sediment sorting

- d_i = sediment diameter (in mm) for size fraction i . They should be given in order of increasing size.
- ρ_i = sediment density (in kg/m³) for size fraction i . The density for size fraction 1 is used to represent the full distribution for some internal calculations.
- $stequ$ = sediment transport equation (table 2.1) to be used for sediment size d_i . Enter one of the following codes: 1 Engelund-Hansen equation, 2 Original Ackers-White equation, 3 Revised Ackers-White equation, 4 Westrich-Jurashek, 7 Parker equation, and 10 Modified Parker equation (1990).
- P_i = proportion of size fraction i in the size distribution ($0 \leq P_i \leq 1$ and $\sum P_i = 1$).

▪ Block (2) Sediment Boundary Conditions

All upstream boundaries must be specified. Either GTBDY (sediment transport rate against time), CTBDY (sediment concentration against time) or QCBDY (sediment rating curve) units may be used. The boundary data are contained in the mobile bed module data file ('filename.sed'). They can be specified in any order in the data file and may use any combination of GTBDY, CTBDY or QCBDY units. An example of the structure of this section of the file is shown in Figure 2.43.

Line	GTBDY	UPSTREAM RIVER BOUNDARY
1	rivul	
2	3	
3	1.000	0.0
4	1.15	3600
	1.150	1e20
3 + n1	NEW	
4 + n1	0.6	
5 + n1	0.3	
4+n1+n _{sed}	0.1	

Datafile Format - sediment boundary data block

Line 1 keyword 'GTBDY' or 'CTBDY' or 'QCBDY' [comment]
 Line 2 Label
 Line 3 n1, [tm]
 Line 4 to Line 3+n1 G_i, t_i for GTBDY
 C_i, t_i for CTBDY
 Q_i, C_i for QCBDY
 Line 4+n1 sizedist= 'BED' or 'NEW'
 (Input files for earlier versions of ISIS Sediment may not include this line. If it is omitted then 'BED' is assumed.)

The following lines are only required if sizedist=NEW

Line 5+n₁ to Line 4+n₁+n_{sed} P_i

Fig. 2. 43: The Sediment Boundary Conditions data files section (ISIS, 2012).

Where

- Label = node label at boundary (section label).
- n₁ = number of ensuing data pairs.
- t_m = optional keyword or value for units of time in following data set, can be any numerical multiplier or one of the following: seconds (default), minutes, hours, days, weeks, months (=30 days) or years.
- G_i = sediment transport rate (kg/s) corresponding to time, t_i (for GTBDY units).
- C_i = sediment concentration (ppm) corresponding to time, t_i (for CTBDY units).
- t_i = time (in units of t_m).
- sizedist = keyword setting the size distribution for sediment inflows. Enter: NEW if new distribution will be used or BED to use default distribution given in General Data.

➤ P_i = new grading data for sediment inflow (only required if sizedist=NEW).

▪ Block (3) Hard Bed Option

The hard bed option will prevent erosion from occurring below the initial bed elevation in the designated sections. If required, a HARD BED data block can be specified in any location after the general system parameters within the sediment module data file. Figure 2.44 present an example for this block.

Line 1 2 2+n ₁	HARD BED 3 SECT3 SECT4 SECT5
--	--

Datafile Format - Hard Bed Option


Line 1	keyword 'HARD BED'
Line 2	n ₁
Line 3 to Line 2+n ₁	label _i

Fig. 2. 44: The Hard Bed Option data file section (ISIS, 2012).

Where

- n₁ = number of ensuing node labels.
- label_i = node labels of hard bed sections.

2.4.2.4 Running the sediment transport analysis

Figure 2.45 displays the running process which start by clicking the run button , then window for selecting the time step and the output time step will appear (Fig 2.45 window 1), select the time step as in window (1) and the simulation time. Before running switch to the options tab (window 2) and activate the sediment module, then start the model running.

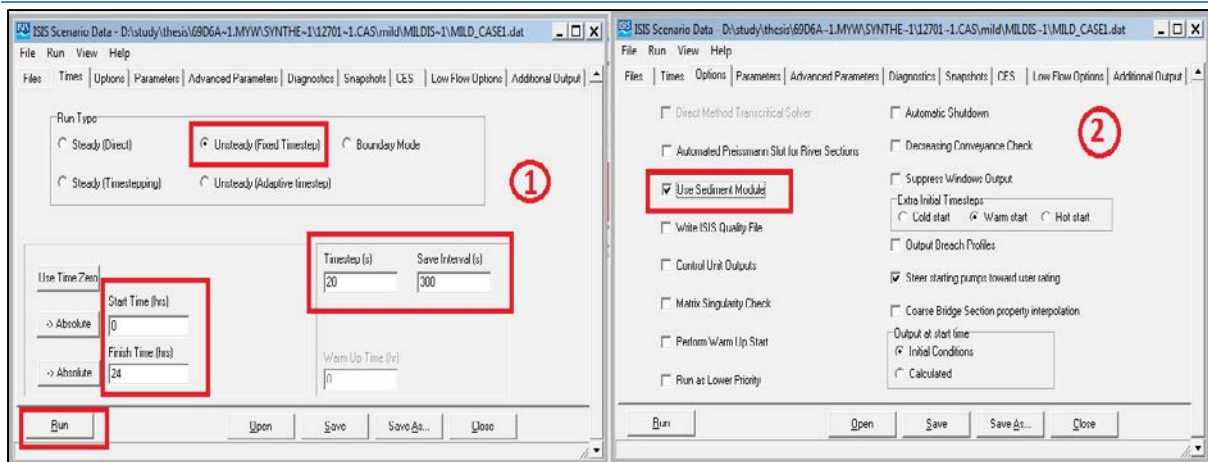


Fig. 2. 45: Running sediment transport model by ISIS (ISIS, 2012).

2.4.2.5 Extracting the outputs.

The time varying results of the mobile bed run are written to the binary file 'filename.zze'. The results can be processed using the ISIS TabularCSV output as shown in Fig 2.46 , be sure from selecting the appropriate file type from the drop down menu, ISIS Sediment Results (*.zze).

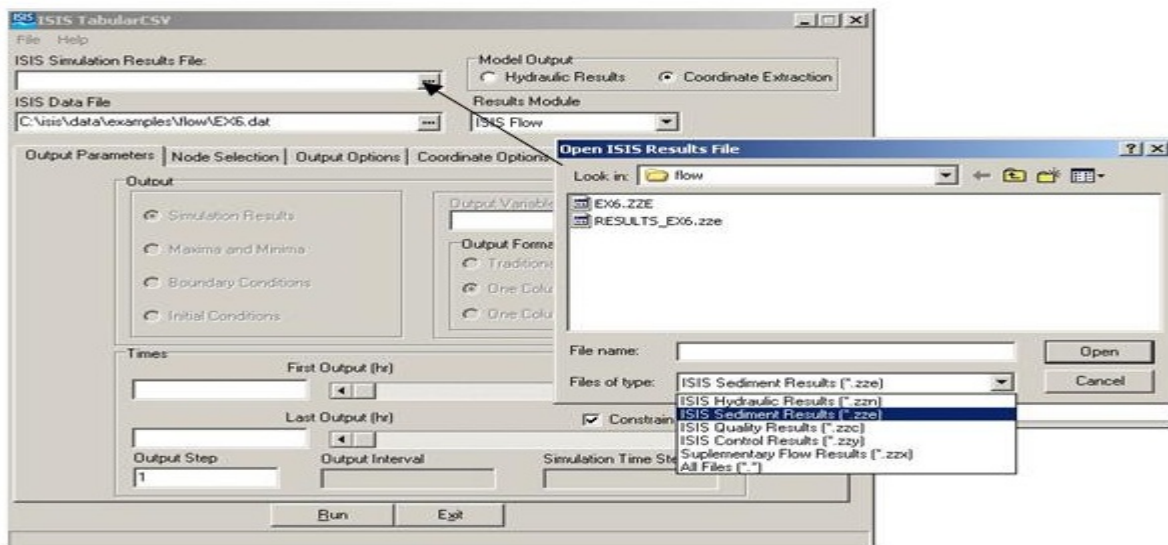


Fig. 2. 46: Opening the mobile bed results binary file 'filename.zze' using the ISIS TabularCSV output (ISIS, 2012).

ISIS TabularCSV output supplies output in comma separated variable (CSV) format for easy access and further manipulation in spread sheet packages, such as Microsoft Excel. The ISIS TabularCSV is accessed from the Tools menu.

The output options are (1) Simulation Results - output at selected time intervals at all or selected nodes, (2) Maxima and minima of all or a single variable at all or selected nodes, (3) Extract new boundary conditions, (4) Initial conditions output. Make sure from selecting the output of the needed choice in the output parameters Tab of the ISIS TabularCSV window, as shown in the left hand side of Figure 2.47.

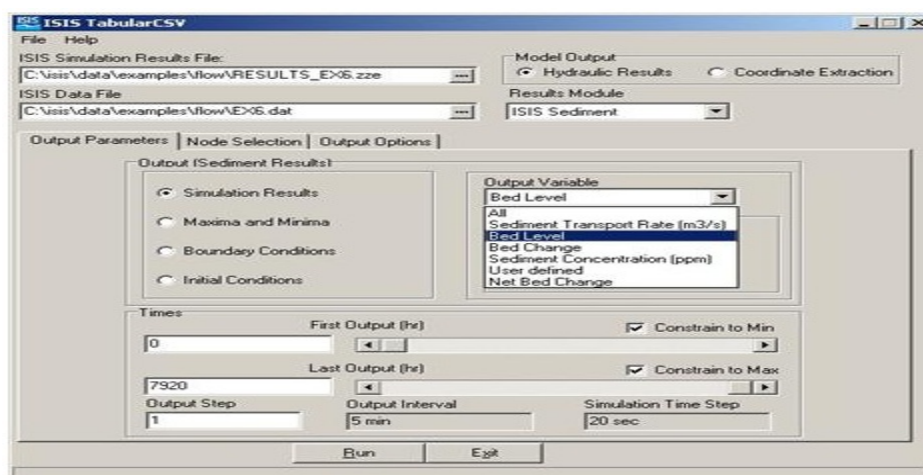


Fig. 2. 47: TabularCSV window and available results Mobile Bed Module results.

The output options can be applied to the following results, which are available for inspection: Sediment transport rate (in m³/s), Bed elevation (in m), change in bed elevation during the last time step (in m), sediment concentration (in ppm), user defined variable, is stated in the data file, and net change in bed elevation (in m).

2.5 Comparative hydraulic analysis by ISIS, Basement, and HEC-RAS

In this part; a comparison among the three software using synthetic case study Fig 2.48 will be discussed. The case is composed of six reaches, while two widths are used in addition to the bed drop. Looking at the differences in the water surface profile and how the software deal with sudden divergent, sudden enlargement, and drops in bed level is the aim from this comparison.

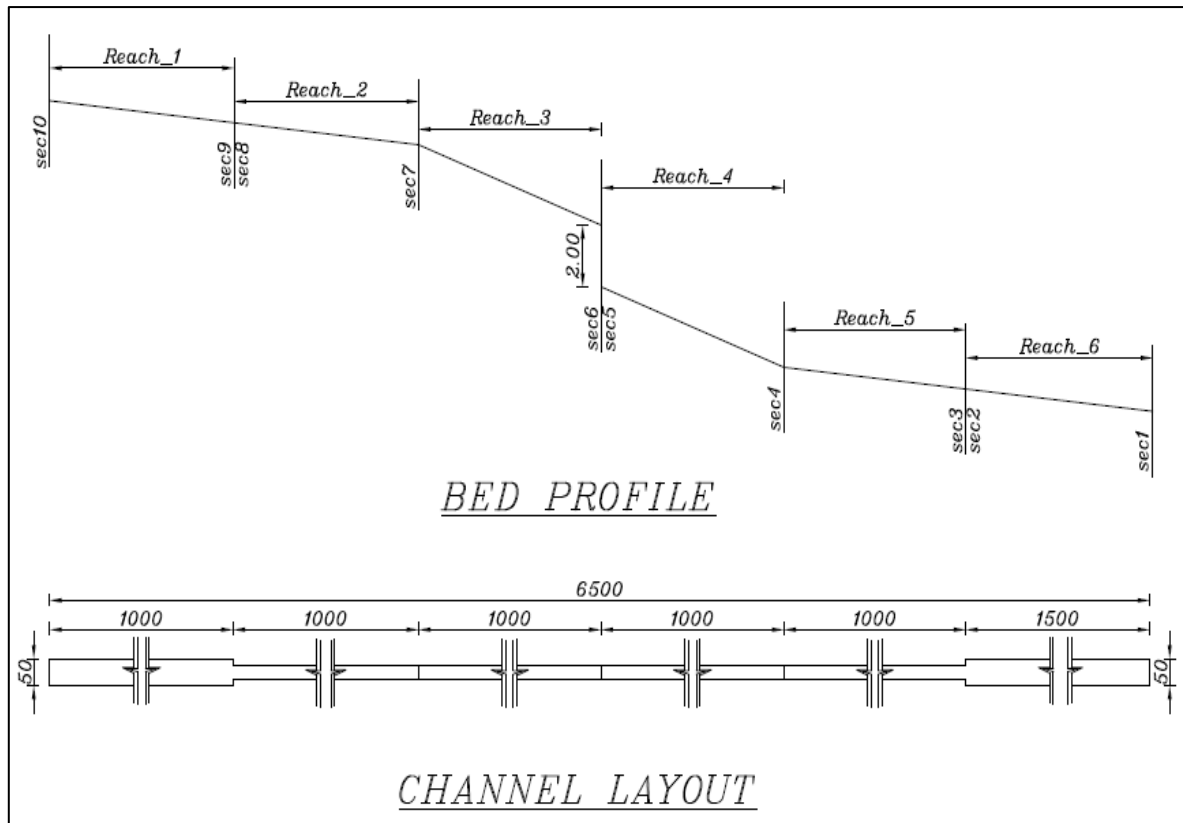


Fig. 2. 48: Synthetic case study with sudden enlargement and bed drop.

As table 2.2 presents; there are four cases studied by the three software: (1) steady case with discharge $3000 \text{ m}^3/\text{s}$ and 250m spatial discretization, (2) steady case with discharge $3000 \text{ m}^3/\text{s}$ and 50m spatial discretization, (3) unsteady case with a peak discharge $3000 \text{ m}^3/\text{s}$ and 250m spatial discretization, and (4) unsteady case with a peak discharge $3000 \text{ m}^3/\text{s}$ and 50m spatial discretization. The table also includes the levels, the width of each reach, the slope, and the manning friction coefficient used in the analysis for each reach. The distance of each section measured from upstream is reported, where the locations of the sections are shown in Fig 2.48.

The previous four cases analyzed by the three software depend on the condition defined in table2.2. Two spatial discretization used to study the effect of spatial discretization in the analysis. The results are described in below.

Comparative study of different scenarios for the morphological evolution in a river stream

Reach	length	slope	width	Friction(n)	Sections levels(m)			
Reach_1	1000	0.002	50	0.04				
Reach_2	1000	0.002	25	0.04	sections	upstream distance	BED LEVEL	BANK LEVEL
Reach_3	1000	0.015	25	0.04	section 10	0	1000	1100
Reach_4	1000	0.015	25	0.04	section 9	1000	998	1098
Reach_5	1000	0.002	25	0.04	section 8	1000.1	998	1098
Reach_6	1500	0.002	50	0.04	section 7	2000	996	1096
units	meter	--	meter	sec/meter ^(1/3)	section 6	3000	981	1081
Cases studied					section 5	3000.1	979	1079
Case_1	steady analysis with 250 m spatial discretization				section 4	4000	964	1064
Case_2	steady analysis with 50 m spatial discretization				section 3	5000	962	1062
Case_3	unsteady analysis with 250 m spatial discretization				section 2	5000.1	962	1062
Case_4	unsteady analysis with 50 m spatial discretization				section 1	6500	959	1059

Table 2. 2: Properties of the synthetic case study.

A- Steady case with discharge 3000 m³/s and 250m spatial discretization.

In the steady analysis; there are no changes in flow features (velocity and discharge) with time, but with spatial distances only. Although of using the same spatial discretization, the three programs give different water profile as shown in Fig 2.49.

Fig. 2. 49: Steady water profile using 250 m spatial discretization.

The differences in the water surface elevation WSE are mainly due to the different factors used to calculate the head losses in the divergent and enlargement, also It is clear that ISIS uses simplified method to calculate the water surface at the bed drop i.e. it assume that no energy lost in the drop, hence the specific energy is the same before and after the bed drop.

B- Steady case with discharge 3000 m³/s and 50m spatial discretization.

With more spatial discretization the three WSE become close but still the differences are due to the losses treatment within each program as shown in Fig 2.50.

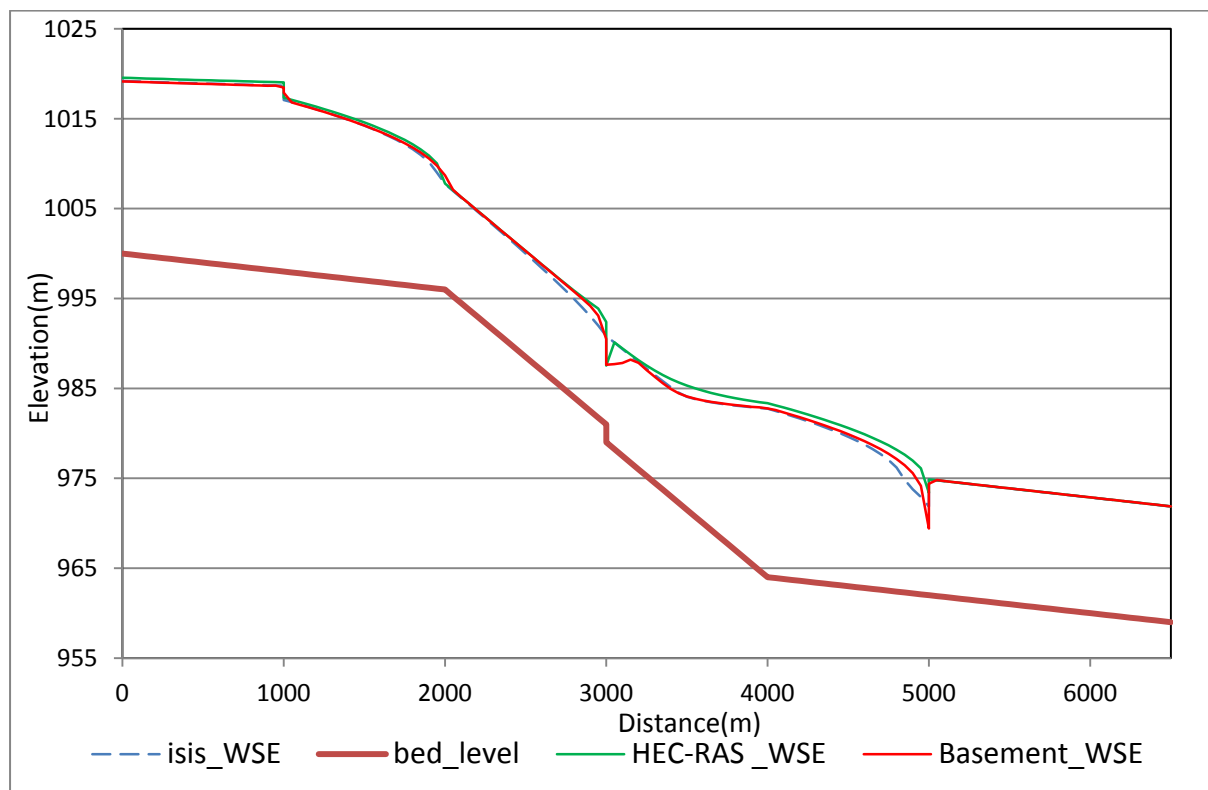


Fig. 2. 50: Steady water profile using 50 m spatial discretization.

The steady analysis using any software from the three used will run whatever the spatial step because there is no condition for the stability , but the benefit from more discretization is getting smooth WSE which is more close to the real one.

C- Unsteady case with 250m spatial discretization.

The same synthetic cases studied considering unsteady flow represented by triangular hydrograph (Fig 2.51) with one day as base time, 3000 m³/s as peak discharge, and 1000 m³/s as base discharge. The aim from selecting this hydrograph is comparing the maximum WSE computed from the unsteady analysis with the steady analysis based on the peak discharge.

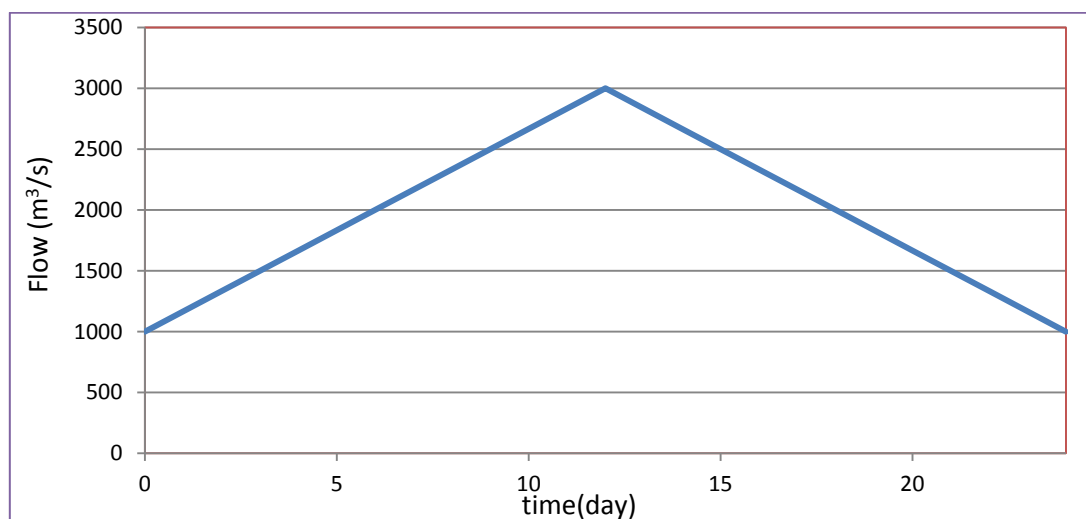


Fig. 2. 51: Considered flow hydrograph for unsteady analysis.

The spatial discretization considered each 250 m. but as described in Fig 2.48 and table 2.2, the distance between the sections at turning points from enlarge sections to narrow section also at the drop is only 10 cm. This means that the spatial steps is not same, but it vary from very narrow value (10cm) to very wide value (2500 cm). With this huge variation in the time step; the CFL range ($0 < CFL < 2$) can't be satisfied in case of using fixed time step. To treat this problem; adaptive time step is needed otherwise the model will become divergent.

HEC-RAS uses only uniform (fixed) time step within the model. So with small time step, the spatial distance (250 m) is not proportional to this time step. Also with wide time step, the spatial distance 10 cm is not proportional to it

and both the two cases can't satisfy CFL limits hence HEC-RAS can't analyze this problem.

ISIS has two types of solvers: unsteady with fixed time step (unified time step within the whole model whatever the spatial step) and unsteady with adaptive time step (ISIS selects the time step depend on the spatial step considering the limits of CFL number). So with the fixed time step solver; the model becomes divergent because unified value for CFL can't be satisfied, hence the only way is using the adaptive time step solver.

With Basement; this type of problem is treated by selecting maximum value for the time step, hence Basement selects adaptive step lower than the maximum time step assigned before. This adaptive time step selects to satisfy the CFL number assigned in the model.

AS a summary; HEC-RAS model for this case is divergent, although of using implicit finite difference scheme because it unifies the time step. ISIS work only for such problems by using adaptive time step solver. In case of divergence with Basement; the maximum time step must be enlarged to allow higher values for the adaptive step which can affect the results accuracy.

The following figure present a comparison between maximum WSE calculated by ISIS and WSE calculated using HEC-RAS as a result of steady analysis with the peak discharge. It shows coincidence between the maximum WSE and the profile of peak discharge, which means that these types of numerical problems can be overcome by using the steady analysis instead of using the unsteady.

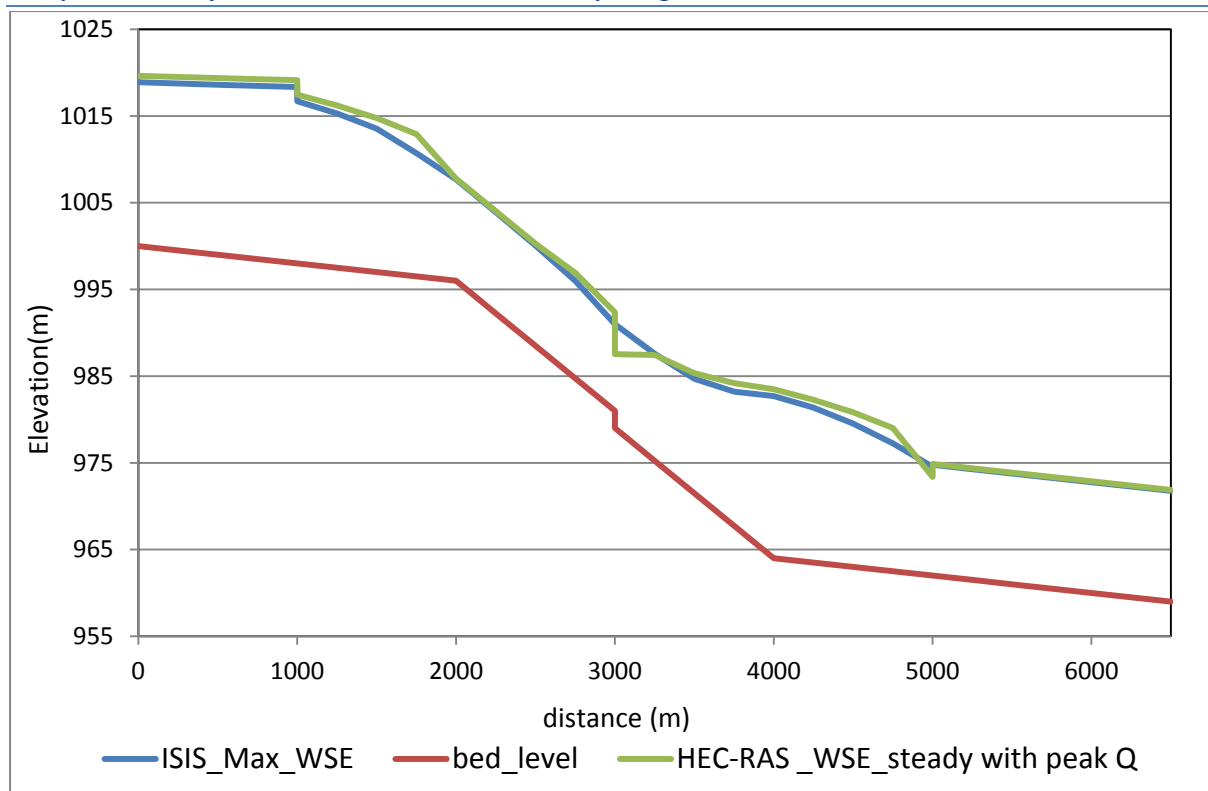


Fig. 2. 52: Comparison between MAX. WSE by ISIS and WSE by HEC-RAS with steady peak discharge.

D- Un Steady case with 50 m spatial discretization.

The more spatial discretization allows the model to be more stable. So HEC-RAS model become stable with 50 m discretization. The profiles of maximum WSE calculated using unsteady analysis by HEC-RAS and ISIS are compared with the WSE calculated using steady analysis by Basement with the peak discharge and the same spatial steps. The result of the comparison is shown in Fig 2.53. It shows that the profile become more smooth and close to each other. This means that the computations cost and the stability problems can be solved by using steady analysis with peak discharge.

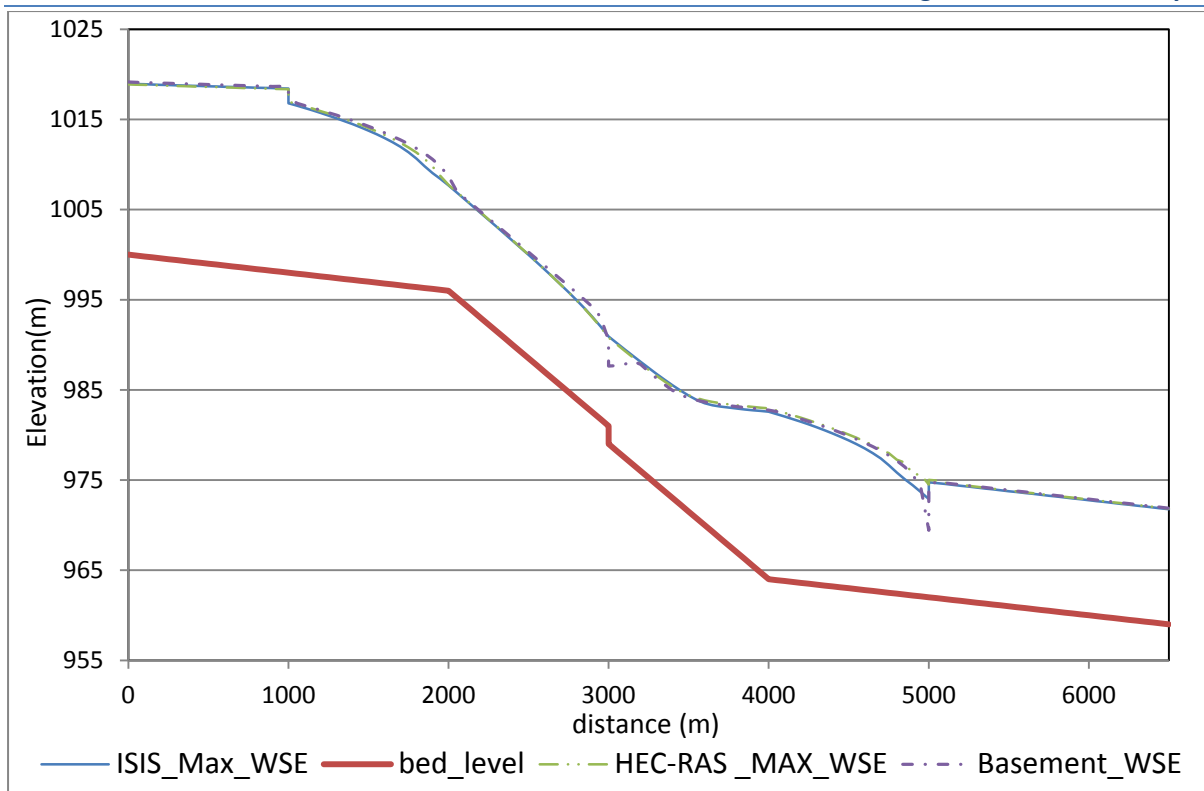


Fig. 2.53: Comparison between MAX. WSE by ISIS and HEC-RAS with WSE by Basement with steady peak discharge.

Finally; the results of this comparison can be summarized in the following points:

- The spatial and time steps have a great influence in the stability of the numerical codes. It must be proportional to satisfy the CFL condition.
- The more discretization gives more accurate results, so the modeler must equilibrate the computation cost with the purpose from the analysis.
- Mainly the differences in the calculations depend on the treatment, by the software, for sudden change in the cross section width or depth.
- HEC-RAS and ISIS use the same numerical scheme (Preissmann scheme), but the treatment of concentrated losses are different.
- It is better to use the numerical solvers with adaptive time step, when the differences in distances are huge.

Comparative study of different scenarios for the morphological evolution in a river stream

- The numerical codes based on finite volumes, like Basement, doesn't suffer from the numerical stability like finite differences codes. Only with more discretization in finite volumes codes the accuracy of the results becomes higher.
- Unsteady analysis is costly from computational point of view, so it can be replaced by the steady analysis with peak discharge if the only aim is the computation of maximum WSE.

In the following chapters; this hydraulic comparison among these programs is going to enlarge to involve the morphological evolution in a river stream.

3 Modelling and Analysis of Synthetic Channel Cases

3.1 Introduction

This chapter introduces an investigative study using the numerical codes discussed in chapter 2 through simple synthetic cases. The need for such simple analysis comes from the complex nature of the reality in case of modeling real cases such as Mallero River, which will be the subject of the next chapters.

In item 1.14, a number of critical objectives and issues were identified, which are aimed to overcome in this work. The modeling strategies followed here want to respond to these objectives and approach to reality in a more precise. The following cases are studied (which were explained in detail in the referred item):

- Upstream feeding by sediment;
- Effect of lateral feeding by sediment in an intermediate river section from external source;
- Sequent movable and hard beds effect.
- Sorting of sediments in case of using multiple non-uniform grain sizes in representing the bed and feeding granulometry.

In-between; the sensitivity of the modeling to some parameters and effects are discussed like the bed friction effect, spatial discretization and control volume thickness. At the tail of the chapter; the results obtained by modeling these cases and the sensitivity analysis will be summarized to be used as a guide in studying the aforementioned Mallero case.

3.2 Properties of the synthetic cases

The analysis aims to make a comparison between the morphological evolution in both the mild and the steep channels, so two synthetic channels are built; the first is mild with bed slope 0.2% while the second is steep with bed slope 2%. The following table summarizes the geometric properties of the two channels.

code	channel type	bed slope	side slopes (Hz/vl)	bed width	banks elevation	channel length	u/s bed level	D/s bed level	manning coefficient (n) s/m ^{1/3}
M1	mild	0.20%	0	50 m	100 m	10 km	1000	980	0.04
M2	mild	0.20%	0.25	50 m	100 m	10 km	1000	980	0.04
S1	steep	2%	0	50 m	100 m	10 km	1000	800	0.04
S2	steep	2%	0.25	50 m	100 m	10 km	1000	800	0.04

Table 3. 1: The geometric properties of the synthetic cases.

The manning coefficient presented in the table represents the total roughness coefficient of the channel’s bed i.e. the roughness due to all the sources of friction (skin, bed forms and vegetation). As discussed in item 1.6; the roughness must be considered in the bed load modeling is the skin friction only, while the bed form and vegetation roughness use along with the skin friction in case of calculating the water surface profile. As discussed in items 2.3.2 and 2.3.3; HEC-RAS calculates the skin friction automatically based on the assigned granulometry and uses it in the calculations of bed load and regardless the assigned value for roughness (it use the assigned value for the roughness only in fixed bed hydraulics). This means that the value of manning in table 3.1 is useless in case of using HEC-RAS. Basement has two options either using the assigned value for friction coefficient, which should be the skin based, or it can calculate the skin friction automatically, while in ISIS the skin friction coefficient must be evaluated and assigned directly. Finally ISIS does the calculations depending on the assigned value of friction while HEC-RAS

uses the skin friction automatically. Basement can work with the two selections either automatically or manually.

Regarding the transport capacity formula; Meyer-Peter and Müller (item 1.7.1) used in all the models use uniform granulometry, while MPPM (1.7.2) formula used for non-uniform granulometry.

As shown in table 3.1; for both the mild and steep cases there are two types of channels, the first is rectangular while the second is trapezoidal with side slope 1:4. The aim of using these two types of channels, e.g. M1 and M2, is checking how the sediment distribution in the cross section will be? Indeed, ISIS uses many cases of sediment distribution depending on the user selection (see Fig 2.41).

The sediment properties and water properties used in the analysis are summarized in table 3.2, while the use of each property is discussed in item 1.4. As shown in the table there are specific median diameter related to the channel type (in case of non-uniform granulometry, the gradation curve will be used instead of d_{50}).

water density	S	shape factor	porosity	kinematic viscosity	Water unit weight	repose angel	d_{50} mild	d_{50} steep
1000	2.65	0.6	0.4	1E-06	9810	30	2	20
kg/m ³	-	-	-	m ² /s	N/m ³	degree	mm	mm

Table 3. 2: Sediment and water properties.

The model initial condition and upstream sediment boundary will be assigned depending upon the in-flow discharge of water. The water downstream boundary is the bed slope (2 ‰ for mild channel), while the constant bed level is the downstream sediment boundary. The upstream water discharge is the uniform flow (with water depth = 4m) which can be calculated by manning formula, so $Q_w = 510.37 \text{ m}^3/\text{s}$ and $1613.94 \text{ m}^3/\text{s}$ for mild and steep

channel respectively. Hence the initial condition for each cross-section equals the feeding discharge, while the sediment boundary (feeding) will be assigned as a ratio of the sediment transport capacity that calculated using the total friction coefficient and MPM by $Q_{sm} = 0.4339 m^3/s, Q_{ss} = 13.72 m^3/s$ for mild and steep channel respectively. The locations where the sediment discharges will be assigned are shown in Fig.3.1.

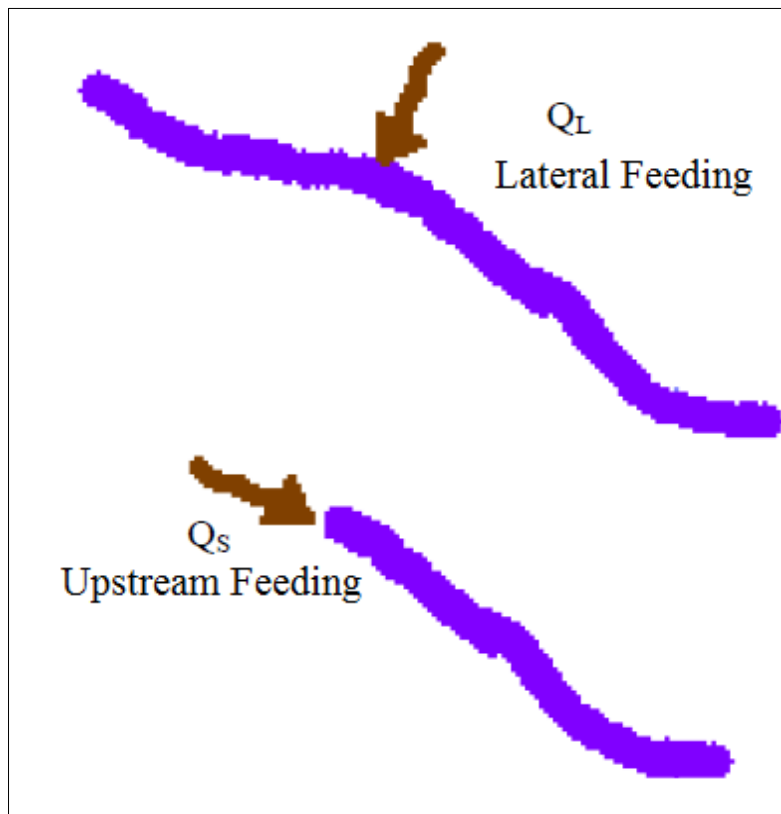


Fig. 3. 1: The locations and symbology of sediment feeding.

The location where Q_s assigned is the upstream section (first section), while the lateral feeding Q_L assigned at the mid of the model (5km from upstream or downstream). The values of Q_s and Q_L is a ratio from the transport capacity Q_{sm} or Q_{ss} , this ratio are expressed as in Eq 3.1.

$$\text{For mild case} \quad Q_s = K_{sm} * Q_{sm} \quad \text{and} \quad Q_L = K_{Lm} * Q_{sm} \quad 3.1$$

$$\text{For steep case} \quad Q_s = K_{ss} * Q_{ss} \quad \text{and} \quad Q_L = K_{Ls} * Q_{ss} \quad 3.2$$

Where K_{sm} , K_{ss} , K_{Lm} and K_{Ls} (or briefly K) are the ratios of sediment feeding as a percentage from the transport capacity. K_{sm} , for example, means the ratio of upstream feeding relative to the transport capacity for the mild channel case.

- $K = 1$ means that feeding discharge of sediment equal to the transport capacity;
- $K = 0$ means no sediment feeding;
- $K < 1$ means that sediment feeding is less than the transport capacity ;
- $K > 1$ means that the sediment feeding is more than the transport capacity.

By using the previous channel geometry and the boundary conditions, the morphological evolution is modeled by considering the simulation time for the entire models is one day.

3.3 Comparative morphological analysis by HEC-RAS, Basement and ISIS

HEC-RAS and Basement use the total friction in calculating the water surface, but in the morphological evolution analysis; HEC-RAS uses the skin friction in calculating the sediment transport capacity, while Basement can be adapted to use either the total or the skin friction in calculating the sediment transport capacity. So the comparison between Basement and HEC-RAS will depend upon the skin friction that calculated automatically by each code.

ISIS uses the assigned value for calculating the water surface and the transport capacity, so another comparison depends on the total assigned roughness will be held between ISIS and Basement.

3.3.1 Comparison between HEC-RAS and Basement

The mild channel M1 (table 3.1) used to held this comparison using the boundary conditions given in previous item (3.2). Two values of K_{sm} are used; the first represent the case of no feeding ($K_{sm}=0$) and the second represent feeding by 3 times the transport capacity ($K_{sm} = 3$). The ways of calculating the skin friction either by HEC-RAS or basement are shown in item 2.3.3. By using the skin friction in the calculations; the results of bed and water level at the start and final time (24 h) are shown in fig 3.2.

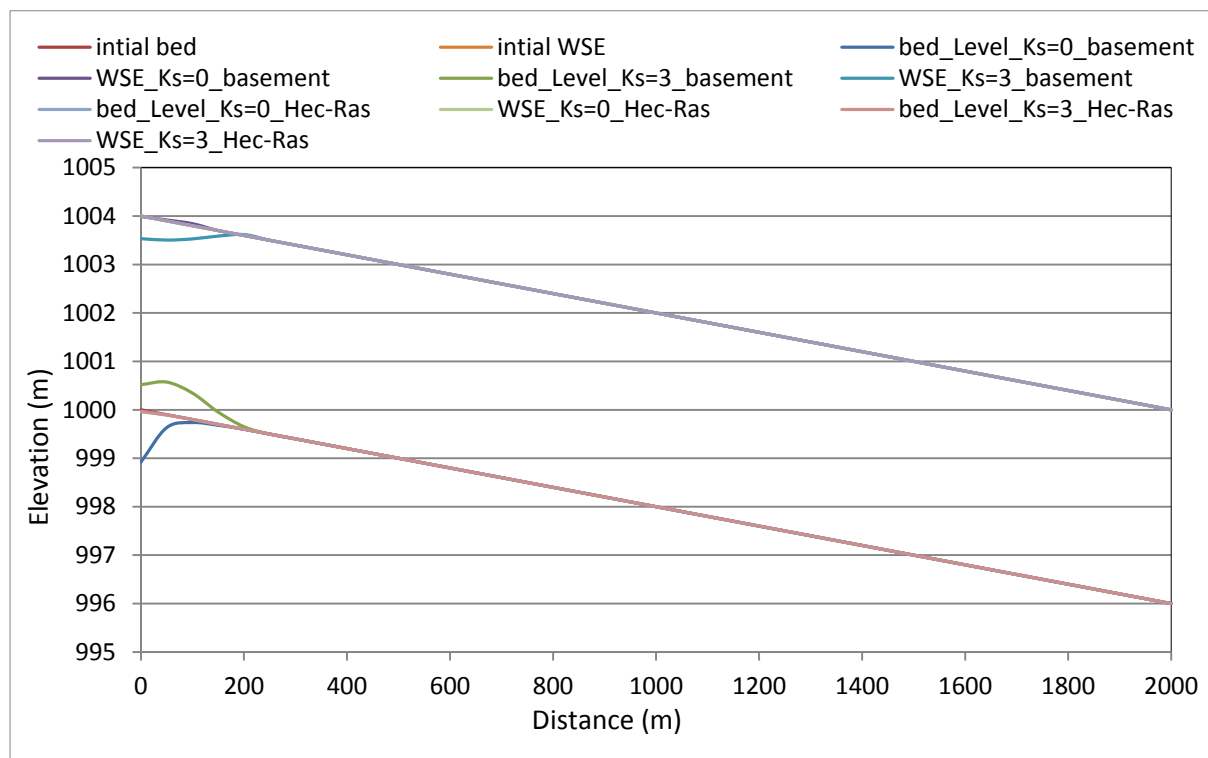


Fig. 3. 2 : Comparison between HEC-RAS and Basement in mild channel with 2‰ bed slope.

As shown; degradation occurs when there no sediment feeding, while aggradation occurs when $k_{sm} = 3$. This aggradation leads to lowering in water surface because of increasing in bed slope and hence the velocity. Only these conclusions belong to Basement, while the differences in bed and water surface by HEC-RAS are not visible. To see the reason for this bug; the skin bed share stress at the final time ($t = 24$ h) is drawn in the following figure.

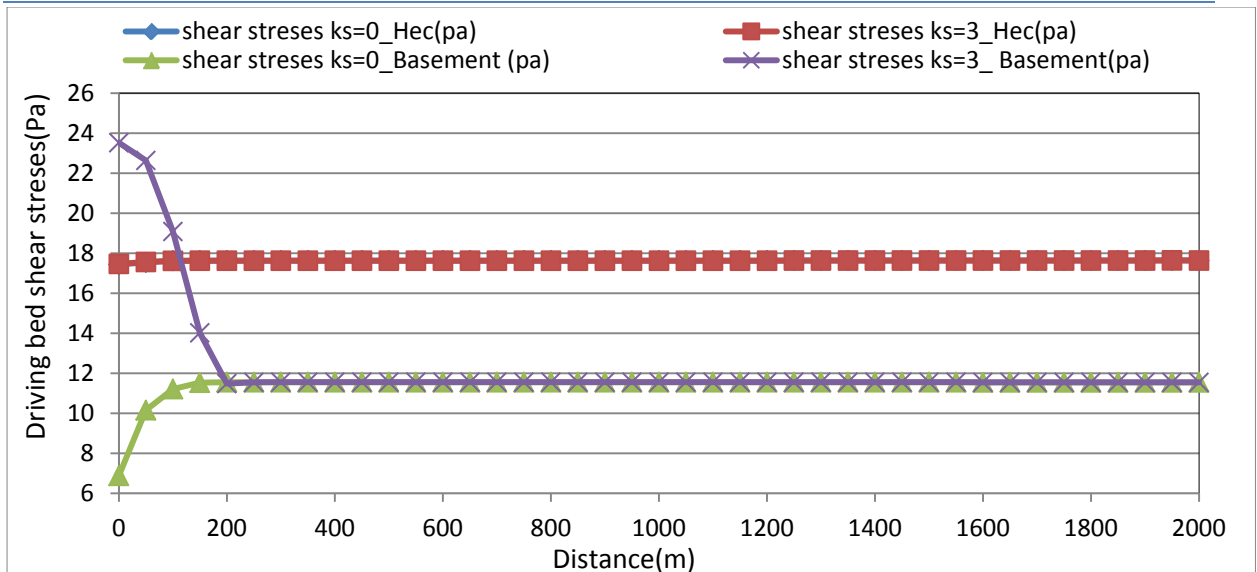


Fig. 3. 3: Bed skin shear friction calculated by HEC-RAS and Basement.

As shown; the skin bed friction calculated by HEC-RAS is more than that calculated by Basement. At the upstream, the skin stresses by Basement increases when $k_{sm} = 3$ and decreases when $k_{sm} = 0$, because of the change in the slope with time, while the skin stresses by HEC-RAS remain constant. Although of the high value of the skin friction more than these got by Basement, the transport capacity is very small as shown in figure 3.4 even by using the same transport capacity formulae (MPM).

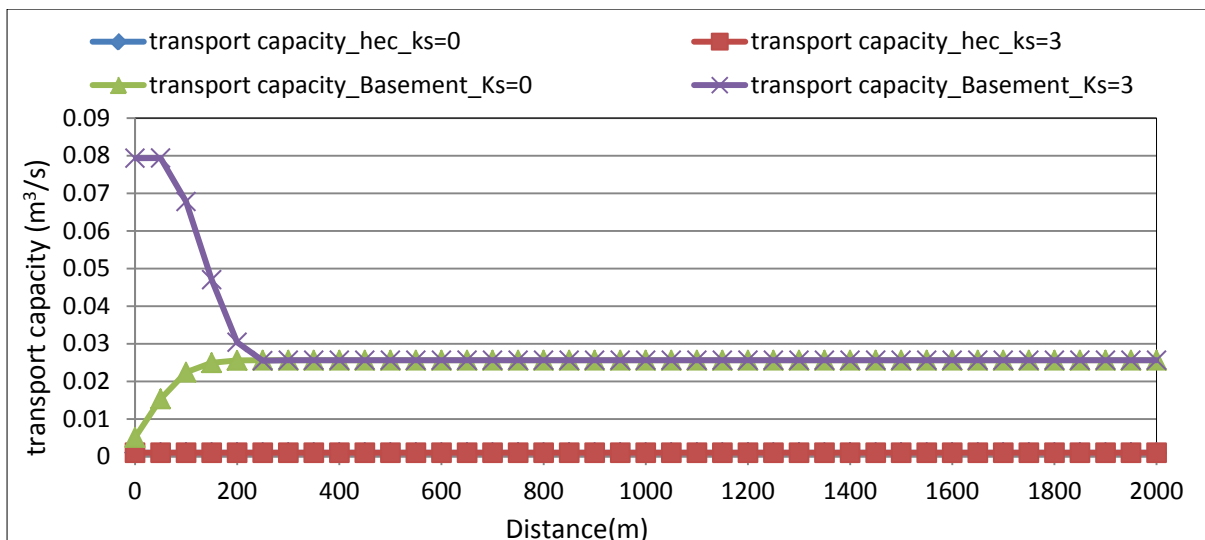


Fig. 3. 4: Transport capacity (MPM) calculated by HEC and Basement.

This wrong estimation may lead to no degradation or aggradation by using HEC-RAS as shown in Fig.3.2, while Basement gives results seem logical. So starting from now, HEC-RAS will be dropped not only because it gives wrong values but it has also some bugs like inconsistently numbers when passing from computation of mass to computation of volume (the transformation from computation of masses to volumes is shown in figure 2.18 in the window named "sediment output options").

Finally; it is important to comment that when there is no sediment feeding the bed degrades gradually at upstream, while at high rates of sediment feeding the sediment aggrade gradually. This aggradation and degradation cause changes in the bed shear stress, the transport capacity and the water profile with each time step, because of the change in bed level.

3.3.2 Comparison between ISIS and Basement

ISIS is very sensitive to the spatial discretization, so 20 m used as a spatial step but still the model divergent (may be because of the potential weak of the used version' 'free version"), which means that ISIS is not practical software to model the sediment transport. So ISIS as well dropped from the analysis in the remainder work.

3.4 behavior of morphology in channels have uniform bed gradation

The morphological evolution is studied through some synthetic models represent the upstream and the lateral feeding in both mild and steep channels as shown in table 3.3.

model	channel	Ks	KL
#1	M1	0.5	0
#2	M1	3	
#3	S1	0.5	
#4	S1	3	
#5	M1	0	
#6	M1	1	3
#7	M2	1	3
#8	S1	1	3
#9	M1	0	3
#10	S1	0	3
#11	M1	0	0
#12	M1	2	0
#13	S1	0	0
#14	S1	2	0

Table 3. 3: The combination of sediment feeding.

3.4.1 Case of upstream feeding by uniform sediment

The case of upstream feeding of sediment can occur due to the erosion in the catchment, then the water carry the sediment with it. Usually the bed slope in the real rivers change, that affect the transport capacity and lead to aggradation by moving from high slope to low slope and degradation by moving from low slope to high slope. In the following; a comparison between the aggradation and degradation in the upstream due to feeding by rates less and more than the transport capacity for mild and steep channels respectively.

3.4.1.1 Mild channels

Model #1 shown in table 3.3 is used to study the degradation in the upstream. The reason for the degradation is the feeding by rate equal to half the transport capacity ($k_s=0.5$), so the upstream erode to provide sediment equal to the transport capacity. Because the feeding is less than the transport capacity in the whole simulation time, the erosion increases with time as shown in figure 3.5.

Comparative study of different scenarios for the morphological evolution in a river stream

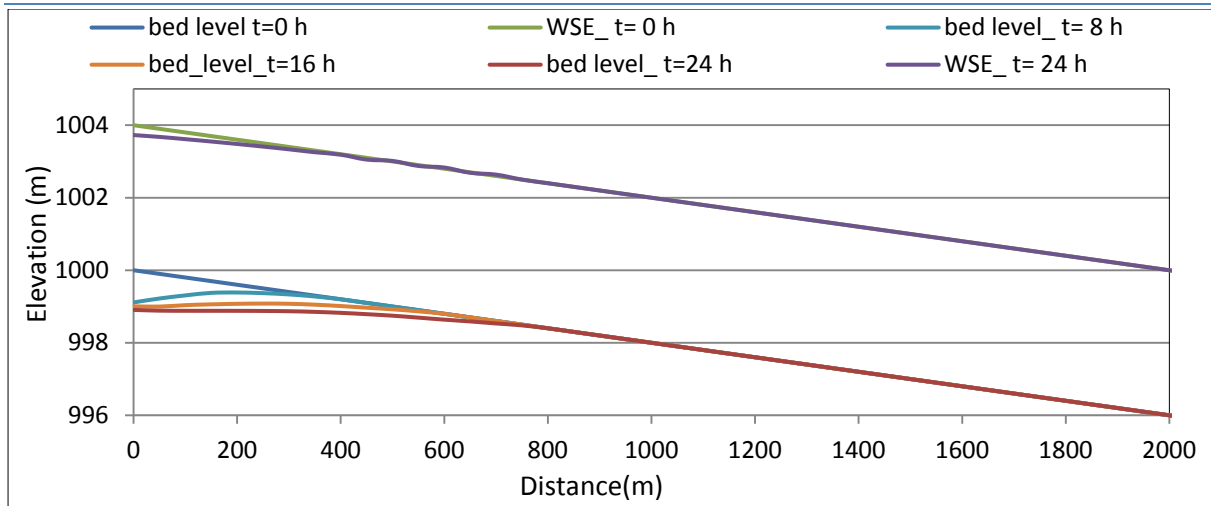


Fig. 3. 5: Degradation at upstream due to low feeding of sediment (Mild channel M1, $k_s=0.5$)

If the simulation time increased, the erosion length and depth will increase. Also by the time the water surface affected by the erosion in the bed i.e. it become lower with the higher erosion (fig 3.5).

The opposite behavior takes place when the feeding rate is higher than the transport capacity as the case of model #2 shown in table 3.3 i.e. the aggradation increases with time as in figure 3.6 which increasing the water level. Hence, if the banks level is less than the new water surface, flooding will occurs in the zone of sediment deposition.

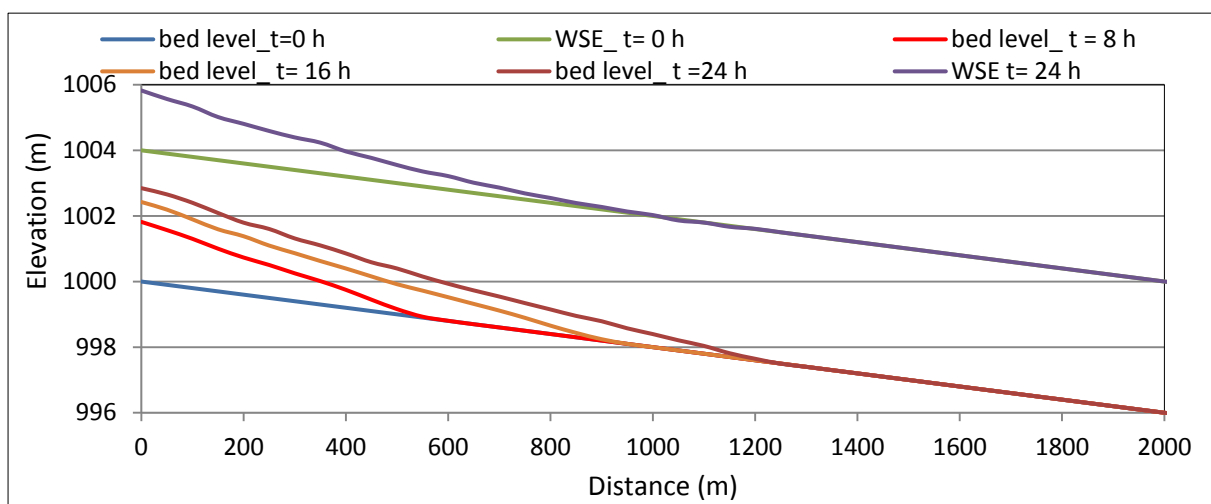


Fig. 3. 6: Aggradation at upstream due to high feeding of sediment (Mild channel M1, $k_s=3$).

3.4.1.2 Steep channels

In case of steep slope channel (S1) that has 10 times the bed slope and median diameter of the mild one (M1); the same case of erosion take place with model #3, that gives higher amount of degradation, since the depth of erosion reaches 10 meters . Also, the length of erosion increases as shown in figure 3.7, which is 10 times the erosion depth in mild channel.

In case of aggradation in steep channel created using model #4, the depth of aggradation (fig 3.8) become more than 10 times the aggradation in mild channel also the erosion length become higher. This means that; it is difficult to relate among the bed slope, the feeding discharge, the median diameter and the erosion or deposition depth and length i.e. it is difficult to generalize a formula that quantify the erosion depth and width by knowing the bed slope, the feeding discharge and the median diameter, but a formula may granulize for mild and steep channels separately.

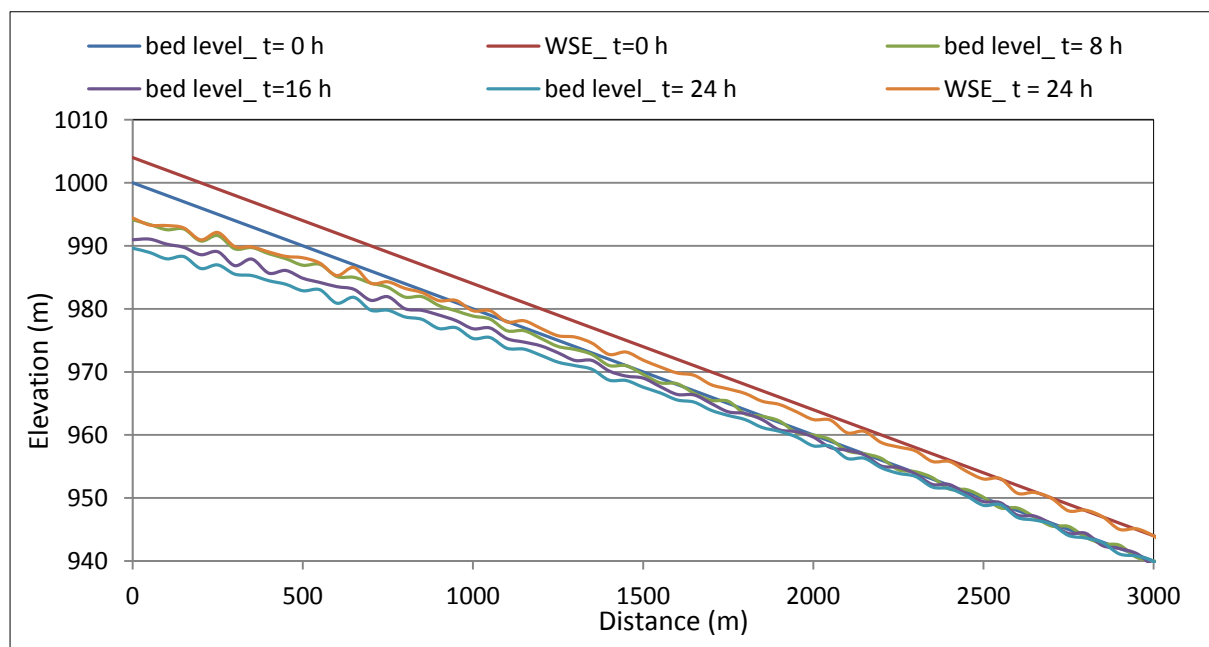


Fig. 3. 7: Degradation at upstream due to low feeding of sediment (steep channel S1, $k_s=0.5$)

Comparative study of different scenarios for the morphological evolution in a river stream

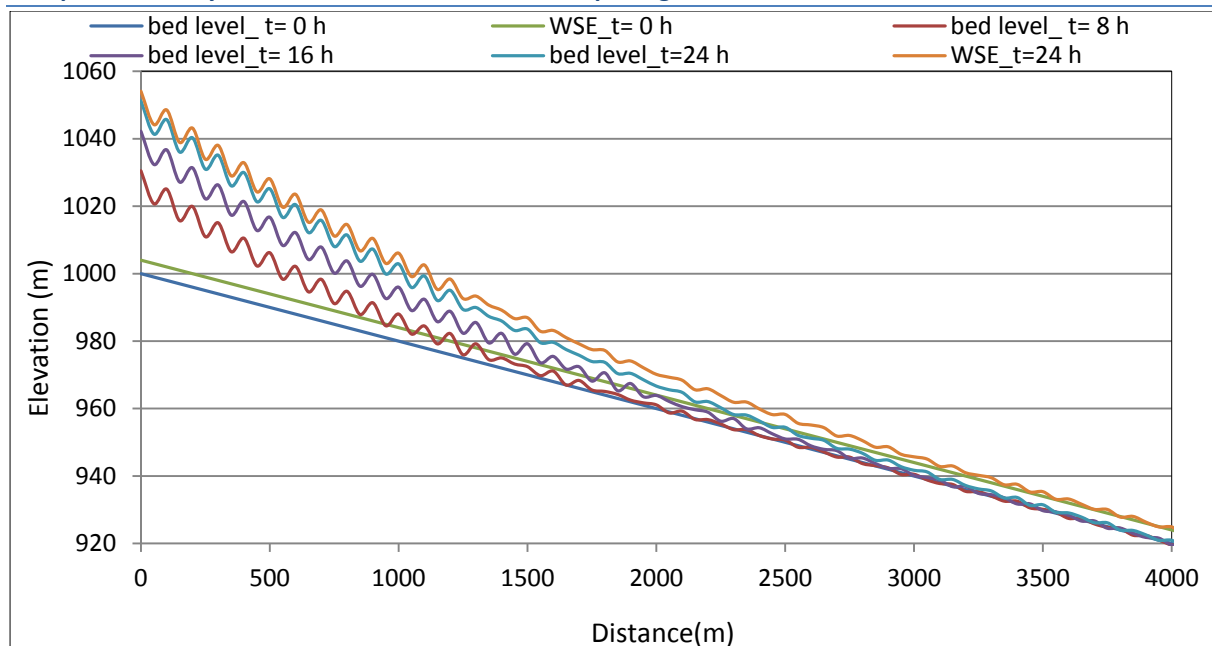


Fig. 3. 8: Aggradation at upstream due to high feeding of sediment (steep channel S1, $k_s=3$).

As may be noted in fig 3.7 and 3.8; the shape of meandering in the bed and water profiles appear in the steep cases, this is because of the numerical effect. These fluctuating shapes can be overcome by using narrow spatial steps (as will be discussed later in item 3.4.2.3).

3.4.1.3 Effect of skin friction

The roughness coefficient used in all the previous models (#1- #4) is the total one given in table 3.1, while the roughness coefficient must be used in the bed load calculations is Nikaradse roughness (grains roughness). Using Nikaradse roughness; decreases the transport capacity since it decreases the driving shear stresses. Hence the erosion and deposition rates must decrease i.e. the volume of sediment transport is less.

A comparison between the using of the skin friction and the using of the total friction in representing the bed shear stresses using model #2 and model #5 given in table 3.3 is shown in Fig 3.9.

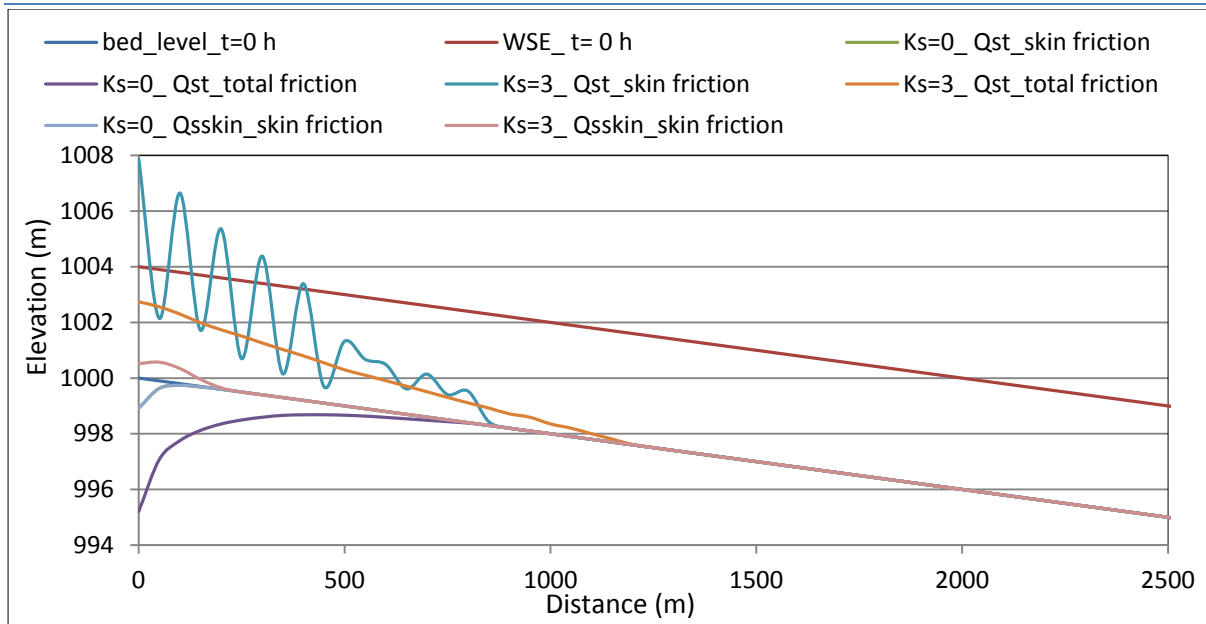


Fig. 3. 9: Effect of using skin friction and total friction in representing the bed shear stress.

The transport capacity by MPM is calculated twice; one based on the total shear stress (Q_{st}) and the second based on the skin friction (Q_{sskin}). Then, the model fed by nothing and 3 times Q_{st} or Q_{sskin} , with considering the total friction or the skin roughness in bed shear stress calculations. The figure shows that, using the skin friction in calculating both the transport capacity and the bed shear stress the degradation or the aggradation is less than that in case of using the total friction, while in case of feeding by ratios calculated using the total roughness along with using the skin shear stress, it seems that the model is fed by high ratio of sediment and vice versa. Finally, the cases of no feeding (skin friction based or total friction based) with skin friction in the bed stress are same i.e. “Ks=0_Qsskin_skin friction” and “Ks=0_Qst_skin friction” are obviously the same, since there is no feeding and the bed shear is computed in the same way.

3.4.2 Case of lateral feeding by uniform sediment

The case of lateral feeding represents in reality the case of landslide (debris flow), so the models #6 to #8 shown in table 3.3 are built and fed by sediment

without water in the mid length of the synthetic case by 3 times the transport capacity ($k_t=3$) along with feeding the model by the transport capacity at upstream ($K_s=1$).

3.4.2.1 Mild channels

The mild channel case is modeled (#6); the results are shown in figure 3.10. The sediment deposits in the feeding location, since the water is able to transport one third the feeding rate only. The remainder two third deposits and forms submerged dam and lake behind this dam. The height of the dam and the stored volume increases with time as long as the sediment feeding is continuous. The figure shows that no erosion or deposition in the upstream since the feeding equals the transport capacity.

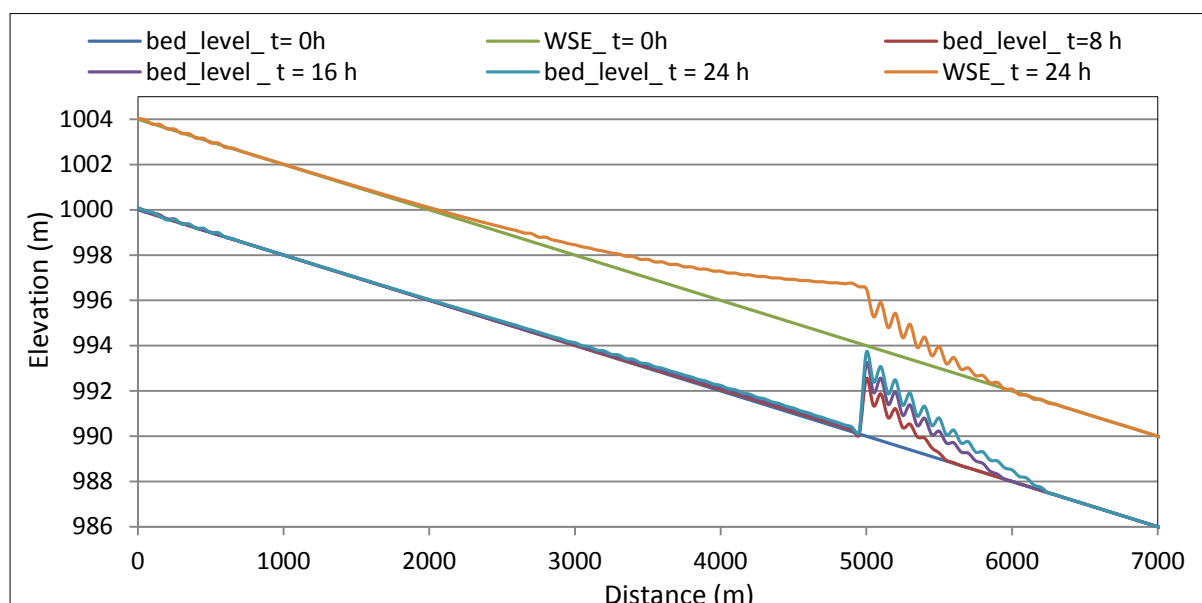


Fig. 3. 10: Dam formation in mild channel due to the lateral feeding of sediment.

As shown in the figure; the water overtops the submerged dam and extends the base of that dam in the downstream while the dam's upstream is sharp, which is contrary to nature because the model doesn't consider the sediment distribution except that moving in the water direction.

To see the sediment distribution in the cross section at the dam, after the deposition; model # 7, which uses the trapezoidal channel M2, is studied. The way of how Basement distributes the sediment is shown in figure 3.11. The figure shows that it distributes uniformly.

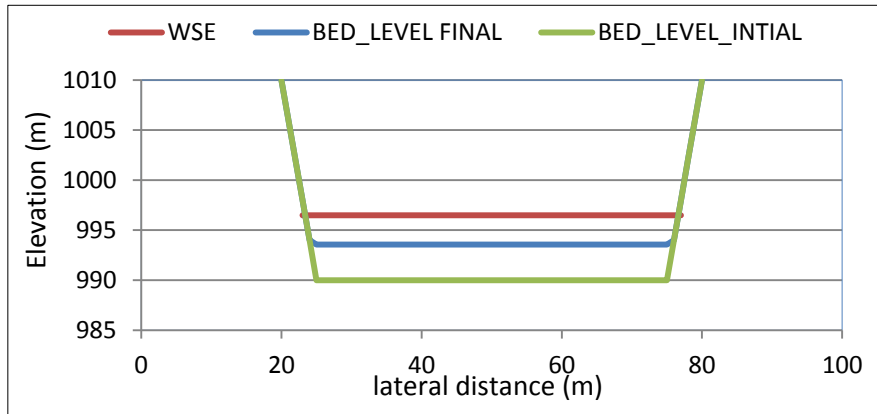


Fig. 3. 11: Sediment distribution in the cross section.

3.4.2.2 Steep channels

In the steep channel, the lake and the dam become more visible. The sediment coming from lake's upstream deposits at the lake entrance, because of the transition from high velocity to low velocity in the lake as shown in fig 3.11.

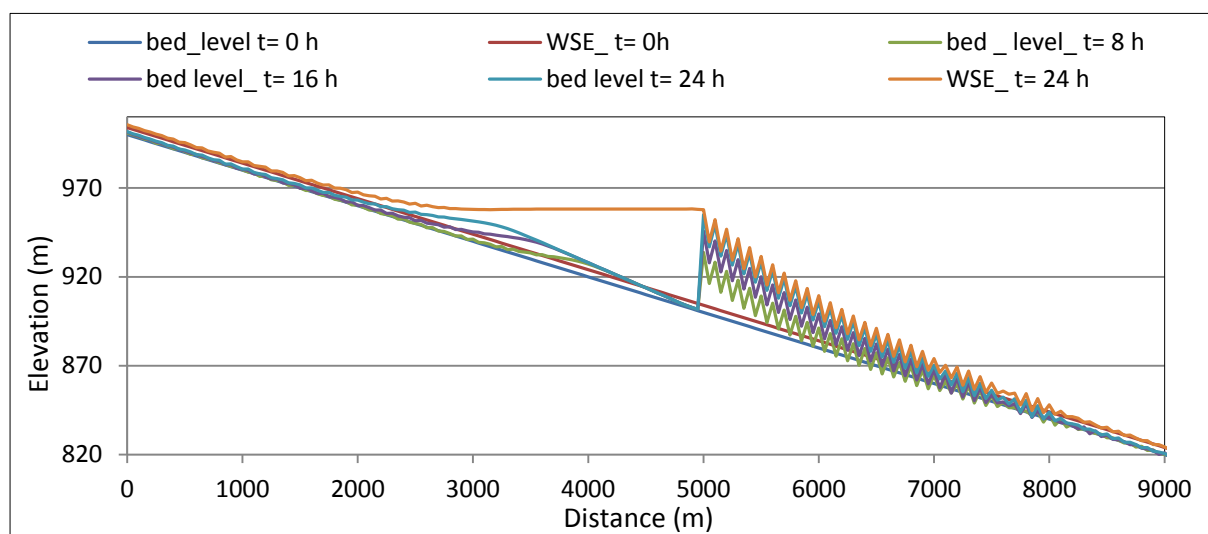


Fig. 3. 12: Dam and lake formation in steep channel due to the lateral feeding of sediment.

3.4.2.3 Sensitivity to spatial discretization

More refinement of the spatial step is important not only in preventing the numerical instability, but also in improving the results and its precision. Model #9 and #10 are studied using two spatial discretization, 50 m and 250 m, to see the effect of the spatial discretization in the dam formation in both the mild and steep channels respectively. As shown in fig 3.13; more refinement gives more precise results and smooth profiles for the bed and water surface, also small spatial steps is required in the zones of the aggradation or degradation because of the increasing in bed slope with time as shown in fig 3.13 and 3.14.

Another interesting issue that the dam height is the same whatever the spatial discretization, only fluctuating shape appear at the dam surface because of the high slope. As shown in case of steep channels; the zigzag's sharpens decreases by using narrow spatial steps; while in the mild slope the special discretization almost has no effect on the results.

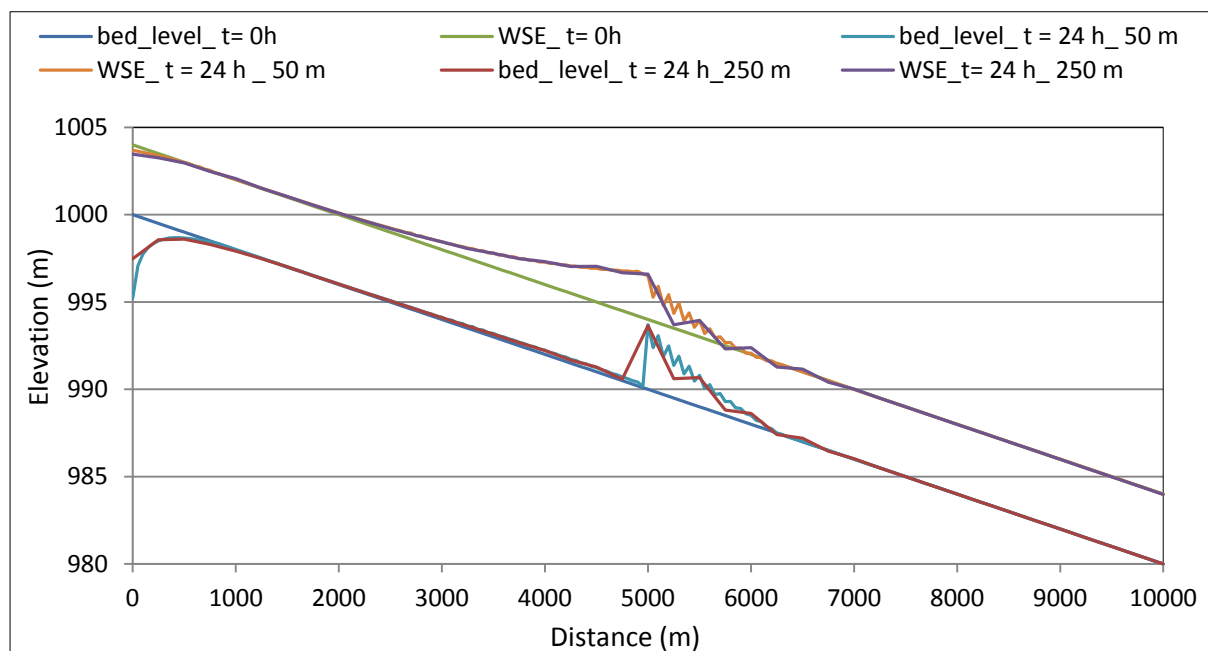


Fig. 3. 13: Effect of the spatial discretization in the results precision (mild channel - model #9).

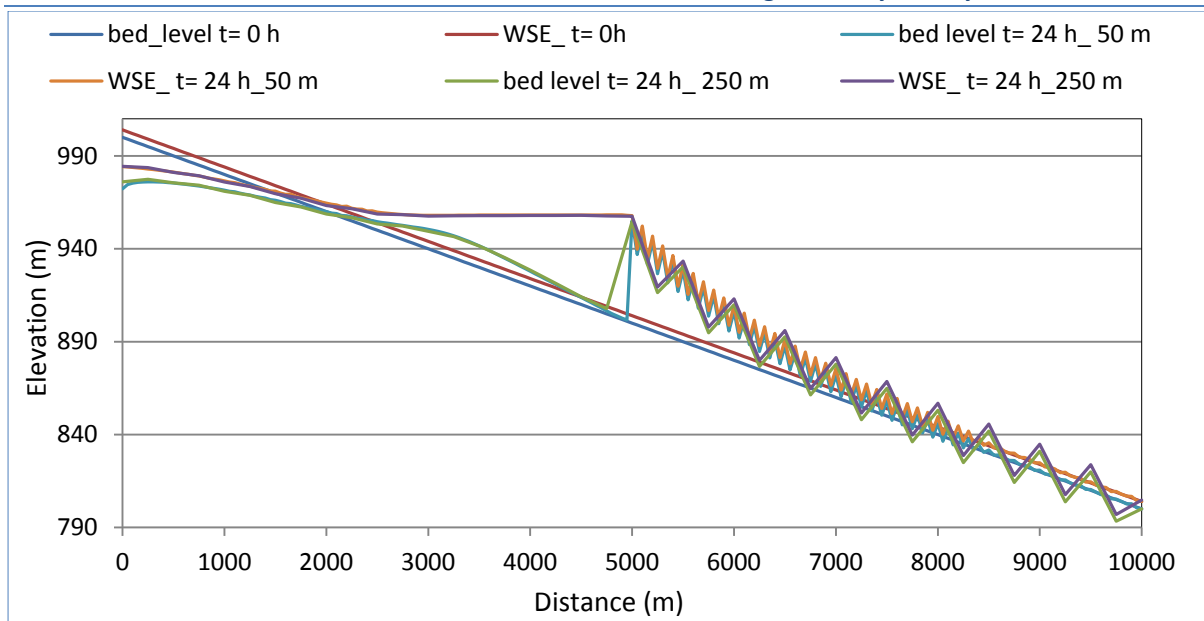


Fig. 3. 14: Effect of the spatial discretization in the results precision (steel channel - model #10).

3.4.3 Case of sequent fixed and mobile beds

The rivers sometimes run above rocky soil, which means that beds are hard in these zones i.e. there is no erosion in these zones, only the sediment deposition can happen. To study Basement ability to model such cases; 3 models are built (#11 to #13), while the results are discussed below.

3.4.3.1 Mild channels

The case of upstream erosion (model #11) is studied twice; the first starts by hard bed(250 m) followed by mobile bed(250 m) and so on along the stretch of the channel, the second starts by mobile followed by hard bed i.e. 250 m hard followed by 250 m mobile soil and vice versa. Because there is no feeding, the bed starts with hard bed didn't erode while the followed mobile bed eroded. The opposite behavior is noted also in case of starting with mobile bed. As shown in fig 3.15; the erosion extends and deepens to provide the transport capacity.

Comparative study of different scenarios for the morphological evolution in a river stream

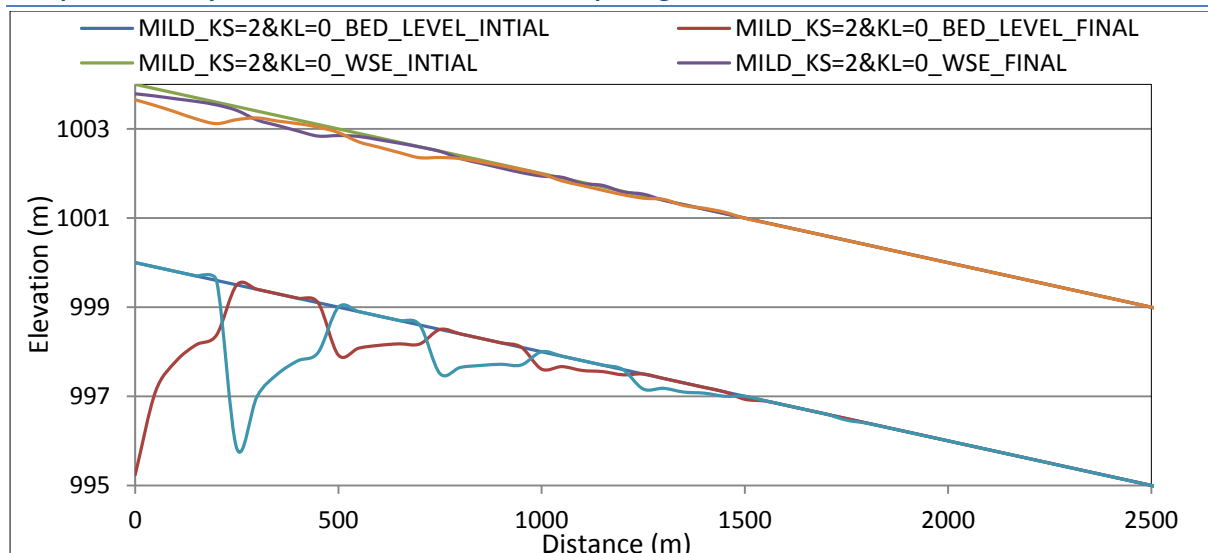


Fig. 3. 15: The bed erosion in sequent hard and mobile bed for model # 11.

In case of sediment feeding by $K_s=2$ as in model #12; the sediment deposits in both the hard and mobile bed as shown in Fig 3.16. It is clear in the figure that; there no effect for replacing the sequence of mobile and hard beds since the sediment deposits in the two beds whatever the sequence.

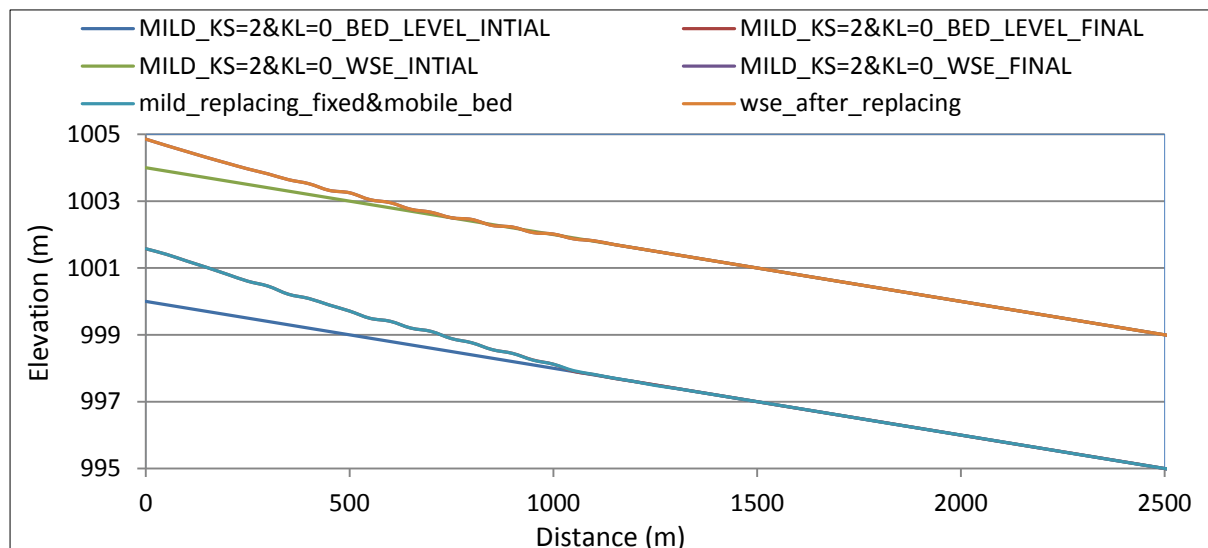


Fig. 3. 16: The sediment aggradation in sequent hard and mobile bed for model # 12.

3.4.3.2 Steep channels

In case of steep slope; the erosion extends in the whole length, but the hard parts remain without erosion. Only the mobile parts erode as shown in Fig 3.17, which shows the result of studying model #13.

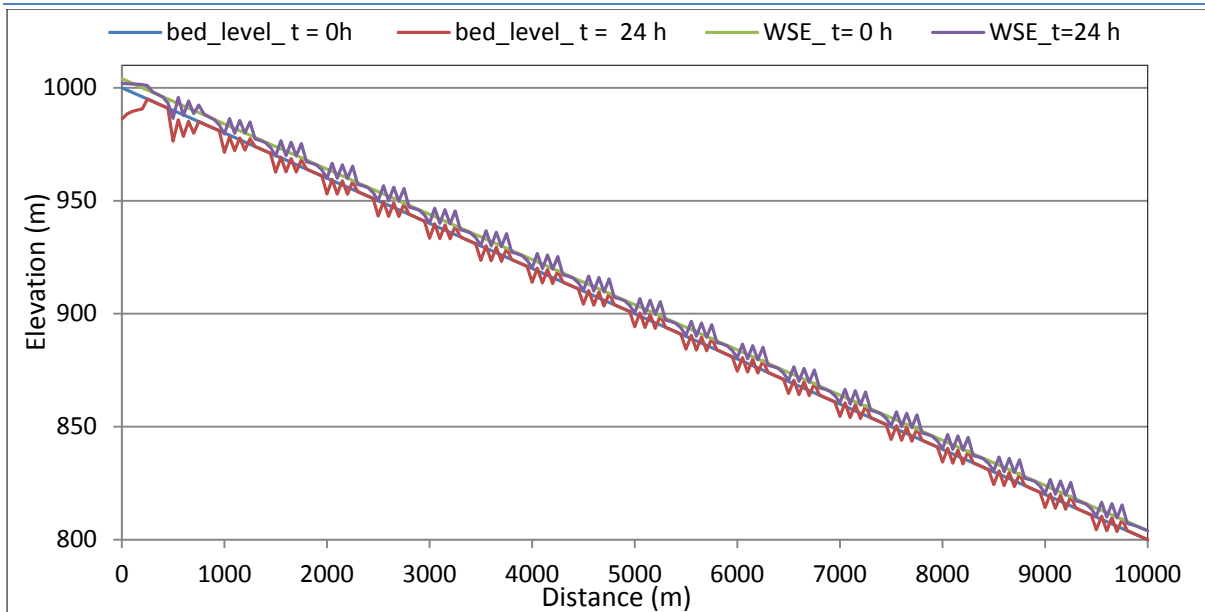


Fig. 3. 17: The bed erosion in sequent hard and mobile bed for model # 13.

In case of sediment aggradation; the sediment deposits in both the hard and mobile bed as shown in Fig 3.18 that shows the result of studying model #14.

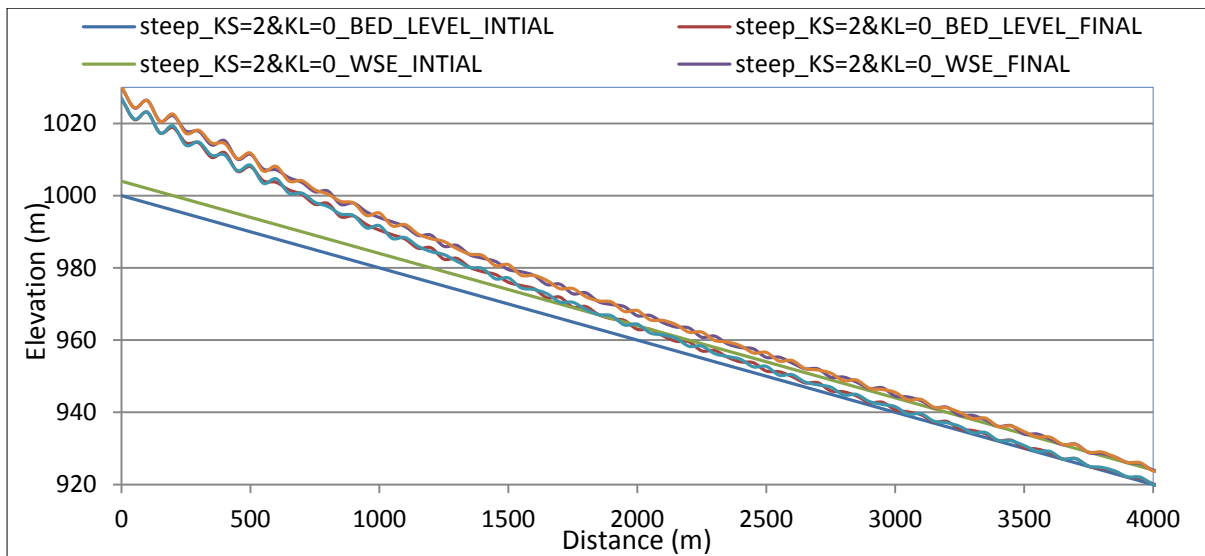


Fig. 3. 18: The sediment aggradation in sequent hard and mobile bed for model # 14.

3.5 Behavior of morphology in channels have non-uniform bed gradation

Indeed; the bed granulometry is very distributed specially in the Mountain Rivers. In the previous analysis; the median diameter d_{50} used on the multi grain sizes behalf. Therefore the characteristics of the bed evolution with a

single value of the diameter are unrealistic, so the gradation curves must be inserted to see how much it affect the sediment transport and consequently the variations in the river's bed.

This section aims to analyze, how the use of multi particle size affects the profile of the riverbed and how the multi granulometry evolve along the stretch of riverbed with time.

3.5.1 Basement treatment for multiple grain sizes

This part is an extension of item 2.3.4.3, since it discuss the assigning of multi grain sizes using Basement as well as extraction of the results.

The section of the program concerned this point is the Basement BED MATERIAL, which belongs to the block MORPHOLOGY (see section 2.3.4.3). The information to be included in order is:

- Grain class: for assigning the grain sizes listed in increasing order i.e. the diameters (in mm) of the sediment involved in the simulation;
- Mixture: for assigning the name of a group of grain sizes belong to the classes defined before and the percentages (contribution) of each size in the mixture (fig 3.19). Many mixtures can be defined depend upon the number of soils describing the bed along it's stretch;
- Soil-def: it defines the name of the soil, the mixture forming it and the thickness of the erodible layer;
- Soil-assignment: it assigns to each soil previously defined an index, which, as already explained in item 2.3.4.3 and fig 2.29. This uses in the geometry file (geometry.bmg) to define the type of soil for each cross section.

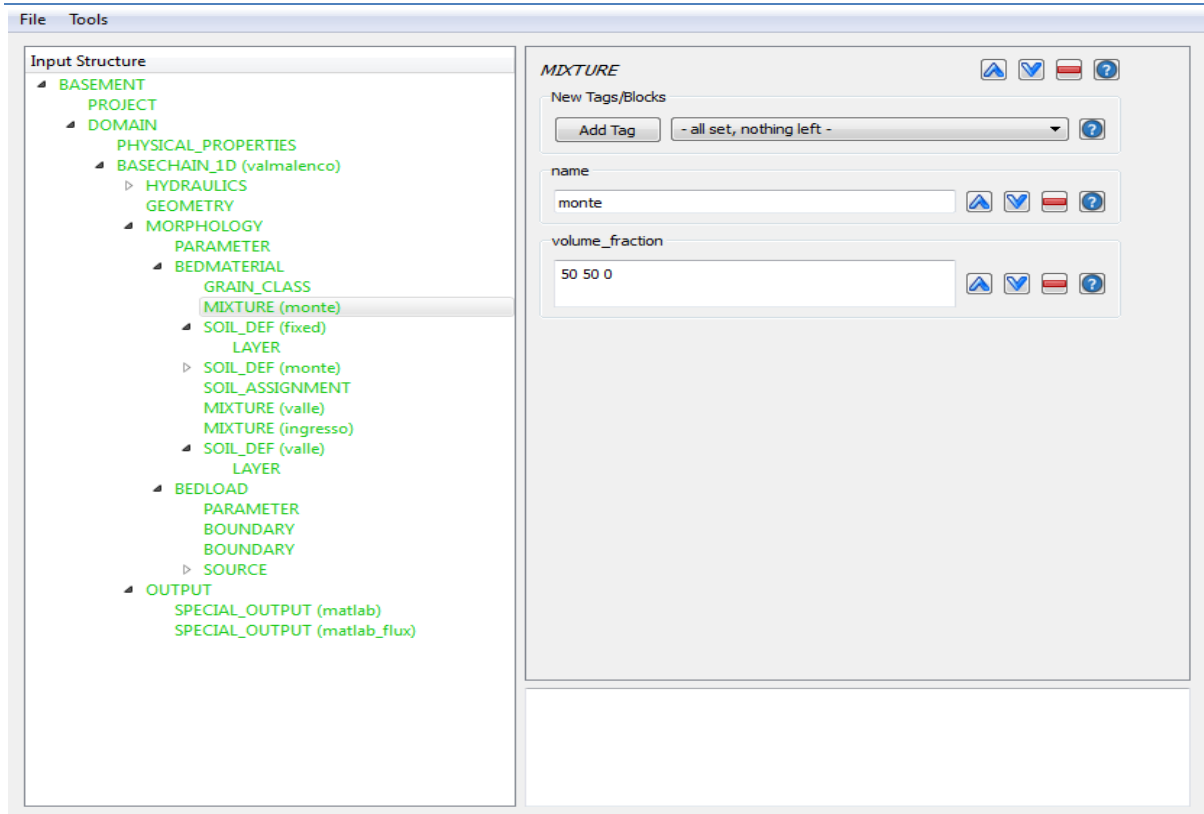


Fig. 3. 19: Assigning of multiple grain sizes in Basement.

In item 2.3.4.3 and Fig 2.36, it is explained what is corresponding to each column of the Matlab output from Basement. in the case of uniform particle size the total number of columns are 17, while in case of more grain sizes the number of columns are 17 plus double the increase in the number of diameters inserted more than the usual single size i.e. in case of 2 diameters the number of columns are 19 and for 3 diameters are 21 and so on. These new columns give the ratio of each grain size in the control volume thickness ($cvt = L_a$), defined in item 1.11, and the sub layer respectively.

In more detail; Starting from column 14 to $(14+n-1)$ in figure 2.36, the ratio of each grain size in the control volume thickness are shown, where n is the number of grain sizes defined. Starting from column $14+n$; the ratio of each diameter in the sub layer is given. The last two columns are fixed; the penultimate column in figure 2.36 shows the thickness of the sub layer (h) while the last gives the number of soils defined in each cross section.

Figure 3.20 displays these two layers (cvt and the sub layer) as well as, it represents the percentage of each diameter in the control volume for a model uses two grain sizes i.e. the model considers that the bed formed by coarse diameter d_1 and another finer size d_2 entering the model and fills the voids among the coarse diameter in the bed.

Along with the representation of the soil; the figure shows a granulometric curves give the ratio of each diameter in the control volume thickness (cvt). The blue curve is related to the percentage of bigger diameter d_1 , while the red curve related to the percentages of smaller diameter d_2 . It is observed that the two curves are intersected when the percentages of the diameters reach to 50%, this means that the percentage of the diameter d_1 is replaced by the percentage of d_2 . As shown in the figure; the cvt has constant value in the model. It is filled by d_1 at downstream, but it is filled by d_2 at the upstream because of the aggradation of d_2 entering the model.

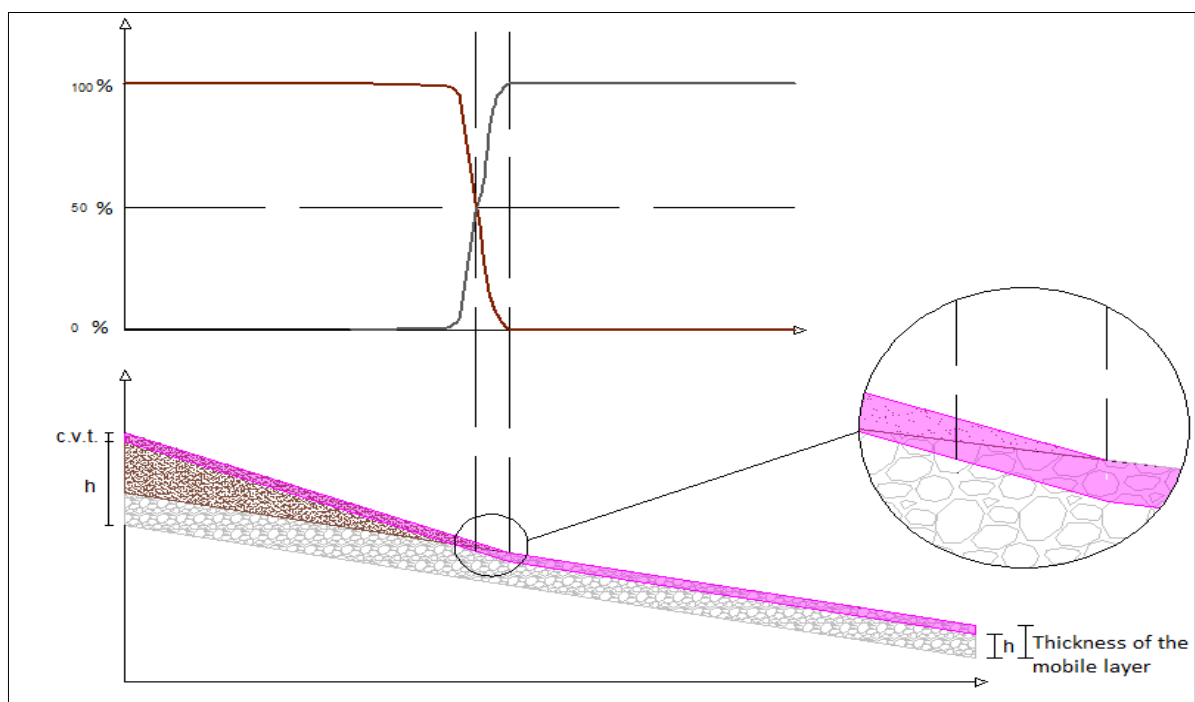


Fig. 3. 20: The sediment mixing in the control volume.

As discussed in item 1.11; the smallest size transport earlier which is known by the sediment sorting, then the coarser sediment remains. The sorting effect leads to change in the gradation curve of each cross-section toward the coarser sizes in the zone of erosion after each time step as in Fig 3.21. These curves can be drawn for each section at each time step by summing the ratios of the diameters in specific section and drawing it versus the diameter sizes.

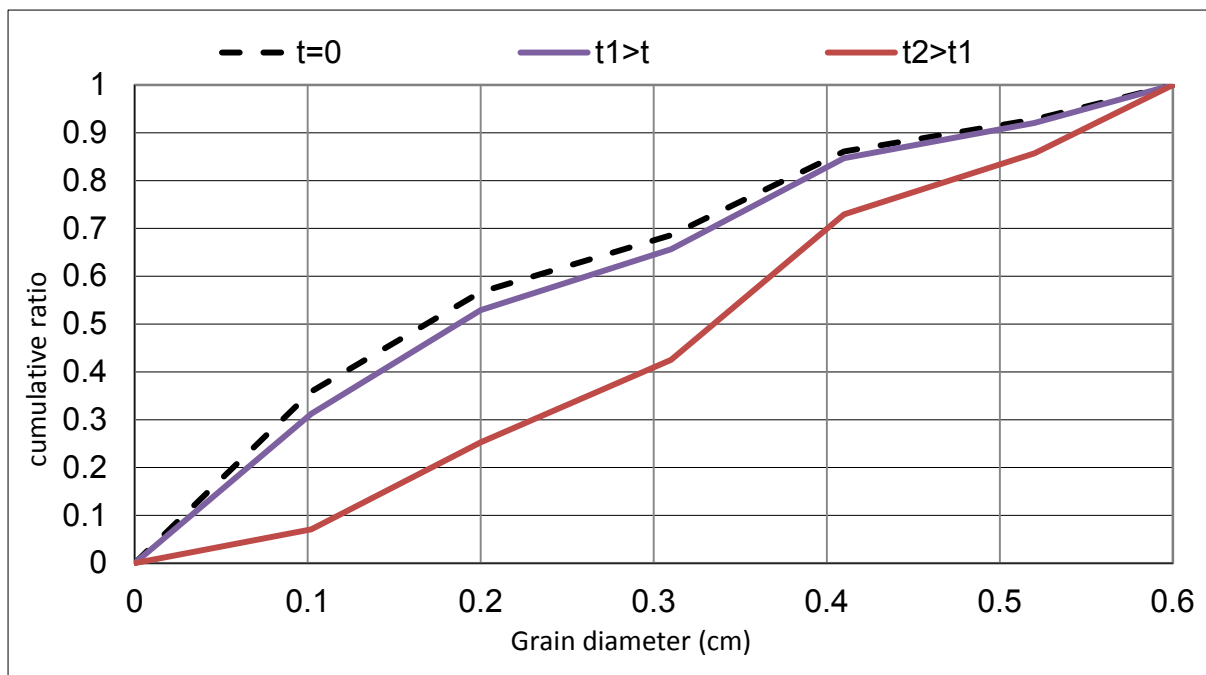


Fig. 3. 21: The change in the gradation curve due to sorting effect at specific cross section.

In the following; the upstream and lateral feedings discussed before will be reanalysed, but with using 2 diameters: one represents the bed granulometry and the second represents the feeding (d_{in}). The bed granulometry is selected to be at the onset of motion ($\tau_* = \tau_{*c} = 0.047$ according MPM), while the in-diameter is selected as a ratio from the bed diameter. As shown in the following table; the in-diameter is smaller or bigger than the bed diameter, so the bigger diameter will not transport, since the bed diameter, which is smaller, is in equilibrium. The transport capacity is calculated for the in-flow diameter, then, the ratios K_s and K_l are used to represent the inflow sediment

as a ratio from the transport capacity. As expected; the in-flow diameters that are bigger than the bed diameter have not transport capacity, so the feeding rate in this case randomly selected e.g. for case #5 the transport capacity of case #4 is selected.

case	channel type	flow type	water depth (m)	Q (m ³ /s)	d_{bed} (mm)	d_{in} (mm)		Q_s (m ³ /s)	KS	KL	Cvt (m)
						ratio	value				
#1	M1	uniform	4	510.37	88.94	$d_{bed}/10$	8.894	0.371	0.5		0.1
#2	M1	uniform	4	510.37	88.94	$d_{bed}/10$	8.894	0.371	3	0	0.1
#3	S1	uniform	4	1613.9	889.4	$d_{bed}/10$	88.94	11.74	3		0.1
#4	M1	uniform	4	510.37	88.94	$d_{bed}/3$	29.65	0.237	0	3	0.1
#5	M1	uniform	4	510.37	88.94	$3 * d_{bed}$	266.81	0.237		3	0.1
#6	S1	uniform	4	1613.9	889.4	$d_{bed}/3$	296.5	7.487		3	0.1
#7	S1	uniform	4	1613.9	889.4	$3 * d_{bed}$	2667.9	7.487		3	0.1

Table 3. 4: The combination of non-uniform sediment feeding.

3.5.2 Upstream feeding by non-uniform sediment

Regarding the upstream feeding by sediment; 3 cases are studied using non-uniform granulometry as shown in table 3.4; the first two for mild channel and the third for steep channel. The analysis of each case individually is discussed below:

- Case#1

Although the feeding ($Q_s/2$) is lower than the transport capacity, the degradation amount is limited in upstream , as shown in fig.3.22, comparing it with fig. 3.5 for single size. This is because of the stability of the bed granulometry, which prevent more erosion from the bed. In the second part of the reach there is some aggradation, whilst in the analogous case for uniform sediments there was a progressive degradation everywhere, which reflects the large complexity of the multi-size case.

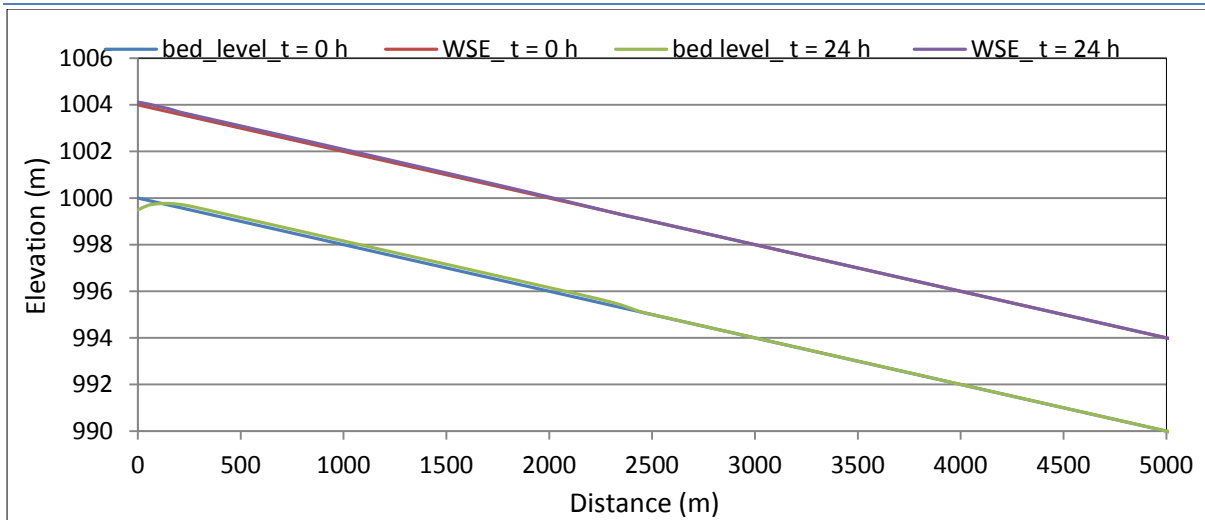


Fig. 3. 22: Bed evolution for case#1 of non-uniform granulometry.

Since the feeding's diameter is smaller than the bed diameter, which in equilibrium, it transport with the water along with mixing with the bed granulometry. As shown in fig 3.23; the ratio of the in-flow diameter increases in the cvt with time, while the bed ratio decreases which means that d1 (the smaller diameter fed to the model) mixes with the bed diameter. Also the in-diameter mixes with the sub layer but with very small ratios as shown in fig 3.24. It showed also that the mixing advances with time toward the downstream.

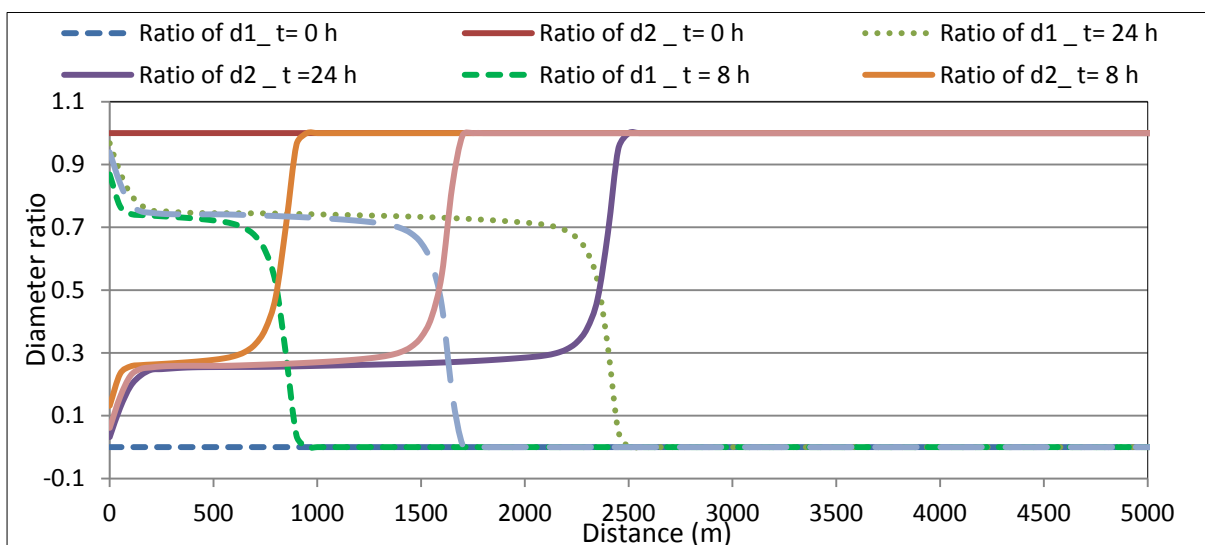


Fig. 3. 23: Case #1; the mixing between the in-flow diameter and the bed diameter in the cvt

Comparative study of different scenarios for the morphological evolution in a river stream

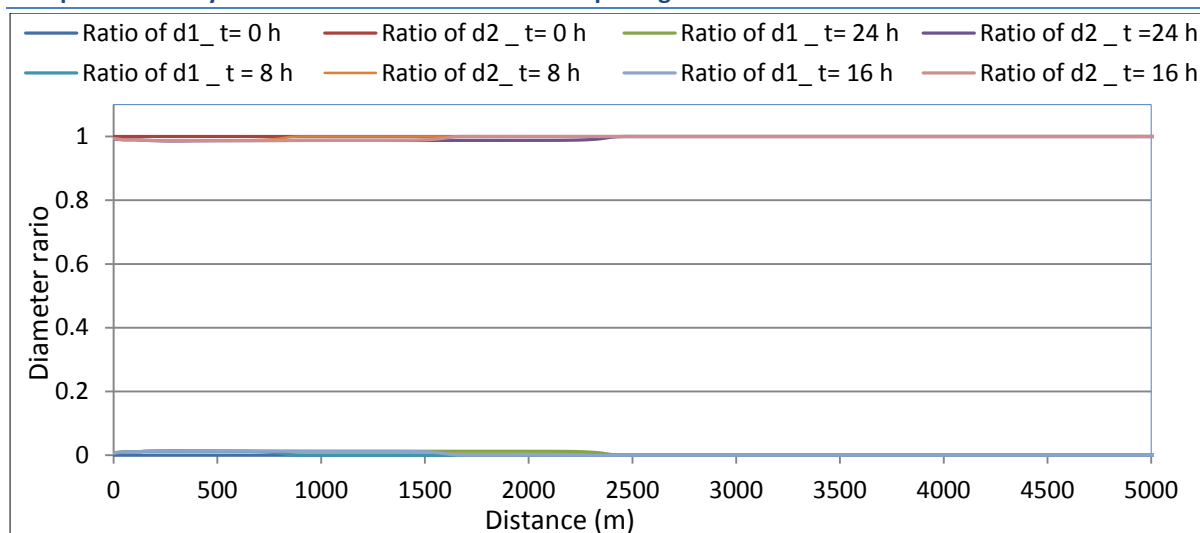


Fig. 3. 24:Case #1; the mixing between the in-flow diameter and the bed diameter in the sub layer.

- Case #2

Here the in-flow rate of sediment is more than the transport capacity, so the aggradation is clear in Fig 3.25. Also the cvt is totally replaced by the inflow diameter, since it take the shape shown in fig 3.20. As shown in fig 3.26 the mixing also advances with time, but d1 usually dominates in the cvt because of the deposition up to 3500 m then it becomes non-existent.

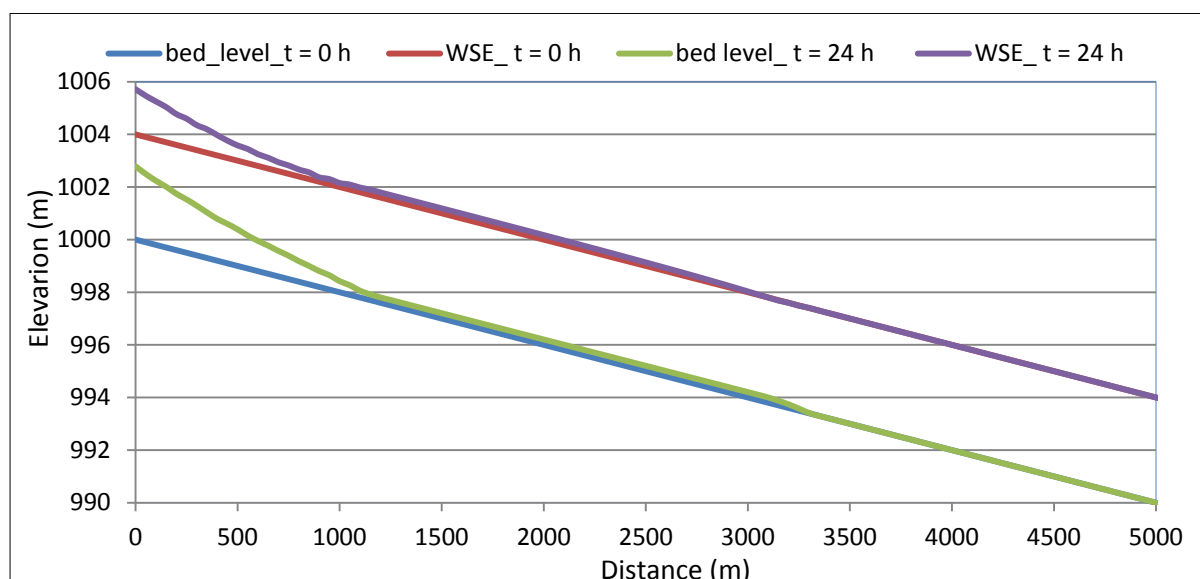


Fig. 3. 25: Bed evolution for case#2 of non-uniform granulometry.

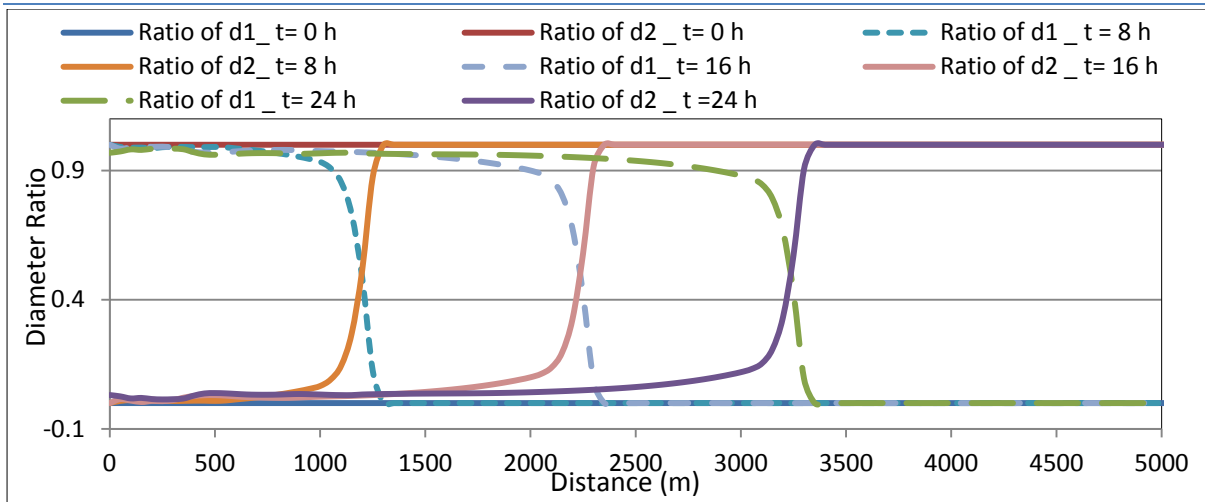


Fig. 3. 26:Case #2; the mixing between the in-flow diameter and the bed diameter in the cvt

- Case #3

It is a case of aggradation (fig 3.27), since the feeding is more than the transport capacity. The striking that; the in-flow diameter is transported along stretch of the channel by big ratio. This means that in steep slope the small diameters sort and transport by high amounts toward downstream while the coarser remains stable. Also the small diameter fills the voids among the bed diameters, then it starts to aggragate above the original bed level. This appears by comparing Figure 3.27, that doesn't show any aggradation after 5500m, with figure 3.28 which shows that d1 is existent after 5500 m in the cvt. So the mixing starts first then after filling the voids the aggradation starts.

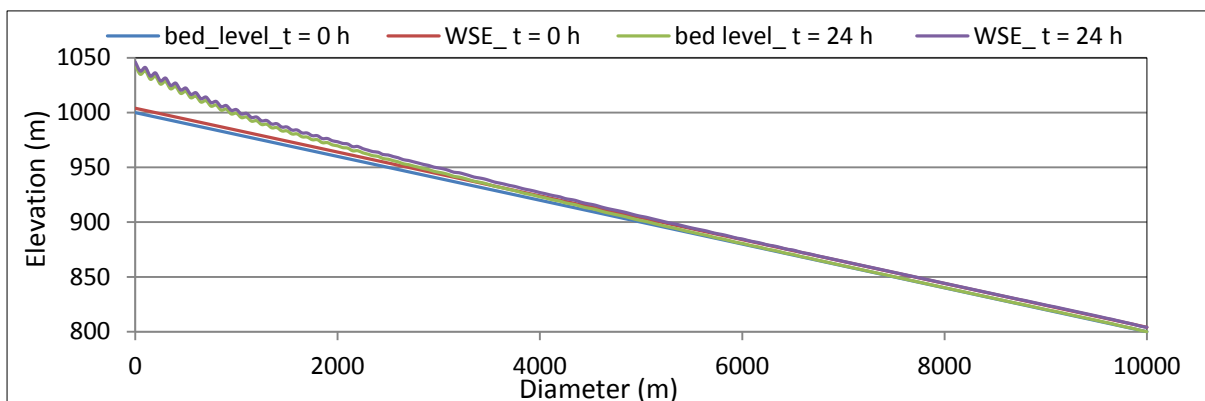


Fig. 3. 27:Bed evolution for case#3 of non-uniform granulometry.

Comparative study of different scenarios for the morphological evolution in a river stream

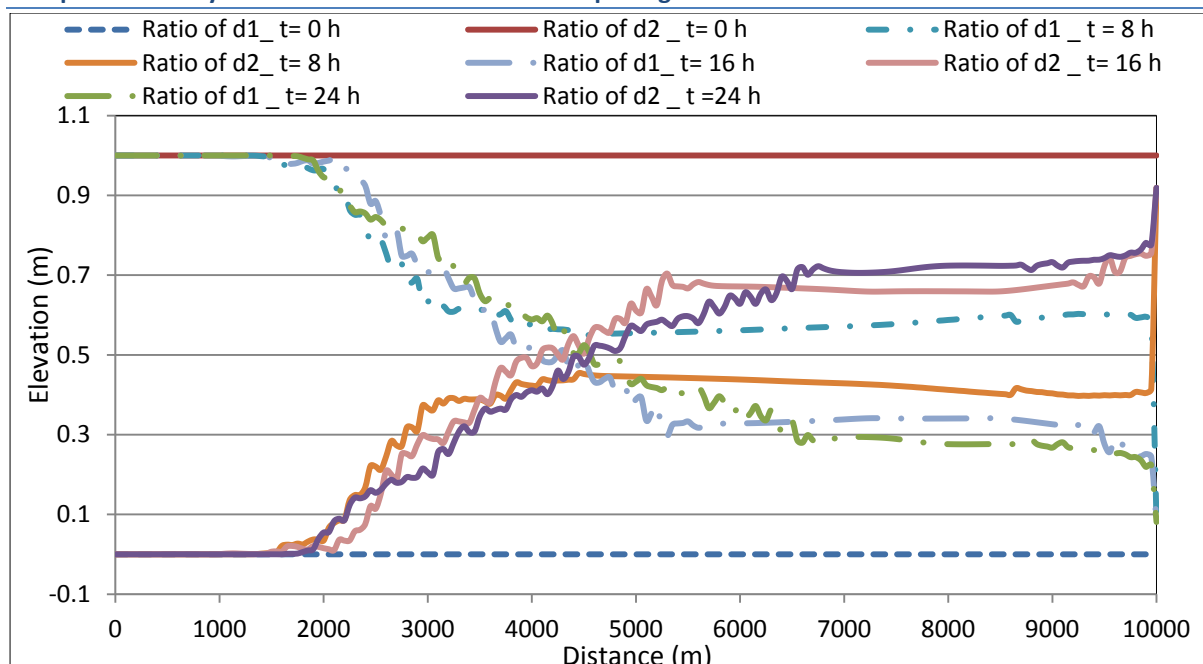


Fig. 3. 28: Case #3; the mixing between the in-flow diameter and the bed diameter in the cvt

3.5.3 Lateral feeding by non-uniform sediment

As discussed; the lateral feeding by rate more than the transport capacity leads to dam formation. The height of this dam may be affected by the inflow diameter, so 2 cases are studied; one uses smaller inflow diameter ($d_{in} = d_{bed}/3$) and the second uses bigger diameter ($d_{in} = 3d_{bed}$). The properties of these 4 cases (2 for mild case and 2 for steep case) are listed in table 3.4, while the results are discussed below:

- Case #4 (mild channel & $d_{in} = d_{bed}/3$)

First of all; there is no change in the bed level takes place at upstream (fig 3.29), because the bed granulometry is in equilibrium. By comparing the dam height in figure 3.10 with the dam height in the following figure; the dam height is less while its base is wider. This is because of the mixing, since the inflow sediment fills the voids first then it starts the aggradation which leads to reduction in the dam height. The mixing limits are confined as in fig 3.30 because of the mild slope and the small transport capacity.

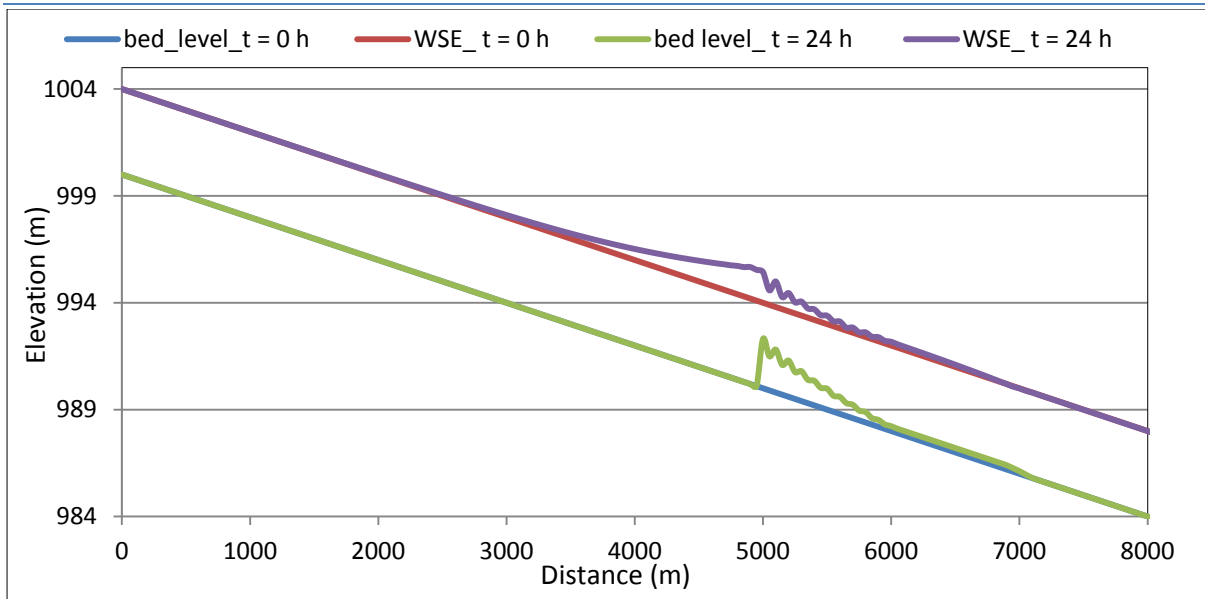


Fig. 3. 29: Bed evolution for case#4 of non-uniform granulometry.

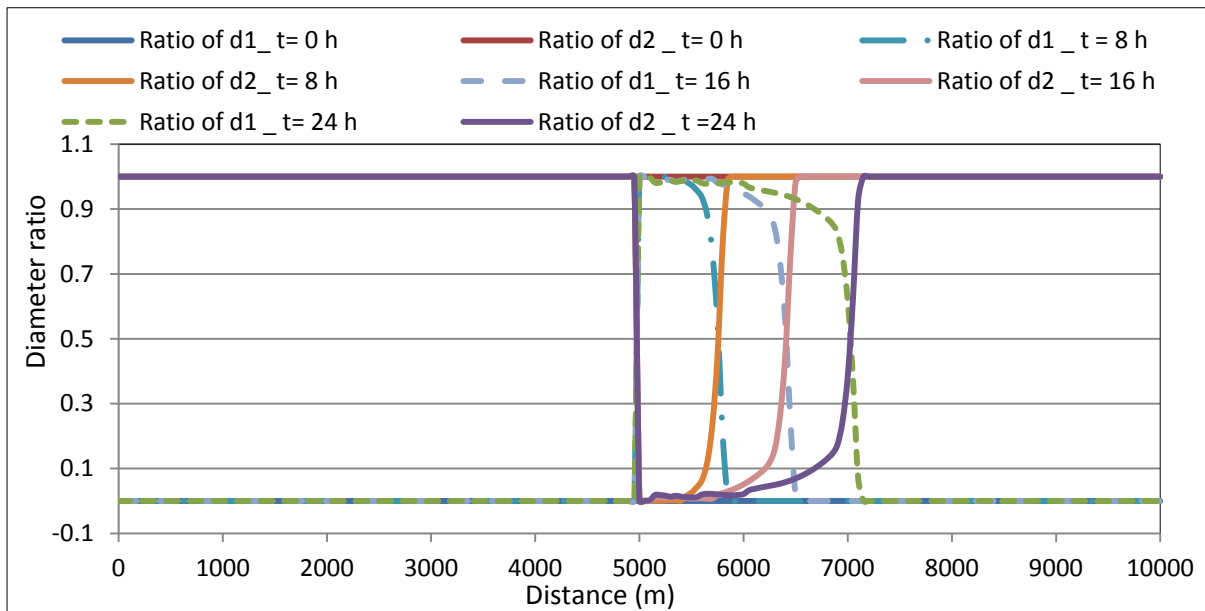


Fig. 3. 30: Case #4; the mixing between the in-flow diameter and the bed diameter in the cvt

- Case #5 (mild channel & $d_{in} = 3d_{bed}$)

The bed diameter is in equilibrium, so there is no changes in the bed at upstream. Regarding the lateral in-flow; the in-diameter size neither able to transport nor mix with the bed granulometry because of it's huge size, so it deposits forming higher dam with narrow base as in fig 3.31.

Comparative study of different scenarios for the morphological evolution in a river stream

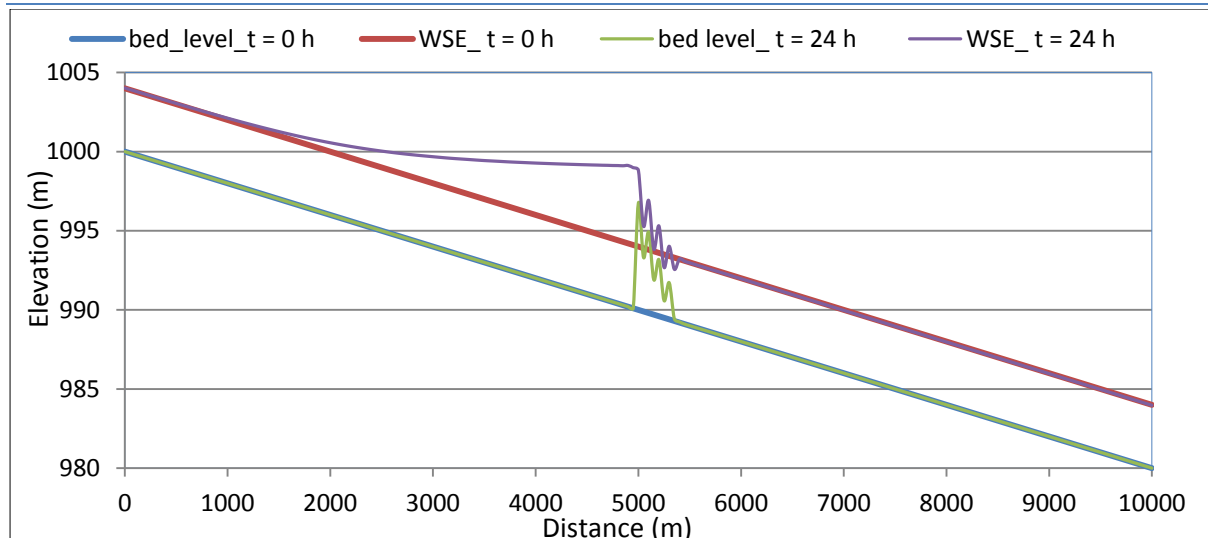


Fig. 3. 31: Bed evolution for case #5 of non-uniform granulometry.

The cvt in the dam zone is totally filled by the in-diameter, then it goes back to it's original case before the feeding as shown in fig 3.32.

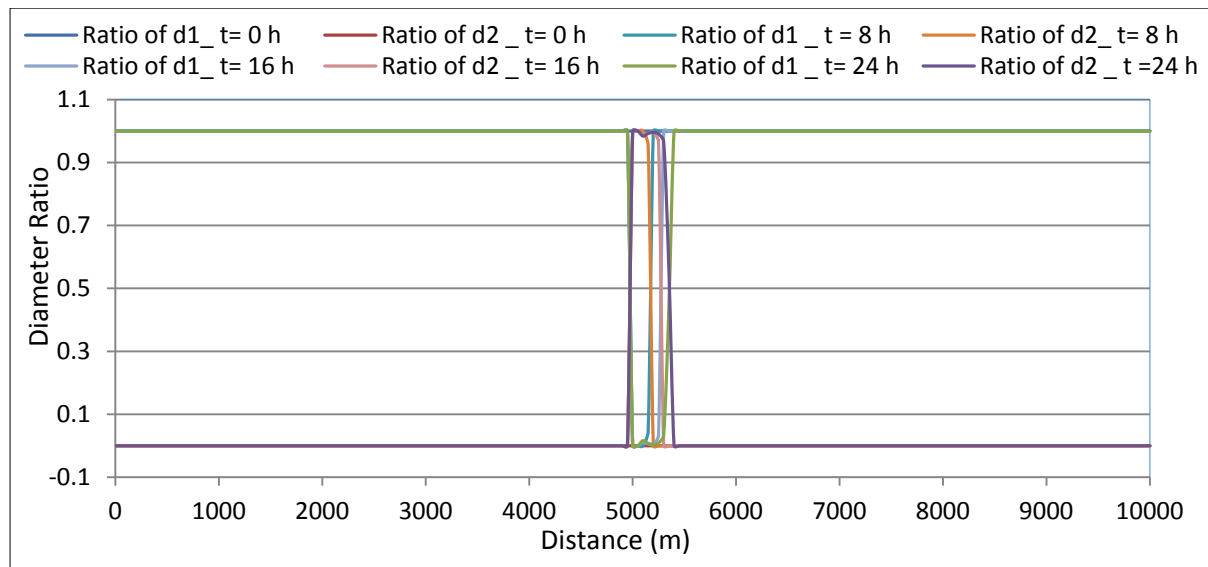


Fig. 3. 32: Case #5; the mixing between the in-flow diameter and the bed diameter in the cvt

- Case #6 (steep channel & $d_{in} = d_{bed}/3$)

The same behavior is noted here, since the inflow diameter is less than the bed diameter. The sediment starts filling the voids among the bed particles primary, then the dam creates. In the tail of the dam; the mixing is equally equilibrated as in Fig.3.34.

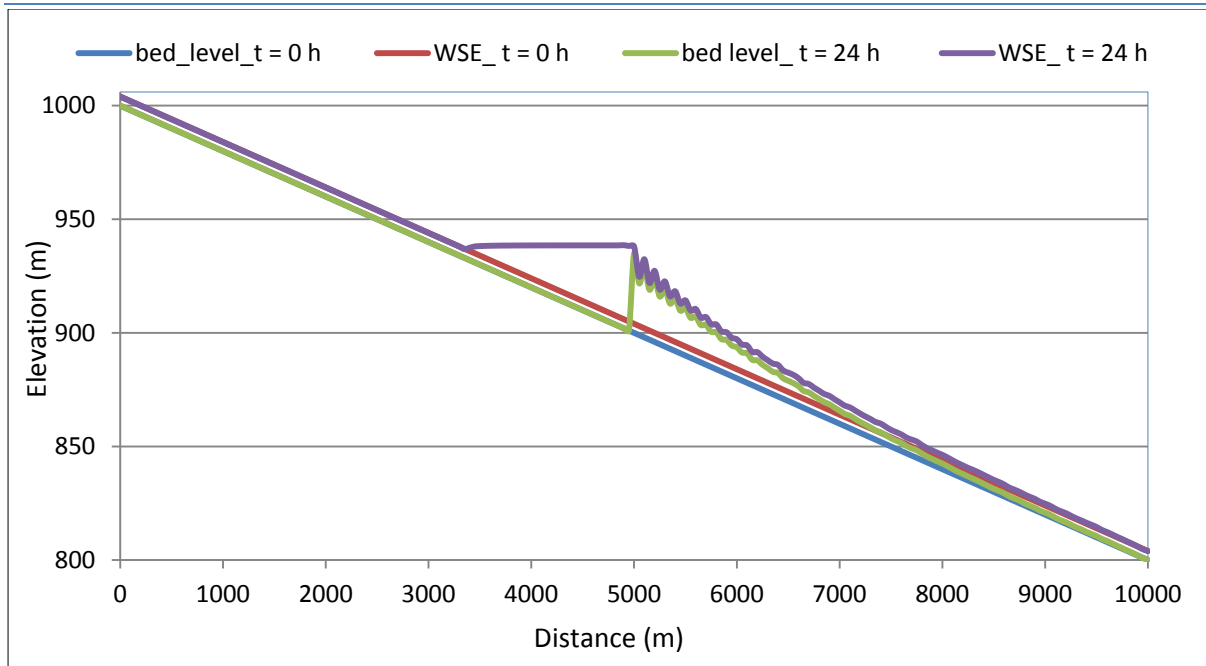


Fig. 3. 33: Bed evolution for case #6 of non-uniform granulometry.

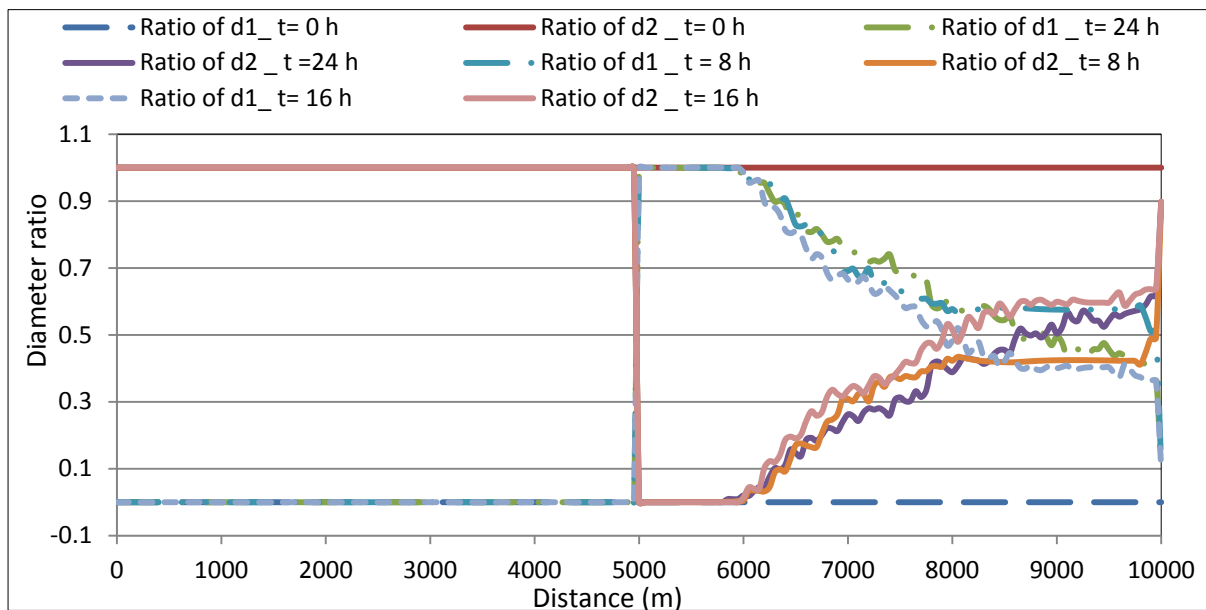


Fig. 3. 34: Case #6; the mixing between the in-flow diameter and the bed diameter in the cvt

- Case #7 (steep channel & $d_{in} = 3d_{bed}$)

In this case also there is neither mixing nor transporting because of the huge size of the in-flow diameter, so all the inflow contribute in creating the dam (fig 3.35). This is the reason why there is no mixing as in fig 3.36.

Comparative study of different scenarios for the morphological evolution in a river stream

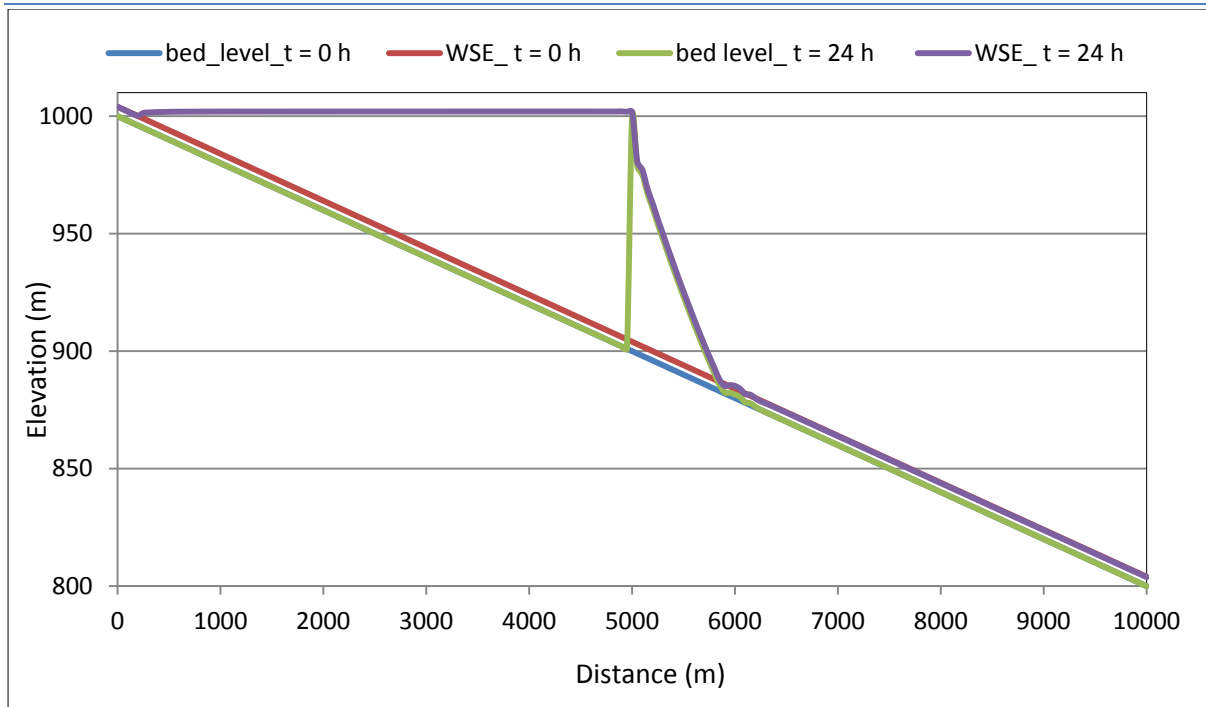


Fig. 3. 35: Bed evolution for case #7 of non-uniform granulometry.

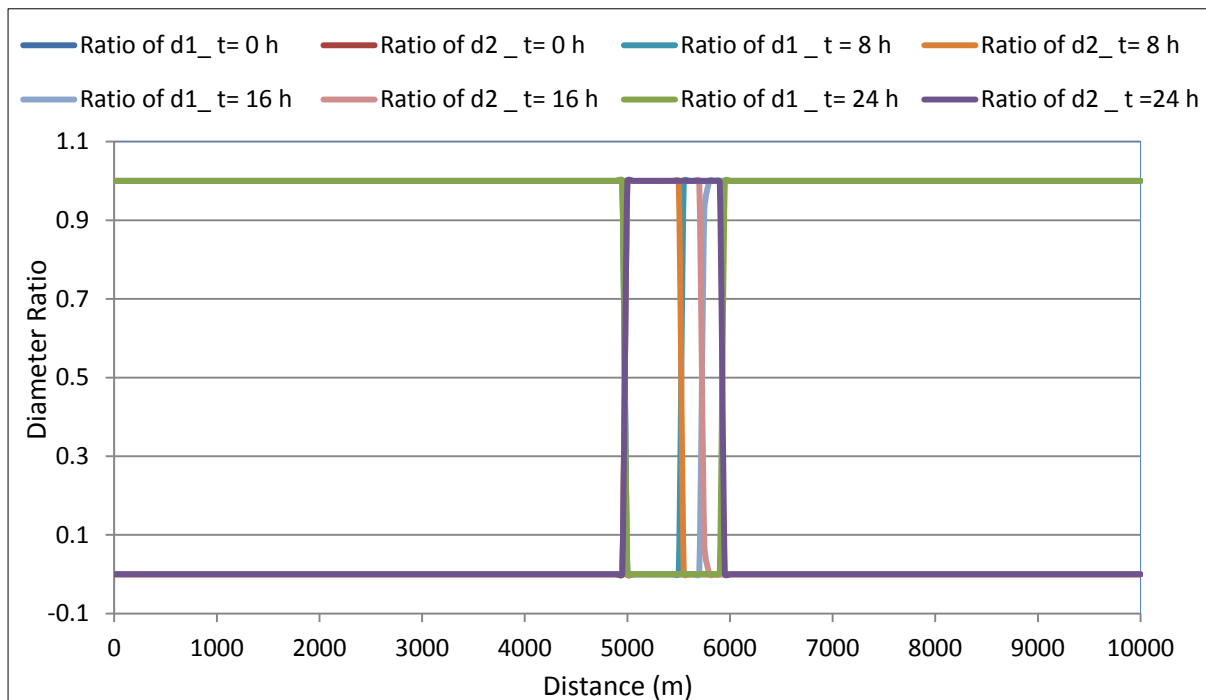


Fig. 3. 36: Case #7; the mixing between the in-flow diameter and the bed diameter in the cvt

Finally, it is noted, especially from figure 3.35, that the lateral feeding can create huge dam and lake behind it. The water overtop the dam without

breaching since the transport can't exceed the capacity, but this dam can't take this shape because it may be structurally unstable.

3.5.4 Sensitivity to control volume thickness

The control volume thickness plays a fundamental role in the calculation of sediment transport. According to Eq 1.23; the smallest value of cvt , the smallest transport capacity. The cvt can't be zero, while it's default value is $2d_{90}$. Increasing the cvt means increasing the field of mixing and sorting, while the values more than the default value will not affect so much because the higher sizes, in level, will prevent the mixing and sorting.

The cvt also has no effect in the transport capacity if the bed gradation is coarse (more than the threshold size) since this type of sizes is in equilibrium, while in case of fine sizes the sorting will be more and consequently the transport capacity.

The cvt value is constant within the Basement model, so to zoom in it's effect the previous cases are studied again, starting from case#2, with different values of cvt as discussed below:

- Case#2

The very small value of cvt as in fig 3.37 means that there is no mixing or transporting, which leads to aggradation at the entrance with depth more than 60 m. in case of cvt by $2d_{90}$; the maximum aggradation width is achieved, while more values of cvt reduce the base of the aggradation because of the mixing in deepest voids. The change in cvt , more than $2d_{90}$, doesn't affect the results so much, since the higher diameters prevent the mixing with or the sorting form the deepest zones in the cvt .

Comparative study of different scenarios for the morphological evolution in a river stream

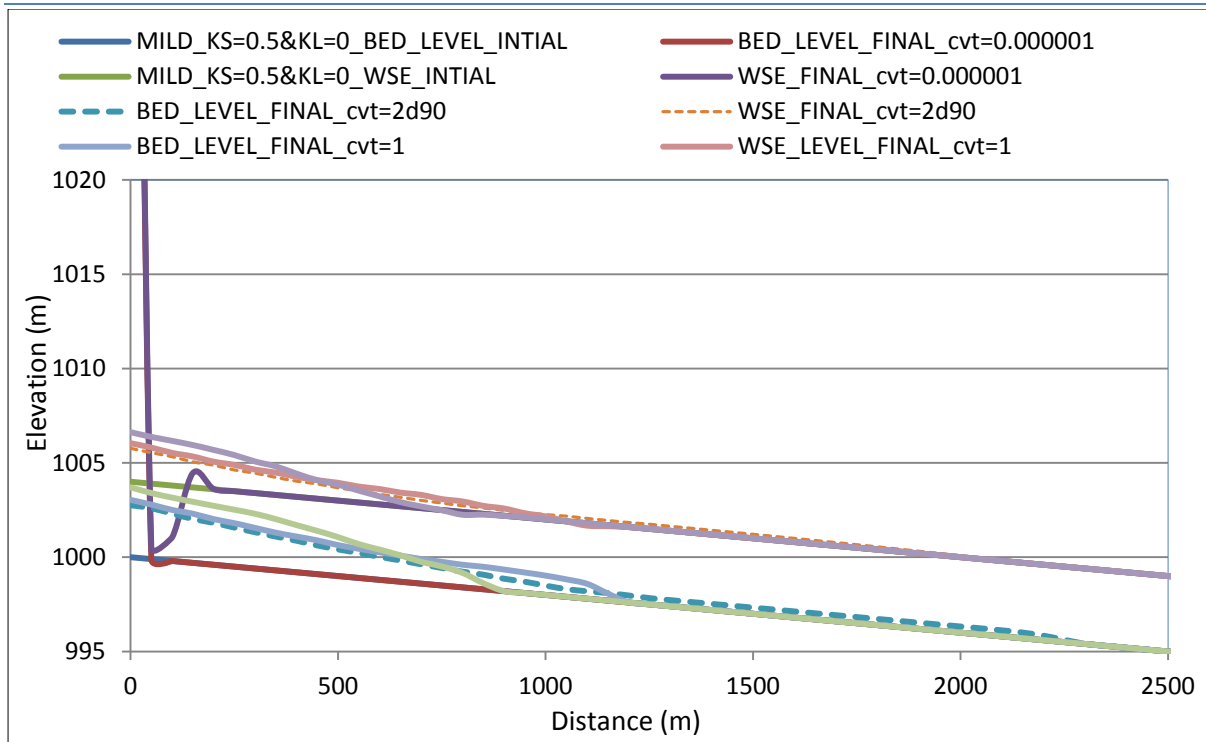


Fig. 3. 37: Sensitivity to cvt for case#2.

- Case #3

In case of steep slopes the cvt doesn't affect the bed evolution except for very small values.

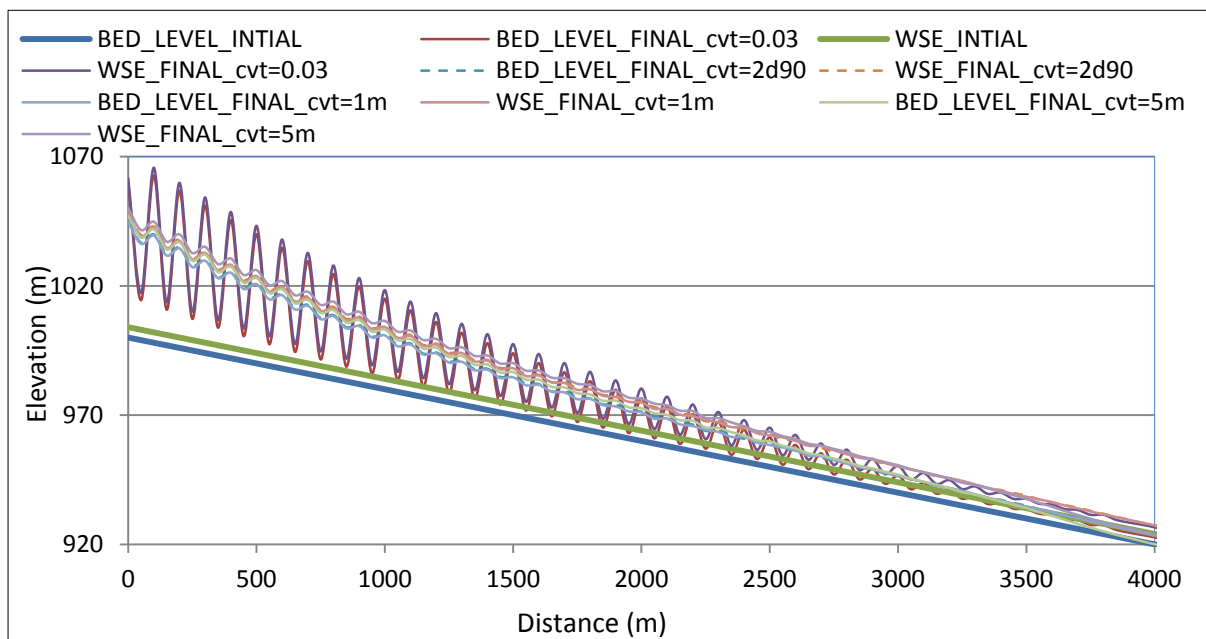


Fig. 3. 38: Sensitivity to cvt for case#3.

- Case #4

This case looks like case #2, since the dam height increases with very small values of *cvt*, while the other values of *cvt* doesn't affect the dam height so much.

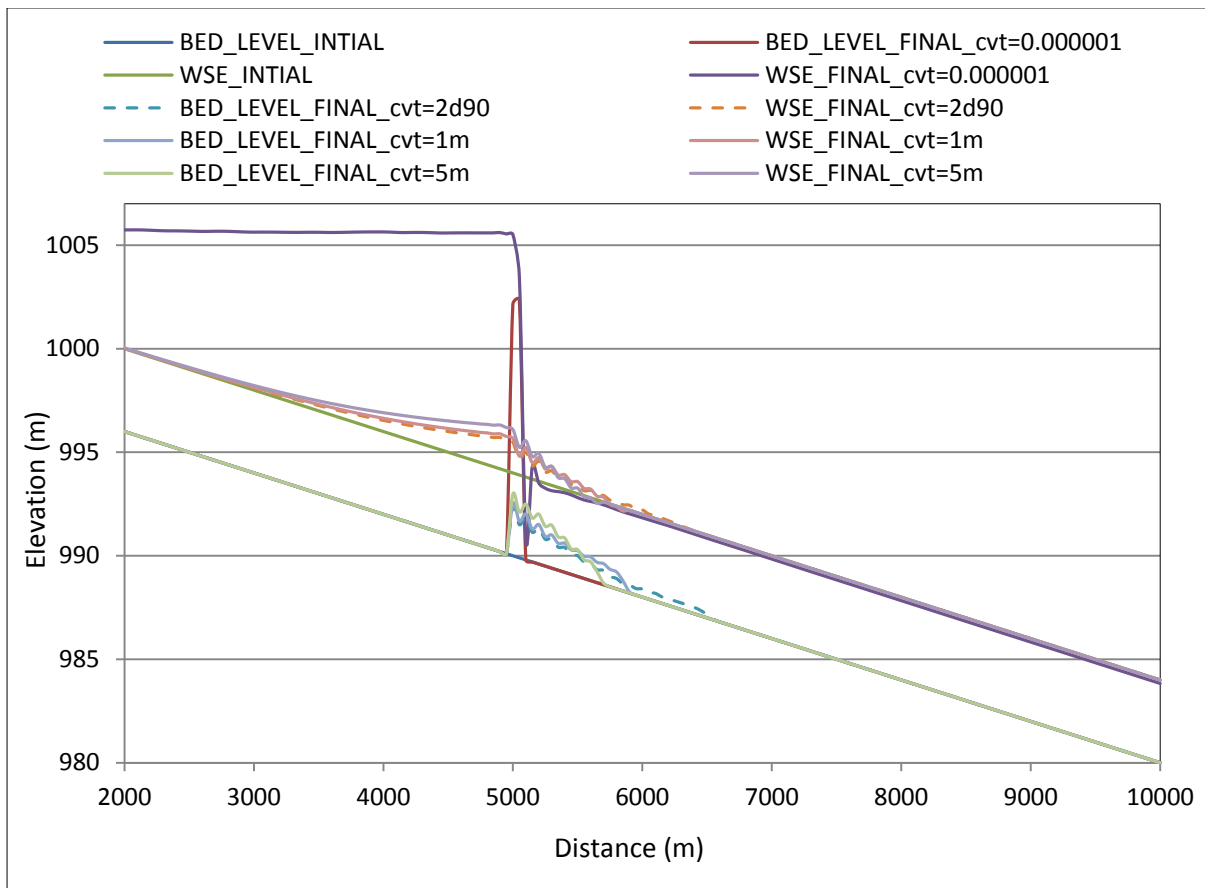


Fig. 3. 39: Sensitivity to *cvt* for case#4.

- Case #5

The in-diameter in this case is bigger than the bed diameter, which prevent the mixing between the in-diameter and the bed. The reduction of *cvt* value amplifies the effect and create very thin and tall dam because of the very small value of *cvt*.

Comparative study of different scenarios for the morphological evolution in a river stream

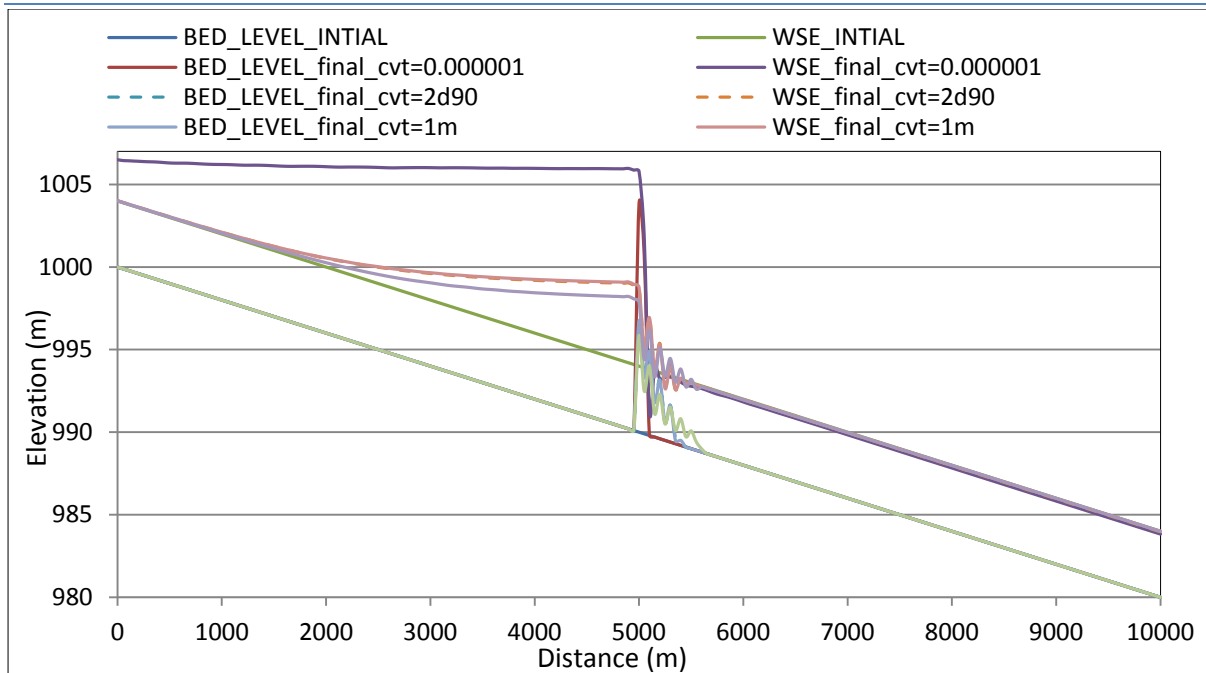


Fig. 3. 40: Sensitivity to cvt for case#5.

- Case #7

This case verifies that the cvt has no effect when the in-diameter is coarser than the bed granulometry.

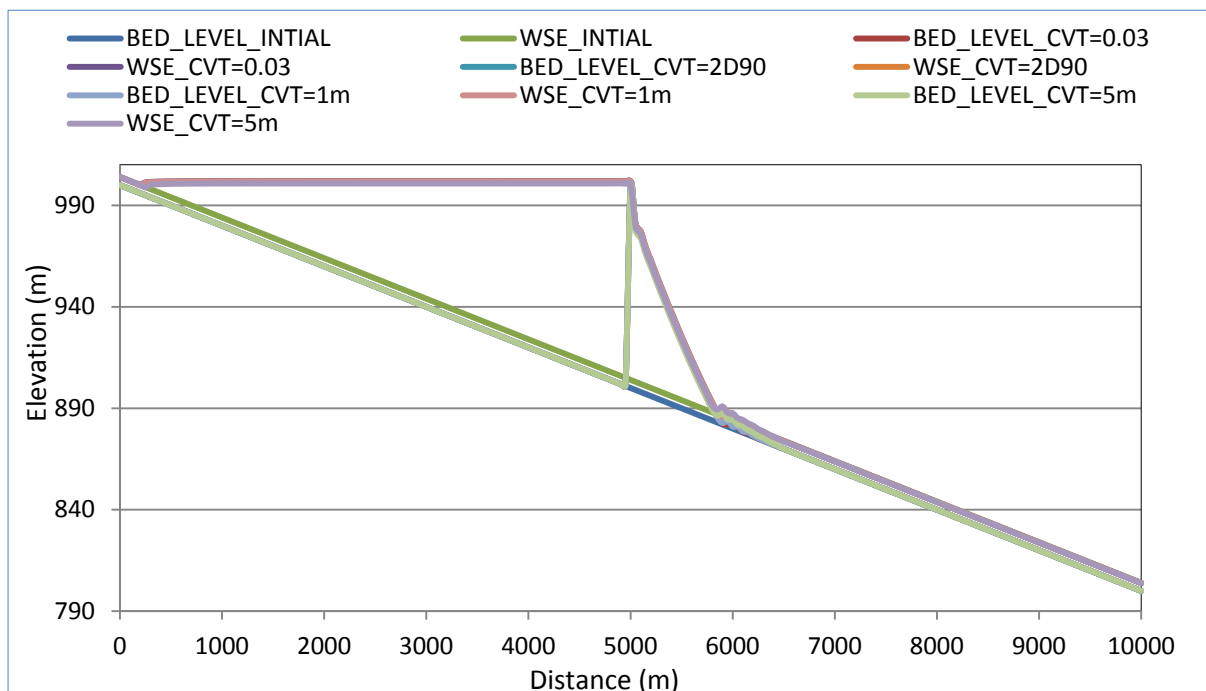


Fig. 3. 41: Sensitivity to cvt for case#7.

3.6 Conclusions

After studying the upstream feeding and the lateral feeding by sediment using single sizes and multiple granulometry, the following notes can be summarized:

- Basement was able to compute more or less all the cases, even if sometimes instability problems or huge variations were observed for certain values of the parameters. By contrast, HEC-RAS and ISIS had problems even for the simplest cases that were considered.
- The erosion of beds depend primary on the granulometry sizes. If the sizes are less than the threshold value of the size, erosion occurs under the condition that the feeding rate is less than the transport capacity. If the sizes are in equilibrium, no erosion will be noted.
- The erosion in the steep channels is higher in rates than the mild slopes since the erosion occurs along the stretch of the river.
- Basement is able to model reasonably erosion and deposition in reaches with movable and fixed portions alternating with each other.
- The skin friction usually uses in the calculation of the bed load, since the total friction produce huge amount of sediment which is unrealistic. Using the total friction gives the same behavior but the amounts of sedimentation are amplified by a specific value.
- The time and special step of the model affects the precision of the solution and wide values lead to numerical instability.
- The numerical analysis of steep channels morphology is more sensitive to the spatial discretization, since irregular bed is noted. For overcoming this irregularity, narrow spatial steps are recommended.

- The lateral feeding of sediment in a channel more than the transport capacity lead to dam formation and lake behind the dam. The dimensions of this lake depend on the dimension of the dam.
- The dam's dimensions are affected by the feeding granulometry and the ability of mixing with the channel bed.
- The default value for cvt is $2d_{90}$, while increasing it doesn't affect the morphological evolution so much, also small values of cvt reduce the transport capacity and cause aggradation.
- If the feeding diameter is bigger than bed granulometry, it neither mixes nor moves. Only it deposits and closes the river valley.

Basement has been tested against the previous typical cases/situations present in Mountain Rivers. Then, the expectation is that Basement can serve as a modelling tool for real cases. This is wanted to investigate in the following chapters with reference to the different scenarios for the case-study.

4 The Case of Mallero: Mallero Description

4.1 Introduction

As a case study; this chapter and the next two chapters introduce the sediment transport problem in Mallero River haunted to the floods in Sondrio city. Sondrio is a city in the north of Italy far from Milan around 100 km (Fig 4.1). It is situated on a conoide formed by the debris that Mallero River had deposited in the outlet of Valmalenco catchment before it reaches to Adda River. The Mallero River catches the water from Valmalenco which has an area around 320 km².

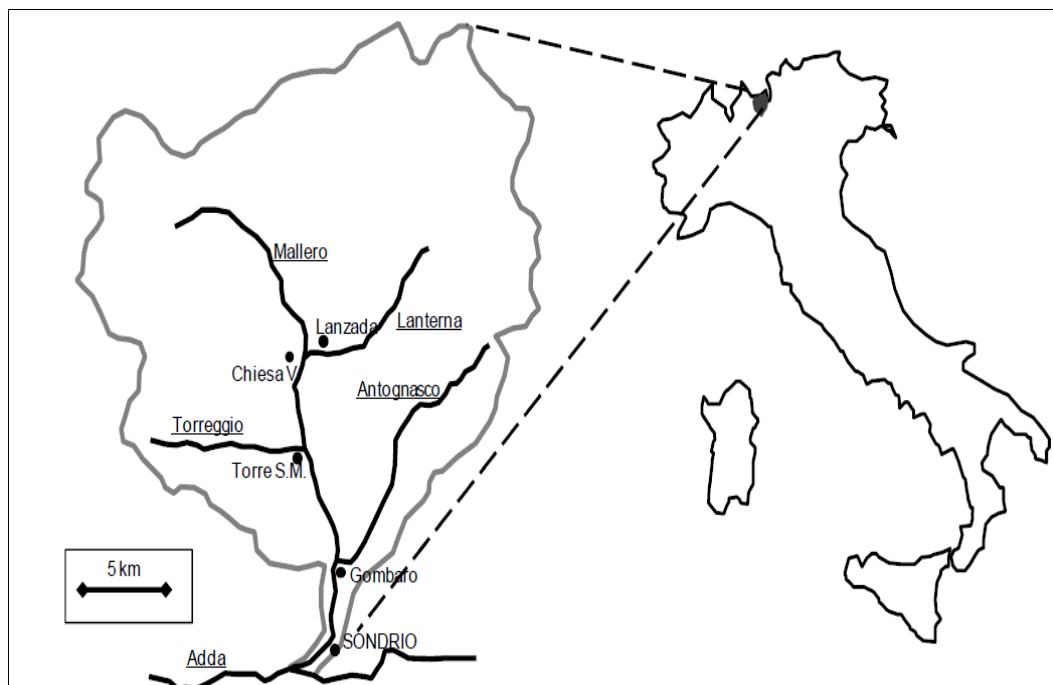


Fig. 4. 1: The Mallero basin (water courses underlined and towns in normal font) (Radice, et al., 2013).

The aim from studying this case is the improving of the emergency plan for Sondrio city by improving the knowledge about the phenomenon through improving its modeling. Of course, better modeling will lead to better planning e.g. the amount of aggravated sedimentation will affect the planning in both the emergency phase and back to normalcy phase. In the emergency phase; more sedimentation will lead to reduction of the river capacity, hence more exposure to the flood which affects the city evacuation during the crisis and the accessibility of the roads available for the emergency purposes. Restoring the river capacity is the second activity will affects the time line and the emergency cost during the back to normalcy phase i.e. more sedimentation will need more time , more cost and more procedures to remove it.

In 1987; Sondrio exposed to a flood haunted and followed by huge amount of sedimentation which forced towards the excavation to restore the capacity of Mallero to avoid the flooding of the city due to the appurtenances of the event or due to next similar events. To study this event; the properties of Valmalenco catchment will be introduced during this chapter, then the results of the numerical modeling for the last 9.48 Km (out of 27 Km) from Mallero by using Basement software will be discussed in chapter 5.

Another scenario will be discussed in chapter 6 related with occurrence of a landslide in Spriana (around 7 Km upstream the confluence point of Mallero river and Adda river), the aim is studying the ability of one dimensional software like Basement 1D to simulate such type of problems (lateral feeding of sediment with huge rates), the properties of the dam will form due to the landslide, the ratability of the results obtained by this complex modelling and finally the amount of sediment will transport due to this event.

This scenario, related with the occurrence of the landslide, will be reintroduced with formation and consequent collapse of an earthen dam resulting in a dam-break wave. Some models will be highlighted for the breaching of the dam created by the landslide, the properties of the lake will create behind that dam, the estimation of the dam break wave due to the breaching of the dam, evaluation of the amount of sediment will generate by the breaching and finally the morphological evolution due to the dam break wave.

The reliability of the modelling of these scenarios will be discussed through either a comparison among the obtained results, those of previous studies and some field measurements or through the sensitivity of the modeling to some related parameters. Finally, a comparison between the consequences of each scenario will be introduced to know which scenario is more dangerous for the town.

4.2 The Mallerio basin

The basin is located in Valmalenco in the province of Sondrio in Italy beside the borders between Switzerland and Italy (Fig 4.2). Mallerio is the main tributary collecting the water from the basin and pouring it in Adda River. it starts in Pian di Lupo at height 1650 m ASL(above sea level) and flows into the Adda river near the town of Sondrio at altitude about 280 m ASL. After around 27 km from Sondrio toward upstream there are numerous tributaries, the main ones are: the stream of Lantern (corresponding to Chiesa Valmalenco, 1000 m ASL), the stream of Torreggio (in Torre Santa Maria, 750 m ASL) and the stream of Antognasco (Arquino, 450 m ASL) (Fig 4.1).

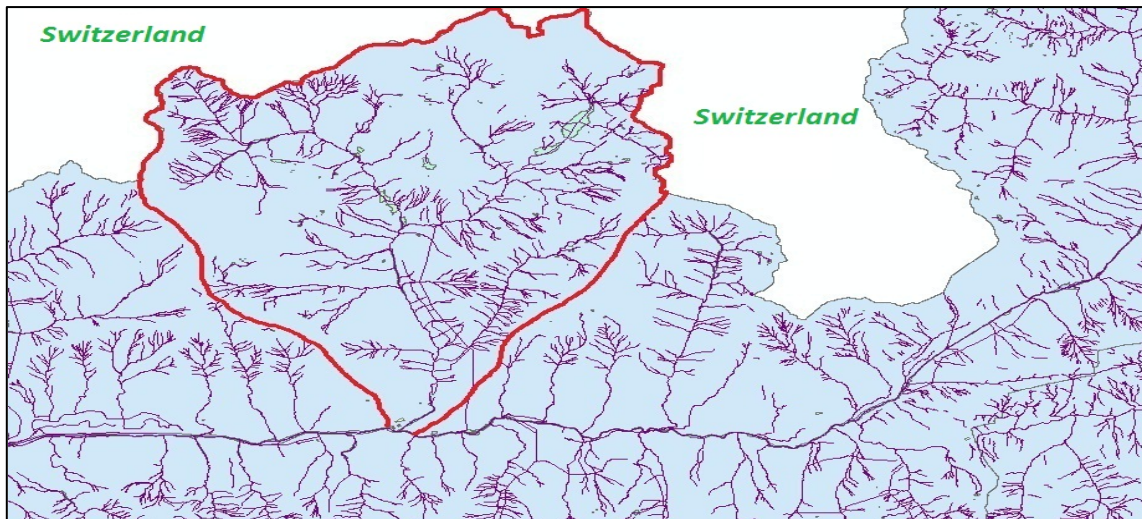


Fig. 4. 2: Mallero River, it's tributaries, it's catchment and it's confluence with Adda River.

The catchment of Mallero covers an area around 320 Km². The boundaries of the river basin are: from north; Piz Bernina (which is the Italy-Switzerland border), from the east by Pizzo Canciano, from the south by the Sasso Bianca and from the west by Monte Sissone. The highest point in the catchment in the north at Piz Bernina (4050 m ASL), while the lowest point in the south at the confluence point of Mallero river and Adda river (280 m ASL). Figure 4.3 shows the topography of the catchment.

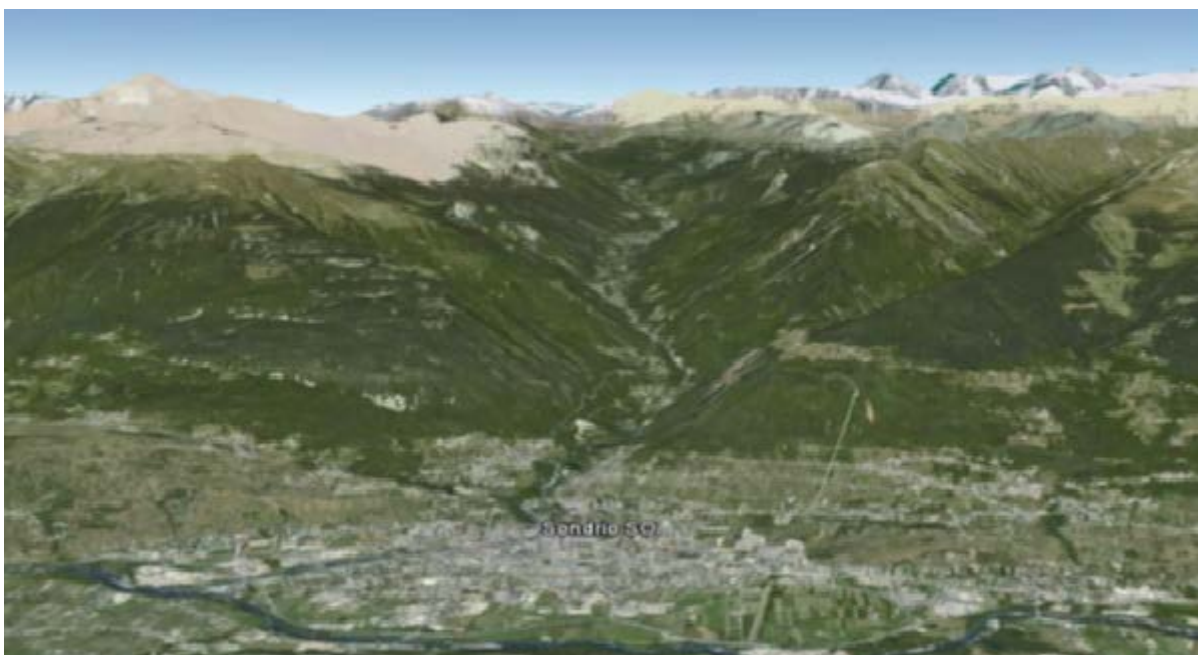


Fig. 4. 3: The topography of Valmalenco valley.

As shown; Sondrio city sites at the south part of the catchment, upstream the confluence point of Mallero and Adda rivers. The slope in Sondrio city is almost flat (Fig 4.4), while the topography is sharp upstream Sondrio. This sharp topography leads to faster runoff of water in a short concentration time.

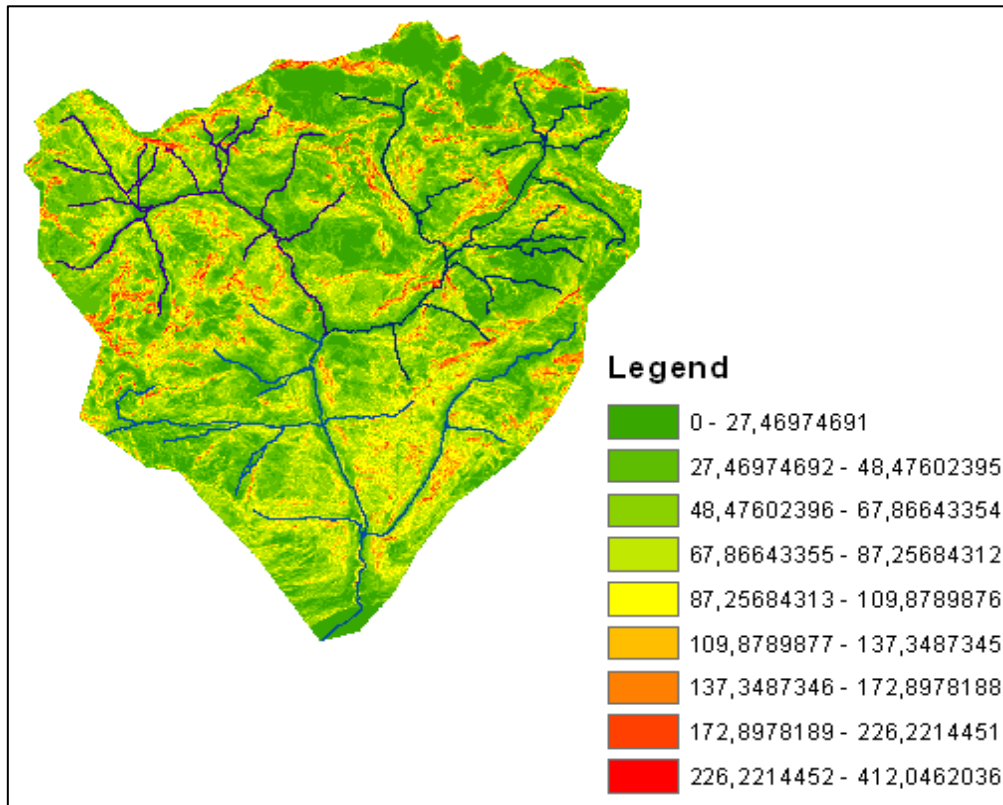


Fig. 4. 4:Slopes in the basin expressed in percentage.

4.3 Grain sizes and bed slopes

The Mallero has a length of 27 km with very variable granulometry among the different cross-sections and variable slopes along its length (Fig 4.4) e.g. in the upper part of the river; the slope values of the riverbed ranging from 4% to 40% with an average of around 8%. In the last 2 km of Mallero before its intersection with Adda, the slope is approximately 1% with some local values of 0.1%. Table 4.1 (Filippetti, et al., 2012) summarizes the particle sizes and average slopes of the different reaches of the river.

Comparative study of different scenarios for the morphological evolution in a river stream

location	slope [%]	d50 [mm]	notes
Pian del lupo	3	167	upstream (US)
A monte di Chiareggio	3	166	
Chiareggio	4	348	
A valle di Chiareggio	7	512	
Sabbionaccio – San Giuseppe	2	79-118	
Val Rosera	7	120	
Cave di serpentino	> 10	360-1640	
Curlo	10	968	
Confluenza torrente Lanterna	5	73-85	
Chiesa Valmalenco	4 – 6	80	
A valle di Chiesa Valmalenco	4 – 6	313-669	
A monte di Torre S. Maria	4 – 6	162-212	
A valle di Torre S. Maria	8	85-140	9Km from DS
A monte di Spriana	4	84-127	
Tra Spriana e Arquino	8	247-772	
A valle di Arquino	8	772	
Cassandre	3 – 6	540-1180	
Sondrio	1	40-73	Downstream(DS)

Table 4. 1: Grain sizes and slopes in different sections of Mallero.

The main reach of the Mallero till a valle di Torre S. Maria is shown in Fig 4.5.

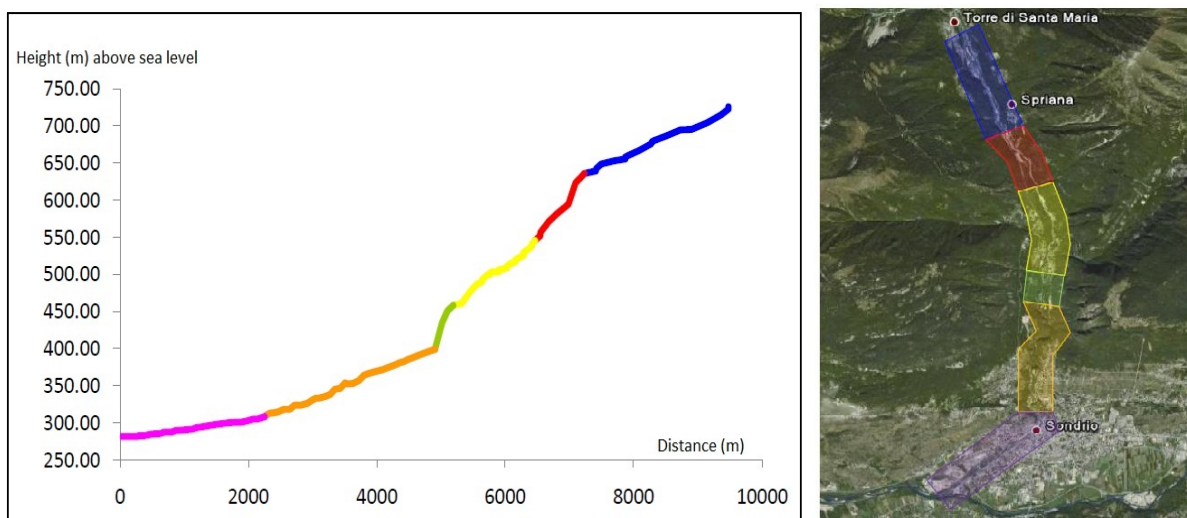


Fig. 4. 5: Traits of Mallero - profile & photo (Mauri, et al., 2009).

The analysis will be proposed in next two chapter focuses only on the part shown in Fig.4.5 (less than 10 km out of 27 Km that the whole length of Mallero). The fuchsia (pink) part in the profile represents the Mallero inside the town of Sondrio. The slope is low there (about 1%), while the cross sections are mainly rectangle with distance between the banks around 30 m (Fig. 4.6) .The particle size of the bed is varied and the average diameter is about 7 cm decreasing towards the outlet.

Before entering the city, the Mallero through 1800 meters (orange part), is formed by a deep and narrow gorge. In this stretch, the slope is not high (around 3%), in addition to presence of some bridges and some natural cascade. The reduced width of the cross sections there generate the maximum values of water depth. The route is not straight but uneven with a double curve at halfway point. Exclusively, the particle size of the bed there compound of large boulders whose average diameter is greater than 60 cm.

After that toward the upstream, the Mallero pass through very steep part called " Cassandre" (the green part), after that the slopes varies as shown in fig.4.5.



Fig. 4. 6: Photo for the Mallero in Sondrio.

4.4 Measuring the precipitation on Valmalenco

This section briefly describes the spatial distribution of rainfall stations. The hydrological records start at 1989, after 1987 flood by using some rain gauges, so the data available for the precipitation are only for less than 25 years. Table 4.2 lists the rainfall stations, while their position identified on the map shown in Figure 4.7.

station name	station code	Altitude MSL [m]	Location
Spriana	P1	650	Ponte sul Mallero
Cucchi	P2	680	Comune di Torre, sponda sinistra
Torre S. Maria	P3	720	Ponte sul Mallero
Ganda di Lanzada	P4	970	Centrale ENEL sul torrente Lanterna
Chiesa Valmalenco	P5	1022	Ponte sul Mallero
Curlo	P6	1051	Ponte sul Mallero
San Giuseppe	P7	1430	Ponte sul Mallero
Campo Franscia	P8	1518	Valle del Lanterna
Laghi di Chiesa	P9	1610	
Alla Braccia	P10	1650	Valle del Torreggio
Alpe Costa	P11	1690	Bassa Val di Tegno
Piazzo Cavalli	P12	1710	Pendici del monte Palino
Alpe Entova	P13	1900	Bacino del Mallero superiore
Campo Moro	P14	1971	Centrale ENEL – valle del Lanterna
Funivia al Bernina	P15	2014	Lago Palù
Alpe dell'Oro	P16	2030	Bacino del Mallero superiore

Table 4. 2 : List of the rainfall stations.

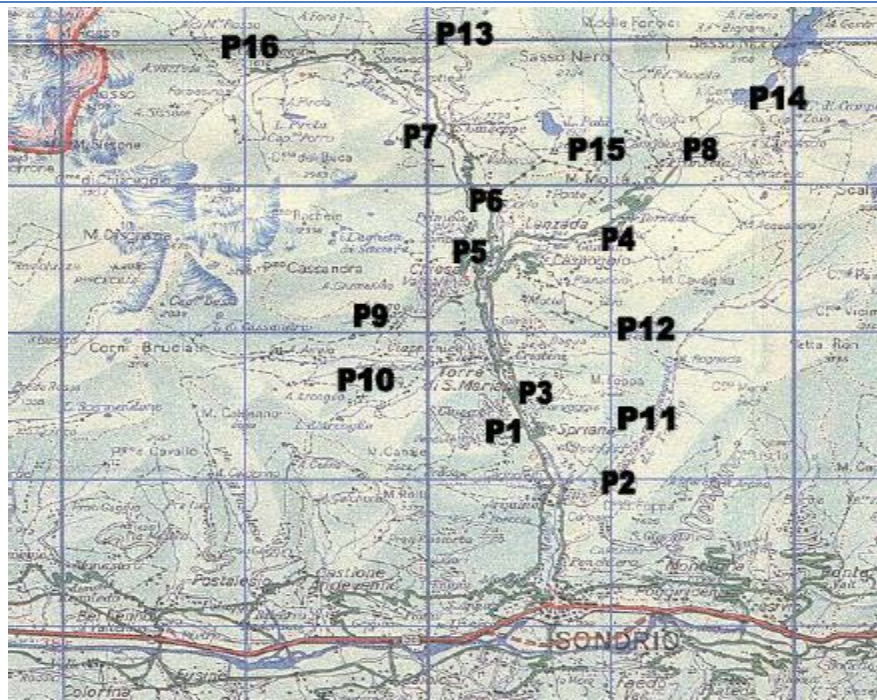


Fig. 4. 7: Locations of rainfall stations.

4.5 Measuring the discharge in Mallero

The Geological Monitoring Centre in Sondrio has provided the values of water height measured every 30 minutes for five gauges on the Mallero River and one on Ganda di Lanzada (Lanternia) for the period January 1992 - July 1999. The list of these stations is shown in Table 4.3.

station name	station code	Altitude MSL [m]
Sondrio, ponte Eiffel	I1	298
Ponte di Spriana	I2	650
Torre S. Maria	I3	720
Chiesa Valmalenco	I4	1022
Curlo	I5	1051
Ganda di Lanzada (Lanternia)	I6	970

Table 4. 3: List of hydrometric stations.

From the measured water depth in some sections during the period from 1992 to 1998 it was possible to draw the so-called rating-curves relates the

water depth with the discharge at specific cross section e.g. Fig 4.8 represents the rating curve in Sondrio, ponte Eiffel.

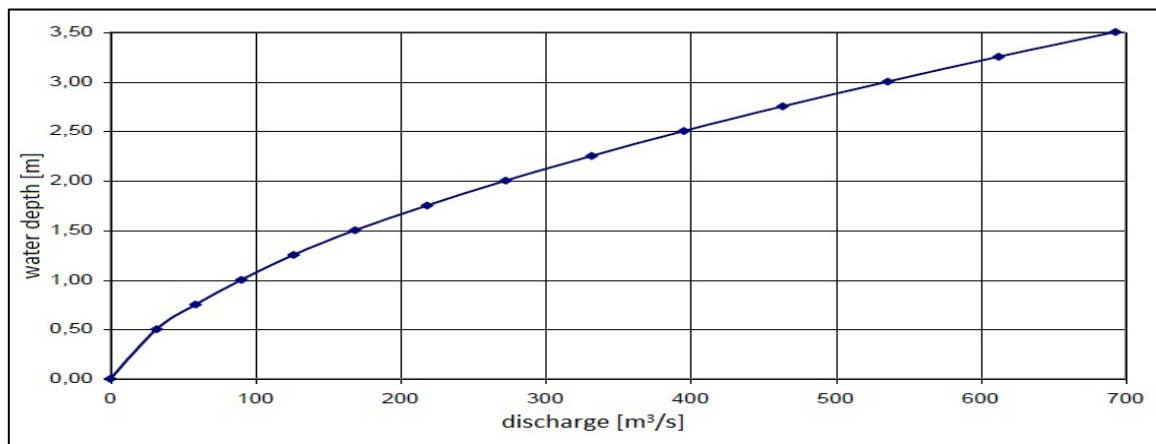


Fig. 4. 8: The rating curve at Sondrio, ponte Eiffel station.

The discharge data recorded at the stations given in table 4.3 from 1992 to 1999 is drawn in the form of annual flow curves (Fig 4.9). The curves show that the maximum discharge measured at Sondrio ponte Eiffelin station in this interval is 160 m³/s, while 100 m³/s exceeded only 17 days in 6 years (1992-1999). Also the ordinary discharge in Mallero is less than 10 m³/s (which is very small value and no sediments can transport with these ranges of discharge).

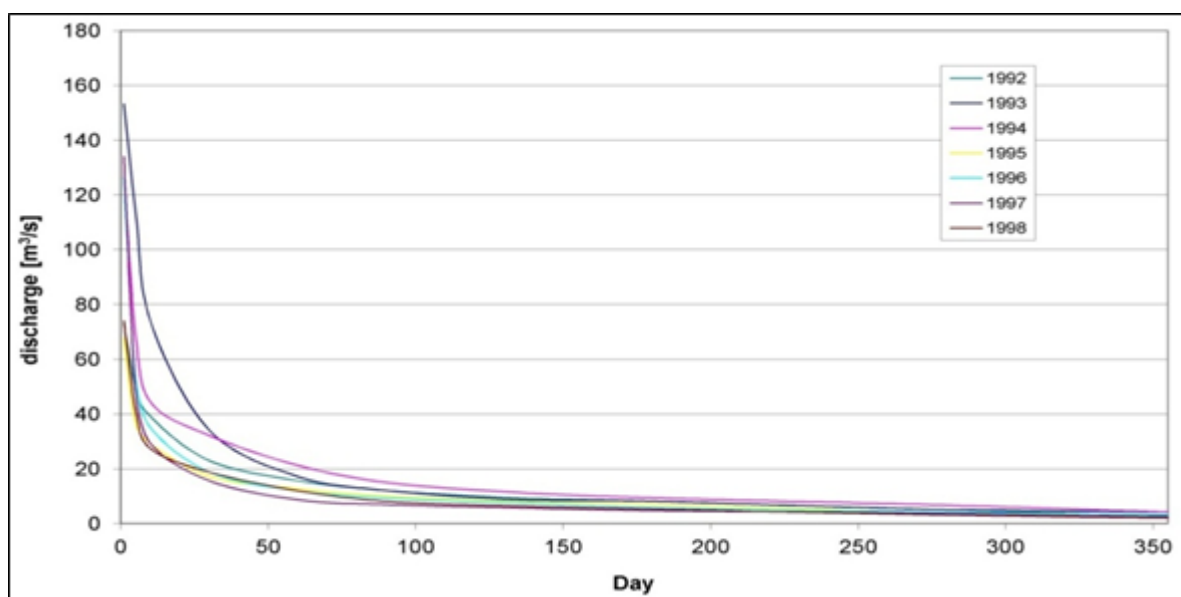


Fig. 4. 9: Annual flow curves from 1992 to 1998 at Sondrio ponte Eiffelin station.

As discussed by (Radice, et al., 2013), in the absence of sediment aggradation, the town would not suffer from a significant flood hazard, since the 100-year discharge is $640 \text{ m}^3/\text{s}$ in Sondrio and the bankfull discharge of the river in the in-town reach is around $690 \text{ m}^3/\text{s}$. Nevertheless, significant increase of the flood hazard may be due to low local slope values, according to which the sediments transported by the river are likely to deposit (as a consequence of the decreased transport capacity of the flow), thus inducing a strong aggradation and reducing the conveyance.

4.6 The 1987 floods in Sondrio

According (Radice, et al., 2013); several flash floods affected Sondrio in the last centuries: events have been documented in 1817, 1834, 1885, 1911, 1927 and 1987. Indeed, the event of 1927 is frequently addressed as the worst one because it involved largest volumes of sediments. On the other hand, unfortunately, this 'ancient' event is not well documented.

According to (Filippetti, et al., 2012); 1987 flood was different and can be summarized as follows: the mid of July was characterized by the presence of a high anticyclone over the Mediterranean started from the Atlantic, while there is cold currents coming from the Arctic. In this context; on 17 the two currents clashes with each other in the zone of Alps, this was the cause of the precipitation. In the province of Sondrio the peak precipitation was 305 mm in that day. The problem that this event had outstripped by a normal precipitation, this rainfall had already made the land covered by alluvial and fully saturated, so all the precipitation ran off without infiltration.

The consequences of the floods in Adda and Mallero were: 53 dead, thousands of the displaced and 4000 billion LIRE (£) was the total cost of the

damage caused. Fig. 4.10 shows the situation in Mallero during this event, it is clear that still the flood within the Mallero thresholds.



Fig. 4. 10: Level reached by the water due to the flood in Mallero at 1987.

The danger of flooding was the excessive water flow and the accumulation of debris that occurred in the part of the river with low slope that led to raising the bed and it drastically reduced the river capacity. This is the reason why the bulldozers were needed (Fig. 4.11) to dredge the deposited materials in order to restore the river capacity, therefore reducing the risk of future flooding.



Fig. 4. 11: Dredging operations after 1987 flood.

The hydrograph estimated in 1987 for that flood (Fig. 4.12) has the following characteristics: The total duration of the hydrograph is 51 hours and the maximum peak is nearly $500 \text{ m}^3/\text{s}$. The estimated volume of sediment that has been eroded from the last 5 km upstream of the confluence with Adda river

equal to $7 \times 10^5 \text{ m}^3$, while $2.2 \times 10^5 \text{ m}^3$ has been settled in the city section. The sediment deposited had 5 m depth at Garibaldi Bridge, while 3 m at the Eiffel Bridge and 2 m at the railway bridge (the bridges location shown in Fig 4.13). Finally; a volume equal to $3.5 \times 10^5 \text{ m}^3$ was poured into the Adda River. The capacity of Mallero, after this event, estimated by $160 \text{ m}^3/\text{s}$ only, because of the drastically increasing in the bed level as a result of the sedimentation, which means that the capacity reduced by 77%.

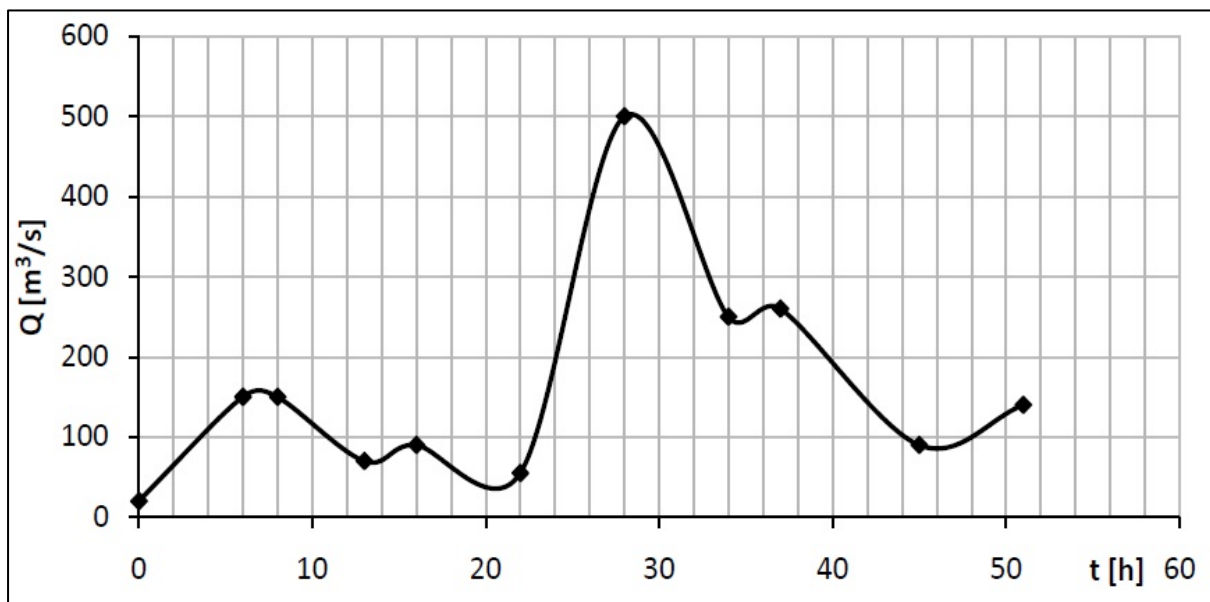


Fig. 4. 12: The hydrograph for 1987 flood.

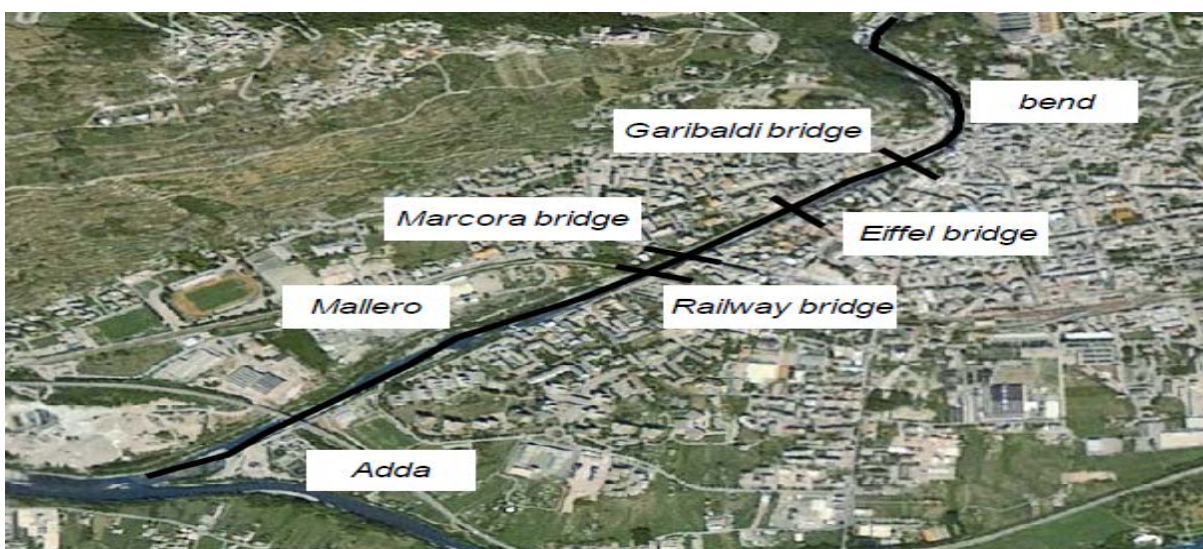


Fig. 4. 13: Google Earth view of Sondrio with indication of bridges location; taken from (Radice, et al., 2013).

4.7 Spriana landslide

There are some landslides likely to occur in Valmalenco. The dominant triggering factor for these landslides is the increasing of the ground water table due to the intensive precipitation for long durations; also it can be induced for any earthquake.

The most important landslide is the Spriana landslide; it is located at the left side of Mallero River (Fig.4.14) in the Valmalenco valley at a distance around 7 km from the confluence point with Adda. The landslide bounded from North West by Vallone di Badoglio and from South West by Val Calchera. The foot of the Landslide is estimated at 700 m ASL, while there are two visible crowns are obvious at the level of 1100 m and 1400 m.

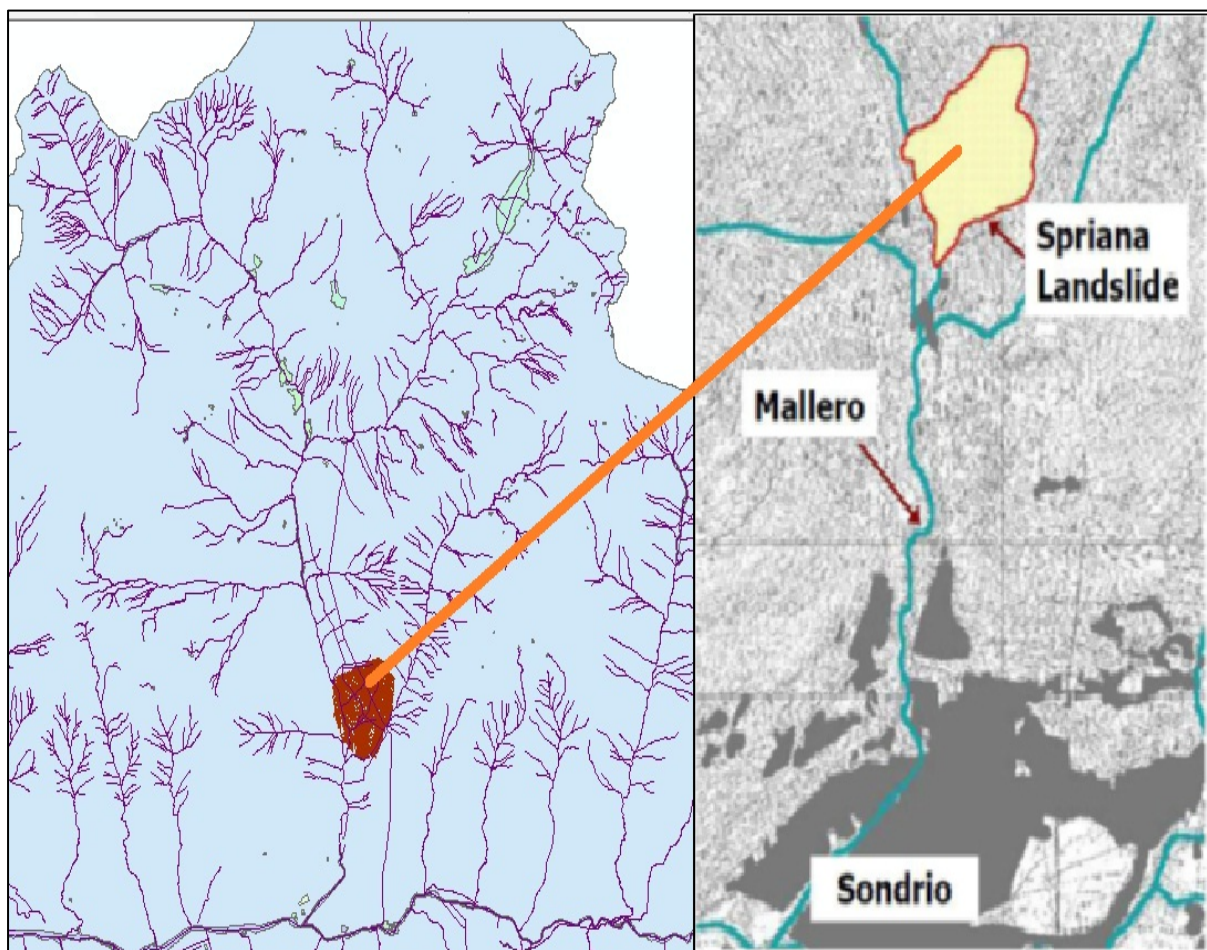


Fig. 4. 14: The location of Spriana.

The failure of Spriana landslide will close, temporary, the valley of Mallerio once it happen, creating an earthen dam and huge lake behind this dam. The body of the Spriana landslide is shown in figure 4.15.

According the emergency plan report prepared by (Franzetti, 2005); the collapse of Spriana landslide will produce $20 \cdot 10^6 \text{ m}^3$ of soil starting from crown at 1400 m AMSL. This amount of soil will create an earthen dam with 80 m height. This earthen dam will store, for a short period, huge amount of water behind it that can cause it's failure due to the seepage effect or due to overtopping effect. The dam break (breaching) is expected to produce a catastrophic wave that lead to Sondrio inundation as will be discussed in chapter 6.



Fig. 4. 15: The body of Spriana landslide.

5 The Case of Mallero: 1987 Flood

5.1 Introduction

There are a lot of studies for 1987 flood prepared before like (Radice, et al., 2013), (Mauri, et al., 2009) and (Filippetti, et al., 2012), some of them considered the bed evolution for a specific length from the whole Mallero most of them focused on the last 5 Km only. So the aim from restudying 1987 flood again is to include more length of Mallero, to make calibration for the used software (Basement V2.1 discussed in item 2.3) and the next work will discussed here, in addition to doing some sensitivity analysis checking the effects of some parameters.

So in the following, the cross-sections used in the model will be described then the water and sediment discharges used in the model. A comparison among obtained results and the previous results will be discussed, then the sensitivity analysis for the used granulometry and the control volume thickness (cvt) will be discussed.

5.2 The model cross sections

Inside the town of Sondrio, the geometry of the sections is characterized by an almost rectangular shape with widths of 20-40 m in average as shown in fig 4.6. While in the other parts, the cross sections is varying between trapezoidal and irregular (fig 5.1 &5.2). The sections used for model building are 92 sections, numbered from CS1 (the upstream) to CS92 (at confluence point with Adda river), the whole distance from CS1 to CS92 is 9480 m, while their shapes are based on a simplified geometry obtained from topographic surveys.

The figures below show two examples of the sections, in which the blue line is the one actually measured, while the red one is the simplification proposed, which keeps the horizontal bottom and keeps the height of the embankments.

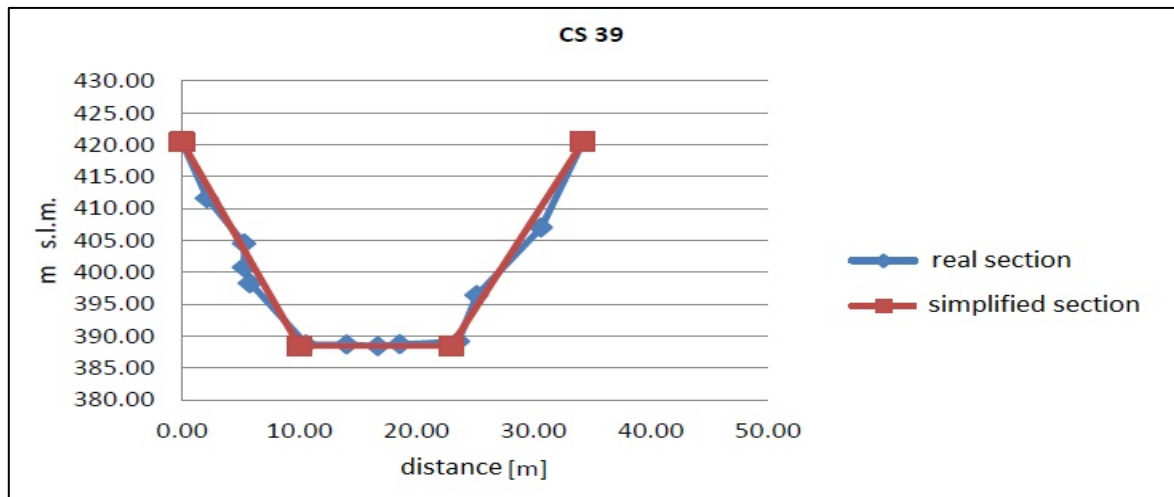


Fig. 5. 1: Simplification for section 39 (4585 m from Adda River).

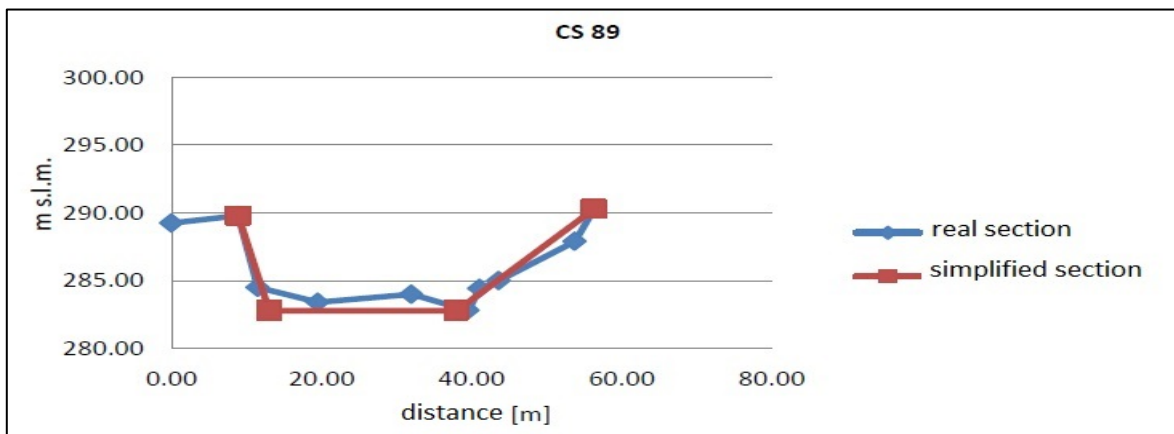


Fig. 5. 2: Simplification for section 89 (389 m from Adda River).

Since the model boundary condition for the sediment flow downstream requires that the height of the bottom remains unchanged (which is totally unrealistic), a dummy stretch of prismatic channel was added with slope 0.1% and geometry of section 92 while the distance among these dummy sections is 60 m. The aim is to make the model independent of the downstream boundary condition which is not entirely representative for the reality and propagate some error. The bed profile is shown in the following figure including this

dummy stretch starts at distance 9480 and the zones of hard (fixed) bed, while the distances among the cross sections considered in the model, including the dummy stretch, are shown in fig 5.4. The distances among the sections are irregular and it vary form 20 m to 256 m, this variations lead to numerical instability as will be discussed and overcome later.

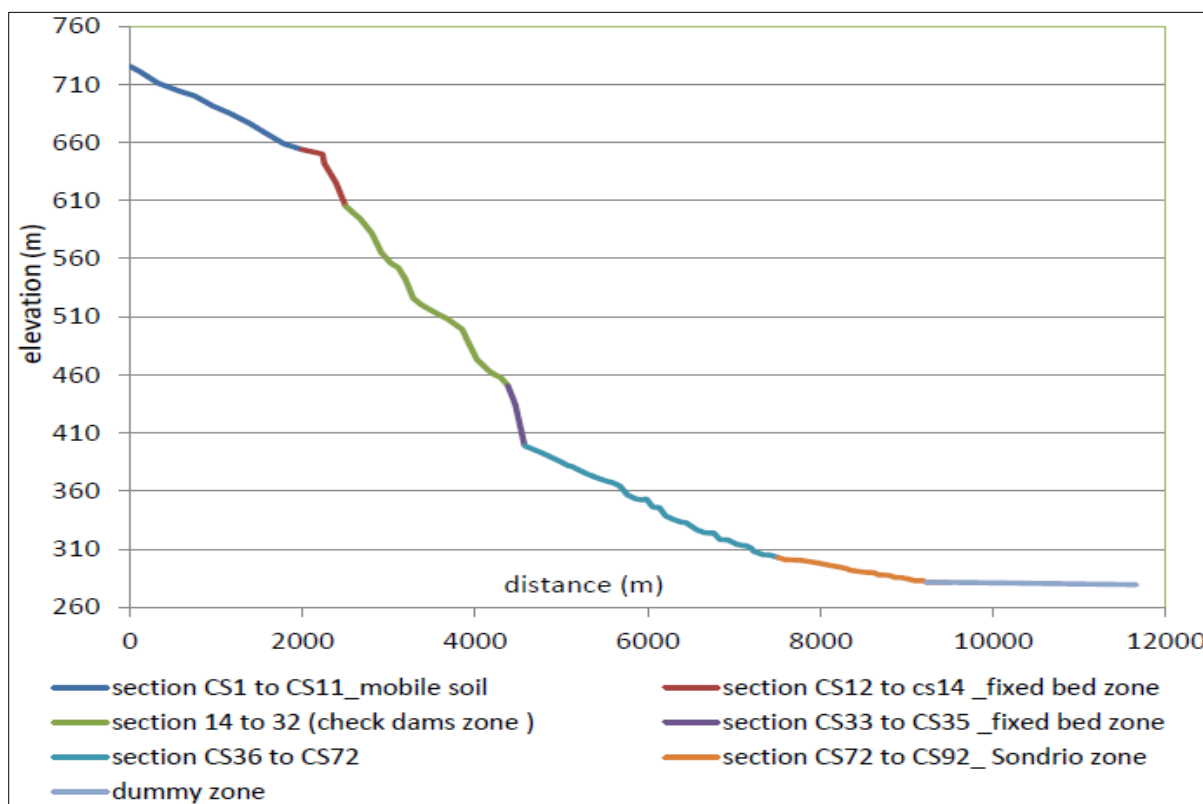


Fig. 5. 3: The bed profile of Mallero and the zones of hard bed.

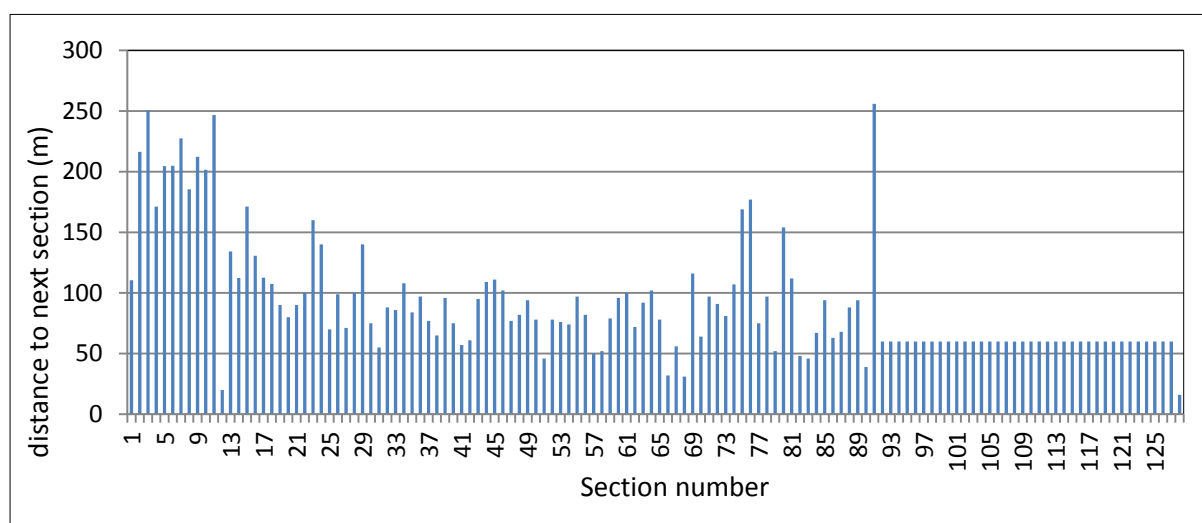


Fig. 5. 4: The distances among the sections used in the numerical modeling.

There are 12 check dams were built along Mallero, the main purpose of them was the reduction of the bed erosion due to the high slope of the river bed, the locations of these check dams are shown in the figure below.

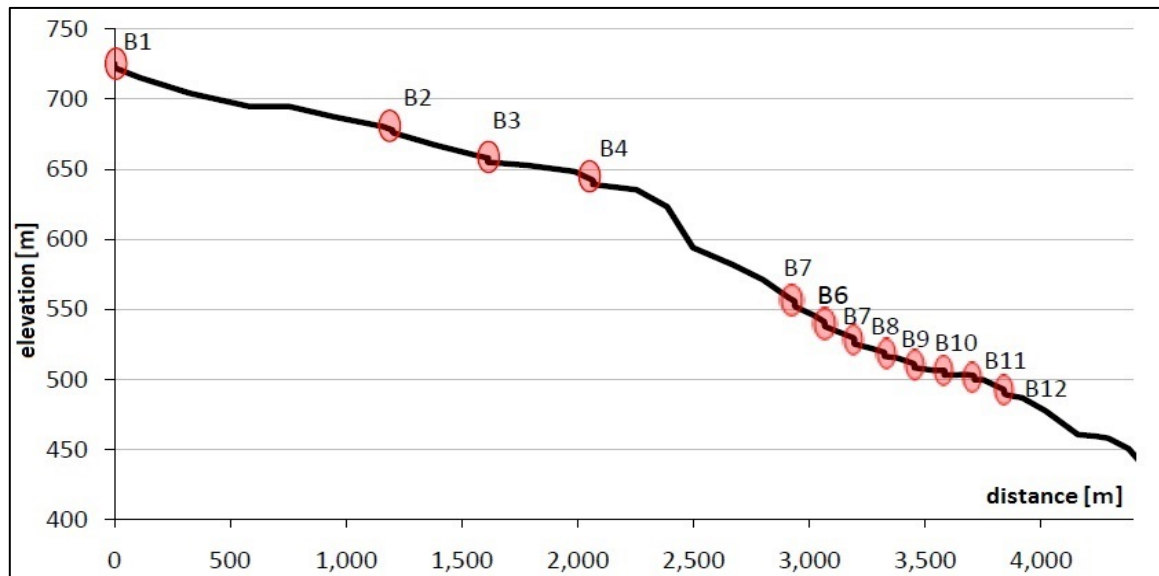


Fig. 5. 5: The bed profile in the zone contains the check dams (Mauri, et al., 2009).

As in (Mauri, et al., 2009); the height of these checks dams is in the range from 1 m to 5 meters. So the bed at these check dams are considered with fixed bed, but there is no simulation for the check dams themselves.

In the downtown there are some bridges built in the Mallero valley their locations shown in the fig 4.13 (taken from (Radice, et al., 2013)). These bridges are not included in the model because of the incapability of Basement to model the hydraulic structures.

5.3 Models granulometry

As discussed in item 3.5; Basement software has the ability to use multi sizes to represent the bed's grain sizes, so this ability has been exploited and the model has been run using different granulometry. Table 5.1 shows the 3 granulometry based models used in the analysis and its relations with the actual median grain sizes d_{50} in the last 9480 m from Mallero River.

The table shows that the particle size, as often happens in the floodplains of the mountain, is very distributed. Table 5.1 zooms only the traits of a part from table 4.1 which represent the last 9480 m of Mallero and the granulometry based models.

location	d50 [mm]	model with 3 diameters			model with 4 diameters			
		10 mm	80 mm	800 mm	10 mm	50 mm	80 mm	800 mm
A valle di Torre S.	85-140	0%	100%	0%	0%	0%	90%	10%
A monte di Spriana	84-127	0%	100%	0%	0%	0%	90%	10%
Tra Spriana e Arquino	247-772	0%	100%	0%	0%	0%	90%	10%
A valle di Arquino	772	0%	100%	0%	0%	0%	10%	90%
Cassandre	540-1180	0%	100%	0%	0%	0%	10%	90%
Sondrio	40-73	100%	0%	0%	10%	70%	20%	0%
feeding mixture		50%	25%	25%	40%	30%	20%	10%

location	d50 [mm]	model with 10 diameters									
		10 mm	50 mm	60 mm	80 mm	100 mm	300 mm	600 mm	772 mm	800 mm	1000 mm
A valle di Torre S.	85-140	0%	0%	0%	30%	70%	0%	0%	0%	0%	0%
A monte di Spriana	84-127	0%	0%	0%	30%	70%	0%	0%	0%	0%	0%
Tra Spriana e Arquino	247-772	0%	0%	0%	0%	0%	50%	30%	20%	0%	0%
A valle di Arquino	772	0%	0%	0%	0%	0%	0%	0%	100%	0%	0%
Cassandre	540-1180	0%	0%	0%	0%	0%	0%	50%	20%	20%	10%
Sondrio	40-73	0%	50%	50%	0%	0%	0%	0%	0%	0%	0%
feeding mixture		40%	20%	10%	10%	10%	2%	2%	2%	2%	2%

Table 5. 1: Basement models according to actual and assumed granulometry

The grain sizes for models with 4 and 10 diameters are selected by the writer, while for 3 diameters model; the diameters and it’s ratios are selected by (Filippetti, et al., 2012). This selection is kept here to enable the comparison with the results obtained by this model as will come later. Any way the diameters are selected to give the most suitable representation for the bed granulometry then, the median diameter ascribed to these diameters by an expected ratio e.g. for model with 3 diameters, the diameters 10, 80, 800 mms are assumed then, the ratio that this diameter represents is selected based on it’s proximity to median diameter domain i.e. for $d_{50} = 85 - 140$ mm, 80 mm is selected by ratio 100% since 10 mm and 800 mm are very far from the median diameter. In the hard bed parts the bed granulometry is selected by

any diameter with regardless the median diameter domain since these parts have fixed bed and no degradation can happen from this zones e.g. in Cassandre the median diameter ranges between 440-1180 mm, while the selected diameter is 80 mm. The feeding is selected to represent the entire diameters used, by using random ratio that represents the expected contribution of each diameter.

5.4 Model boundary and initial conditions

A steady model with a discharge 20 m³/s, which represent the ordinary discharge, has been used to find the initial condition for all the sections together, so the considered initial condition used is the initial discharge 20 m³/s.

As a boundary condition in upstream; the hydrograph corresponding to that calculated by post-event analysis for 1987 event, using Nash rainfall-runoff model (item 4.6), has been used as a boundary (Fig 5.6). The duration of the hydrograph is 60 hours with a peak flow of 500 m³/s. In addition to this hydrograph; the slope defined at upstream is 40 ‰ as a second boundary condition.

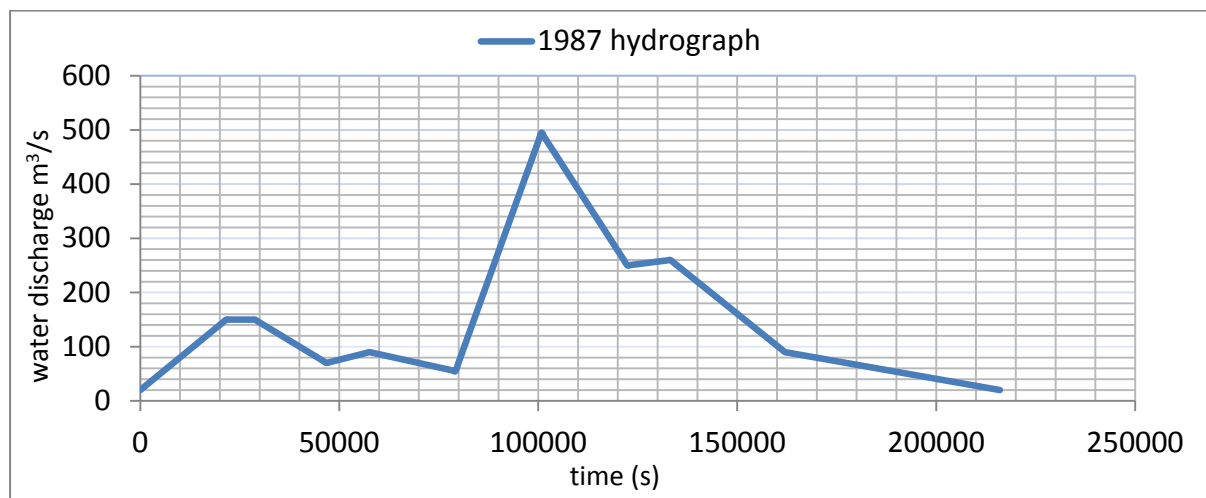


Fig. 5. 6: The feeding discharge corresponding to 1987 hydrograph.

The sediment upstream boundary condition used is the sediment hydrograph computed depend on the whole sediment measured as an aggradation in Sondrio which is $7 * 10^5 \text{ m}^3$. Set this condition; the pattern chosen for the sediment hydrograph (Fig 5.7) is proportional to the square of the water hydrograph. The volume of sediment due to this assumption is 697000 m^3 which near from the volume $7 * 10^5 \text{ m}^3$ stated previously.

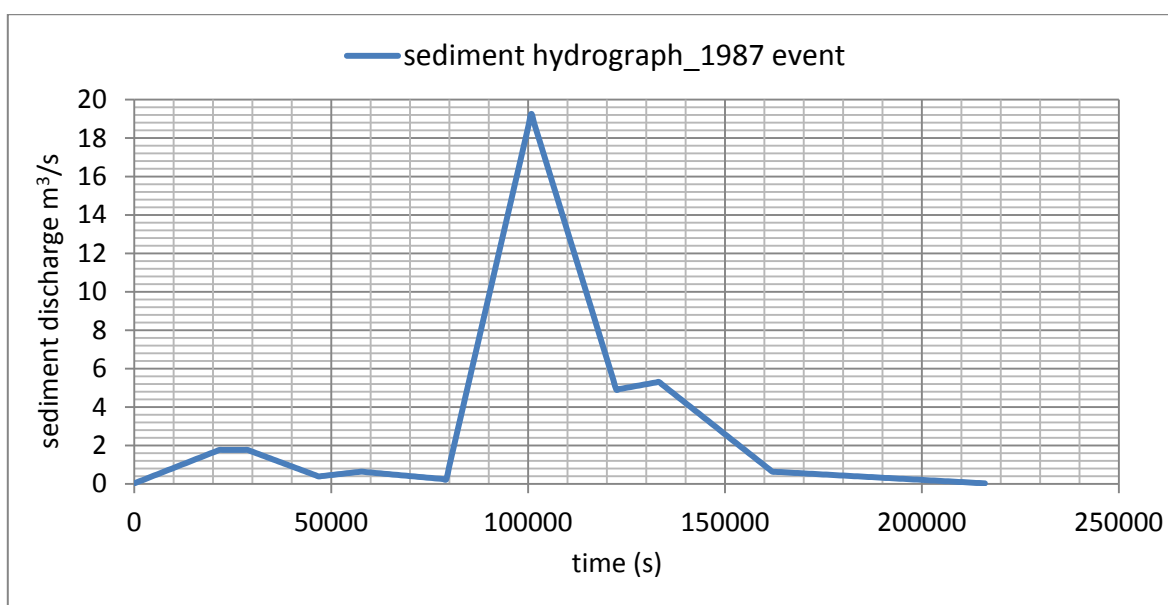


Fig. 5. 7: The feeding sediment discharge corresponding to 1987 event.

The used downstream boundary is the slope of the dummy stretch (1‰) with the fixation of the bed level at downstream and this is the reason why the dummy stretch added.

5.5 Model results and comparison with previous analyses

The following figure (5.8) shows the bed evolution due to the previous boundary conditions with model using 3 diameters to represent the bed and feeding granulometry (Table 5.1). The results show that the sediment starts to deposit in Sondrio from the beginning of the simulation, while it start to degrade at the upstream then start again to aggrade.

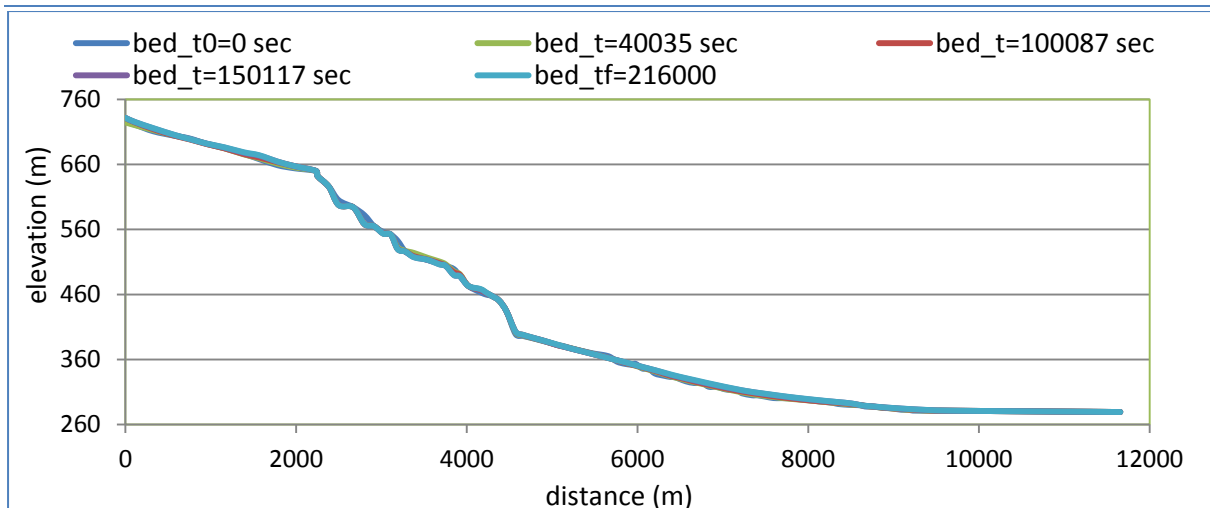


Fig. 5. 8: The bed evolution for 1987 event.

As noted; figure 5.8 doesn't show the bed differences, so in figure 5.9 the bed differences represented with respect to the initial bed level. It shows that the deposition increases in the city zone and also at the upstream, while the zero zones represent the check dams and the fixed bed reaches. Also the dummy stretch zone doesn't have any change in the bed level, although it's bed is mobile type. The zone among the check dams showing sharp erosion for the bed. It is clear that the sediment depth in Sondrio exceeded 5 m in some zones, this elevation of bed increases the vulnerability to the flooding in Sondrio due to the decreasing in the river capacity in the town down.

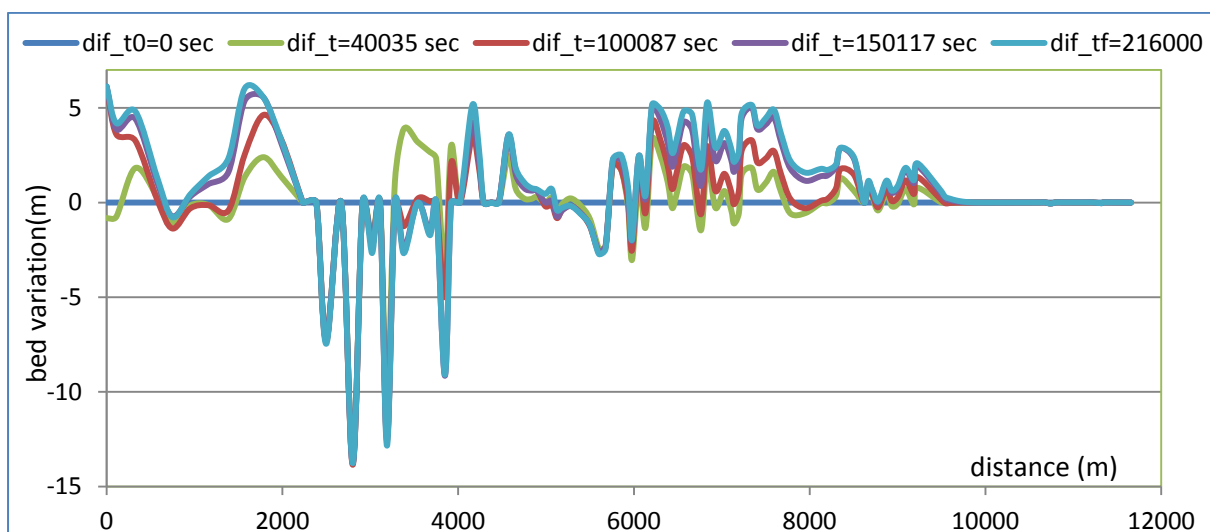


Fig. 5. 9: Bed differences for 1987 event.

It is clear that the majority of the river length exposed to aggradation except the very high slopes exposed to erosion, while the existence of the check dams reduces the sharpness of these erosions.

By comparing the aggradation volumes above the datum (0) in Fig 5.9, with the degradation volumes from the bed in the whole length; the aggregation volumes overcome the degradation volumes, this means that the sediment fed in the upstream transported and distributed in the zones of aggregations, and the contribution of the bed erosion in the aggregated sediment is really small.

As discussed in item 3.5, Basement divides the soil layers into two parts: the active layer with a thickness (cvt) assigns by the modeler and a sub layer equals to the remainder of the soil layer. Usually most of the migration and the sorting processes occur in the active layer, while the changes in the sub layer are insignificant. So let's see how the sediments mix and migrate.

At zero time according the table 5.1; the bed consist of 100% of the 10 mm diameter in the down town and in the followed dummy stretch, while the bed upstream Sondrio consists of 100% from the diameter 80 mm or 800 mm. The migration of sediment diameters calculated by model consists of these 3 sizes is shown in the following figures; figure 4.10 shows the migration of the 10 mm diameter. The figure says that the ratio of this diameter increases at the upstream due to the feeding by the mixture contains 50 % of this diameter, while this ratio reduces again although of the same rate of feeding because the discharged at the event's tail decreases. With this decreasing of the discharge, the 10 mm diameter will be the only diameter can be sorted and migrate so its ratio decreases again with the end of the event. At the downtown, this diameter moves to Adda River and the bed totally replaced by the 80 mm size which can be noted by the shifting of the vertical line in figure 5.10.

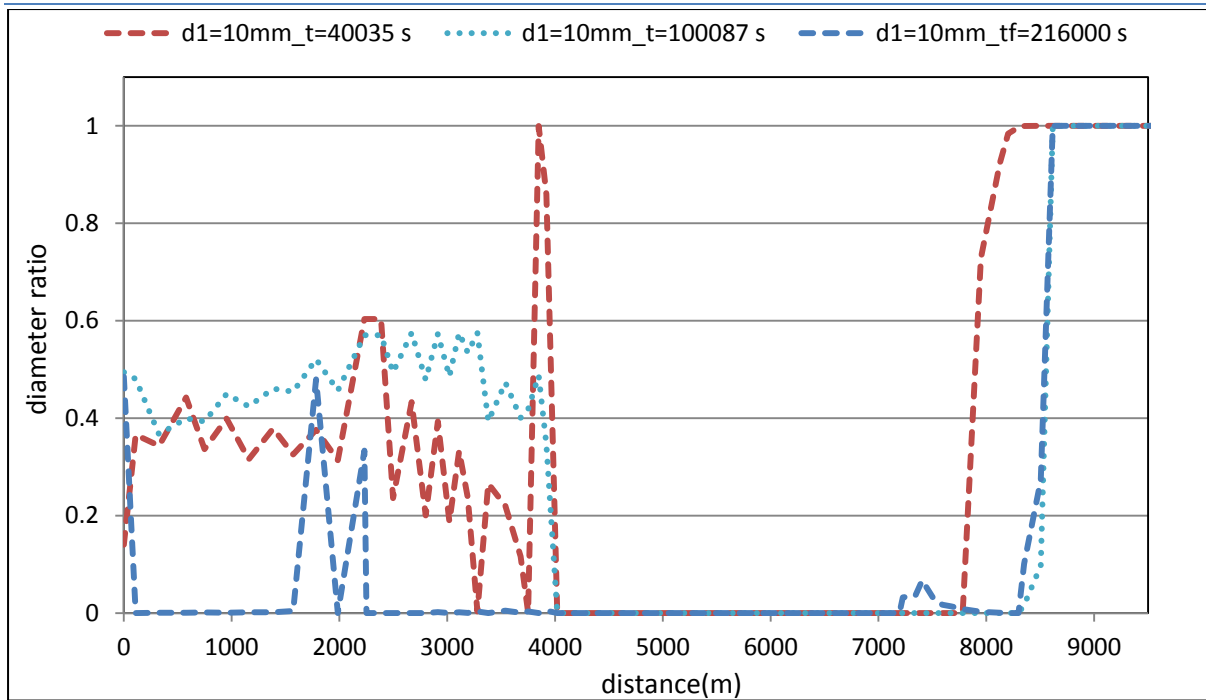


Fig. 5. 10: The migration of the 10 mm diameter in the active layer.

For the 80 mm diameter (Fig5.11); it is almost the complements of 10 mm diameter i.e. the summation of the 2 curves almost equal to one. This means that the decreasing in the ratio of 80 mm diameter will be compensated by the 10 mm diameter and vice versa.

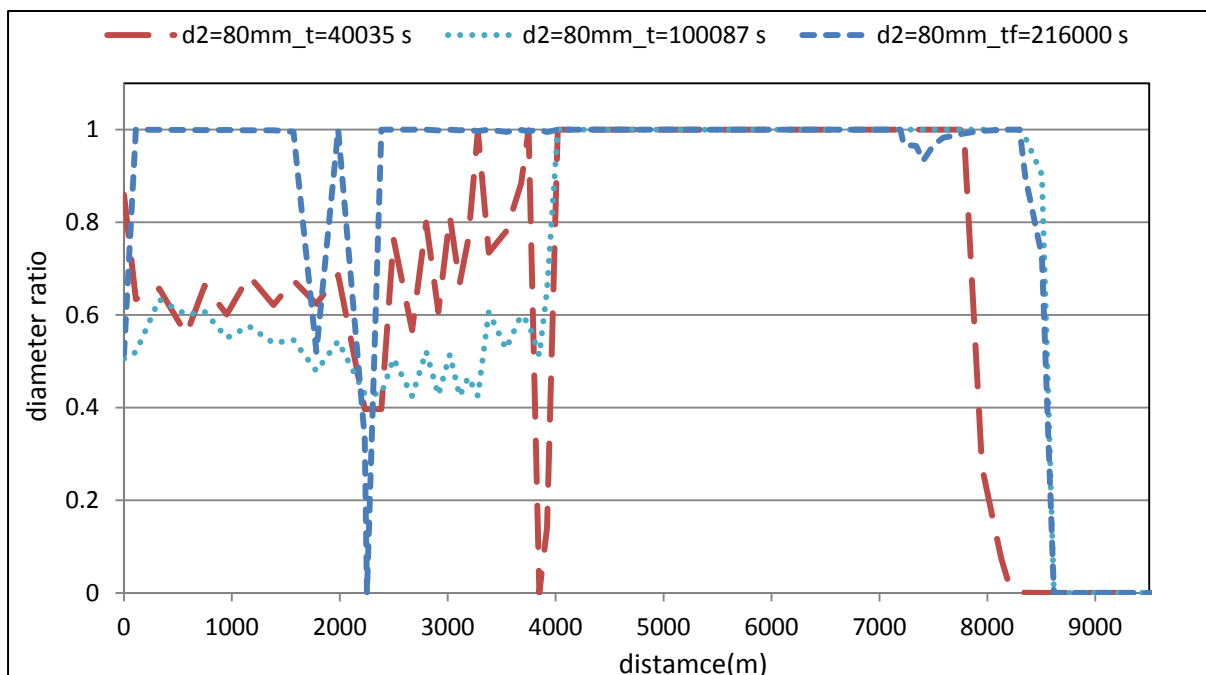


Fig. 5. 11: The migration of the 80 mm diameter in the active layer.

Although the feeding mixture usually includes 25% of the 800 mm diameter, it will not be transported to the downstream but it will deposit in the eroded zone after 2000 m from the model starting as shown in figure 5.12.

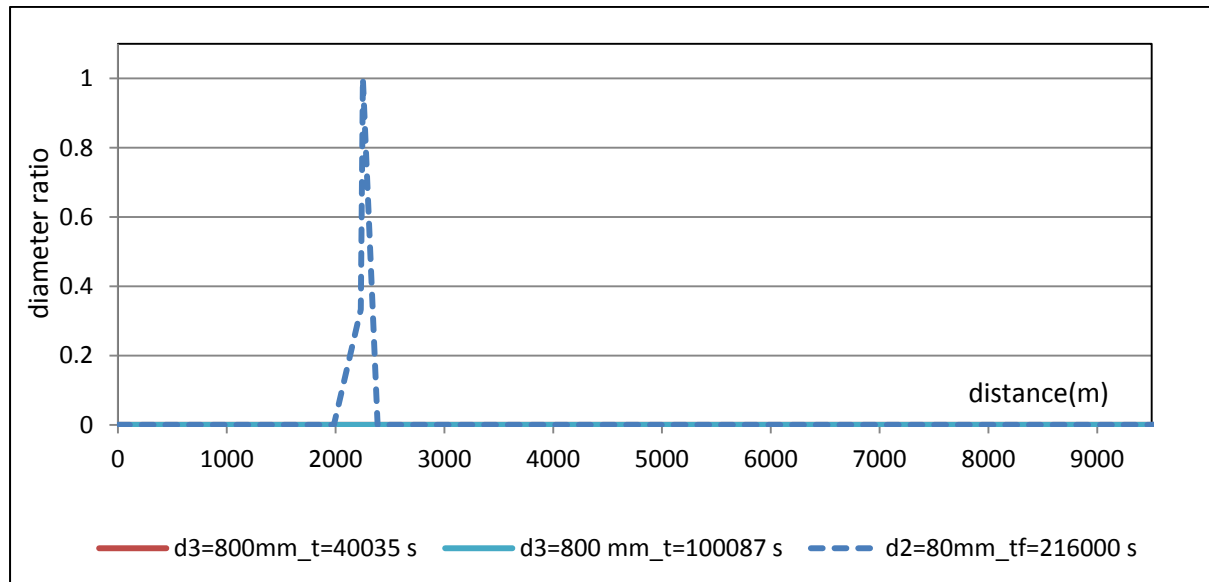


Fig. 5. 12: The migration of the 800 mm diameter in the active layer.

(Filippetti, et al., 2012) studied the last 5 km from Mallero using a model consist of the same 3 diameters used in the analysis here, the same feeding hydrograph and the same sediment feeding (0 distance in Filippetti's model = 4656m in this model) . Their results showed in the following figure (5.13) taken from their work. By Comparing it with the model here, it shows that the sediment depth in Sondrio exceeds 5 m in the same zones although the increasing of the model length, which means that the sediment depth in Sondrio didn't affected by the model length. The small differences in the two results are only because of the effect of the boundary conditions (Unfortunately, fig 5.13 can't be merged with fig 5.9 to highlight the differences). Finally neither (Filippetti, et al., 2012) model nor the model proposed here represents the reality especially at the end of Mallero because of the effect of the downstream boundary condition (dummy stretch with fixed tail) which in reality is the intersection with Adda River.

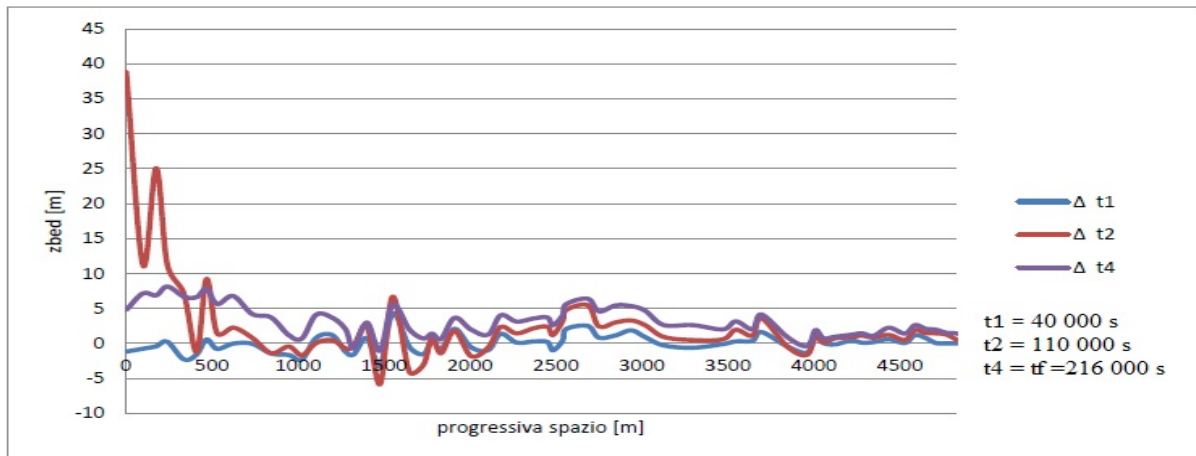


Fig. 5. 13: Bed differences for 1987 event by (Filippetti, et al., 2012).

Comparison between the observed bed level after 1987 event and the calculated bed levels made by (Filippetti, et al., 2012) in the downtown part using single size and multi sizes presented in Fig 5.14. Also this comparison made using 3, 4 and 10 diameters based models, the results shown in fig 5.15 (in the next section, the effect of these classes will be explored in details). As noted in the figures, both the models give very accurate results whenever going away from the downstream because of the boundary effect. Also it is clear that using less number of solid diameters in representing the bed and feeding granulometry gives more accurate results as will be discussed in the following item.

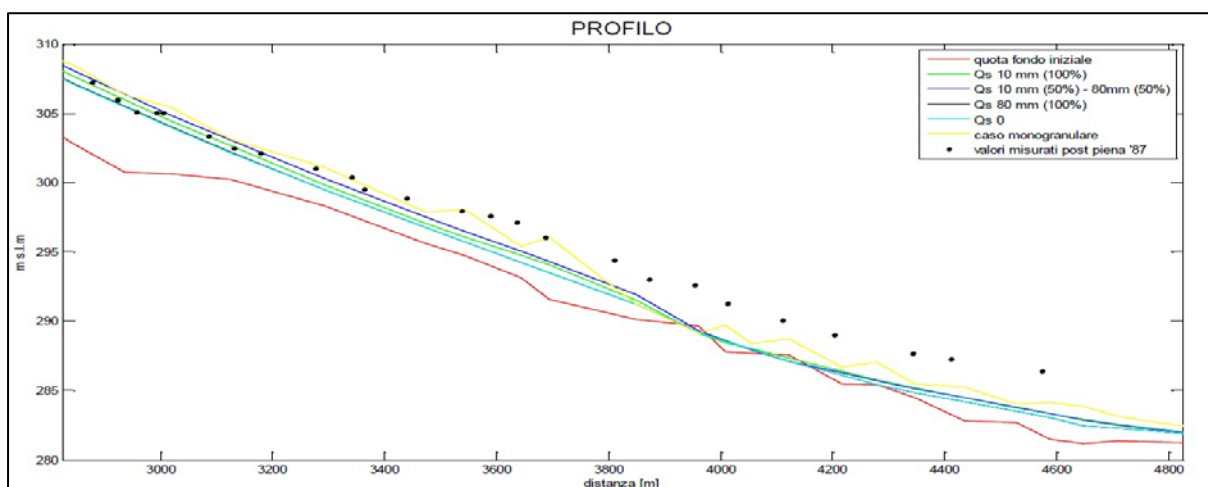


Fig. 5. 14: Comparison between measured values and calculated values by (Filippetti, et al., 2012) for the Mallero in the city section.

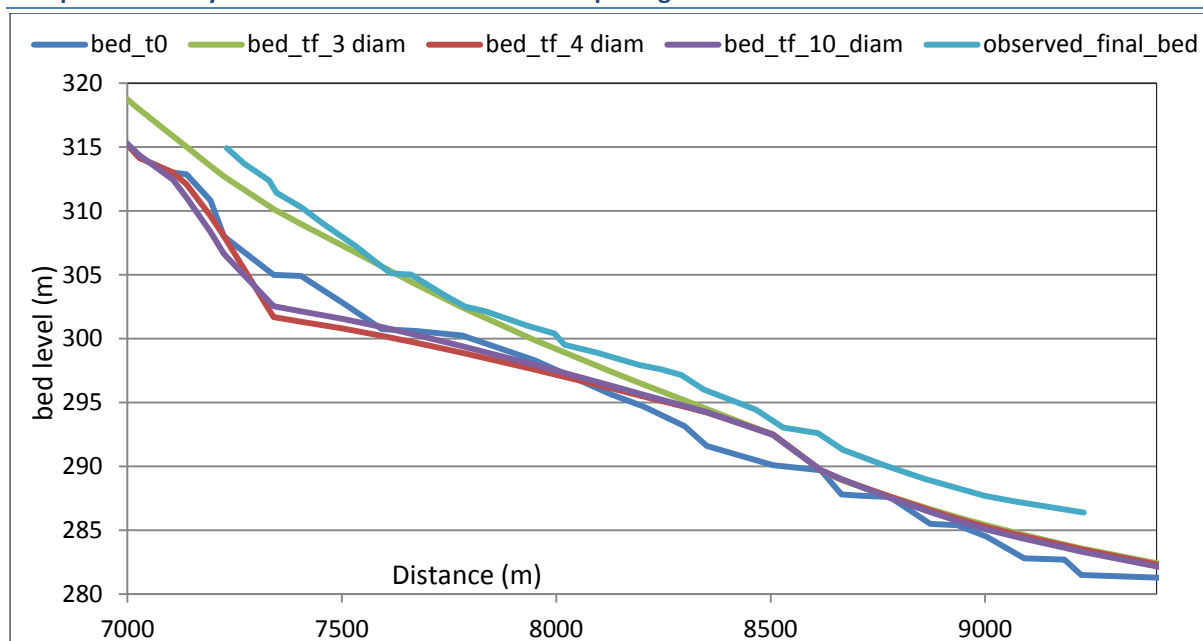


Fig. 5. 15: Comparison between measured values and calculated values in the in-town part.

5.6 Model sensitivity to bed granulometry

As shown in tables 4.1 and 5.1; the mean diameter ranges are wide. So, what will happen in case of using more diameters in representing both the bed granulometry and the feeding mixture is the point of discussion here? According to table 5.1; two additional model ran; the first using 4 grain sizes(10, 50, 80, and 800 mm) to represent the bed granulometry, while the second uses 10 grain sizes (10, 50, 60, 80, 100, 300 ,600, 772, 800, and 1000 mm). The spatial distribution and the ratios of these sizes in the feeding mixture are shown in table 5.1. The following figure (5.16) shows the bed evolution by using the three models (3, 4 and 10 diameters model). Since the differences are not clear in this figure, figure 4.31 shows only the differences between the final bed levels computed using these different 3 models. As shown in the two figures; the model is very sensitive to the grain sizes used. This sensitivity produced because of more sorting and transporting expected with more refinement of the sizes. Hence the aggradation and degradation

zones may be changed. But simplifying the granulometry as possible needed to arrive to more reliable results.

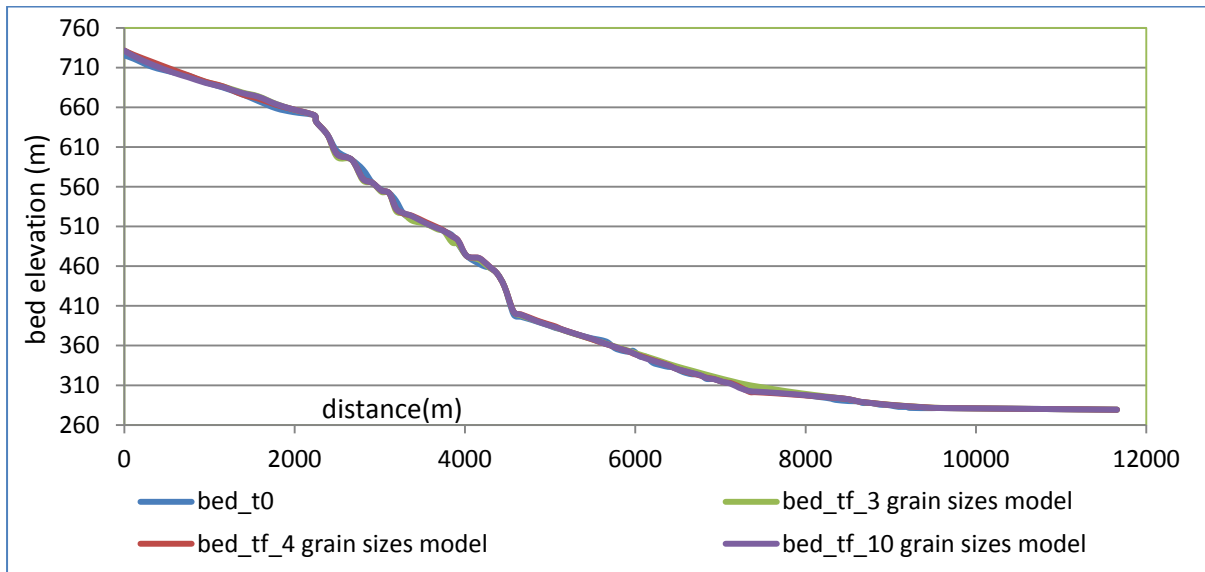


Fig. 5. 16: The bed evolution due to 1987 event using different granulometry.

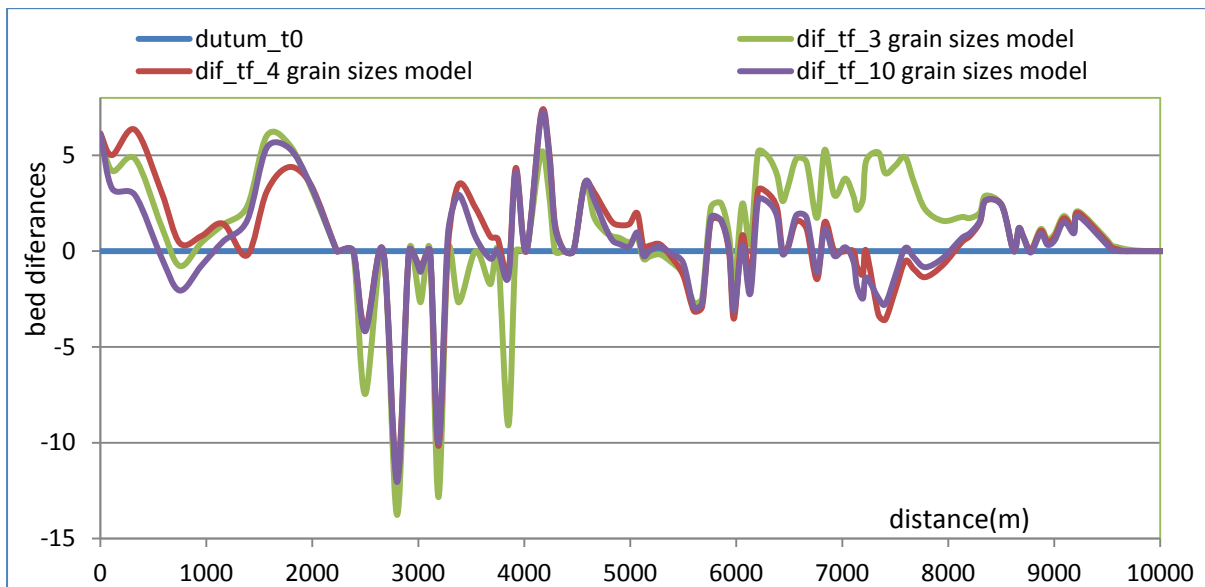


Fig. 5. 17: The bed differences using different granulometry.

The following two figures show the granulometry distribution at the final simulation time ($t_f = 216000$ sec), while the initial distribution of the bed granulometry and feeding mixture showed in table 5.1. The predominant character in these two figures is that the coarse sediments are the dominant upstream, while the finer are dominant downstream. The reason for this fact is

Comparative study of different scenarios for the morphological evolution in a river stream

the sorting effect i.e. the finer sediment will move firstly, keeping the big sizes up stream in the higher slopes as in figure 5.20. As shown, the mixing zone for the 3 diameter model is 4 km and for the 4 diameters model is more than 3 km, which means that the feeding affect only the first part only of the river and the aggradation source is not the feeding but the bed erosion. Also it may be noted that, with multiple diameters may the migration of sediment can't be understandable as in fig 5.19.

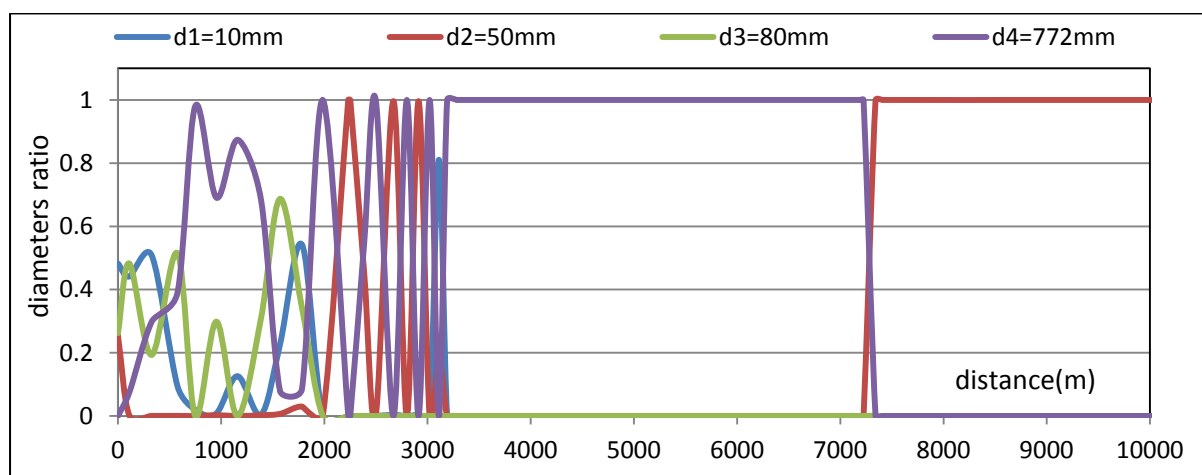


Fig. 5. 18: Granulometry distribution along Mallero at the end of simulation time using 4 sizes model.

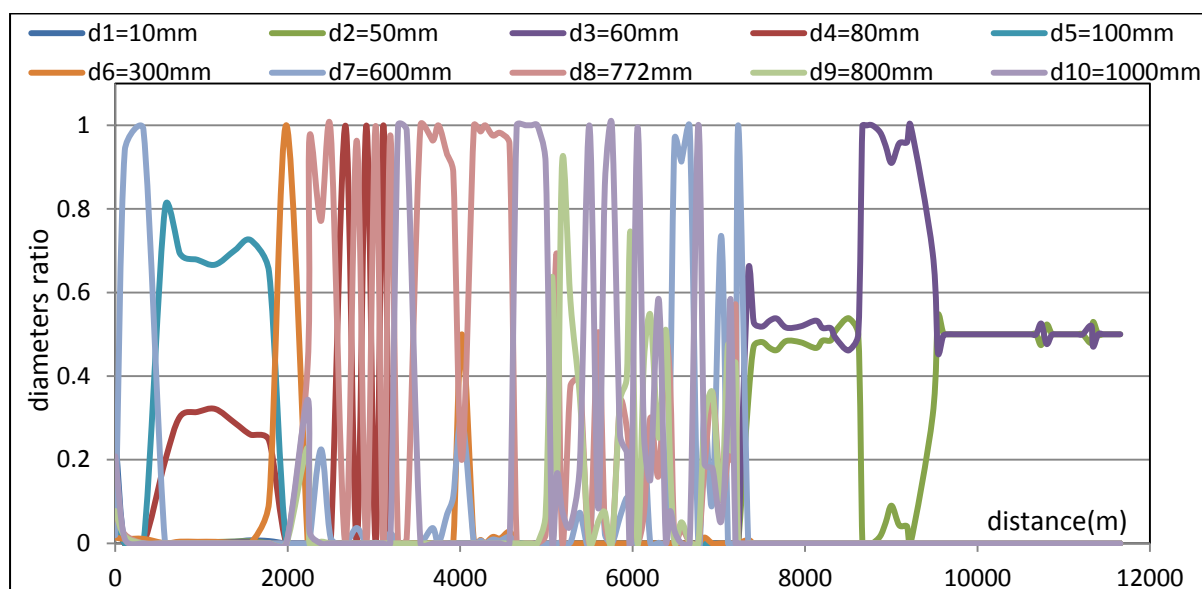


Fig. 5. 19: Granulometry distribution along Mallero at the end of simulation time using 10 sizes model.

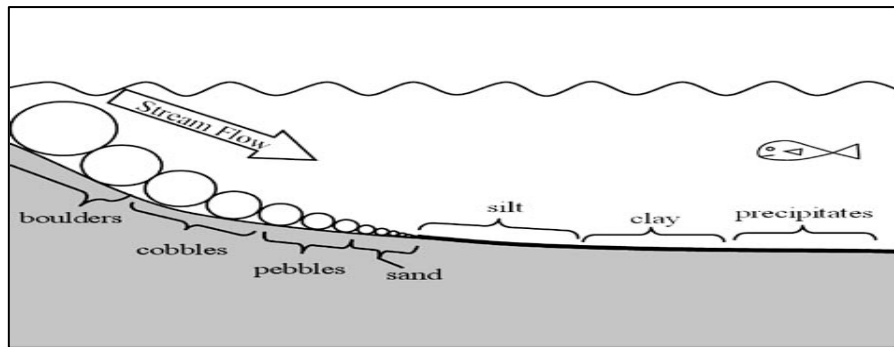


Fig. 5. 20: The sorting effect in open channels.

5.7 Model sensitivity to bed friction

According to item 1.6, speaking about the effective bed friction, there are two types of bed friction; the skin friction computed depend on the granulometry sizes and the total friction which include the skin friction, the bed form effect, the friction due to vegetation and any other sources of friction.

According to item 2.3.2; Basement software has the capability to calculate the skin friction depend on the granulometry assigned to it, while the total value must be assessed and assigned in the form of either Manning, Strickler, or Chezy friction coefficients, if the total friction effect is the required. The value assigned for Strickler coefficient for all the analysis done before was $30 \text{ m}^{1/3}/\text{s}$. The following figures show the differences between the bed levels using the skin friction (calculated by Basement) and the total friction (assigned to the program). For model uses 3 grain sizes as shown in figure 5.21, the bed levels at the end of the simulation time ($t_f=216000\text{s}$) are identical. This means that, the model considered only the skin friction in calculating the total friction i.e. skin friction calculated by Basement equal to the total friction equal to $30 \text{ m}^{1/3}/\text{s}$ for this special case and with the same grain sizes. This means that the other sources of friction like the bed form and vegetation effects were neglected during the estimation of the total friction.

Comparative study of different scenarios for the morphological evolution in a river stream

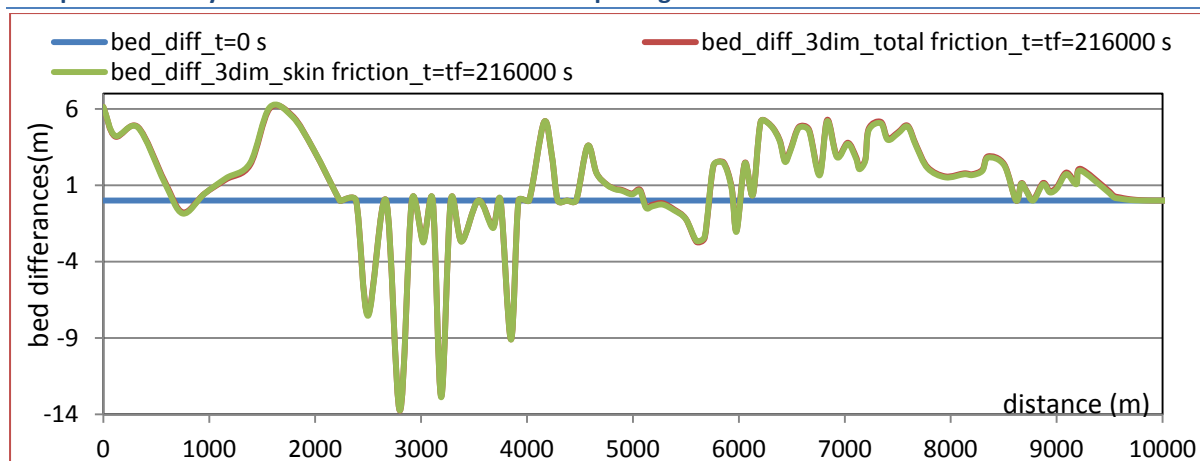


Fig. 5. 21: Effect of the skin friction on the morphological evolution for bed consist of 3 diameters.

With using more grain sizes the bed granulometry can be described by bigger sizes, hence the skin friction exceeds the assign value for total friction ($30 \text{ m}^{1/3}/\text{s}$). The skin bed friction decreases in the aggradation zones because of its smooth surface, so finally the model is sensitive to the bed grain sizes used. Hence, for each model uses different grain sizes, different value for the total friction must be calibrated and assigned to reach to the same result. Figure 5.22 and 5.23 show the differences between the two beds in case of using 4 and 10 diameter models respectively. The common feature among the three figures (5.21 to 5.23) is the coincidence of the bed levels in the down town where the zone of interest is.

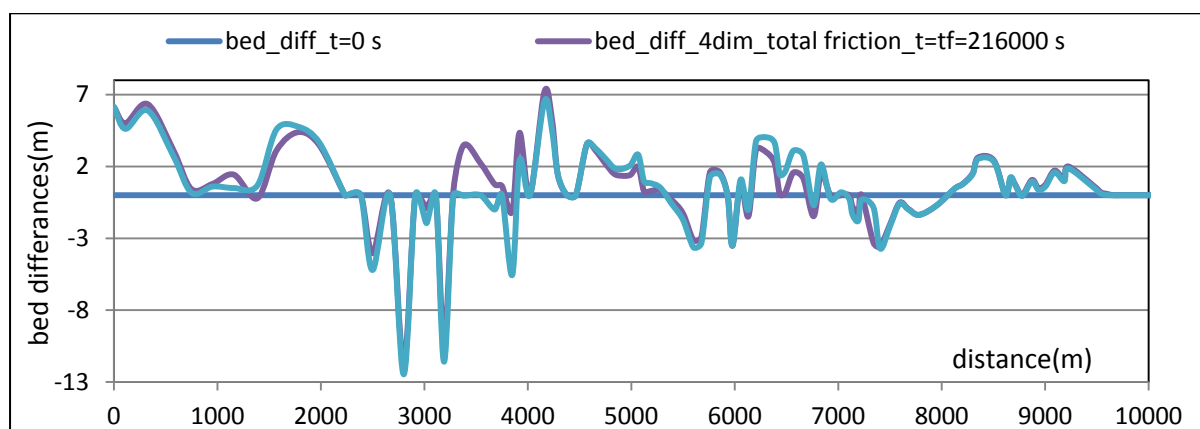


Fig. 5. 22: Effect of skin friction on the morphological evolution for bed consist of 4 diameters.

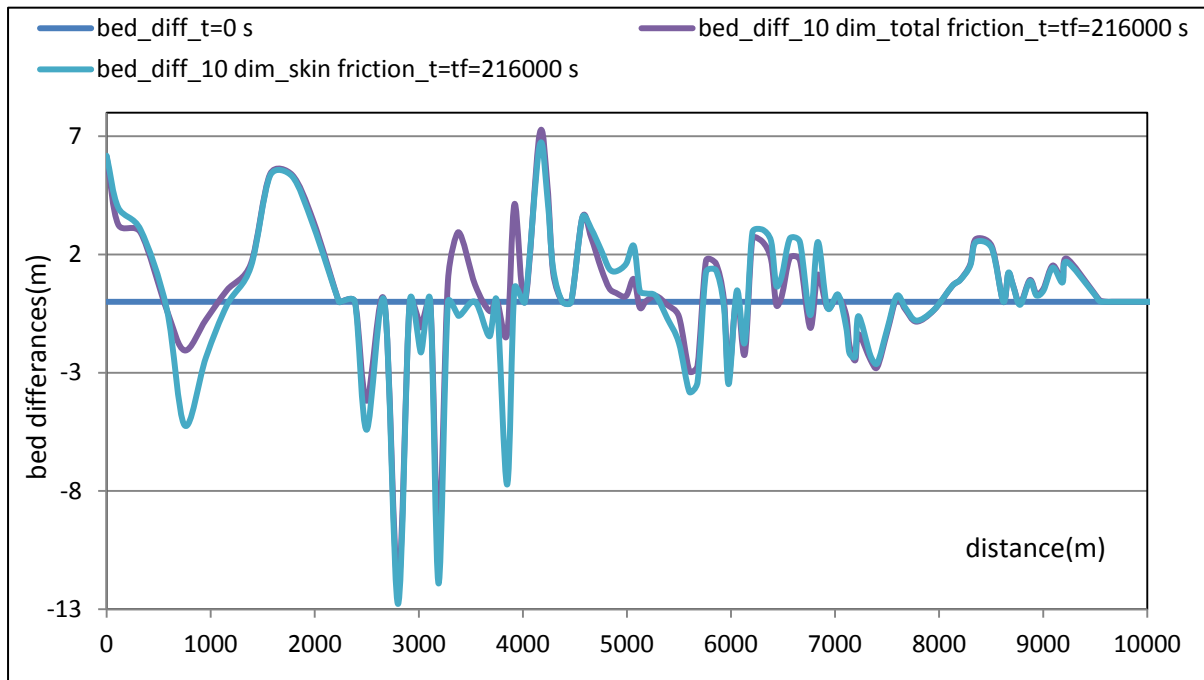


Fig. 5. 23: Effect of skin friction on the morphological evolution for bed consist of 10 diameters.

5.8 Model sensitivity to control volume thickness

As discussed in items 1.11 the thickness of the active layer shown in figure 1.24 has an effect on the transport capacity for bed with multiple sizes. In fact there is no specific value for the thickness of this active layer, but it depends only on the bed granulometry and it is in the range($2 d_{90}$). The following three figures show the influence of this thickness; for model using 3 grain sizes the bed evolution didn't affected by it, while its influence in the other models is small and increases with more used granulometry to describe the bed because of the capability of more sorting. But at all cases the effect of the cvt can be neglected.

As mentioned in item 3.5.4; the very small values of cvt lead to no transportation of sediment, hence aggradation at the model entrance by huge values. In case of logical values for cvt, as chosen here, the model becomes insensitive to the value of cvt.

Comparative study of different scenarios for the morphological evolution in a river stream

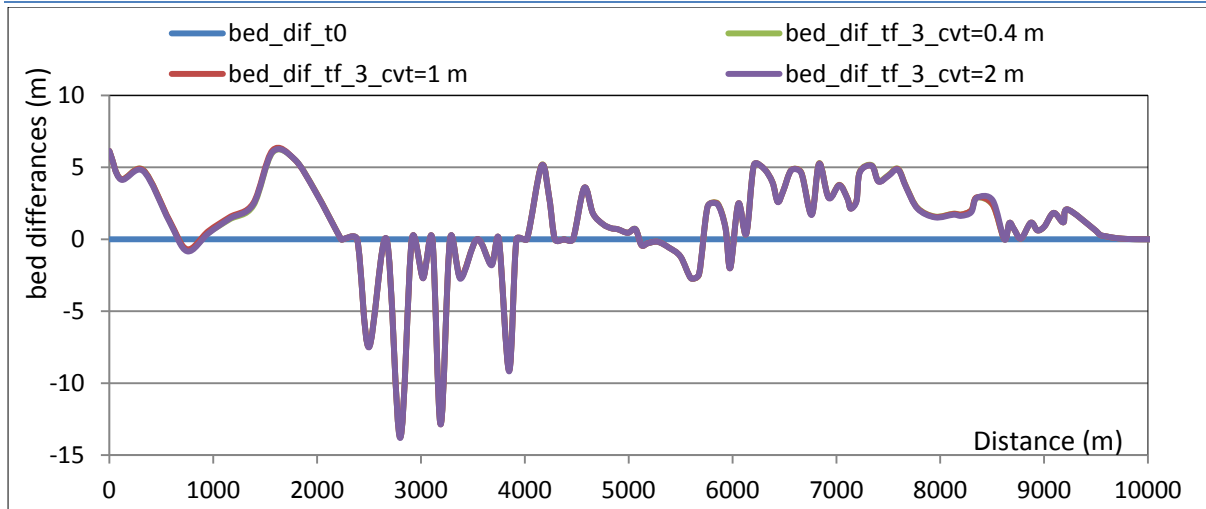


Fig. 5. 24: Influence of changing the control volume thickness on the bed evolution for 3 grain sizes model.

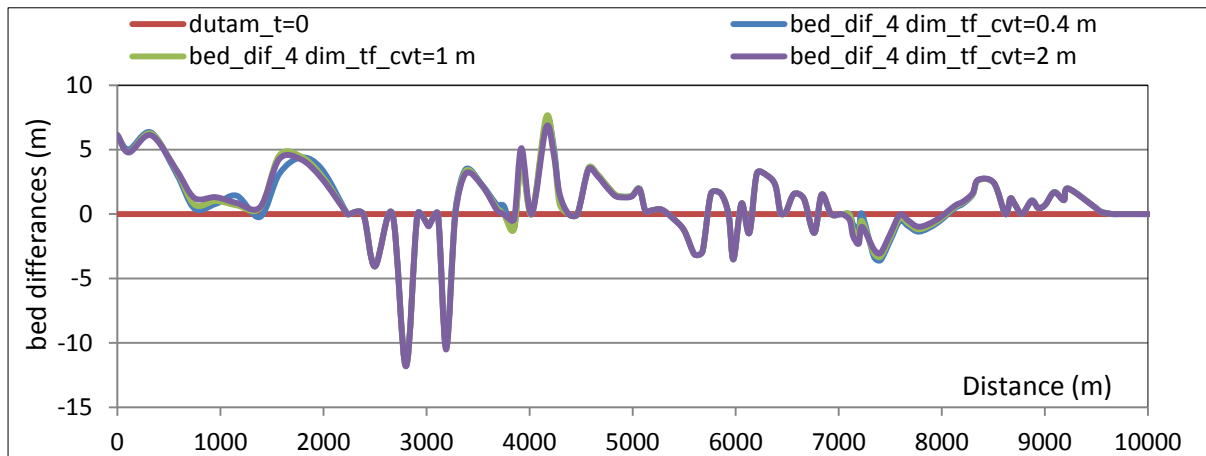


Fig. 5. 25: Influence of changing the control volume thickness on the bed evolution for 4 grain sizes model.

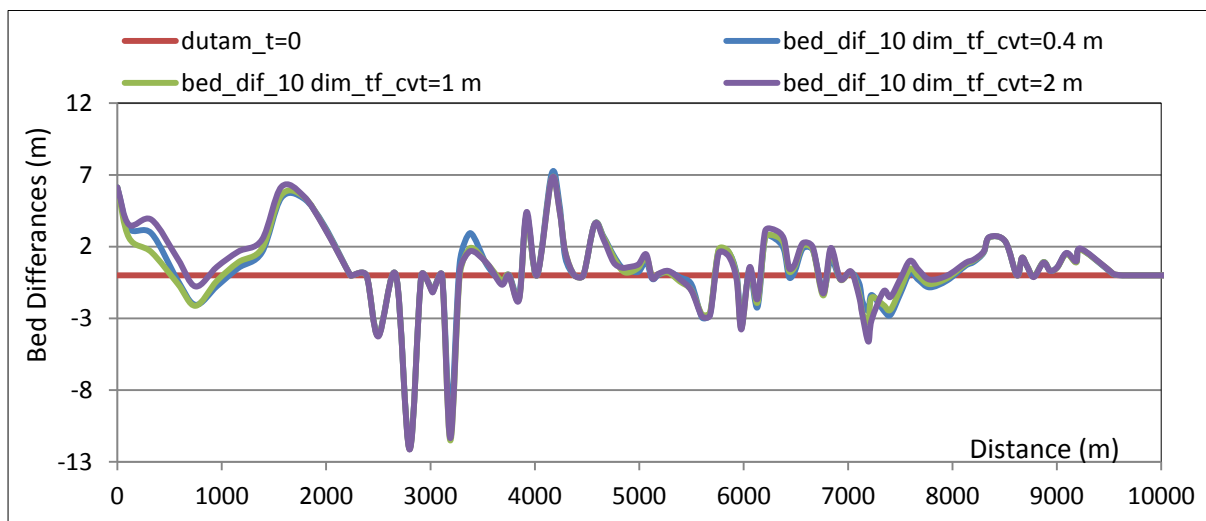


Fig. 5. 26: Influence of changing the control volume thickness on the bed evolution for 10 grain sizes model.

5.9 Numerical Issues

The number of sections used in 1987 event modelling is 129 sections starts from CS1 to CS129. Starting from CS92 to the end; it is dummy sections used to add dummy stretch with length 2176 m to overcome the downstream boundary condition effect. The whole real length from CS1 to CS129 is 9480 m, while the distances among these sections are shown in Fig 5.4.

As shown in the figure, the distance among the section are not uniform, it vary from 20 m (the minimum) to 256 m (the maximum). These huge differences in the spatial discretization among the sections must be treated to reach to the numerical stability (model convergence) either by sub-discretizing the wider distances to small distance and interpolating the sections features or by treating it numerically. Unfortunately; the interpolation way is not available yet by Basement because, still, it is experimental and usually gives wrong interpolation of sections features, so the numerical treatment is the only way to overcome this problem.

As discussed in item 1.13, the numerical treatment in Basement is usually done by selecting valid Courant-Friedrichs-Lewy number (CFL for short) given by Eq 1.29 and maximum value for the time step. The software selects automatically the valid time step which satisfies both the CFL number and the compatibility with the variant spatial steps. This time step generated by the software is also variable but within the maximum given time step i.e. to overcome the stability problem the CFL number or the maximum time step can changes until convergence.

The numerical analysis by spatial finite volume software like Basement usually needs to reduce the spatial discretization and the maximum time step to get accurate results. But ,as discussed, the spatial discretization is not by

choosing, so small time step must be selected at least with keeping CFL number within the range ($0 < CFL < 1$ and the best range from 0.5:1).

For all the models discussed before the maximum time step is 100 sec, while CFL is 0.5. Once this value increases to 0.6 the models become unstable, also the maximum time step must has higher value which affects the results accuracy, if it exceeded. It seems that this treatment procedure for the numerical stability is really good and no model can be unstable but it can be inaccurate once the time step becomes wider.

Increasing the time step has another side effect which appears when there is feeding source (either water or sediment) with short duration less than the time step, as will be discussed in chapter 6, where the software may not realize this short duration feeding.

5.10 Final considerations and conclusions

Finally, after analyzing 1987 flood using multiple classes of granulometry and performing the sensitivity analysis, there are some points should be summarized as a parameterization to the following study in chapter 6:

Regarding the modeling:

- Increasing the model length doesn't affect the model results in Sondrio, because the sediment feeding will not arrive to Sondrio (maximum it affect 4 km measured from upstream), but the source of sedimentation in Sondrio is the bed erosion not the sediment feeding from the catchments.
- Using less grain sizes to represent the bed and the feeding granulometry is better from reliability, computational cost and results presentation points of view than using multi grain sizes.

- The modeling by Basement gives accurate results as long as the boundary conditions are simulated correctly or as long lags from the boundaries locations.
- The modeling shows small sensitivity to bed friction computation, this small sensitivity appears because of using different granulometry classes. The more distributed granulometry class is the more sensitivity to bed friction, because of the big sizes involve in the distributed classes that increases the skin friction.
- The sensitivity to the cvt is small in general, when logical values for the thickness of the active layer are used. This small sensitivity increases with using multi grain sizes, while it vanishes by using limited number of granulometry (no effect for the cvt in case of uniform granulometry).
- Basement uses finite difference scheme in time and spatial finite volumes, so the model stability is controlled by adapting the maximum time step or/and CFL number i.e. with any spatial discretization, one can find a solution for the model as long as the CFL is respected with adapting the maximum time step.
- Finite time steps are preferred from computational point of view also in case of pulse feeding by water and/or sediment.

Regarding 1987 event

- The 1987 flood has 4 peaks, 3 maxima and 1 maximum, so it produces a lot of sedimentation in Sondrio because the sediment moves in maxima tail will be urged by the sequent maxima or maximum. While the sediment transport is fewer in case of waves have one peak and same maximum value i.e. the wave shape has a

role in the transported amount (this will be verified in details in next chapter).

- The aggradation happened in Sondrio because of the transition from very steep slope to mild slope i.e. transition from high transport capacity to less transport capacity.
- The aggradation source in Sondrio is not the sediment feeding coming from the catchment but the bed erosion in the last 4 km before the entrance of Sondrio, hence the amount of sediment fed from the catchment didn't affect the aggradation depths in Sondrio.
- The check dams built upstream Sondrio plays an important role in erosion prevention, since it reduces the aggradation amount in Sondrio.
- The check dams are an important structural mitigation measure for the flood risk, since it helps in saving the river capacity by reducing erosion, so building more check dams especially in the last 4km before the entrance of Sondrio is recommended.
- The capacity of Mallero must be restored after any similar event by re-excavating and transporting the deposited sediment outside the city.

6 The Case of Mallero: Integrated Scenario for Spriana Landslide

Spriana landslide has a high likelihood to fail at any time. It can be triggered by intense precipitation, sudden earthquake or any other triggering factor. Once the failure happens, the produced soil will close the valley of Mallero in the front of Spriana. In this chapter, a comparison is aimed, through two different ways of modelling for the landslide, between the amounts of sediment will aggrade in Sondrio due to the morphology of the sediment that will produce by the landslide and that aggraded due to 1987 flood.

6.1 The scenario of lateral feeding from Spriana

Basement software has the capability to simulate such type of lateral feeding with sediment as discussed before, so this capability was exploited here to zoom in the interaction between the flow in Mallero and the lateral feeding of sediment from Spriana and to see what are the sediment depths will deposit in Mallero at in-town due to the evolution of Mallero bed and the sediment fed laterally from Spriana.

To start this type of analysis, some data were needed about the geological behavior of the landslide like: what is the discharge will be in Mallero during the landslide? What is the volume of soil will generate due to this landslide? How much the period of the landslide? What is the rate of soil feeding from the landslide?

Regarding the first point, there is no specific expectation for the landslide time or at least the season, so the only way is assuming a deterministic scenario or some scenarios for the discharge in Mallero within the historical ranges of the observed discharges shown in figure 4.9 (annual flow curves). According this figure, the maximum discharge observed in 6 years (1992-1999) is $160 \text{ m}^3/\text{s}$, while $100 \text{ m}^3/\text{s}$ exceeded only 17 days. Also the usual discharge in Mallero is less than $10 \text{ m}^3/\text{s}$, so the deterministic scenario assumed here is using of $100 \text{ m}^3/\text{s}$ for the discharge during the landslide failure then the results due to any different scenario can be assessed to get rough estimation depend on the results obtained by the scenario using $100 \text{ m}^3/\text{s}$ as a feeding discharge.

About the soil volume will generate due to this landslide, (Franzetti, 2005) in the emergency plan report prepared for Sondrio expected a volume around $20 * 10^6 \text{ m}^3$ of sediment that will generate due to the landslide starting from the crown at 1400 m above sea level.

The question now, what is the rate of sediment feeding in Mallero valley during the landslide, what is the velocity of the landslide or what is the duration of the land slide? Indeed, there is no certain answer for these questions simply because it didn't yet collapsed, so let's speak about the duration of the sliding in similar case.

(Crosta, et al., 2004) studied 1987 Val Pola Landslide in Italian Alps which is near from Spriana (figure 6.1), they arrived to the following conclusions; the landslide velocity is unsteady with maximum velocity more than 70 m/s (fig 6.2) and the landslide duration is around 5 minutes (300 second) as shown in this figure.

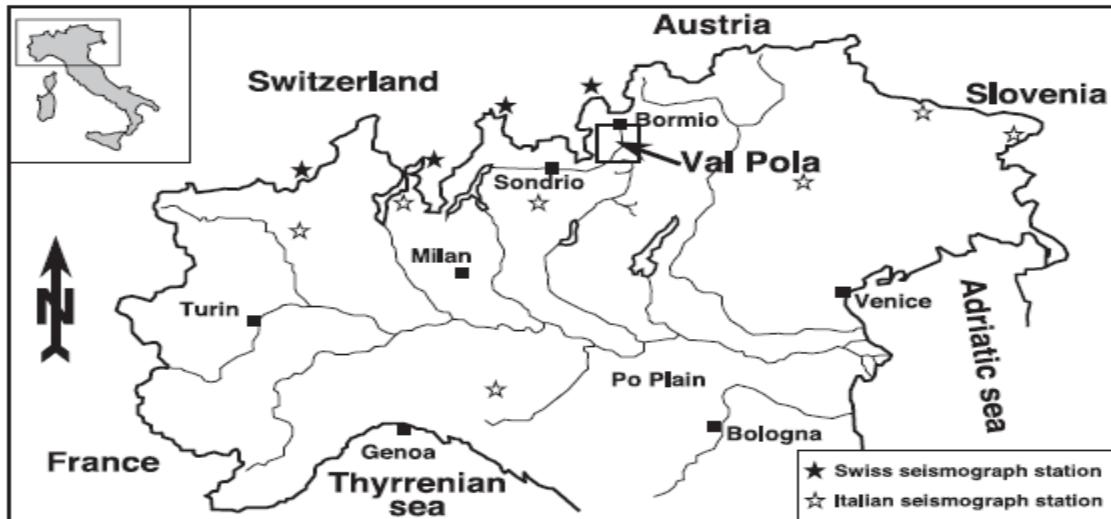


Fig. 6. 1 : Location map of the 1987 Val Pola rock avalanche (Central Alps, Northern Italy).

So considering a steady flow for Spriana landslide having volume $20 * 10^6 \text{ m}^3$ and considering the same duration for Val Pola, the rate of lateral feeding of sediment created by the landslide will be $66666.67 \text{ m}^3/\text{s}$.

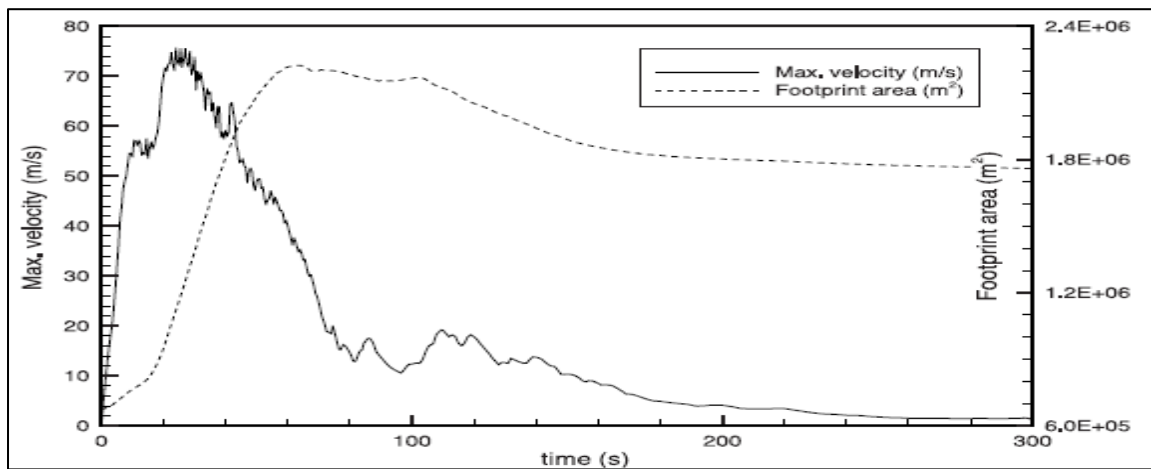


Fig. 6. 2: Time histories of the local maximum velocity and footprint area for 1987 val pola landslide (Crosta, et al., 2004).

6.1.1 The model description

The model cross sections are the same described for 1987 event in the previous chapter with the same length and features, while the bed granulometry is the same described in item 5.3 and Table 5.1. So there are also 3 models built depending on the bed granulometry, one uses 3 grain sizes, the second uses 4 grain sizes and the third uses 10 grain sizes.

The model used $100 \text{ m}^3/\text{s}$ as initial discharge condition at each cross-section, while the same downstream boundary conditions described in item 5.4 are used also here in these models. The hydraulic upstream boundary condition represents the catchment feeding, as discussed before, is steady discharge that equals $100 \text{ m}^3/\text{s}$, while there is no sediment feeding from the upstream which means that degradation will be expected in the upstream.

Regarding the lateral feeding, the models fed by two types of scenarios figures 6.3, 6.4; the first is unsteady with peak $83333.34 \text{ m}^3/\text{s}$ and base time 5 minutes, while the second is steady feeding with sediment discharge $92.59 \text{ m}^3/\text{s}$. The first scenario is trying to represent the actual behavior for the feeding depending on the Val Pola's failure time (Fig 6.2), while the second scenario will be more clearly supported after presentation of the first scenario. The feeding done only on Spriana front (2000 m starting from upstream), while the simulation time is 60 hour like 1987 flood. The volume of the two feedings is $20 * 10^6 \text{ m}^3$.

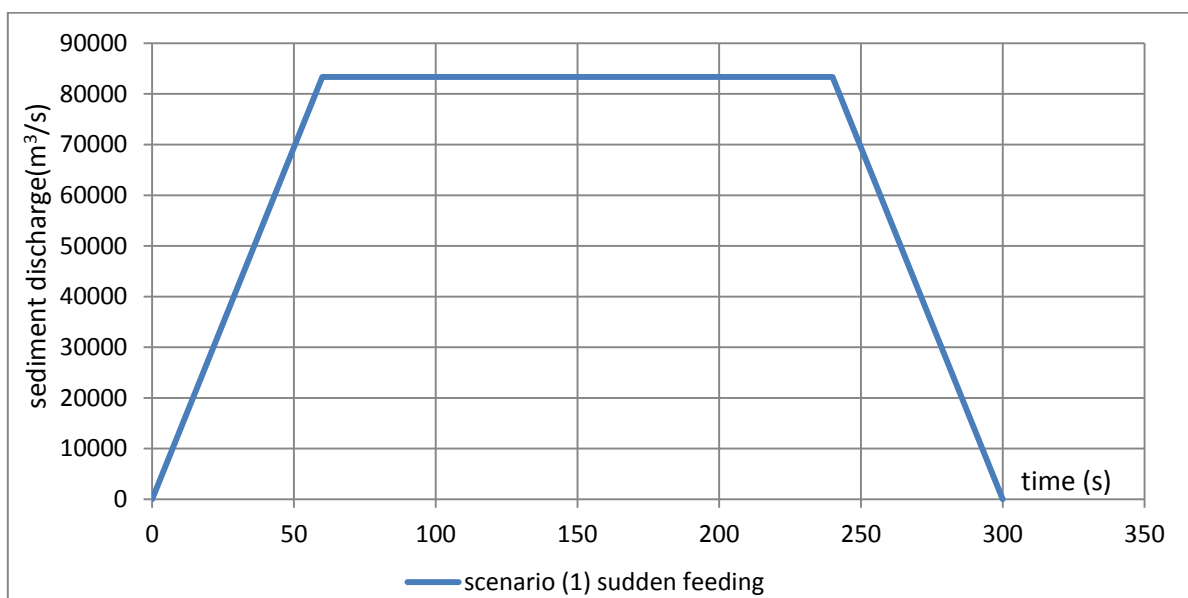


Fig. 6. 3: Scenario(1) for lateral feeding (sudden feeding).

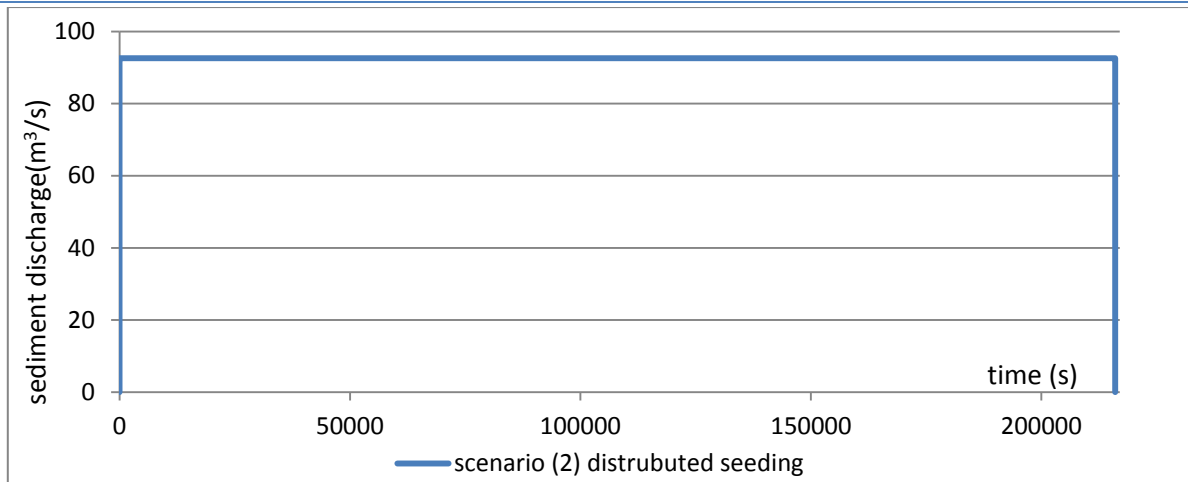


Fig. 6. 4: Scenario(2) for lateral feeding (distributed feeding).

6.1.2 Results of scenario (1)

The sediment feeding by these huge amounts, which is higher than the transport capacity, leads to the deposition of sediment in this site creating a dam of sediment as discussed in chapter 3. Figure 6.5 shows the first 2500 m of the model, it visualize the dam and the overtopping of water above this dam for model uses 3 grain sizes in description of bed granulometry and scenario(1) for sediment feeding.

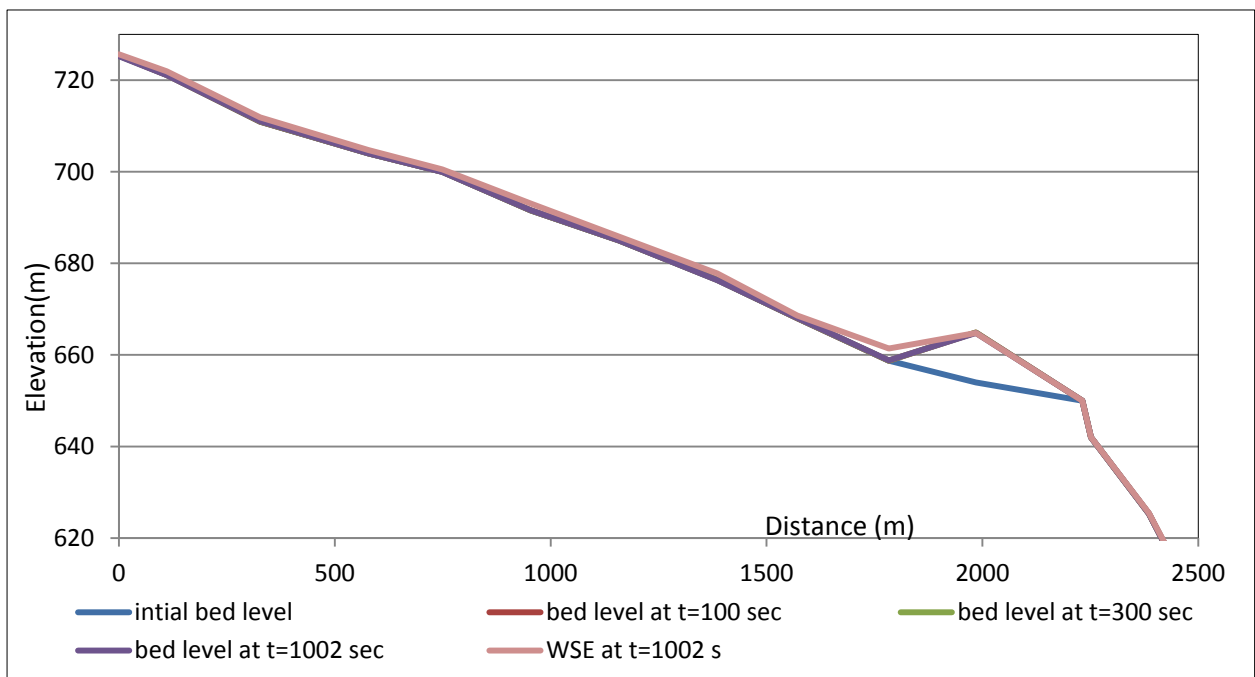


Fig. 6. 5: The bed and the WSE profiles at intermediate times of the simulation.

For better visualization of the dam and its dimensions, the differences between the initial bed level and bed levels at time 0, 300, 1002, 100090 and 216000 seconds showed in the following figure.

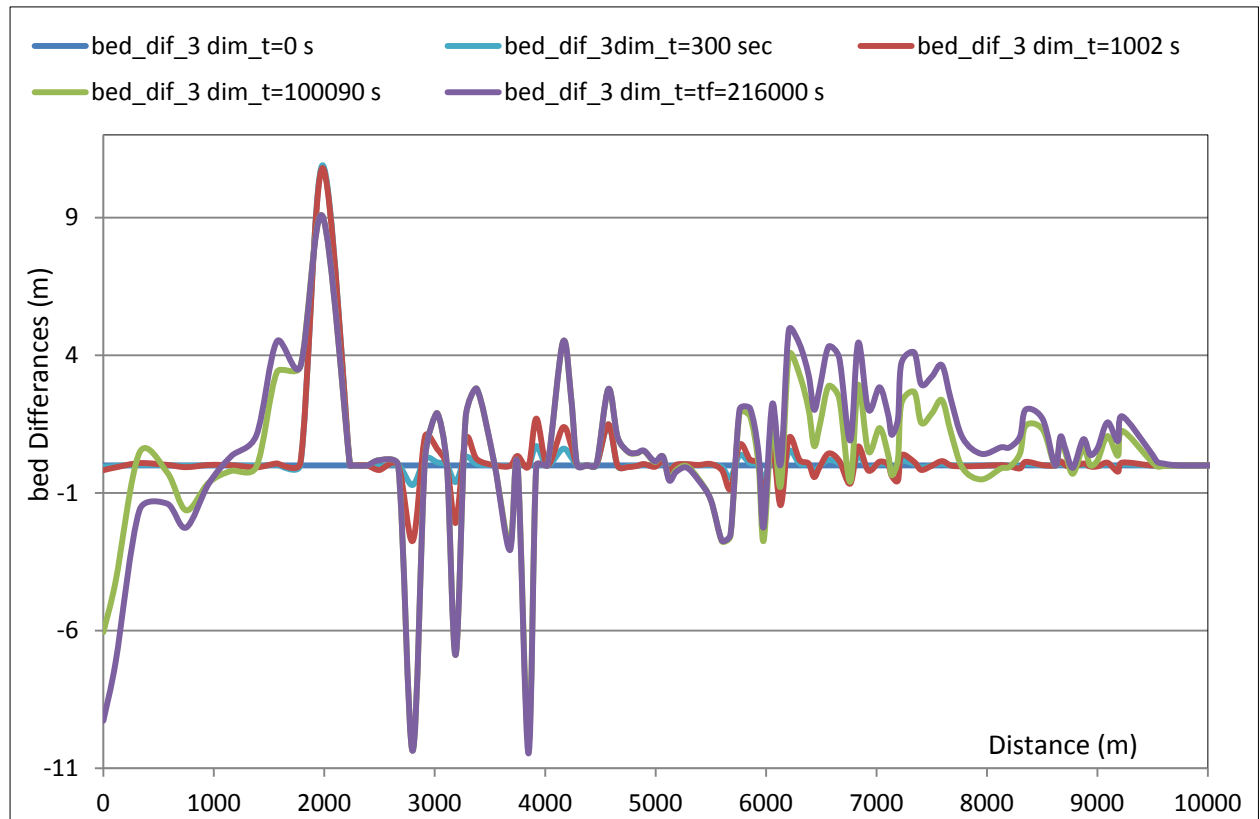


Fig. 6. 6: Bed differences in case of lateral feeding according scenario (1) and using model of 3 grain sizes.

It is clear that, the profile starts with degradation at the upstream because there is no upstream feeding of sediment, this degradation at upstream increases with time to reach to around 10 m. Due to the lateral feeding, a dam has around 11 m height created with 450 m base. The height of this dam decreases with time because of the sediment transportation.

In the downtown, the sediment deposits, with time, to reach to its maximum value (5m) in some section, but still the sedimentation depth is lower than that noted in 1987 flood, although the volume of the sediment fed

from Spriana is higher than that fed in 1987 flood for the same simulation time.

In case of using model uses multi sizes e.g. 10 grain sizes (Fig 6.7), the behaviour is near to the results obtained by model uses 3 grain sizes. The dam dimensions are quite similar, but still the model is sensitive to the granulometry used.

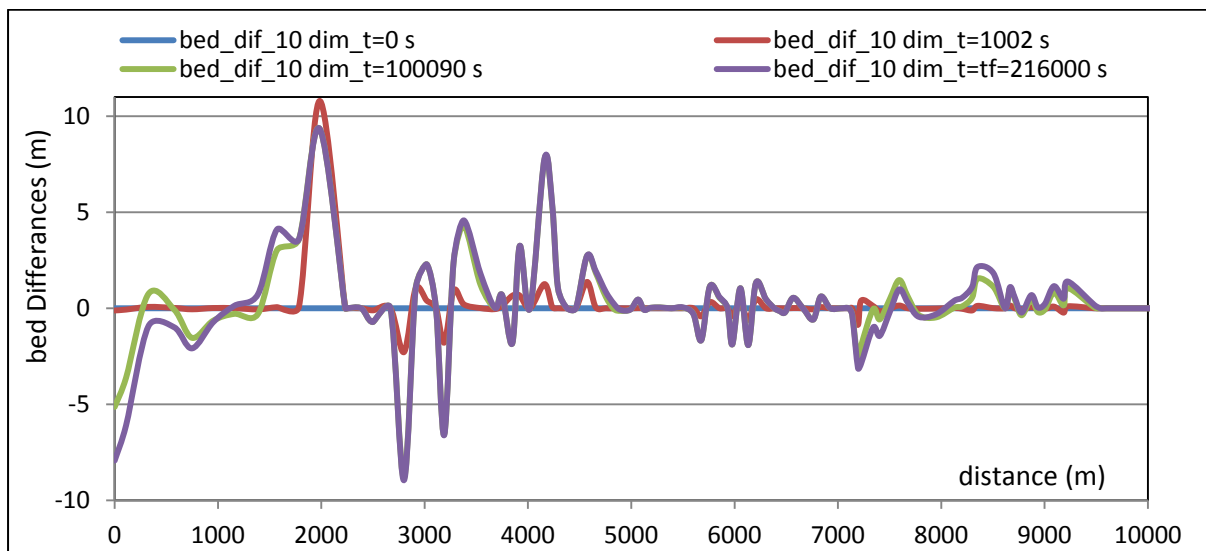


Fig. 6. 7: Bed differences in case of lateral feeding according scenario (1) and using model of 10 grain sizes.

As shown in results of scenario (1), the dam dimensions are small, the volume of the dam is around 75000 m^3 after 300 sec, while the volume of the sediment fed is $20 * 10^6 \text{ m}^3$ till this time. This means that, the average transport capacity must be $16604.2 \text{ m}^3/\text{s}$ to satisfy the principle of mass conservation. On the other hand, the maximum calculated transport capacity in Mallero in this time is $6.65 \text{ m}^3/\text{s}$. This means that, Basement software doesn't respect the principle of mass conservation.

Another note about the water surface in fig 6.5 is that, the water surface is not horizontal behind this dam as it supposed to be. So Basement software doesn't have the capability to simulate this type of huge feeding of sediment.

To be certain from this conclusion, let's assume the distribution of the sediment along the simulation time presented by scenario (2).

6.1.3 Results of scenario (2)

By using scenario (2) that represents the distributed feeding instead of the scenario of pulse feeding, the upstream degrade at upstream but not by the same amount noted in the previous scenario. In the dam zone, the dam height increased with time then erosion appeared in it's upstream portion although of the feeding. In the in-town zone, the same deposition showed but with heights less than that noted in scenario (1). It noted that, the final state of the bed differences is totally different from that at previous times as shown in fig 6.8. Finally, although of using distributed feeding, the volume of the dam doesn't affected so much which means that Basement is not able to simulate this type of complex analysis with this huge amount of sediment feeding either with pulses or distributed feature.

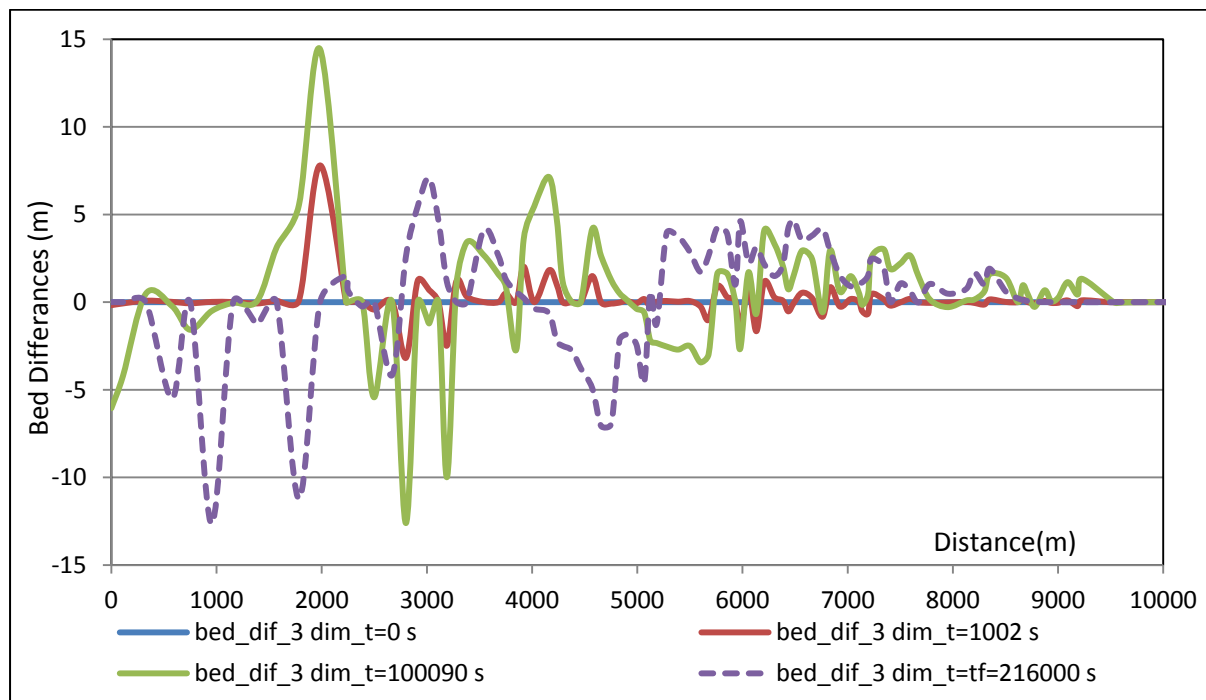


Fig. 6. 8: Bed differences in case of lateral feeding according scenario (2) and using model of 3 grain sizes.

6.2 Integrated scenario for the sequent landslide and dam-break in Spriana.

As discussed, the landslide failure in Spriana will take place in few minutes creating a dam in front of Spriana. In the previous item 6.2; Basement software was not able to calculate the real dam dimensions, because it doesn't respect the principle of mass conservation i.e. input mass \neq output mass. So in this item produces another scenario that describes the consequences of the landslide failure.

This second scenario tries to find an integrated modelling for the phenomenon using some sub models that describes the parts of the phenomenon. This models in sequent are: (1) model describes the landslide features, the soil volume created by it, the distribution of this sediment in Mallero valley and estimates the height of the created dam, (2) model estimates the discharge in Mallero in the slide time, (3) model estimates the volume of water will be stored behind the created dam, (4) model for the dam break and the generated water and sediments hydrographs and (5) the morphological evolution of the sediment that will generate from the dam break. The relation among these models is described in the following flowchart (Fig 6.9).

First of all, the discharge in front of Mallero must be estimated using either rainfall runoff model or using the flow annual curves (Fig.4.9), then a model is needed that estimate the slide duration, the volume generated, the distribution of the soil produced and the dam height. Once the height of the created dam and the valley geometry known, the lake formation model uses to estimate the stored volume, the surface area for this lake and the time needed to fill this lake. This dam will collapse either due to structure defect, the piping

effect or the breaching due to the water overtopping, so a discussion about the dam collapse will be held then some models describe the generated water and sediment discharges will be discussed. Once the water and sediment discharges, produced by the dam failure, are known, a morphological evolution model uses Basement software can be used to know the expected water and sediment depths in the downtown due to the dam break.

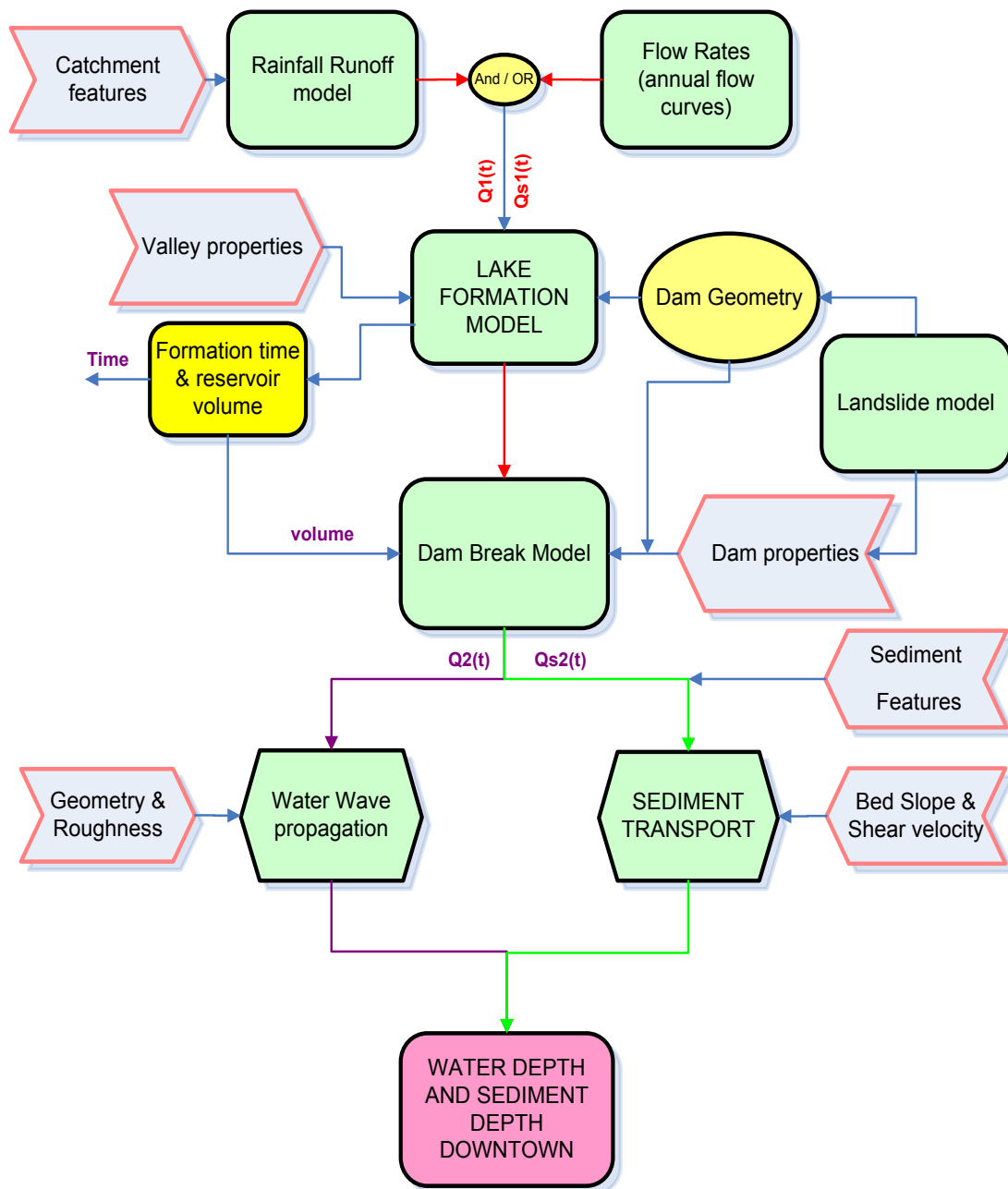


Fig. 6. 9: Relation among the sub-models relating dam failure in Spriana.

6.2.1 The sub model for the landslide distribution.

As discussed in item 6.1, the likely surface of rupture for Spriana landslide starts from a crown at level 1400 m above the average sea level. The previous geological studies like this by (Franzetti, 2005) show that, the volume of produced soil in case of collapse will be $20 * 10^6 m^3$. A 3D model for the landslide must be used to know the evolution of this huge sediment mass, it's distribution in the valley and the height of the dam will create.

Indeed, there are no models built for the evolution and the distribution of the landslide, but the work depended on the analogy with Val Pola 3D model (Fig 6.10) that built by (Crosta, et al., 2004) and the results of the emergency planning report authored by (Franzetti, 2005).

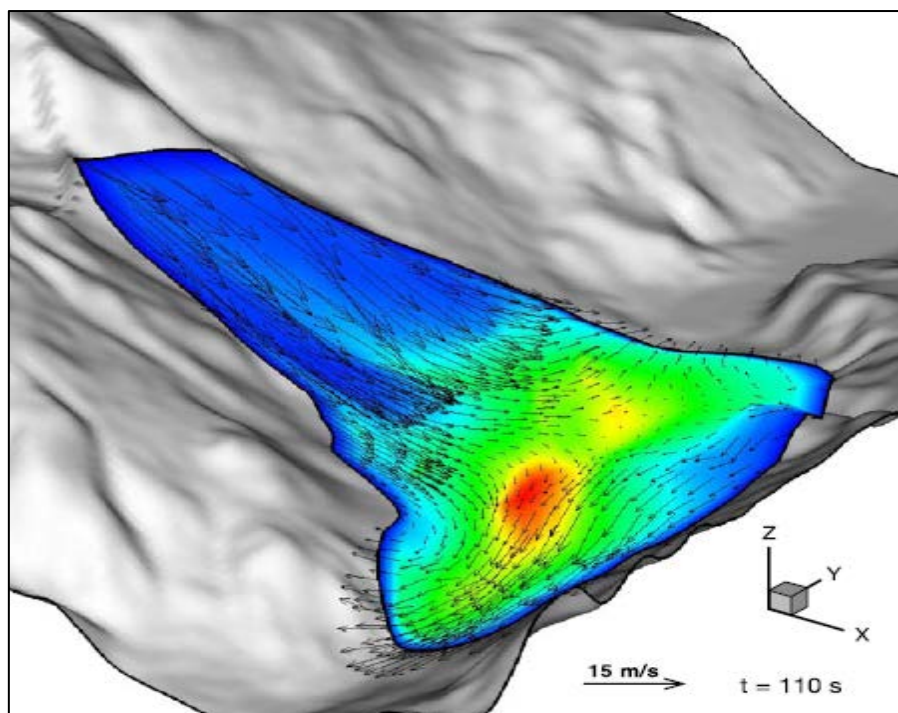


Fig. 6. 10: Instantaneous velocity field at the indicated instant (110 s) with fully 3D features (Crosta, et al., 2004).

Figure 6.11 shows the evolution of the landslide in Val Pola 1987, it is clear that the dam closes the valley and stops the water flow in the valley. By measuring from the figure, the average height (the average of top level and the

minimum crest level) of the dam created is a round 250 m with a base length around 1280 m which means that the side slopes in y direction is 0.39.

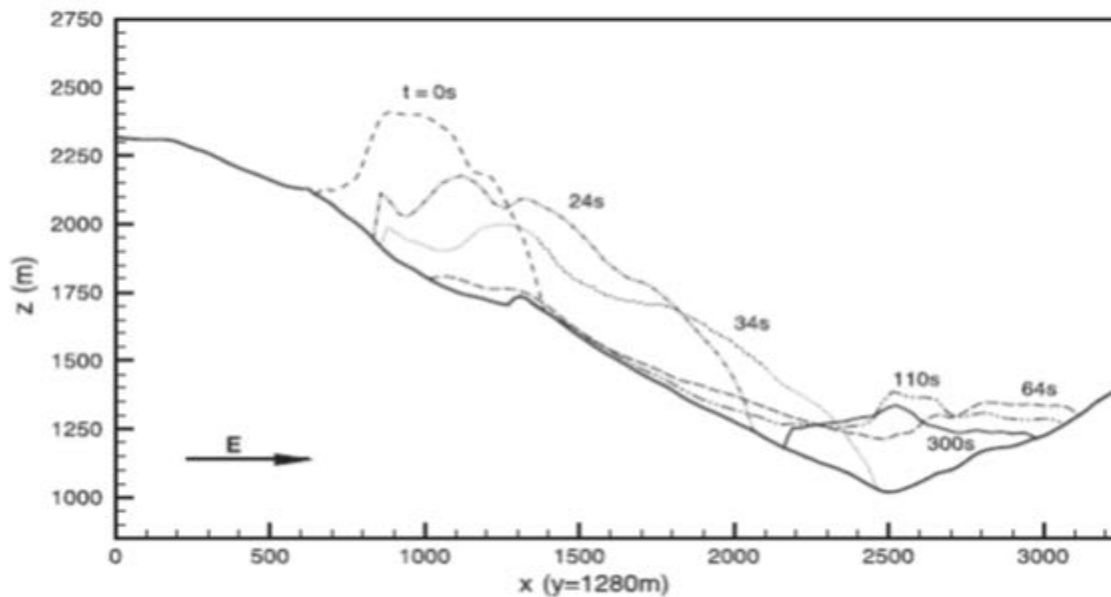


Fig. 6. 11: Debris profiles in Val Pola extracted along the longitudinal section $y = 1280$ m (Crosta, et al., 2004).

By analogy, the sides slopes for the created dam in Spriana will be 0.39, while the dam height is 80 m, taken from (Franzetti, 2005) emergency report, so the base of the dam in y direction is 410 m and considering the average valley width at Spriana around 220 m (bed width at Spriana is around 20 m) but still this dimensions of the dam doesn't satisfy the volume of the land slide $20 * 10^6$ m³.

By fixing the minimum dam height, 80 m, with average dam height of 120 m and considering the volume of the landslide with assuming a triangle distribution of soil in the valley direction(y direction); the base of the landslide will be 1515.2 m (regardless that the discretion of the sediment in downstream must be wider than upstream because of the steep slope at the feeding zone) . This means that, the side slopes of the dam in y direction is 6.31, so table 4.5 describes the features of the created dam for different scenarios according the

dam height with the same consideration for dam volume and triangular distribution of the sediment in y direction.

	scenario 50		scenario 80		scenario 100		scenario 150	
Average dam height	100	m	120	m	150	m	200	m
Min. Dam height	50	m	80	m	100	m	150	m
Crest width	0	m	0	m	0	m	0	m
Average valley width	220	m	220	m	220	m	220	m
Dam base	1818.182	m	1515.152	m	1212.121	m	909.0909	m
Side slopes s_u (y/z)	9.09		6.31		4.04		2.273	
Dam volume	20000000	m ³	20000000	m ³	20000000	m ³	20000000	m ³

Table 6. 1: Different scenarios for the dam features.

Where Min. dam height= the minimum level for the dam crest- the average local bed level at Spriana; Average dam height = the mean of the max. and min. dam height; Scenario xx= the scenario that has min. dam height of xx; S_u (dam side slope)= is the change in the dam length in y direction (the water flow direction to the change in the dam height).

6.2.2 The sub model for estimating the discharge in Mallero.

The feeding discharge varies with the season as it depends on precipitation in the catchments; also it depends on the meteorological conditions. So the value of the discharge coming from the catchment is uncertain and no specific value for the discharge that comes from the catchment can be considered. It is needed to estimate the maximum discharge at the collapse time which can be done by using a statistical models based on the historical data for the precipitation, the discharge or both of them. By using the return period for having an intense precipitation that can trigger the landslide collapse or the return period for having earthquake excites the slide and causes the collapse.

Unfortunately the data collected for both the precipitation and the earthquake are not enough to build such type of statistical model, so ,as discussed in item 6.1, by using the annual duration curves (Fig 4.9); the value

100 m³/s can be assumed as a reference value for the discharge. In fact, the importance of estimating this discharge at the collapse time not the use in the morphological evolution, but this discharge is triggering for the lake filling and the time between the landslide and the induced flood due to the expected dam-break.

6.2.3 The sub model for lake formation

The aim from this model is the estimation of the storage capacity, the lake surface area, the lake parameters and the filling time for the reservoir formed by the created earthen dam. Those are depending on the valley geometry, dam properties and the feeding discharge from the catchment at upstream. The relation among the filling time, feeding discharge and storage capacity is simply given by the following formulas:

$$Q(t).dt = dV \quad 6.1$$

$$\text{or } \int_0^T Q(t).dt = \int_{h_i}^H A(h) dh \quad 6.2$$

For steady feeding Q , the lake filling time T can be given by Eq 6.3

$$T = \frac{\text{lake volume}}{Q} = \frac{\int_{h_i}^H A(h) dh}{Q} \quad 6.3$$

The terms of the formula described in Fig 6.12, where H is the minimum dam height given in table 6.1 according the scenario, s_0 is the average bed slope of Mallero at dam location, h is the water depth, h_i is the initial water depth, B is the average bed width and s_u is upstream slope of the dam (given in table 6.1 according to the scenario), while n_l and n_r are the right and left average side slopes of the river in front of Spriana.

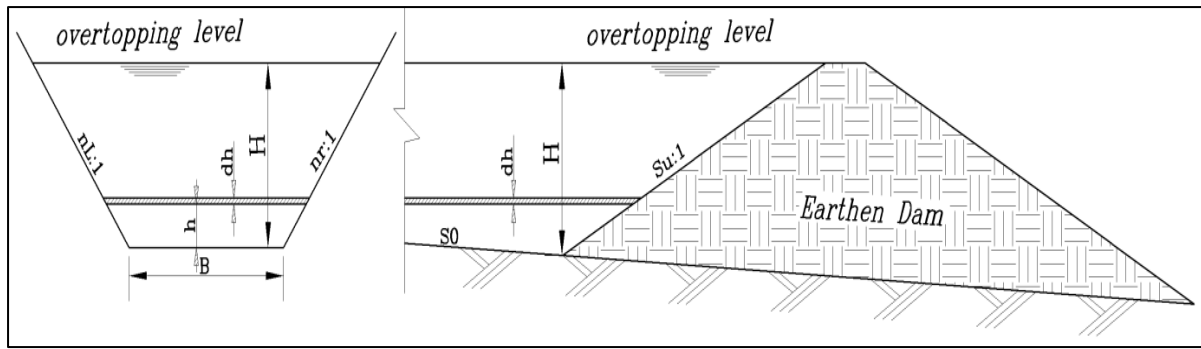


Fig. 6. 12: The parameters of the lake formation model.

Considering those parameters; the area of the lake at height h is given in Eq 6.4. By integrating this area with respect to h ; the volume of the lake, as a function of the water depth, is given by Eq 6.5.

$$\text{Surface Area} = h[B + h(n_l + n_r)] \cdot \left[s_u + \frac{1}{s_0} \right] \quad 6.4$$

$$\text{Lake volume} = \left[\frac{B(h - h_i)^2}{2} + \frac{(h - h_i)^3}{3} \cdot (n_l + n_r) \right] \left(s_u + \frac{1}{s_0} \right) \quad 6.5$$

The values considered for B , h_i , n_l , n_r and S_0 calculated based on the valley geometry, so they have the values 20m, 1m, 1.325(Hz/VI), 1.325 and 4 % (VI /Hz) respectively. The values of the left and right side slopes concluded from the field by considering the tilting angle of the slopes = 37° measured from horizontal as in Fig 6.13.

Regarding the filling time (Eq 6.3), it depends on both the feeding discharge and the dam characteristics which are uncertain variables. To deal with uncertainty, multi cases of dam height (table 6.1) and discharges studied to identify how it affects the behaviour of the lake formation. Figure (6.14) represents the relation among the filling time, different discharges and various dam heights. The figure shows that, the filling time decreases with the discharge increasing and increases with increasing of the dam height.

dam will be flooded along 2 km at 80 m dam height. Figure 6.15 shows the relation between the dam height and the reservoir surface area for different scenarios. As shown for each scenario, the lake has different area curve this because of the upstream slope of the dam s_u (given in table 6.1).

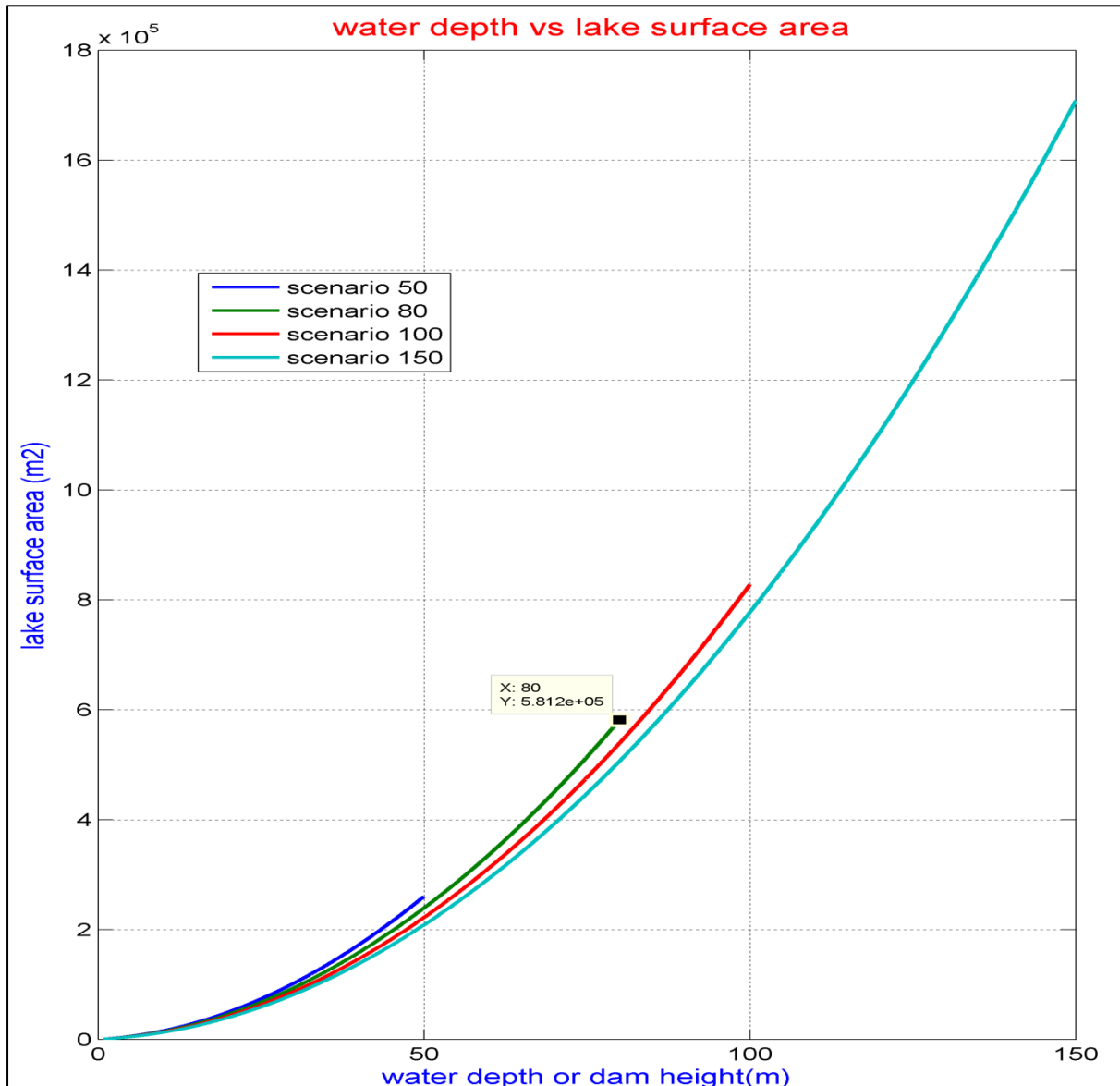


Fig. 6. 15: The surface area curves for different dam height scenarios.

The water storage volume upstream the dam depends on the dam height, so with higher dam huge amount of water will be stored that means that once this dam collapsed it will produce a huge discharge that may lead to flood in downtown. Figure (6.16) gives the relation between the reservoir volume and

dam height. Also the figure shows that, the reservoir volume is independent from the discharge. Only it depends on the valley and the dam features. The differences in the curves are due to the difference in the upstream dam slope.

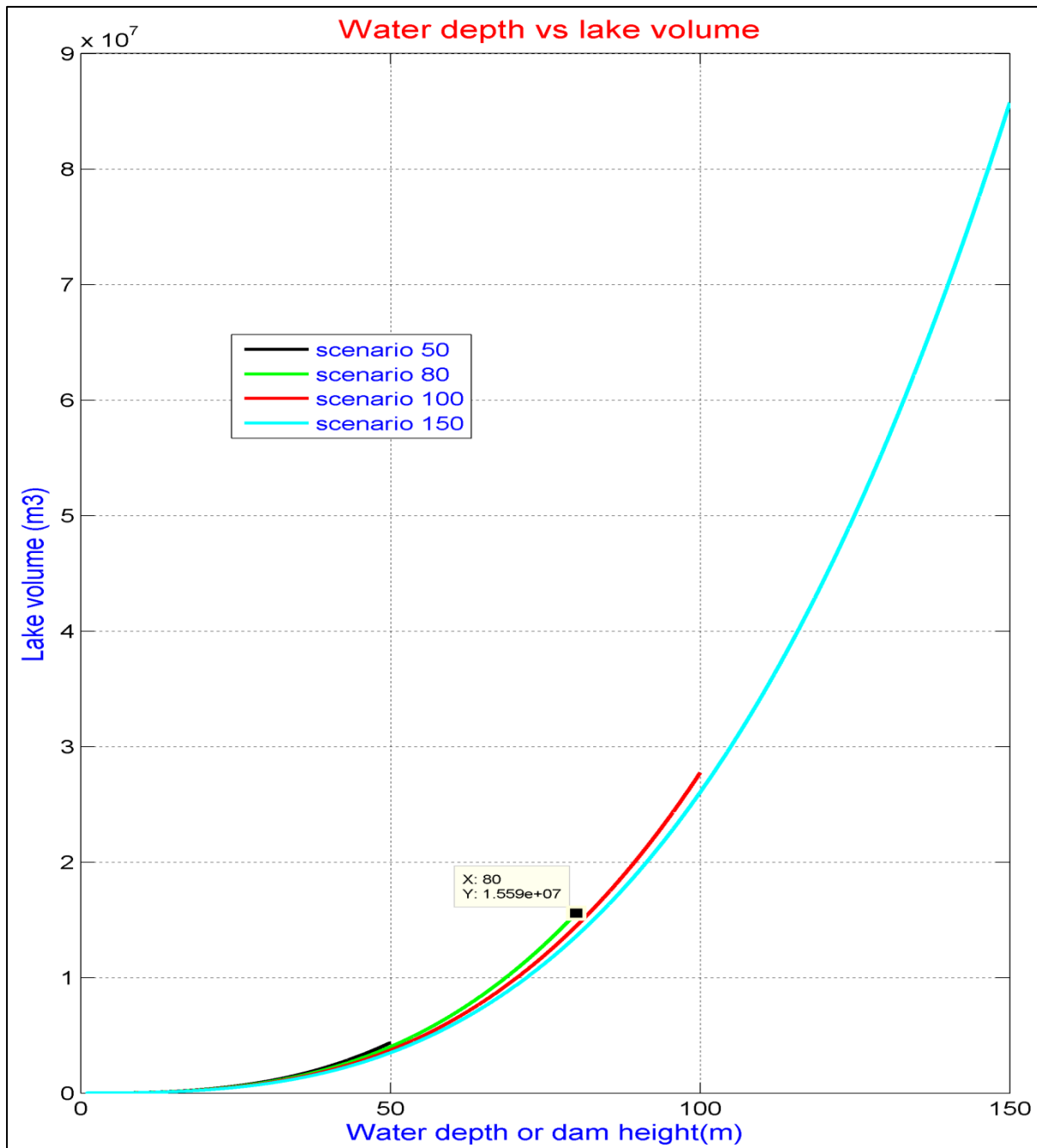


Fig. 6. 16: The lake volume curves for different dam height scenarios.

Since the target is the estimation of filling time under many discharges and with various dam heights. The relation among discharge, dam height and filling

time is studied. The following figure shows that with small discharges at specific dam height, the filling time is higher than that with high discharges.

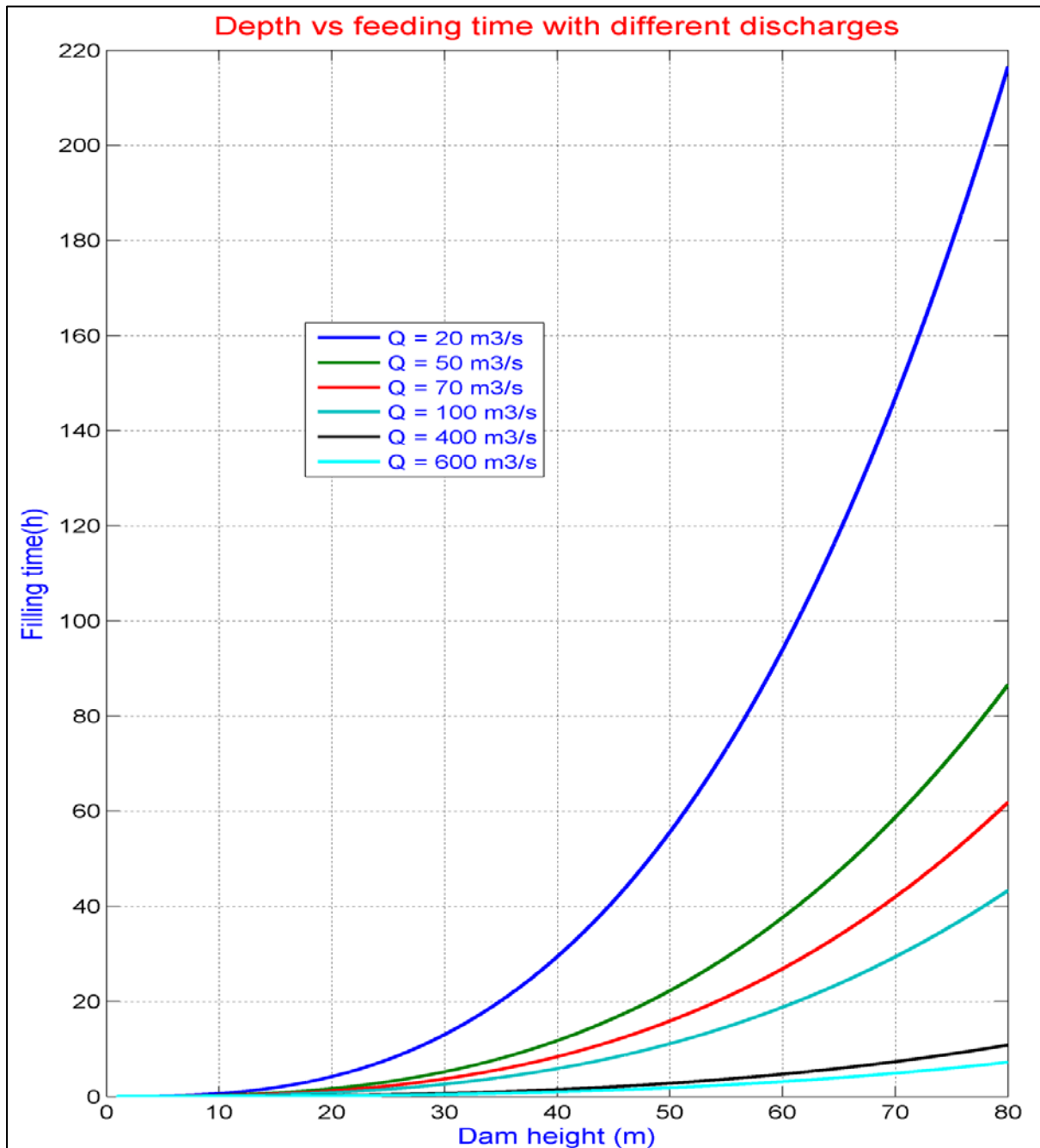


Fig. 6. 17: Effect of feeding discharge on the relation between dam height and filling time (scenario 80).

Since the filling time depends on the reservoir capacity and the feeding discharge, the following figure shows the relation among the reservoir volume feeding discharges and filling time.

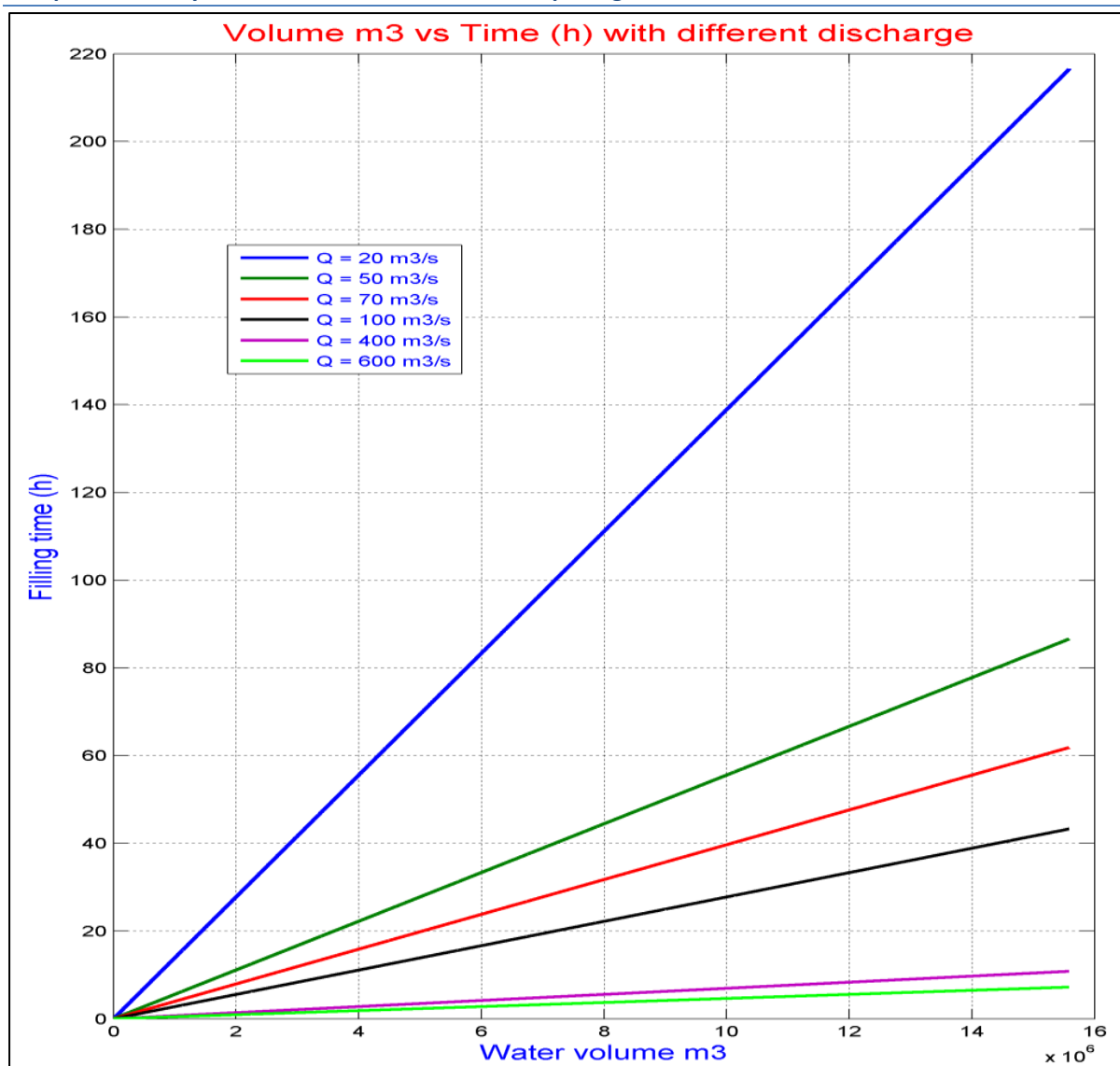


Fig. 6. 18: Relation among the feeding discharge, the filling time and the storage volume.

The importance of lake filling time (T) comes from the ability of exploiting this time in the city evacuation before flooding due to the dam break. Large value for (T) means that, the lake (reservoir) capacity is larger and the warning time increases. Small value for (T) means that, the reservoir capacity is smaller hence dam collapse will happen earlier and the warning time is shorter. The balance point is: when the time valid for the warning is less, the event severity is less, while higher dam give not only more filling time but also sharp severity.

As a summary, both the discharge and dam height are uncertain, but the most likely scenario is a dam with height 80 m (scenario 80). However table 6.2

summarizes the results for the four scenarios considered in table 6.1, while figure 6.19 shows the relation among dam height, filling time and lake volume for scenario 80.

Scenario	Min. Dam height (m)	S_u	surface area(m ²)	lake volume(m ³)	filling time (h)	α_0	$W_0(m^{3-\alpha_0})$
scenario 50	50	9.09	2.60E+05	4.36E+06	12.11	2.76	87.71
scenario 80	80	6.31	5.81E+05	1.56E+07	43.31	2.79	75.60
scenario 100	100	4.04	8.28E+05	2.77E+07	77.05	2.80	68.98
scenario 150	150	2.273	1.71E+06	8.57E+07	238.16	2.83	58.83

Table 6. 2: The results of the lake formation model for different scenarios.

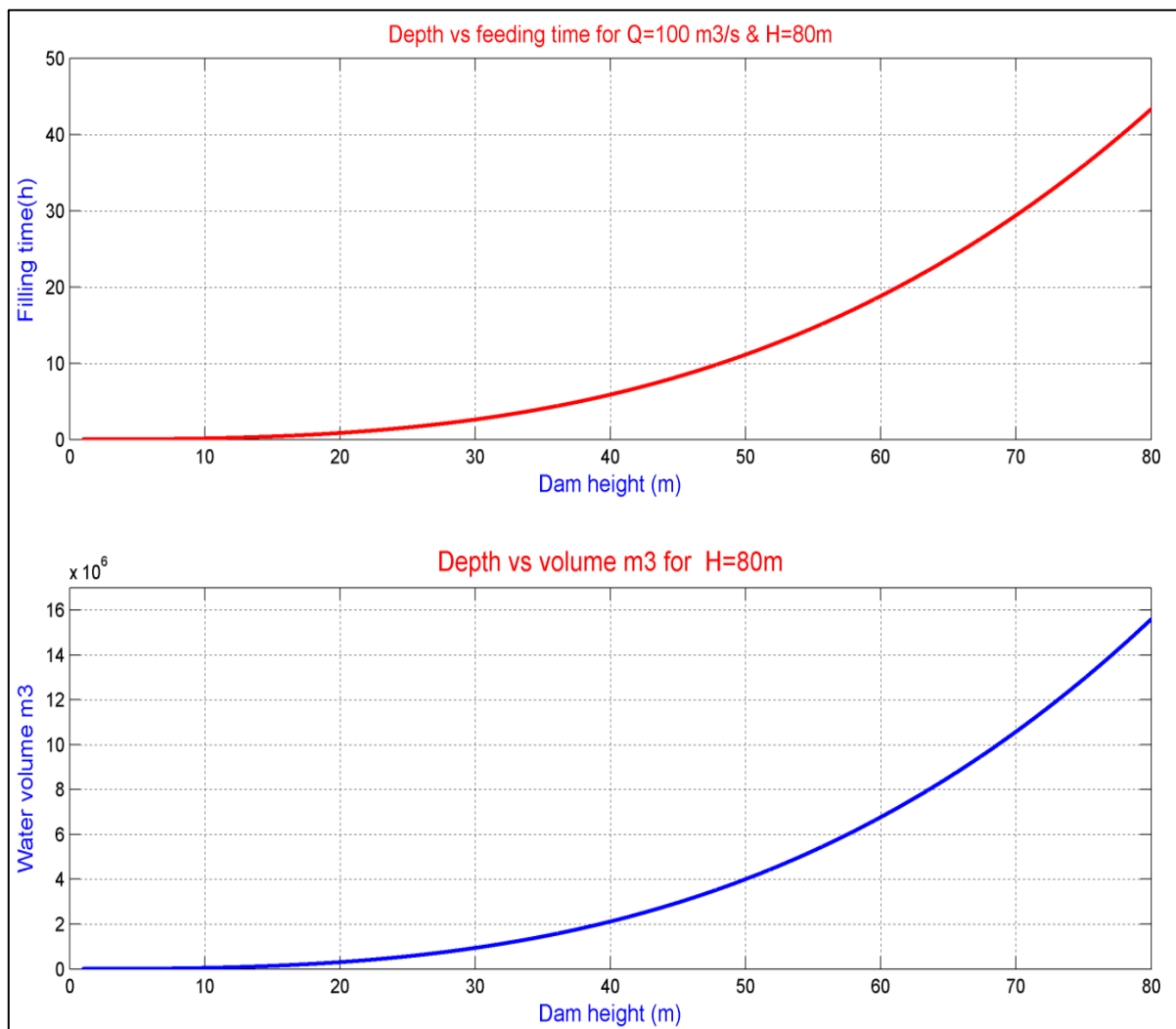


Fig. 6. 19: The calculated filling time and stored volume for scenario 80.

As discussed in (Macchione, 2008), for reservoirs where the water surface A and the corresponding volume V at a given elevation h known; values α_0

(storage exponent parameter represents the vertical distribution of the water mass in the reservoir, in the real world $1 \leq \alpha_0 \leq 4$, reservoirs with high values of α_0 store most of the volume in the upper levels) and W_0 (coefficient of level reservoir volume curve) can be estimated considering the derivative $\frac{dV}{dh}$:

$$\left. \frac{dV}{dh} \right|_{h=H} = V_s \cdot \alpha_0 \cdot H^{\alpha_0-1} = \frac{V_s \cdot \alpha_0 \cdot H^{\alpha_0}}{H} = \frac{V_s \cdot \alpha_0}{H} = A_s \quad 6.6$$

Where V_s and A_s are the total volume and the maximum surface area that can be achieved by the water in the lake. Therefore, the value of α_0 can be calculated as:

$$\alpha_0 = \frac{A_s \cdot H}{V_s} \quad 6.7$$

Once α_0 is obtained, the value of W_0 can be given by:

$$W_0 = \frac{V_s}{H^{\alpha_0}} \quad 6.8$$

For a reservoir where at least two water levels h_1 and h_2 and corresponding volumes V_1 and V_2 known, the parameters α_0 and W_0 can be evaluated as follows:

$$\alpha_0 = \frac{\log V_1 - \log V_2}{\log h_1 - \log h_2} \quad 6.9$$

So by drawing the relation between $\log V$ and $\log h$ (Fig 6.20) and by calculating the slope of the straight part of this curve gets α_0 . Table 6.2 shows also the final results of the lake formation model for the different scenarios identified in table 6.1 in addition to the lake parameters for each scenario. Because there is a different value for the upstream dam slope S_u , the values of α_0 are different.

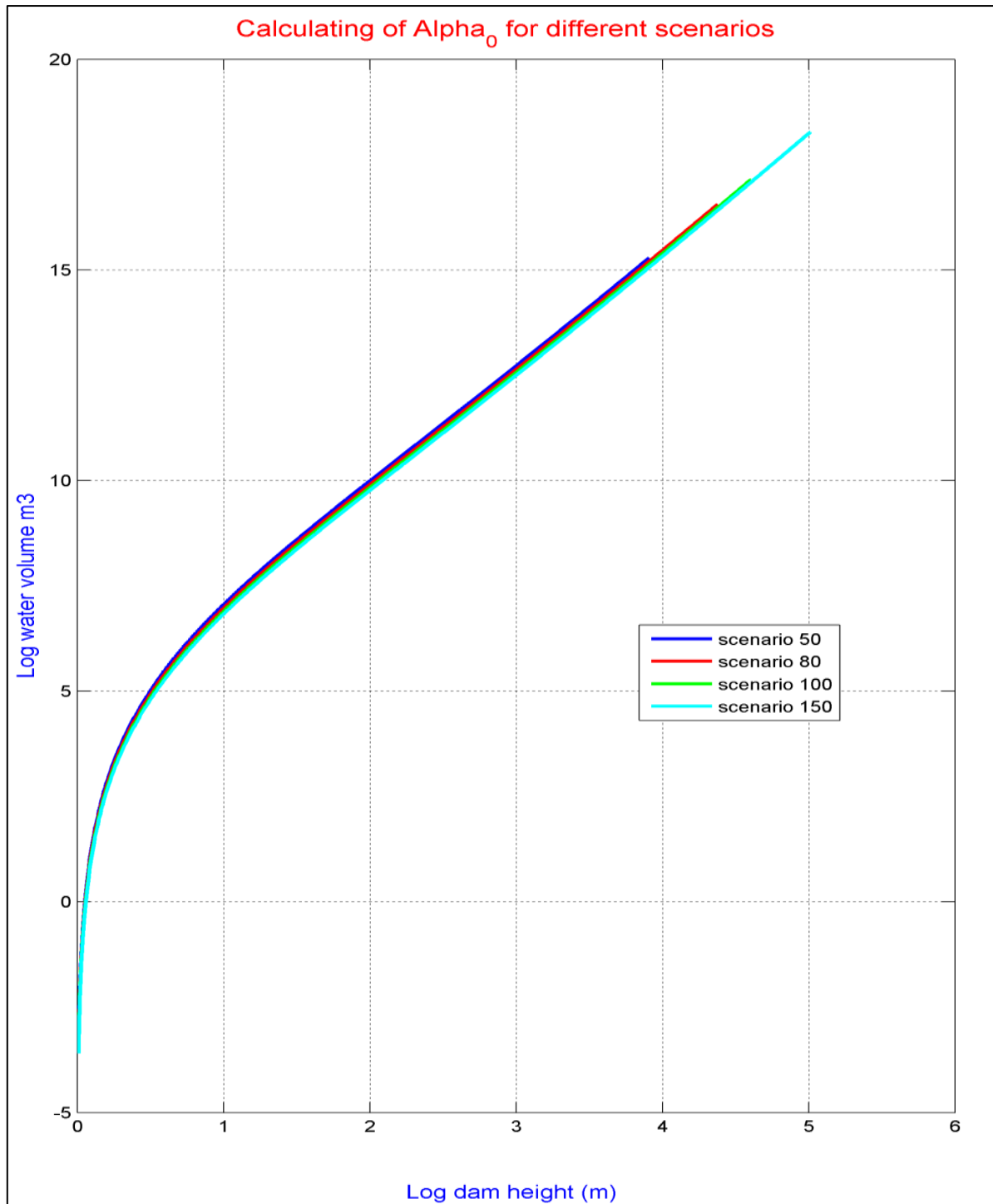


Fig. 6. 20:Level reservoir volume curve.

6.2.4 Dam failure causes, modelling and consequences

Dams provide many benefits for our society, but floods resulting from the failure of dams have also produced some of the most devastating disasters of the last two centuries. When dams fail property damage is certain but loss of

life can vary dramatically with the extent of the inundation area, the size of the population at risk and the amount of warning time available (almost equal to the lake filling time in Sondrio case).

As in (Wahl, 1998); (Costa, et al., 1985) reports that sixty percent of more than 11,100 fatalities associated with all dam failures worldwide have occurred in just three failures: Vaiont, Italy, 1963 (2,600 dead; overtopping of concrete arch dam by landslide-generated wave); Johnstown Dam, Pennsylvania, 1889 (2,200 dead; overtopping of embankment dam); and Machhu II, India, 1974 (2,000+ dead; overtopping of embankment dam during construction). In each of these cases, large populations were given little or no warning. In fact; (Costa, et al., 1985) reports that: the average number of fatalities per dam failure is 19 times greater when there is inadequate or no warning.

Earthen dam failures are very sensitive to the structure materials and configurations, impacting forces and other environmental factors. In general, a concrete embankment is prone to fail instantaneously (break) when the entire structure or only a portion loses stability under certain loading conditions; thus, the breach dimensions are often determined on the basis of structural stability analysis, then the resulting flood can be simulated by using numerical tools. An earth embankment, however, is likely to fail gradually (breaching) because of erosion of its materials by water flow or wave action involving mixed-regime flows, strong sediment transport, and rapid morphological changes. Therefore, determination of the earth embankment breach characteristics (e.g., width, shape, peak outflow, failure time) is quite complex and challenging, requiring the prediction of complex interactions among soil, water and structure. The following figure shows failure causes.

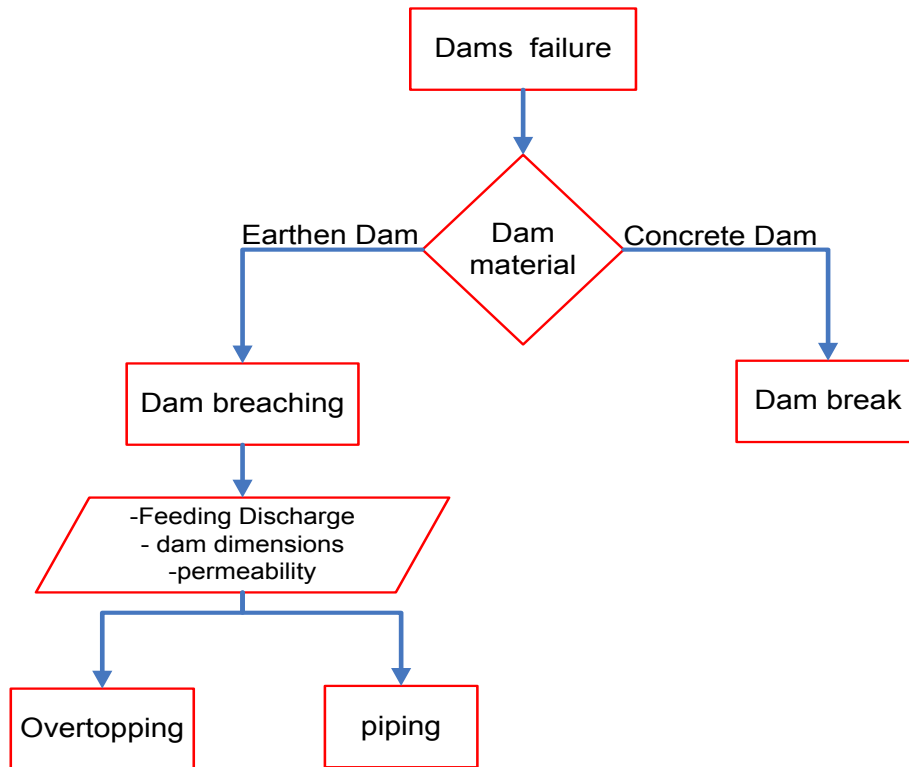


Fig. 6. 21:Flowchart for dam failure types.

Common causes of earthen dam failure

The major causes of earthen embankment failure are overtopping, foundation and structural defects and piping. Although additional failure causes may exist for individual structures. According to (Costa, et al., 1985), approximately 34% of dam failures are caused by overtopping, 30% by foundation defects and 28% by piping.

● Failure of dams due to overtopping

In this type of failure, overtopping of the crest results in channel erosion over the crest and downstream face is driven by shear forces. Observations in laboratory experiments and case studies suggest a distinct difference among the erosion processes of non-cohesive and cohesive earthen embankments attributable to overtopping flow. The critical overtopping erosion mode is usually progressive surface erosion (sediment transport in dispersed particles)

for non-cohesive embankments but headcut erosion (formation and migration of a vertical or nearly vertical drop on the bed) for cohesive embankments. However, non-cohesive heavily compacted embankments may also erode in the form of a headcut and the point of transition between the headcut and surface erosion modes is not well defined. Erosion usually starts at the downstream slope and advances upstream, resulting in a decrease of the width of the embankment crest. In the case of surface erosion, the downstream slope may flatten, steepen and erode back parallel, depending on the soil type and state. In the case of headcut erosion, initial overtopping flow results in sheet and rill erosion, with one or more master rills developing into a series of cascading overfalls and then a large headcut on the downstream slope, as illustrated in Fig. 6.22 (from (Weiming, 2011) taken by permission from (Hanson, et al., 2005)). The breach bed erosion is often accompanied by lateral erosion and mass failure of side walls. When the embankment crest vanishes, the breach flow starts to increase significantly and the breach is then further lowered and widened at a much greater rate until the headwater depleted or the tailwater elevation increases.

Overtopping may occur for a variety of reasons, such as large inflows into the reservoir caused by excessive rainfall or by the failure of an upstream dam, extreme waves and surge, inadequate design, construction and maintenance of the structure, debris blockage in the spillway and flood channel and settlement of the embankment crest.

In figure 6.22; (a) rills and cascade of small overfalls at $t = 7$ min; (b) consolidation of small overfalls at $t = 13$ min; (c) headcut at downstream crest at $t = 16$ min; (d) headcut at upstream crest at $t = 31$ min; (e) flow through breach at $t = 40$ min; (f) transition to final breach stage at $t = 51$ min.



Fig. 6. 22: Phases of cohesive dam breaching by overtopping.

- Failure by piping or internal erosion

Piping is the process by which seepage forces can result in the removal of fines along a path between the upstream and downstream faces. If unchecked, larger sediment particles are washed out by a process known as backward erosion ultimately leading to the formation of a pipe or tunnel carrying a significant discharge. The pipe increases in diameter because of removal of material at the wall primarily attributable to shear stress forces until local collapse or slumping of the crest roof occurs. After the collapse of the crest, overtopping breach characteristics dominate including downcutting and lateral widening. The typical piping failure process is documented in Fig. 6. 23 (from (Weiming, 2011) taken by permission from (Hanson, et al., 2005)). Some case studies have shown that the pipe initiation and erosion stages may take several days or weeks, whereas the subsequent embankment breaching may take only

a few hours or less. In figure 6.23; (a) initiation; (b) $t = 5$ min; (c) 8 min; (d) 13 min; (e) 13 min, following collapse of piping roof; (f) 60 min, continued widening.



Fig. 6. 23: Dam breaching attributable to piping.

- Failure due to foundation and structural defects

Foundation and structural defects include differential settlement, sliding and slope instability, high uplift pressure and uncontrolled foundation seepage. Differential settlement may cause cracks and weaken layers in the embankment, in which internal erosion may develop to initiate piping failure. Excessive foundation seepage through permeable substrata is often accompanied by the formation of sand boils, which often look like miniature volcanoes ejecting water and sediment and may result in piping failure, if not

controlled. High uplift pressure and saturation of foundation materials may give rise to slope instability and sliding failure. The piping failures caused by foundation defects are similar to those described in the preceding subsection, but the initial breaches may involve the whole height of the embankment. Sliding failures can form a large rupture much more rapidly than piping failures. Geotechnical conditions limit the extent of initial sliding failure and the amount of forward movement and determine the actual size, shape and position of failure.

Dam failure modelling

The dam in Spriana is not a constructed dam, but it will create due to the landslide failure. This means that, it is not compacted embankment so it is expected that the soil permeability will be high. The likely failure is mainly dominant by the feeding discharge, the soil type and the dam dimensions i.e. low permeability of the dam material leads to failure due to overtopping not piping and wider dam will reduce the probability of failing by piping. However in the following section, a discussion about the seepage process and its effect on dam breaching will be opened then, discussion about different models of breaching due to overtopping.

- **Modelling the seepage process**

According the lake formation model (item 6.2.3) and by regardless the feeding discharge, the filling time for the lake depends on the dam height e.g. scenario 80 (Dam with 80m height) takes 43.31 hours (around two days) to fill the lake. During this time, the dam can fail due to piping. For this reason, the finite element based software named Geostudio/seep⁵ version 7.1 used to

⁵ <http://www.geo-slope.com>

check the seepage flux considering the dam dimensions given in table 6.1 that is according the dam height scenario.

The first and the only challenge is the estimating of reasonable value for the hydraulic conductivity of the dam material known that the soil is disturbed after the landslide. For this purpose the stratification of the soil formation must be studied. Figure 6.24 shows a 150 m long borehole located in the central area of the landslide slope at an altitude of 1041 m in the area known as Casa Piazza. The borehole passes through three different sections: the first from 0 to 35.6 m in debris, the second from 35.6 to 145 in much fractured rock and the third from 145 to 150 m is rock of good quality. From the lithological point of view both debris and rock masses were homogeneous and composed of mica schist. In the debris section that goes from 0 to 35.6 m one can distinguish two areas with different soil characteristics: in the first, extends from 0 to 24 m, the coarse fraction (larger boulders, gravel) clearly prevails over that fine (sand, silt). in the second, from 24 to 35.6 m, the coarse fraction (few large boulders, pebbles, gravel) is rather less than the fines (sand, silt, clay).

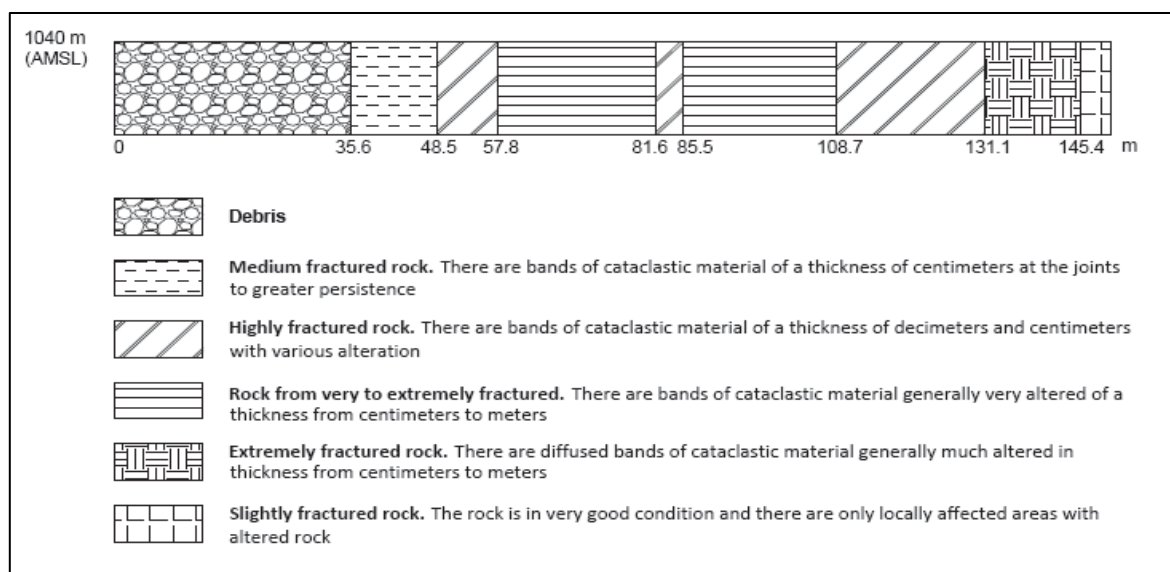


Fig. 6. 24: The soil stratification at Spriana slide.

Depending on the pre-described soil formation, It is necessary to define a hydraulic conductivity (or permeability) function (a function that describes how the permeability varies with changes in suction (negative pore-water pressure = suction)). At low suctions (i.e. near saturation), the coarse material has a higher hydraulic conductivity than the fine material, which is intuitive. At high suctions, the coarse material has lower conductivity, which often appears counterintuitive. The following figure shows the assumed permeability function, it assumes high values of the permeability due to the disturbance of the soil after landslide collapse.

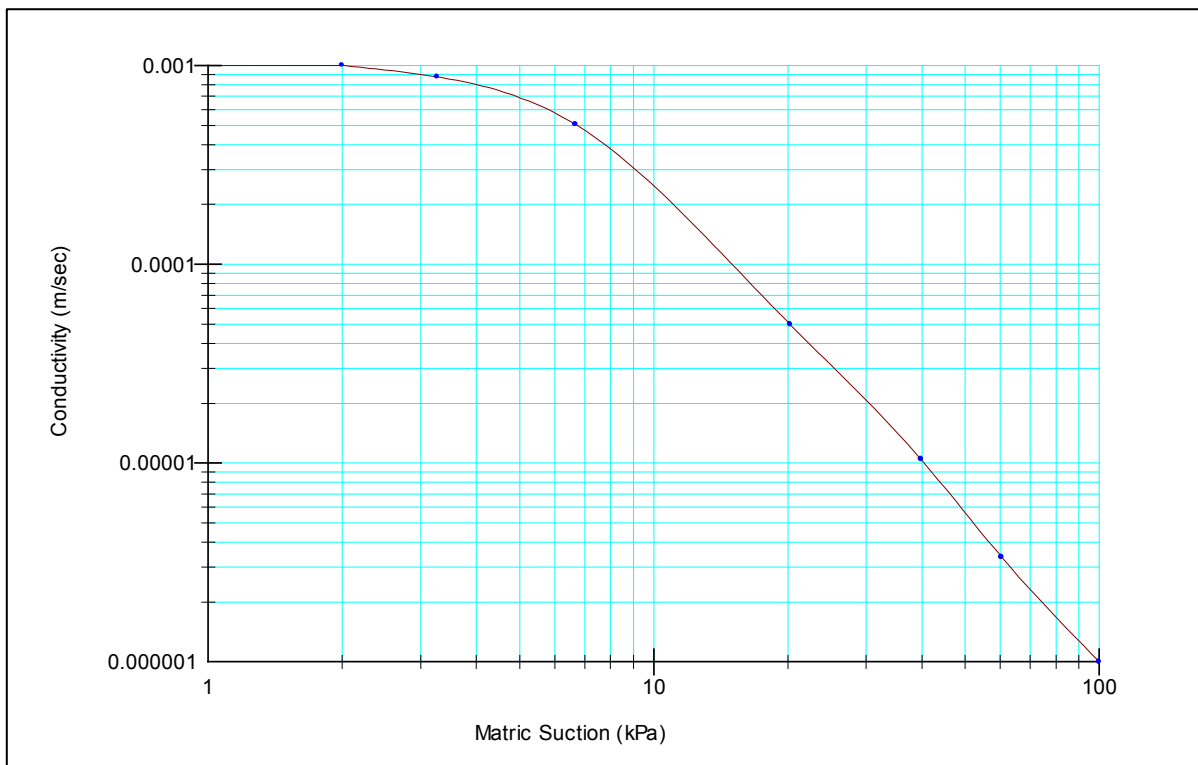


Fig. 6. 25:The assumed hydraulic conductivity function.

➤ Seepage analysis for scenario 80

A 2D seepage model built in the Geostudio software considering the dimensions given for scenario 80 in table 6.1 and the hydraulic conductivity function given in fig 6.25. The model ran as a steady state analysis with four sequent phases of lake's water depth starting from water depth = 20 m up to

80 m. For each phase; the equipotential lines (labeled contour lines), the flow paths lines (green lines starts from left to right) and the line of zero pressure represent the water surface inside the dam (blue continuous line) have been drawn for each phase (fig 6.26,28,30, and 6.32). In addition a dashed line for the flux label has been drawn to calculate the flux per unit depth of the dam.

For a phase with 20 m depth (figure 6.26); the equipotential lines are labeled from 20 to 0 (from the water side to the right side) where each contour line represents the total water head. As shown, there are some water passed the dam body and the water flux per unit depth at the mid of the dam is shown =0.000163 m³/s.

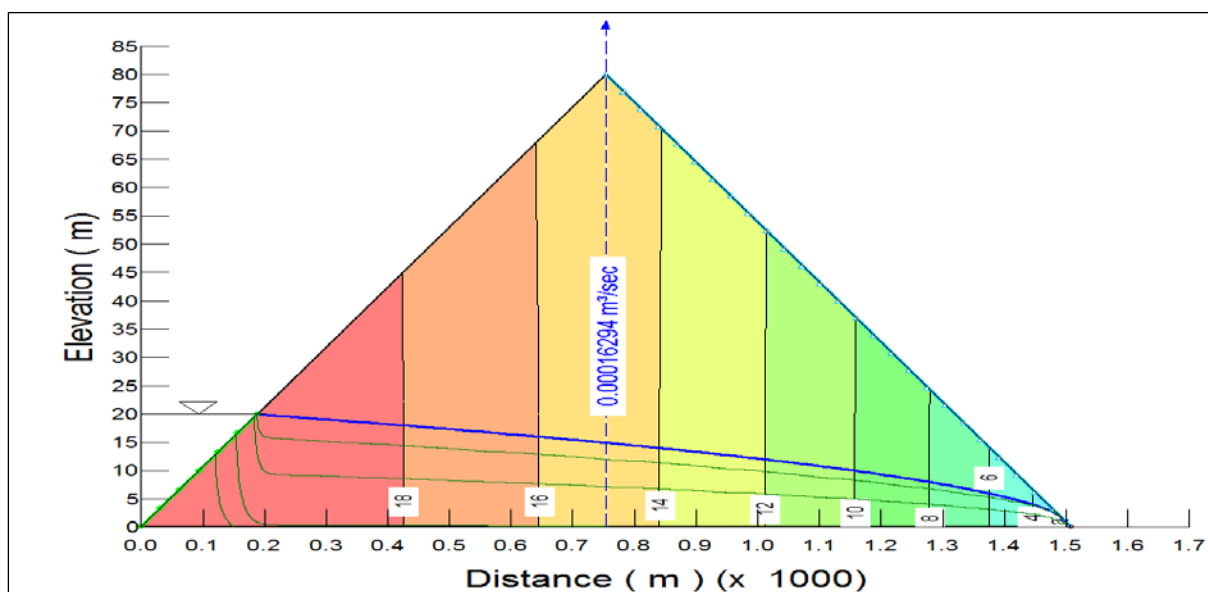


Fig. 6. 26: Seepage analysis at water depth in the lake = 20 m.

At the dam tail there are waters passed the whole dam. The discharge at the dam tail from the seepage face (downstream face) is given in figure 6.27. The minus values of the discharges refer to the outflow per unit depth from the last 20 m of the dam (measured horizontally). This behaviour is similar to that shown in figure 6.23 (photo a), but still the out flow is less than feeding discharge which means that the water arise with time in the lake.

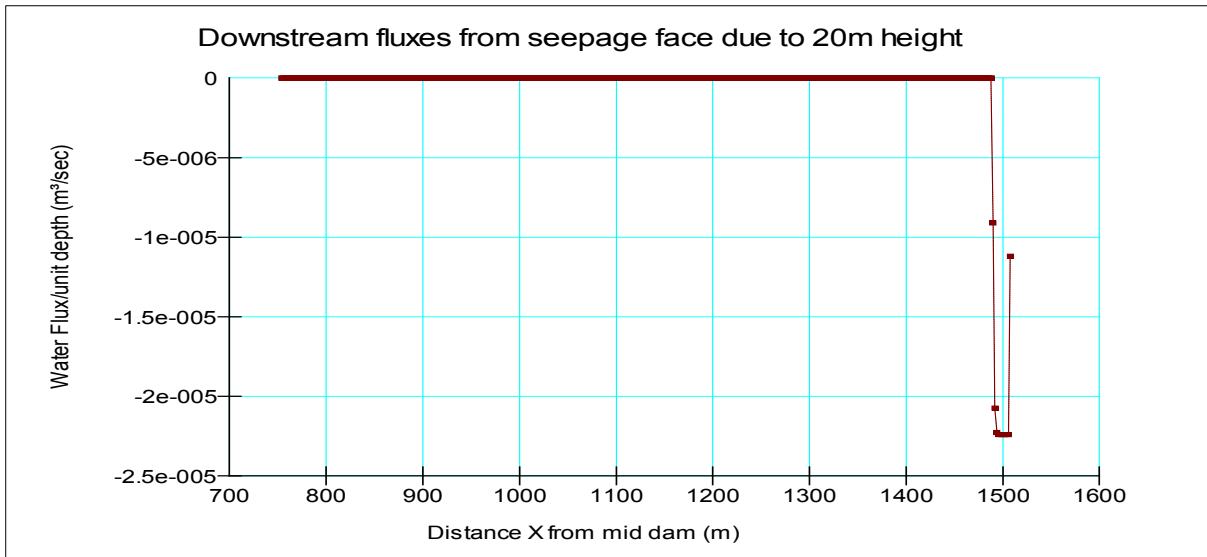


Fig. 6. 27: Downstream fluxes from seepage face due to 20 m water height at upstream.

With increasing water depth as in figure 6.28 to 40 m depth, the discharge at the mid-section of the dam increases in addition to the increasing of the water level inside the dam. Also the discharge at the tail of the dam increases to $0.00074 \text{ m}^3/\text{s}$ and the seepage length increases to round 100 m as in figure 6.29.

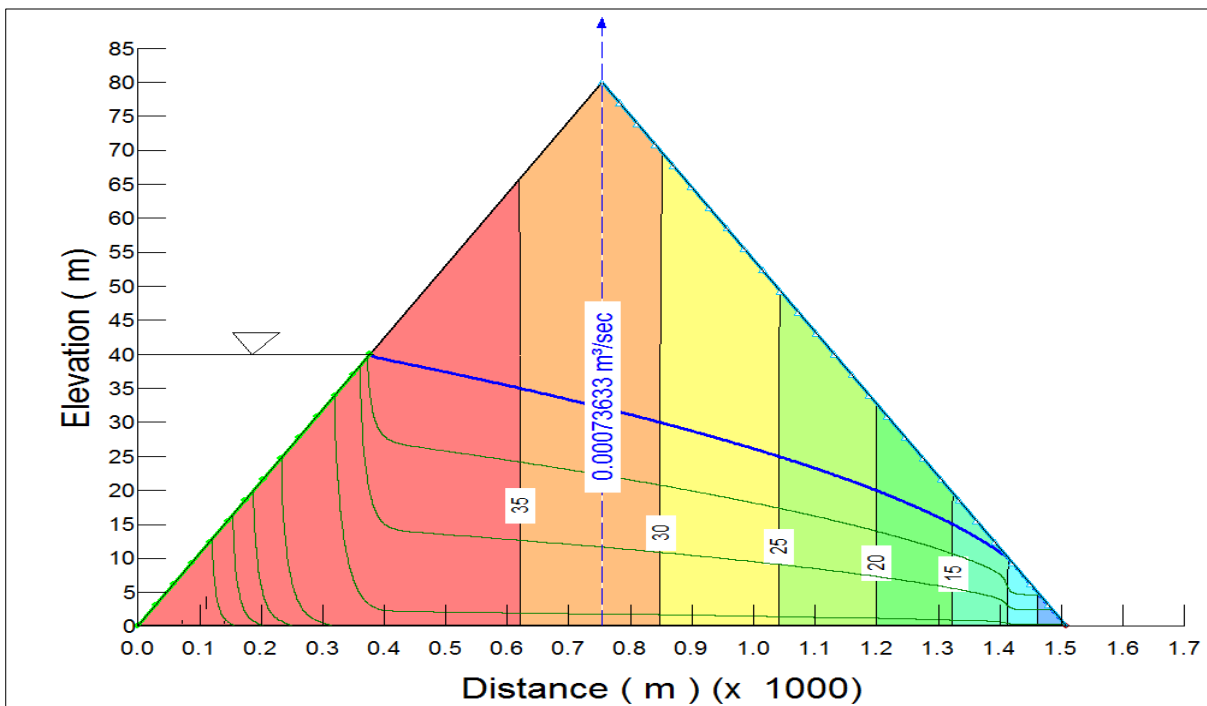


Fig. 6. 28: Seepage analysis at water depth in the lake = 40 m.

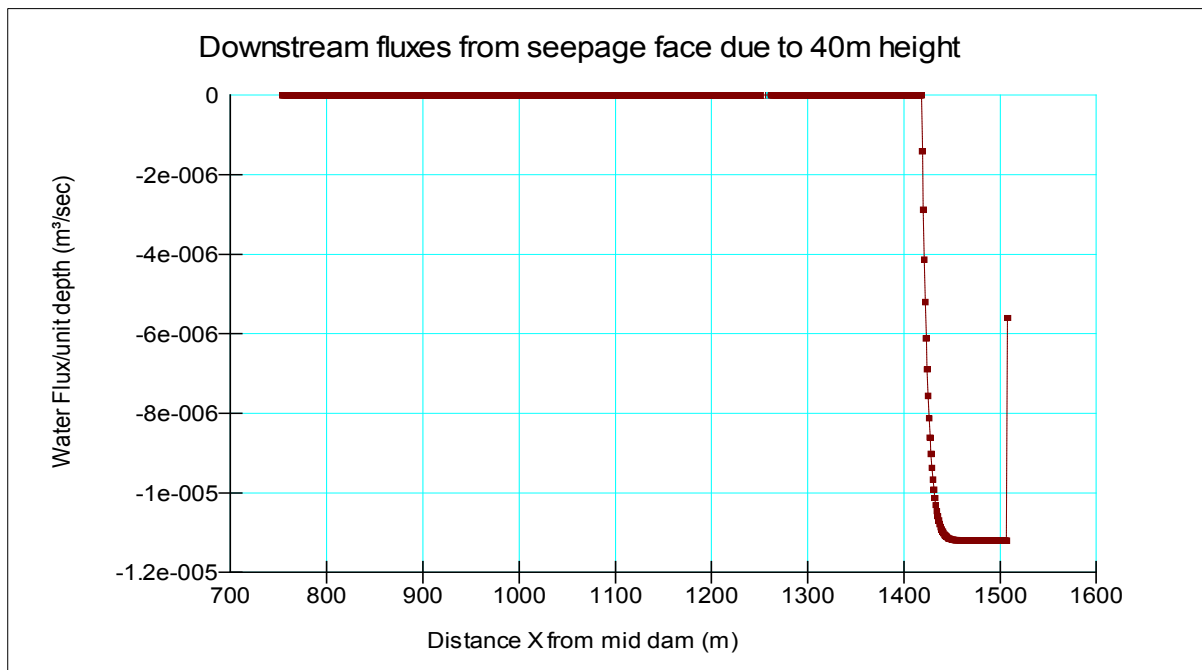


Fig. 6. 29: Downstream fluxes from seepage face due to 40 m water height at upstream.

The same behaviour takes place with further increasing of water level in the lake to 60 m. The seepage distance at the tail reach to 200 m as shown in figures 6.30, 6.31 respectively.

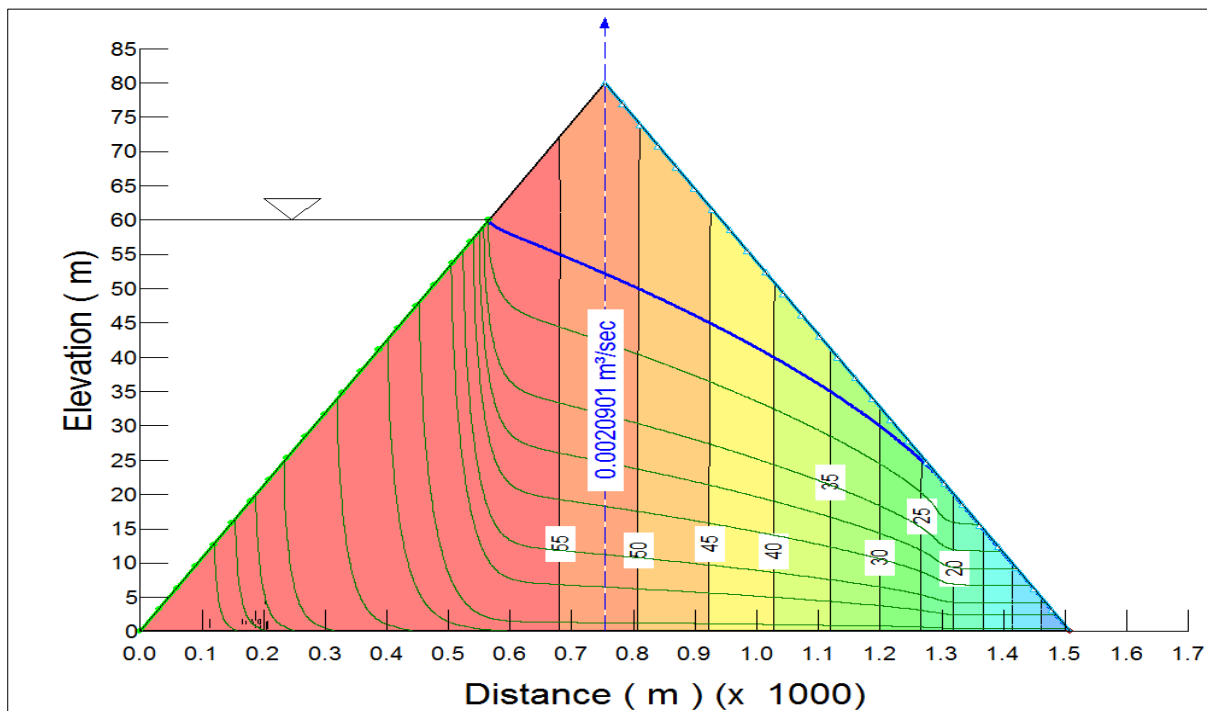


Fig. 6. 30: Seepage analysis at water depth in the lake = 60 m.

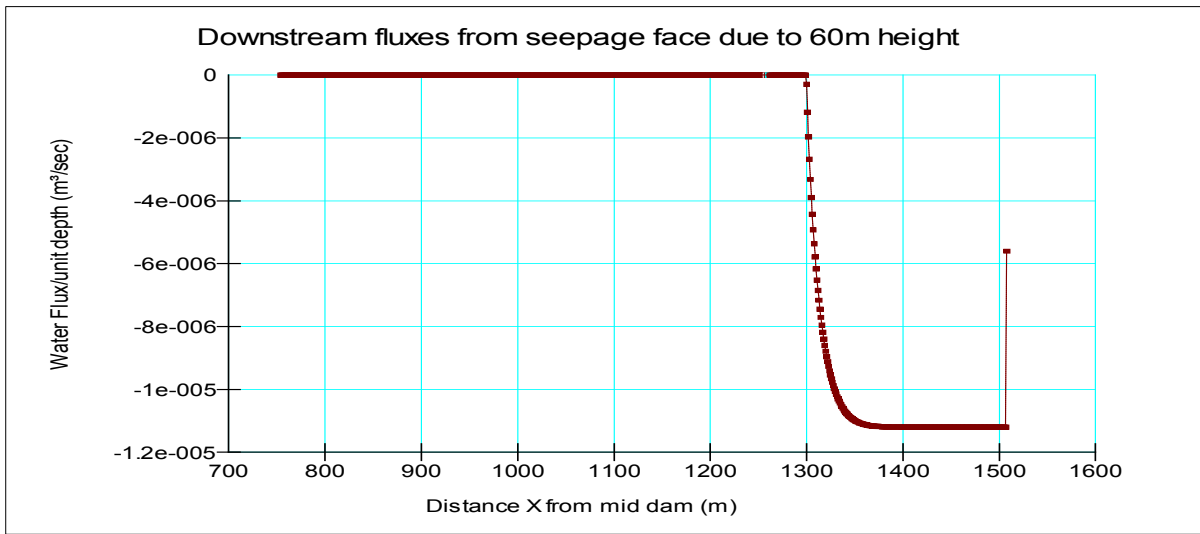


Fig. 6. 31: Downstream fluxes from seepage face due to 60 m water height at upstream.

When the water depth increases up to the overtopping level, the dam become fully saturated (figure 6.32) and the seepage length (figure 6.33) becomes the whole seepage face, but still the out discharge is less than the feeding, which means that the overtopping will start in dam breaching beside the seepage.

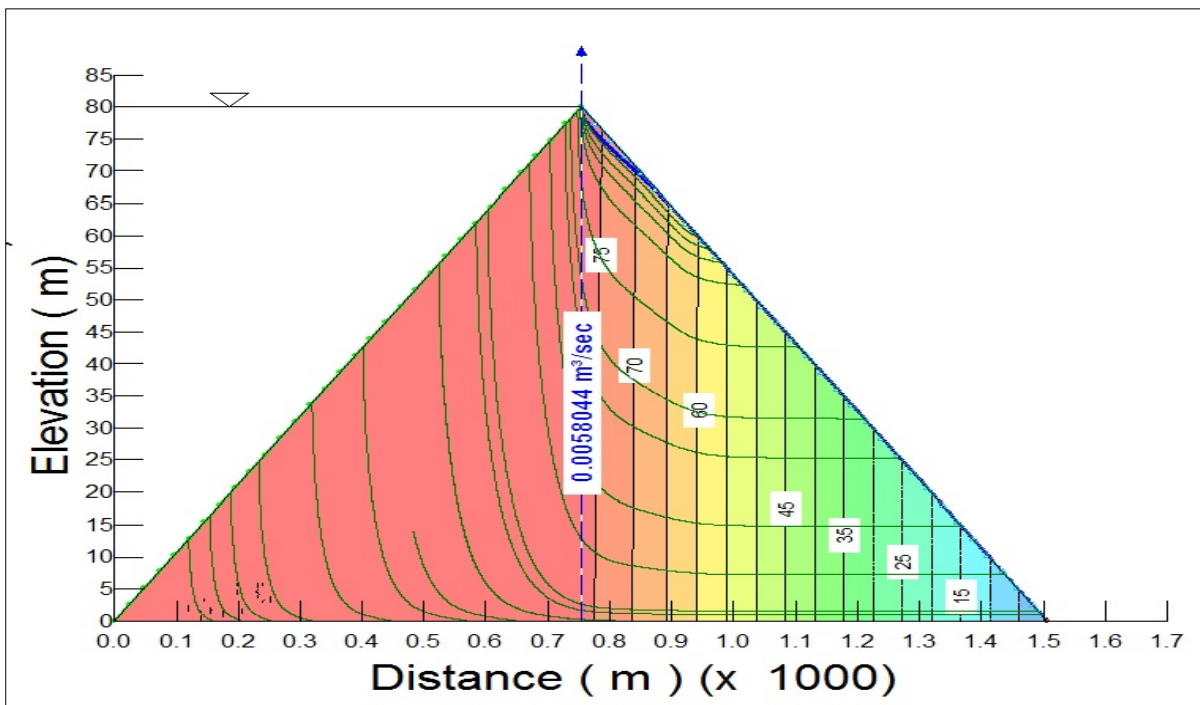


Fig. 6. 32: Seepage analysis at water depth in the lake = 80 m.

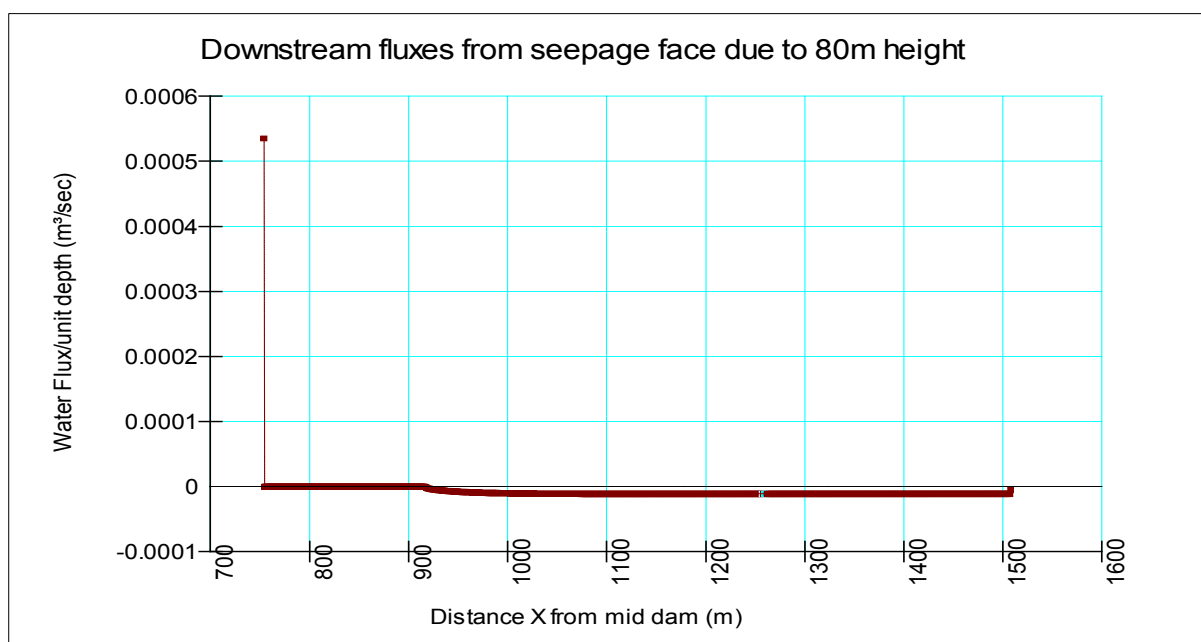


Fig. 6. 33: Downstream fluxes from seepage face due to 80 m water height at upstream.

➤ Sensitivity of the seepage model to the hydraulic conductivity

It is very important to refer to the sensitivity of a seepage model to the hydraulic conductivity not only globally but also locally from zone to another in the dam. Usually the estimation of the hydraulic conductivity function depends on the soil classification as done before. The permeability ranges are small in value, so one can estimate different permeability value which affects the discharge values for specific hydraulic gradient i through cross sectional area A_{sp} according the relation:

$$Q = K \cdot i \cdot A_{sp} \quad 6.10$$

As shown, the discharge is proportional to the permeability K , so any wrong estimation for the permeability will produce wrong results for the discharge and may be wrong description of the failure cause i.e. assuming high permeability instead of actual lower value can lead to collapse due to piping,

while in reality the collapse will be due to the overtopping. The problem related to Spriana is the disturbance of the soil due to the slide, so no one can find accurate value for the permeability. To study the effect of this wrong estimation, a different hydraulic conductivity function (Fig 6.34) is assumed (ten times the estimated one).

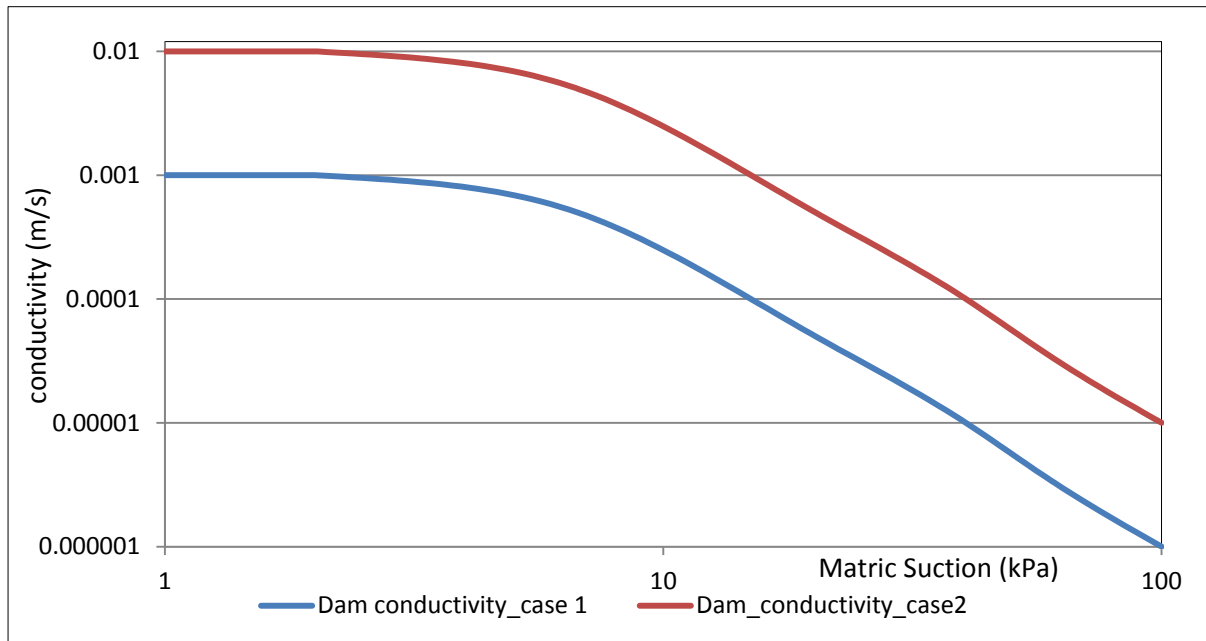


Fig. 6. 34: Different hydraulic conductivity functions (case 2= 10*case 1).

The model re-ran again using this new conductivity function and 60 m depth of water in the lake. The results are shown in fig 6.35. By comparing it with fig 6.30; the zero pressure lines are identical in both the cases, which mean that the flow area within the dam is the same. The values of the discharges increases 10 times due to the increasing of permeability which means that the value of the discharge depends only on the permeability value with the same hydraulic gradient and cross sectional area. Figure 4.36 shows the differences between the values of the outflow discharge from the seepage face due to the two cases of hydraulic conductivity.

With high discharges the toe of the dam will erode faster causing the dam failure due to piping, while with lower permeability the overtopping is the dominant case for dam breaching.

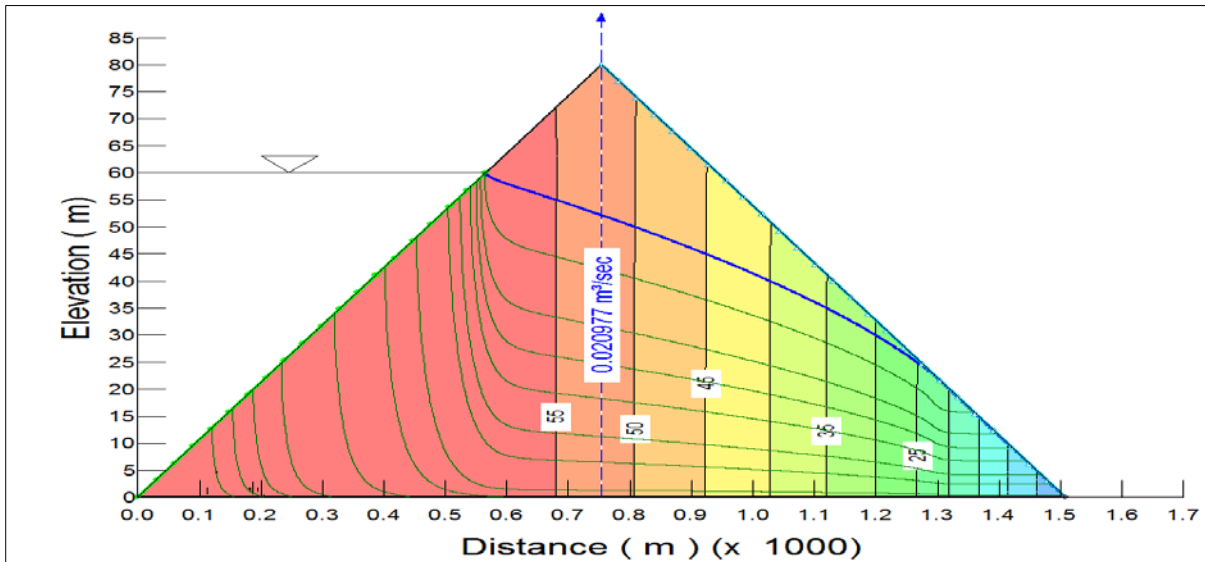


Fig. 6. 35: Seepage analysis at water depth in the lake = 60 m (case 2).

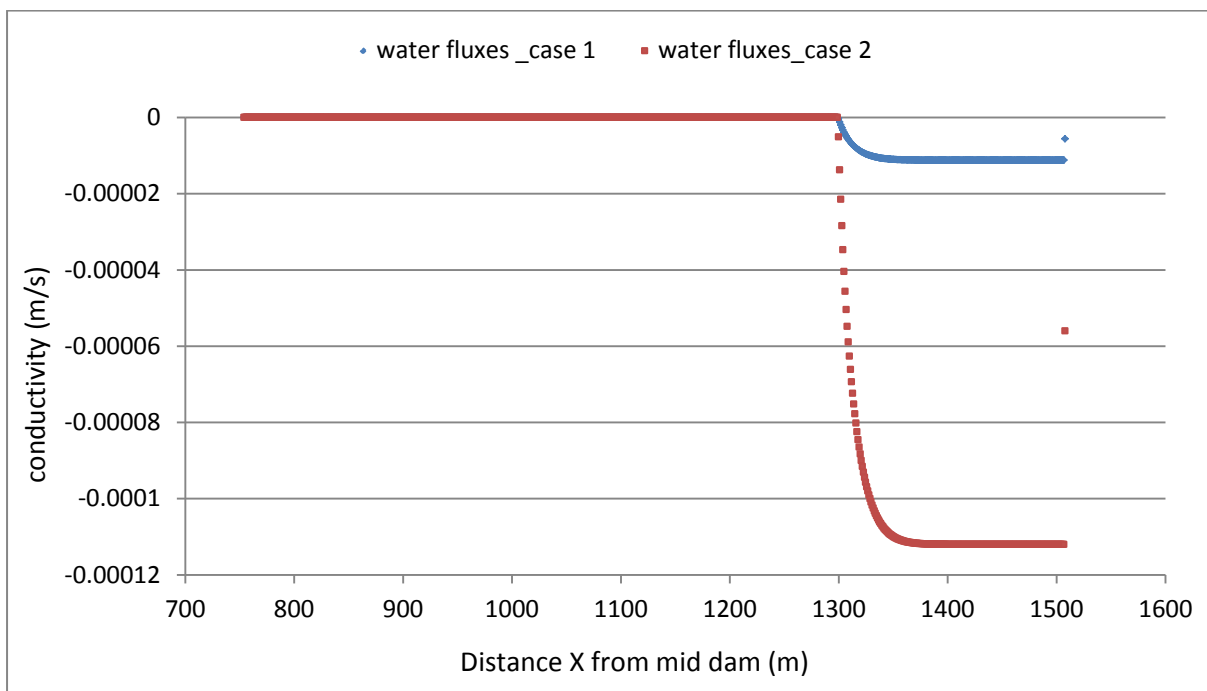


Fig. 6. 36: Downstream fluxes from seepage face due to 60 m water height at upstream with different permeability ($K_2=10.K_1$).

As shown, the discharge values are very small which can't lead to the breaching during the filling time e.g. the scenario 80 for the dam can't collapse

by piping in 43.31 hour that is the time of filling the lake at feeding discharge $100 \text{ m}^3/\text{s}$. For very small discharges, the filling time will be more and the probability of breaching due to piping will increase but still this probability is less than the breaching due to the water overtopping.

- **Models for overtopping breach**

As discussed, the water increases with time in the lake, with this increasing may by some water will ooze. If the permeability of the dam material is high, it can lead to failure of the dam by piping before reaching the overtopping level. In case of lower permeability, the seepage discharge can be negligible hence the water level will increase till reaching the minimum crest level. The overtopping will start exciting the dam's soil causing enlargement of cross-section of the breach and producing catastrophic water and sediments waves.

The hydraulic analysis of a dam or levee breach and the resulting flood includes three primary tasks: (1) Predicting the breach characteristics (e.g., shape, depth, width and formation time) and processes. (2) Routing the upstream inflows. (3) Routing the breach outflow and sediment hydrographs through the downstream area.

In the last decades, numerous models have been developed for prediction of earthen embankment breaching processes. These models can be classified as parametric, simplified and detailed multidimensional physically based breach models. The parametric breach models estimate the breach width, breach side slope, peak outflow and failure time using regression equations statistically derived based on data from dozens of historic dam failures, without considering the detailed breaching processes. In the simplified physically based breach models, the breach cross section is usually simplified as a rectangle, trapezoid or triangle; the flow at the breach is estimated using

the weir relationships; and the erosion estimates by using different simplified models. Multidimensional physically based models simulate in more detail the flow and morphodynamic processes resulting from embankment breaching.

The simplified physically based breach models are attractive for engineering applications. The simplified models may be based on either analytical or numerical solutions. To solve the models analytically or with simple numerical algorithms, simplifications have to be made by approximating the reservoir rating curve with a linear or simple power function between the water level and surface area (or volume) and assuming the erosion rate at the breach to be a power function of the flow velocity (Weiming, 2013) or shear stress (Macchione, 2008).

➤ Breaching model by Macchione

(Macchione, 2008; Macchione, et al., 2008) model is physically based breach model, it predicts not only the peak discharge but also the whole outflow hydrograph and breach development. The aspects are taken into account are: the geometry of the embankment, the shape of the reservoir, the hydraulic characteristics of the flow through the breach and its erosive capacity and the shape of the breach.

▪ Model assumptions

The dam material is impermeable and no seepage can happen before reaching the overtopping level. Also the cross section of the breach is assumed to develop at first in a vertical direction with a triangular shape until its lower vertex reaches the base of the dam. Further development of the breach leads to an enlargement owing to erosion of the sides alone. The model also assumes the occurrence of critical flow through the breach, the critical shear

stress in the breach is negligible in calculating the transport capacity and the inflow rate to the reservoir Q_i is negligible with respect to outflow discharge Q .

▪ Model description

This model considers only the dams totally constructed of earth materials. It computes the outflow discharge and sediments through the breach. The main inputs are: the height of the dam, the initial water level in the reservoir, the reservoir parameters (W_0 & α_0), the crest width of the embankment and the dam side slopes. The considered shape of the breach is triangular and trapezoidal respectively. Referring to the sketch in Fig. 6.37, the area A_b of the triangular breach is:

$$A_b = (Z_M - Y)^2 \tan \beta \quad 6.11$$

In which Z_M indicates the height of the dam; Y = vertical distance between the vertex of the triangular breach and the base of the dam; and β is the angle that the sides of the breach form with the vertical. The considered value of $\tan \beta$ is 0.5 according to (Macchione, et al., 2008).

For the trapezoidal breach, A_b is:

$$A_b = (Z_M - 2Y)Z_M \tan \beta \quad (Y < 0) \quad 6.12$$

In which $(Y < 0)$ now indicates the difference in elevation between the intersection point of the lengthened sides of the breach and the base of the dam. The enlargement of the breach can be described by the equation

$$dA_b \cdot l = c \cdot q_s \cdot dt \quad 6.13$$

In which, c is erodible wetted perimeter; and l = mean length of the breach. Assuming the occurrence of critical flow through the breach, the erodible wetted perimeter c can be expressed as:

$$c = \frac{2h_c}{\cos(\beta)} \tag{6.14}$$

In which h_c =critical water depth in the breach calculated in table 6.3.

Breach	Hydraulic radius R	Velocity in Breach V=	Critical depth h_c	$\frac{(dA_b)}{dY} =$	Breach length l
Triangular	$\frac{1}{2} h_c \sin\beta$	$\left(\frac{1}{2} g h_c\right)^{\frac{1}{2}}$	$\frac{4}{5}(Z - M)$	$-2(Z_M - Y)\tan\beta$	$(Z_M - Y) \cdot \frac{s_u + s_d}{2} + w_c$
Trapezoidal	$\frac{h_c(h_c - 2Y)}{2\left(\frac{h_c}{\sin\beta} - Y\right)}$	$\left[g \frac{(h_c - 2Y)}{2(h_c - Y)} h_c\right]^{\frac{1}{2}}$	$\frac{1}{5} \left[2Z + 3Y + (9Y^2 + 4Z^2 - 8YZ)^{\frac{1}{2}} \right]$	$-2Z_M \tan\beta$	$Z_M \cdot \frac{s_u + s_d}{2} + w_c$

Table 6. 3: Expressions for Macchione model's parameters.

Assuming that the transport capacity is proportional to the 3/2 power of mean shear stress $\tau(N/m^2)$ (as, for example, in the Meyer-Peter and Muller formula, if the critical shear stress is negligible in comparison with τ), the following equation for the volumetric sediment load per unit width, q_s , is:

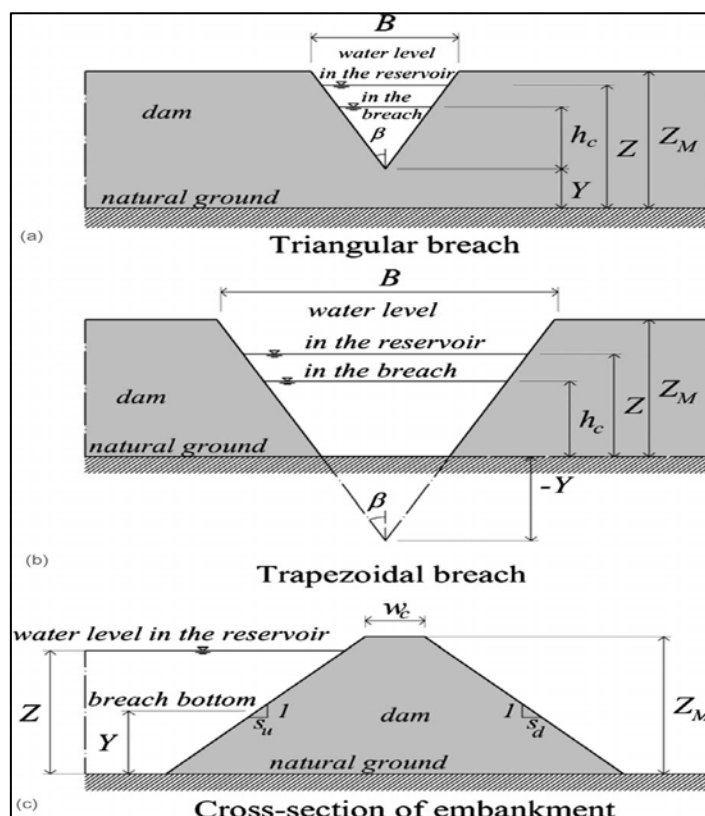


Fig. 6. 37: Definition sketch of breach section by Macchione.

$$q_s = k_0 \tau^{3/2} \tag{6.15}$$

Where the coefficient k_0 ($m^5 s^{-1} N^{-3/2}$) depends on the properties of the material and the conditions in which the erosion occurs.

Since $\tau = \gamma \cdot R \cdot S$ and $S = \frac{V^2}{k_s^2 R^3}$ so Eq 6.15 can be rewritten in the form

$$q_s = \frac{k_0}{k_s^3} (\gamma g)^{\frac{3}{2}} \cdot \frac{V^3}{g^{\frac{3}{2}} R^{\frac{1}{2}}} = v_e \cdot \frac{V^3}{g^{\frac{3}{2}} R^{\frac{1}{2}}} \quad 6.16$$

V =flow velocity in breach, k_s = Strickler roughness coefficient and v_e is the characteristic velocity that affects the erosion velocity dY / dt , hydraulic and geometric conditions being equal, the velocity of erosion is proportional to velocity v_e . The characteristic velocity depends on coefficient k_0 of the volumetric sediment load and the Strickler coefficient k_s therefore depends on the overall susceptibility of the embankment to be breached.

Since $\frac{dA_b}{dt} = \frac{dA_b}{dY} \cdot \frac{dY}{dt}$; Eq. 6.13 can be rewritten as

$$\frac{dY}{dt} = c q_s \left(\frac{dA_b}{dY} \right)^{-1} \cdot l^{-1} \quad 6.17$$

Taking into consideration Eqs. 6.14 to 6.16, Eq 6.17 can be written as follows:

$$\frac{dY}{dt} = \left(\frac{2h_c}{\cos(\beta)} \right) \left(v_e \cdot \frac{V^3}{g^{\frac{3}{2}} R^{\frac{1}{2}}} \right) \left(\frac{dA_b}{dY} \right)^{-1} \cdot l^{-1} \quad 6.18$$

The expressions for $R, V, h_c, \frac{dA_b}{dY}$ and l as functions of Z and Y are given in Table 6.3. The symbols s_u and s_d indicate the upstream and downstream embankment slopes and w_c =crest width of the embankment.

The value of Z over time is provided by the continuity equation of volume W stored in the reservoir

$$Q_i - Q = \frac{dW}{dt} \quad 6.19$$

In which, Q_i =inflow rate to the reservoir and Q =outflow discharge through the breach. To take the reservoir shape into account, the stored volume W is given as a function of Z by the level-reservoir volume curve Eq 6.9. If Q_i is negligible with respect to Q , the continuity equation can be expressed as:

$$-Q = \frac{d}{dt}(W_0 Z^{\alpha_0}) = W_0 \cdot \alpha_0 \cdot Z^{\alpha_0-1} \cdot \frac{dZ}{dt} \quad 6.20$$

Discharge Q is given by the following equations for the triangular breach and for the trapezoidal breach respectively:

$$Q = \left(\frac{1}{2}g\right)^{\frac{1}{2}} \left[\frac{4}{5}(Z - M)\right]^{\frac{5}{2}} \cdot \tan \beta \quad 6.21$$

$$Q = \left(\frac{1}{2}g\right)^{\frac{1}{2}} \cdot [h_c(h_c - 2Y)]^{\frac{3}{2}} \cdot (h_c - Y)^{-\frac{1}{2}} \cdot \tan \beta \quad 6.22$$

By substituting Eqs 6.21 and 6.22 into Eq. 6.20, one obtains Eq 6.23 and 6.24 valid for the triangular breach and the trapezoidal breach, respectively.

$$\frac{dZ}{dt} = -\left(\frac{4}{5}\right)^{\frac{5}{2}} \left(\frac{1}{2}g\right)^{\frac{1}{2}} \cdot \frac{Z^{1-\alpha_0}}{W_0 \alpha_0} [Z - M]^{\frac{5}{2}} \cdot \tan \beta \quad 6.23$$

$$\frac{dZ}{dt} = -\frac{Z^{1-\alpha_0}}{W_0 \alpha_0} \cdot h_c(h_c - 2Y) \cdot \left[g \frac{(h_c - 2Y)}{2(h_c - Y)} h_c\right]^{\frac{1}{2}} \cdot \tan \beta \quad (Y < 0) \quad 6.24$$

Eqs 6.18 and 6.23 describe the generation of the outflow hydrograph for the first part of the phenomenon, characterized by triangular breach, and the discharge Q is given by Eq 6.21. When the breach reaches the trapezoidal shape, the phenomenon is described by the system of Eqs 6.19 and 6.24 and Q

is given by Eq 6.22. The initial conditions are given by the initial water level $Z(0)$ in the reservoir and by initial breach bottom elevation $Y(0)$, at time $t=0$.

The sediment transport calculates using Eq 6.16 considering the value of the characteristic velocity $v_e=0.059$ m/s as calibrated by (Macchione, 2008). For scenario 80 described in tables 6.1; the following hydrograph gives the results of the model.

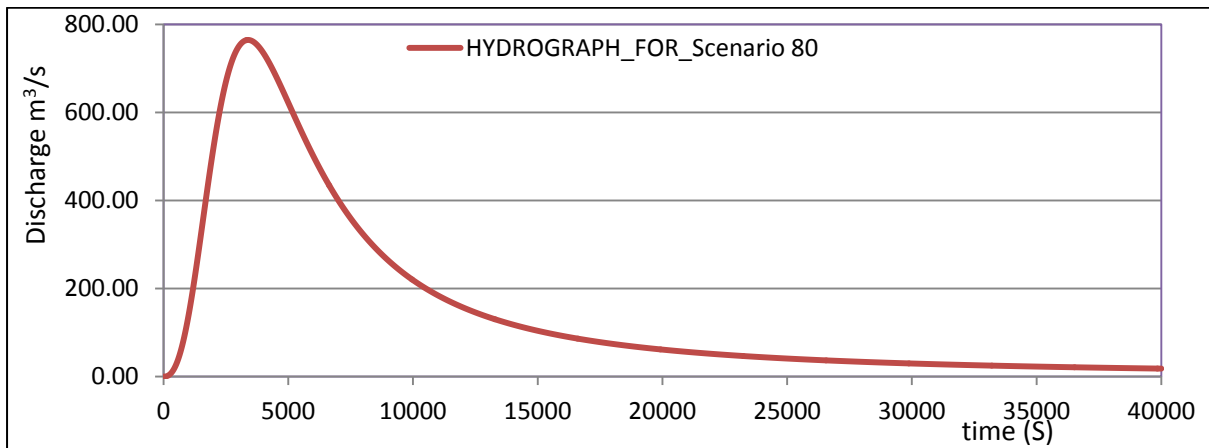


Fig. 6. 38 : The produced hydrograph for scenario 80 according Macchione breaching model 2008.

The figure shows that, once the breaching starts the discharge grows very fast to reach the maximum value for discharge ($754 \text{ m}^3/\text{s}$) after 50 min, then it goes back to the ordinary flow in Mallero after 11 hour. This hydrograph will be accompanied by sediment discharge shown in the following figure.

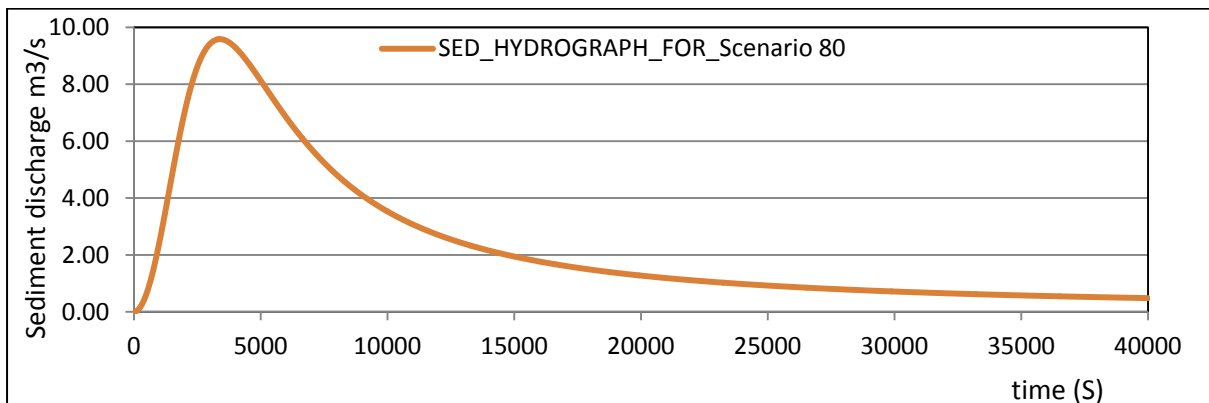


Fig. 6. 39: The produced sediment hydrograph for scenario 80 according Macchione breaching model 2008.

As shown in Fig 6.39, it seems that the dam-break scenario is not going to be critical in terms of sediments. Let us compare fig. 5.7 (that represent the sediment yield for 1987 flood) and 6.39 (that is the sediment produced from the dam-break). In the first one there is a sediment yield with base time of roughly 50,000 s (just the big triangle) and peak of $20 \text{ m}^3/\text{s}$; in the second one, values are 15,000 s and $10 \text{ m}^3/\text{s}$. Therefore the sediment supply in the dam-break case is much lower than that for the flood case and the risk for the town would be related to just water, possibly increased by the redistribution of sediments along the reach if time is enough.

▪ Sensitivity to dam height

Increasing the dam height increases the storage volume and the peak discharge for the hydrograph that is produced by the breaching calculations. The following figure shows multiple hydrograph with various dam heights scenarios (scenario 50, 80, 100, and 150) with crest width $w = 0$.

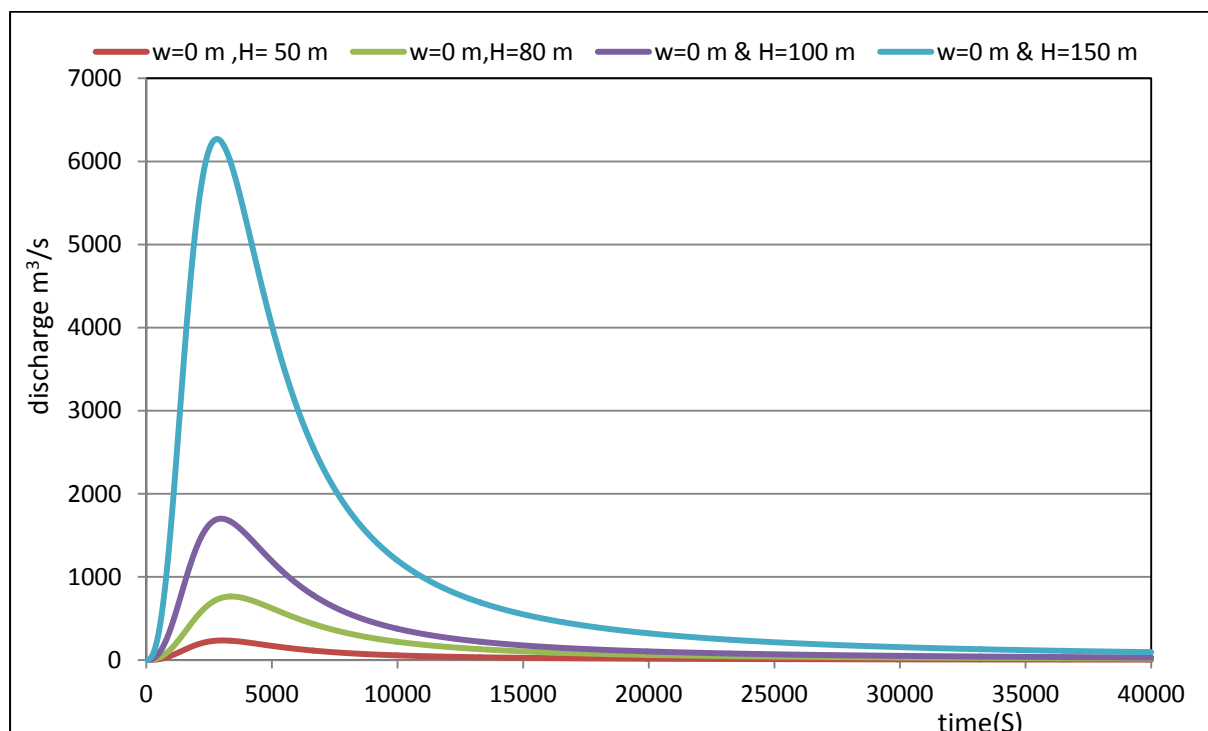


Fig. 6. 40: Macchione model sensitivity to dam height (water hydrograph).

It is clear from the figure that, duplicating the dam height will duplicate the discharge around 10 times. The peak value takes place in approximately the same time, so the peak time will not be affected by the dam height. Regarding the sediment discharges, the effect of the dam height on the produced sediment is shown in (Fig 6.41) that showed that the sediment hydrographs have the same peak time which increases with the dam height. With higher discharges a huge amount of sediment erodes and transports toward the dam toe, then it transport with water to the down town which will be discussed later. The following figure shows that sediment discharge produced due to the dam erosion is around 1% of the water discharge.

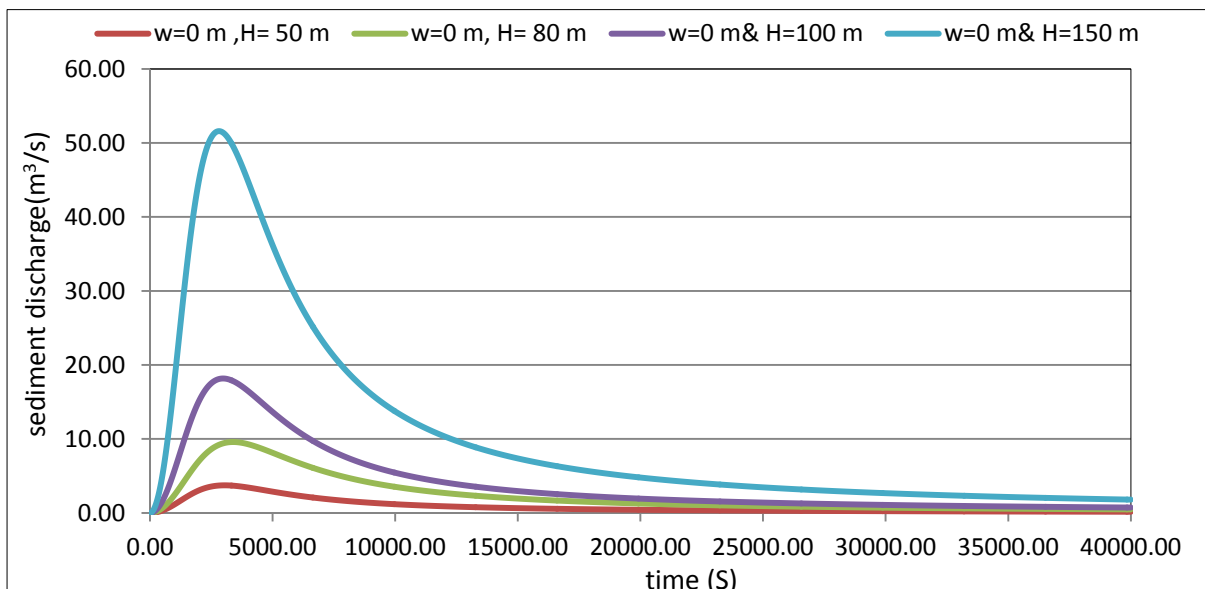


Fig. 6. 41: Macchione model sensitivity to dam height (sediment hydrograph).

■ Sensitivity to crest width

The crest width has a great effect on the water and the sediment discharges. When the crest width increases, the breach length increases which reduces the peak discharge while the base time increases. The following figures show that the peak time for both water and sediment are delayed, also with wider crest width.

Comparative study of different scenarios for the morphological evolution in a river stream

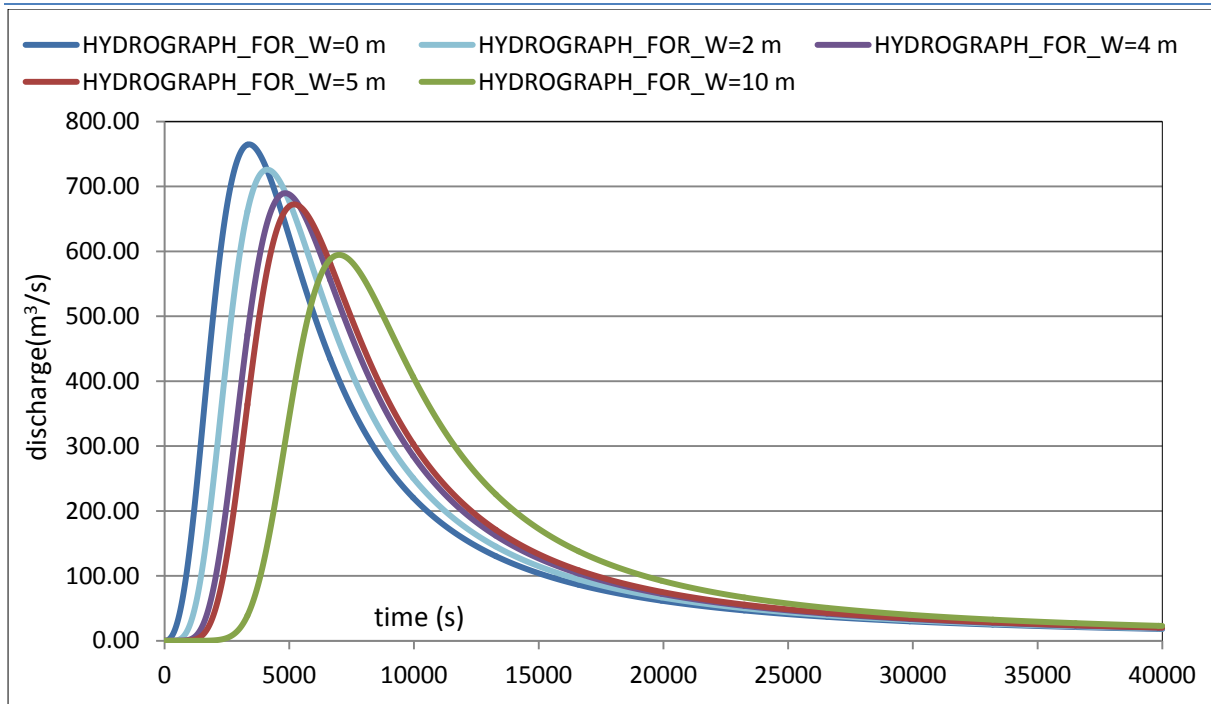


Fig. 6. 42: Macchione model sensitivity to crest width (water hydrograph for scenario 80).

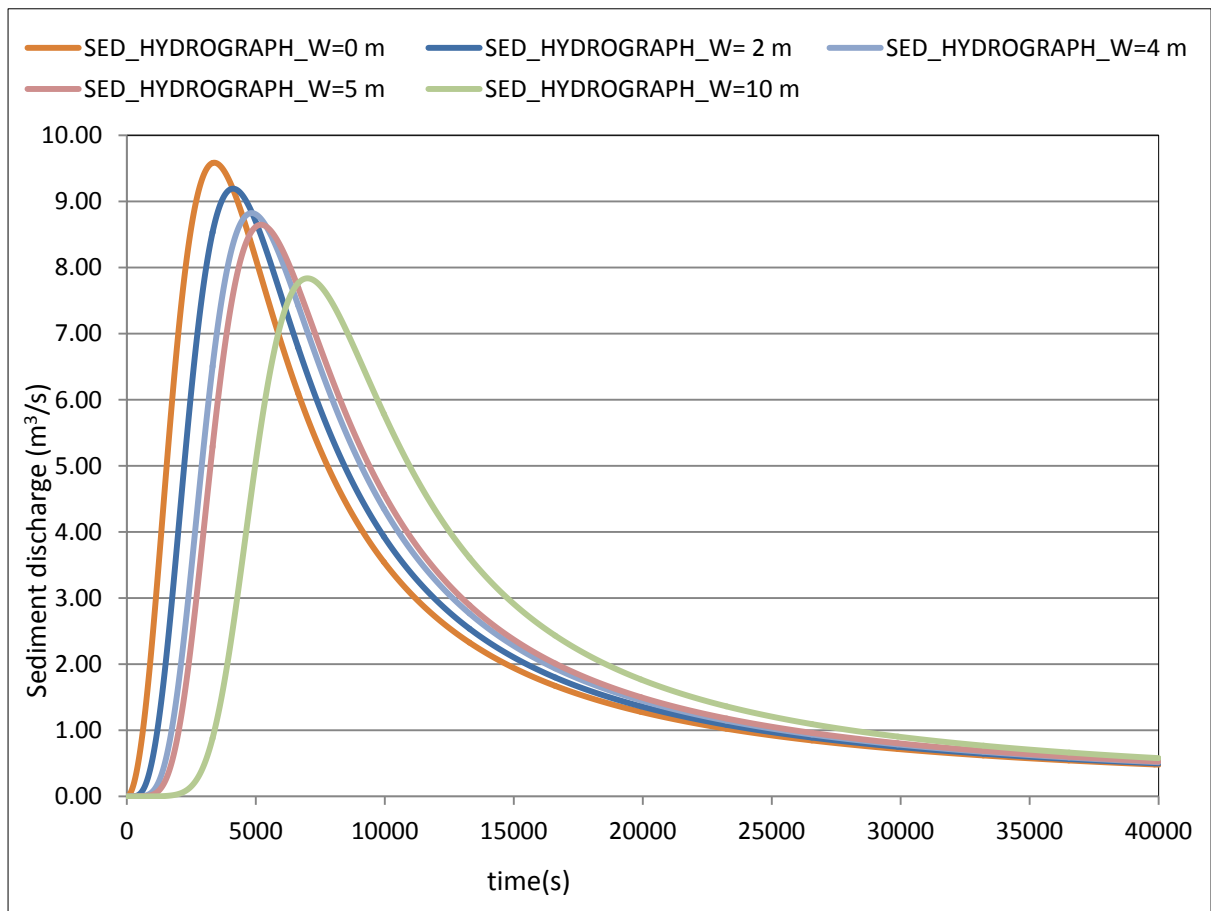


Fig. 6. 43: Macchione model sensitivity to crest width (sediment hydrograph for scenario 80)

■ Sensitivity to dam’s side slopes

As shown in table 6.1, the scenarios assumed based on assuming dam height and with considering the principle of mass balance the slopes are calculated. In reality forecasting the dam shape is really uncertain, hence the side slopes of the dam in addition to affecting the lake formation model it also affect the breaching wave. Reducing the side slope (HZ/VL), decreasing the breaching length and increasing the peak discharge. By the time the bed of the breach lowers and the differences in breach length become negligible, so the discharge becomes the same as in figure 6.44.

Regarding the sediment discharge, it depends on the discharge so its peak increases with the water peak as in figure 6.45.

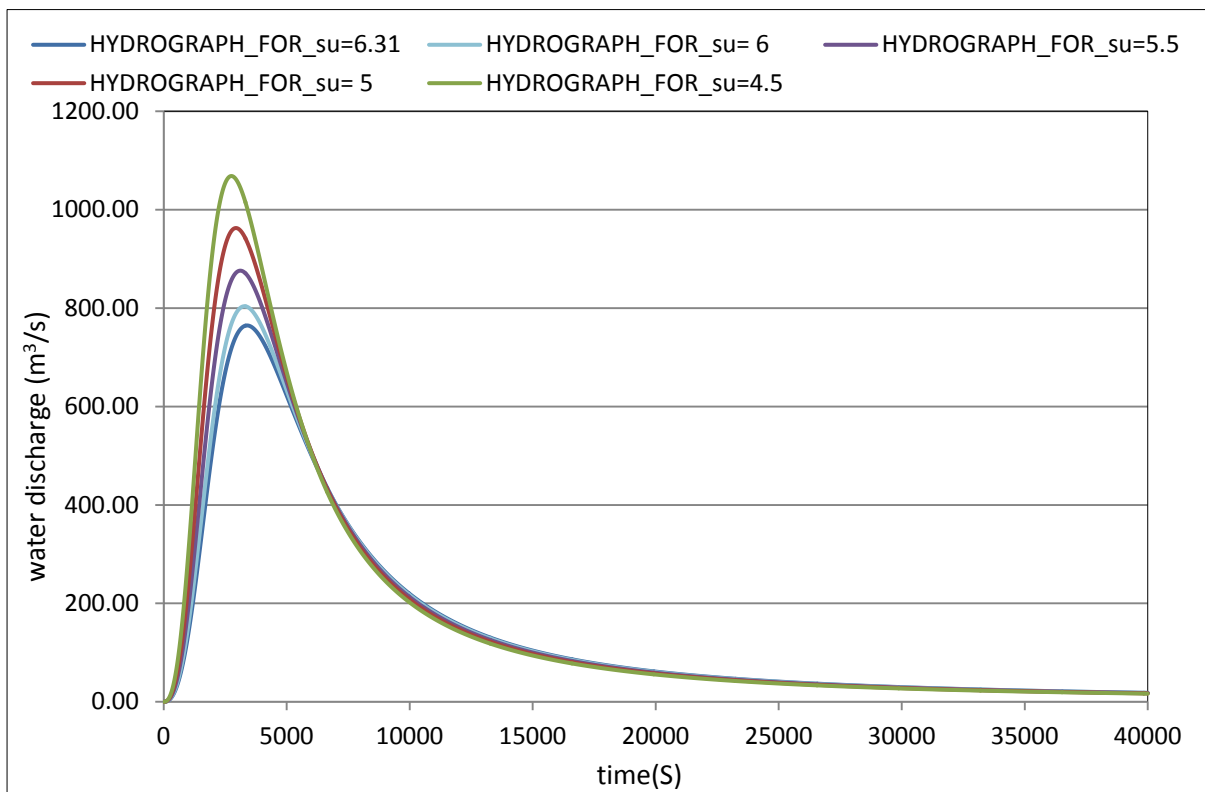


Fig. 6. 44:Macchione model sensitivity to dam slopes (water hydrograph for scenario 80 with different slopes).

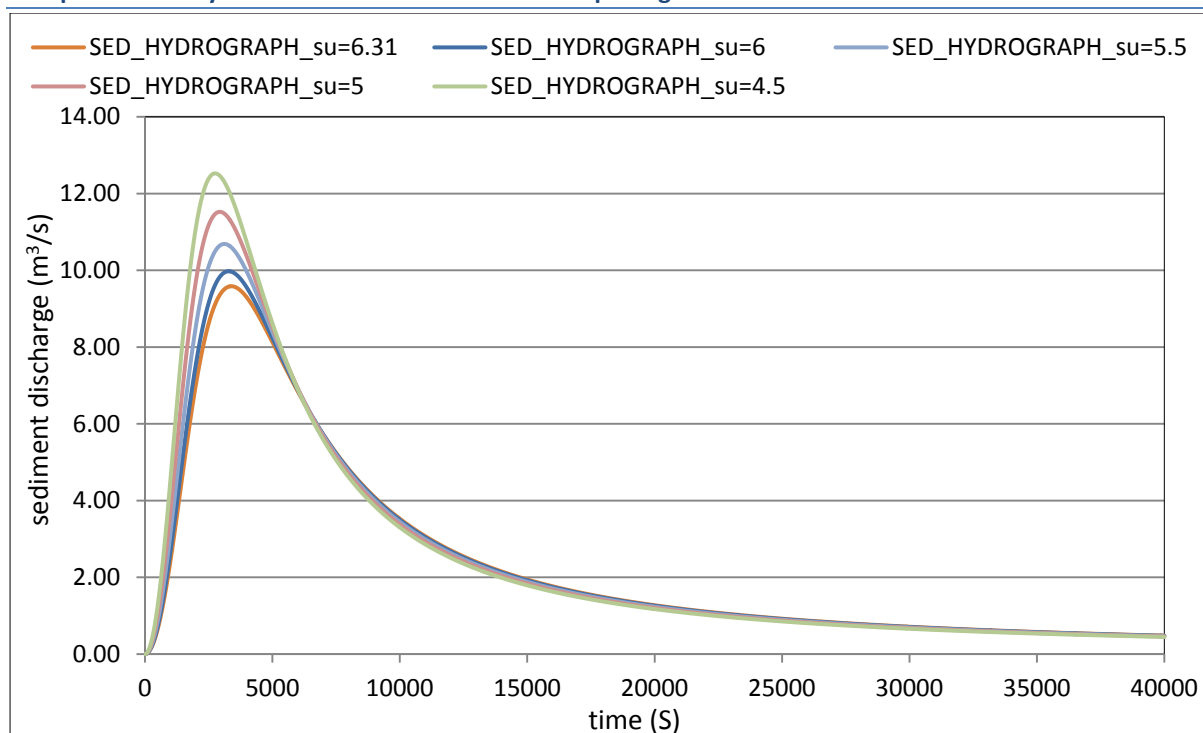


Fig. 6. 45: Macchione model sensitivity to dam slopes (sediment hydrograph for scenario 80 with different slopes).

Finally, the results of the scenario 80 that showed in fig 6.38 and 6.39 for the water and the sediment wave respectively will be used as an upstream boundary for the morphological evolution (that is the last sub-model of this integrated model).

➤ Breaching model by Weiming Wu

(Weiming, 2013) proposed a simplified physically based breach model. It is a comprehensive model which is able to simulate the breaching processes of noncohesive and cohesive, homogeneous and composite embankments owing to overtopping and piping.

▪ The model assumptions

The breach caused by overtopping flow is approximated as a flat broad-crested weir with a trapezoidal cross section (fig 6.46), downstream connected with a vertical drop (headcut) and a straight slope for cohesive and

noncohesive homogeneous embankments, respectively. Sediment transport and morphology changes on the breach top flat section and downstream slopes are calculated using a non-equilibrium total load sediment transport model, whereas the time-averaged headcut migration rate is determined using an empirical formula.

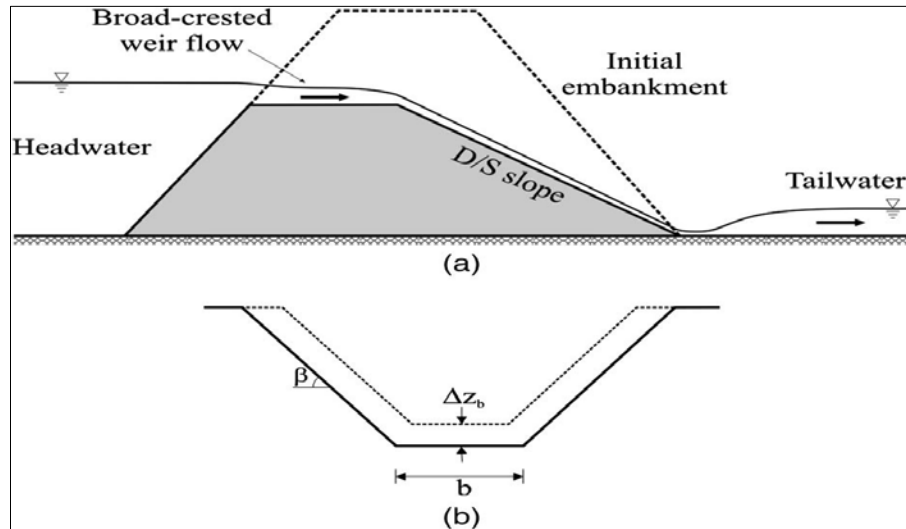


Fig. 6. 46: Noncohesive embankment breach by overtopping: (a) longitudinal;(b) cross section.

■ Model description

The water volume in the reservoir changes because of inflows from the upstream basin and outflows from the breach according the formula:

$$\frac{dV}{dt} = S \cdot \frac{dz}{dt} = Q_{in} - Q \quad 6.25$$

Where, t = time; V = volume of water in the reservoir; S = surface area of reservoir; z = water surface elevation; Q_{in} = inflow discharge; Q = breach flow. The overtopping flow at the breach is estimated using the broad crested weir equation:

$$Q = k_{sm}(c_1 b h^{1.5} + c_1 m h^{2.5}) \quad 6.26$$

Where, b = bottom width of the breach; $h = Z - Z_b$; Z_b = elevation of breach bottom; m = side slope (horizontal/vertical) of the breach; $c_1 = 1.7$; $c_2 = 1.3$; and k_{sm} = submergence correction for tailwater effects on weir outflow. K_{sm} is determined by an empirical relationship. Because the breach flat top section is treated as a broad-crested weir, critical flow is used to represent the flow condition responsible for breach erosion on the flat top section. A uniform flow is assumed on the downstream slope section. Therefore, the bed shear stresses on these two sections are determined from the estimated flow depths and discharge by using the Manning equation:

$$\tau_b = \frac{\rho g n^2 Q^2}{A^2 R^{\frac{1}{3}}} \quad 6.27$$

Where, τ_b = bed shear stress; ρ = water density; A = flow area; R =hydraulic radius; g = gravitational acceleration; and n = Manning roughness coefficient. The Manning's n is related to sediment median size d_{50} (in meter) by:

$$n = \frac{d_{50}^{\frac{1}{6}}}{A_n} \quad 6.28$$

Where, A_n is an empirical coefficient. A_n is approximately 20 on fixed streambeds and may reduce to approximately 10 resulting from bed forms on movable streambeds. The surface area is thus assumed to be a power function of water depth.

$$S = \alpha_r h^{m_r} \quad 6.29$$

Where, α_r and m_r are coefficients. Integration of Eq. (6.28) from the bottom to the water depth h leads to the volume and depth relationship

$$V = \int_{hi}^h S dh = \frac{\alpha_r}{m_r + 1} h^{m_r+1} \quad 6.30$$

If both the reservoir storage, V_R , and surface area, S_R , at the normal pool level (or the water level before the failure), $h_R = Z_R - h_b$, are known, one can derive the following relationship of exponent m_r by substituting these two conditions into Eqs. (6.29) and (6.30) as follows:

$$m_r = \frac{S_R h_R}{V_R} - 1 \quad 6.31$$

The exponent m_r has values between 1.0 –3.0 and an average value of 2.0. This implies that if only the reservoir storage or surface area is known, m_r can be assumed to be 2. Once the coefficient m_r is determined or assumed, the coefficient α_r can be derived by using Eq. (6.28) or (6.29).

The noncohesive sediment transport along the breach top flat section and the downstream slope can be described with the following total-load non-equilibrium transport equation

$$(1 - p') \left(\frac{dV_b}{dt} \right) = Q(C_{t_{in}} - C_{t_{out}}) \quad 6.32$$

C_t = Actual total-load sediment concentration; p' = porosity of dam materials. In the case of cohesive sediment, the bed erosion rate, $\frac{d\varepsilon}{dt}$, is determined using the following formula

$$\frac{d\varepsilon}{dt} = k_d(\tau_b - \tau_c) \quad 6.33$$

Where τ_c = critical shear stress determined using the Shields diagram; and k_d = erosion coefficient in m/h Pa, related to soil properties as follows:

$$k_d = \frac{0.063\gamma}{\gamma_d} \exp\left(-0.121c_{\%}^{0.406} \left(\frac{\gamma_d}{\gamma}\right)^{3.1}\right) \quad 6.34$$

Where $c_{\%}$ = ratio (fraction) of clay in the soil; γ = specific weight of water; and γ_d = dry specific weight of the soil. Eqs (6.32) and (6.33) give the volumetric bed change, ΔV_b , for each time step, Δt . This volume is converted to the bed elevation change, z_b , and width change, Δb , as shown in Fig. 6.46. Δz_b and Δb are assumed to have the following relationship:

$$\Delta b = n_{loc} \cdot \frac{\Delta z_b}{\sin\beta} \quad 6.35$$

Where β =breach side slope angle with respect to the horizontal; n_{loc} = indicator of breach location ($n_{loc} = 1$ for one-sided breach and 2 for breach located at the middle of embankment length). The one-sided breach means that one side of the breach is not erodible, and the breach can extend only on the other side.

The breach side slope depends on the soil properties, breach bank height, water table, and so on. Fig. 6.47 shows the force diagram of a side slope with angle β , the steepest stable slope angle, denoted as β_s . H = slope height; W = weight of the failure block; γ_s = bulk specific weight; φ = friction angle; and C = cohesion of the soil.

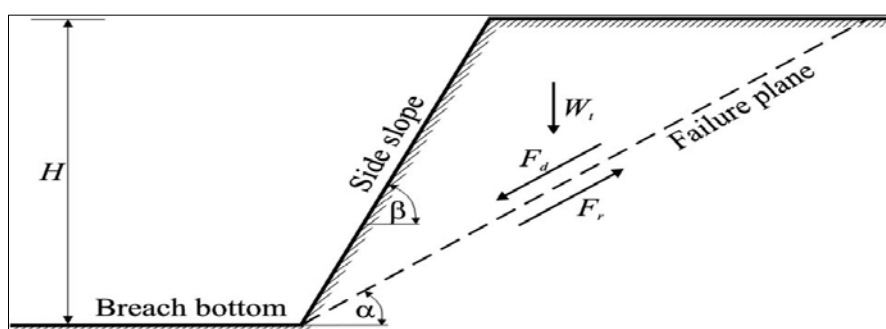


Fig. 6. 47: Breach side slope stability analysis.

By Studying the equilibrium of the breach slopes considering planar failure mechanism for a noncohesive soil, $C = 0$, get $\beta_s = \alpha_s = \phi$, while for cohesive soil with any value of α the following condition uses to calculate the value of β .

$$\frac{1}{\tan\beta_s} = \frac{1}{\tan\phi} + \frac{1}{\tan\phi^2} \left[\frac{4C}{\gamma_s H} - \sqrt{\left(\frac{16C^2}{\gamma_s^2 H^2} + \frac{8C}{\gamma_s H} \tan\phi \right) (1 + \tan\phi^2)} \right] \quad 6.36$$

An embankment breaching usually starts from a side slope less than β_s . As the breach erodes vertically on the bottom and laterally at the side slope toes, the side slopes become steeper until the angle β_s is reached and a failure occurs. The new slope will have the angle of α_s . The breach will repeat this deepening, widening, and failure process. Therefore, the breach side slope is between the steepest stable angle, β_s , and its corresponding failure angle, α_s . The present model assumes the breach side slope, β , as the average of β_s and α_s

$$\beta = \frac{\beta_s + \alpha_s}{2} \quad 6.37$$

The preceding model suggests that for noncohesive soils, β is close to the repose angle; and for cohesive soils, β tends to be steeper.

6.2.5 Dam breaching effect on Mallero morphology

The last step from the integrated scenario corresponding to the landslide in sprains, after studying the dam breaching cause and the generated water and sediment hydrographs, is the morphological evolution of Mallero bed using those hydrographs as upstream boundary conditions. The aim is estimating the bed differences either as erosion or deposition in Sondrio due to the dam breaching wave.

For this purpose a numerical model by Basement software, uses the same cross section described in item 5.2, is used to model this morphological evolution. the only difference in this new model that it starts from cross section CS15 (the cross section in Spriana front) instead of CS1 i.e. this new model is shorter than 1987 model by 2 km which is the distance from section CS1 at Torre S. Maria to CS15 at Spriana. The zones where is the check dams (Fig 5.5) considered as fixed cross sections i.e. deposition in this section is allowed while the erosion from it is not allowed.

The granulometry of the cross sections' beds are the same described in item 5.3 and table 5.1, so different scenarios for bed granulometry are considered also in this model. The composition of the sediment feeding for each scenario is described also in table 5.1.

Regarding the downstream boundary conditions, it is the same used for describing the boundaries of 1987 model in item 5.4 with using the same 2km dummy stretch. The hydrograph (figure 6.38), produced by (Macchione, 2008) breaching model for scenario 80, is used as upstream water boundary condition. The sediment hydrograph produced by the same model (figure 6.39) is used as sediment upstream boundary condition. Owing to the dam formation, the Mallero valley is assumed to be

totally dry during the filling time of the lake, but due to the seepage process the valley downstream Spriana will not be dry, but the flow will depend on the permeability of the dam material. Since the permeability value is uncertain, hence $0.5\text{m}^3/\text{s}$ is assumed as initial condition for the flow in all the cross sections.

The dam height scenario considered here is 80 m because of its likelihood. The simulation time used is 60 hour (216000 sec) which is the same for 1987 event that allow making comparison between changes in bed levels due to the two events with the same time.

The model ran using the previous geometry and flow initial and boundary conditions. To check the water wave propagation in Mallerio, the water wave at upstream, entrance of Sondrio, and confluence point are drawn in figure 6.48. As shown in the figure; the wave from Spriana to the entrance of Sondrio behave kinematically (i.e. no diffusion) because of the steepness of bed profile (that reach to 8% in average), after that within downtown, there is decreasing in the peak flow because of the mild slope but not much since the wave is very fast. The figure shows that the wave will take only 10 minutes from Spriana to the confluence point with Adda i.e. the wave average velocity is 11.67 m/s or 42 km/h so it can cause many damages. According to this scenario (scenario 80), the water discharge is more than Mallerio capacity ($690\text{ m}^3/\text{s}$) which means that around 60000 m^3 of water will inundate Sondrio according this scenario. The lesson learnt that with more dam height the inundation will be more e.g. with scenario 100, the inundation volume is $2.5 * 10^6\text{ m}^3$ and with scenario 150 m is $30 * 10^6\text{ m}^3$ (this volumes for scenario 100 and 150 are calculated from figure 6.40 that shows the sensitivity of the dam-break discharge to the dam height).

Comparative study of different scenarios for the morphological evolution in a river stream

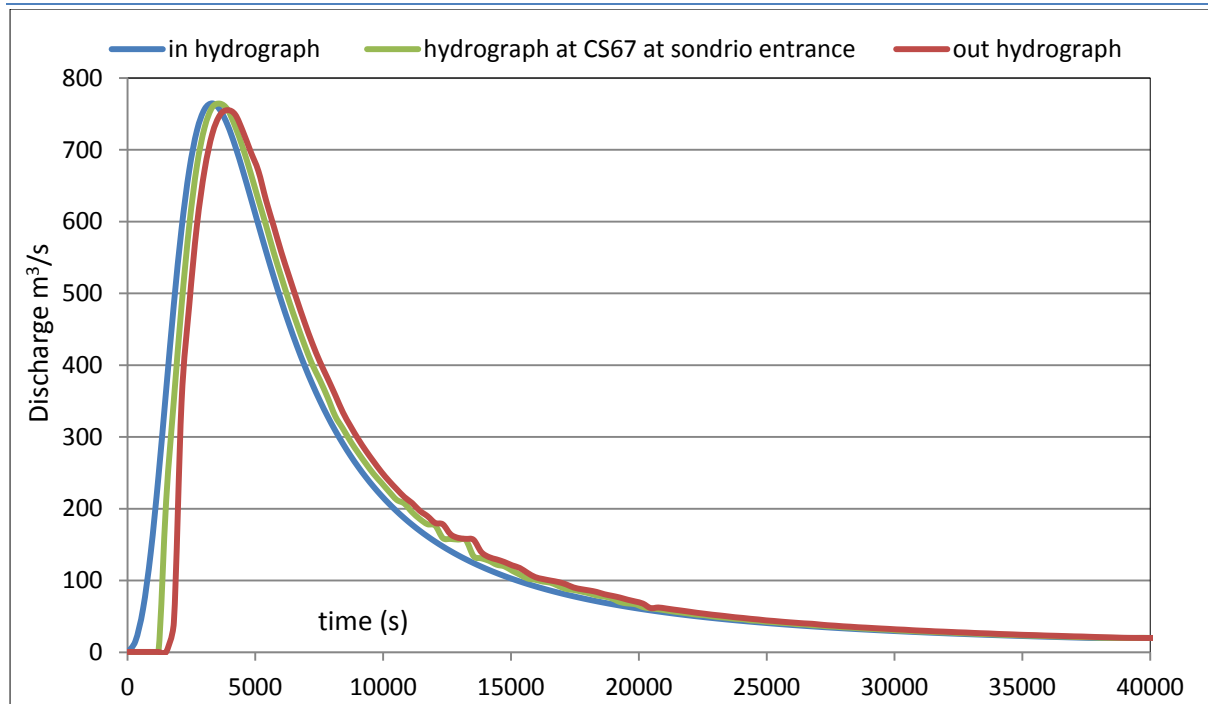


Fig. 6. 48: In, mid and out-flow hydrographs for scenario 80.

The water depths also is calculated in some sections as in figure 6.49 that shows that the water depth at Sondrio increases because of the mild slope of Mallero in the downtown. It reaches its maximum before the confluence with Adda River, but in the middle there are some high water depths in some sections because of its narrow bed width.

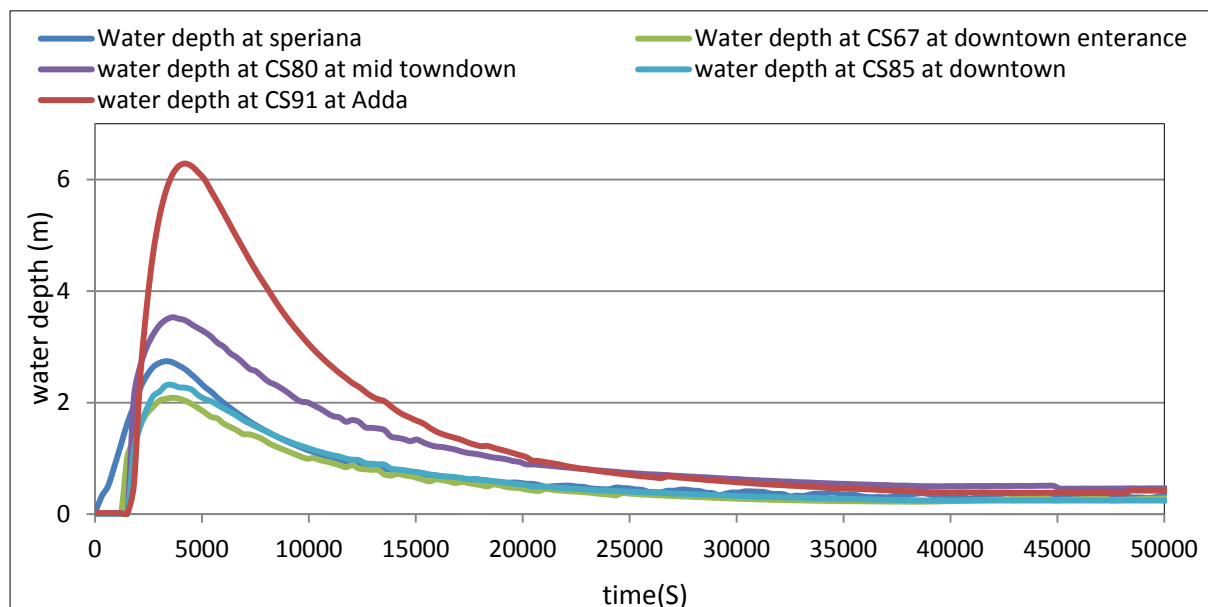


Fig. 6. 49: Water depths in some section due to scenario 80.

It is important to refer to some existing bridges (figure 4.7) that are not included in the model, because of the incapability of Basement to model it. In reality this bridges will affect the water depth and mainly the flood will start at the bridges especially the upstream one, because the river cross-sections decreases at bridges that lead to high water depth hence inundation.

Although the sediment inflow is continuously fed due to dam breaching, this fed deposits behind the dam and only the transport will be according the capacity. Figure 6.50 shows the sediment discharge at Spriana, Sondrio entrance and confluence with Adda respectively. The sediment wave peak decreases because of sediment deposition i.e. at Mallero exit the sediment discharge will become very less than the inflow as shown in the figure. This decreasing in sediment peak leads to noting that sediment wave vanishing due to deposition.

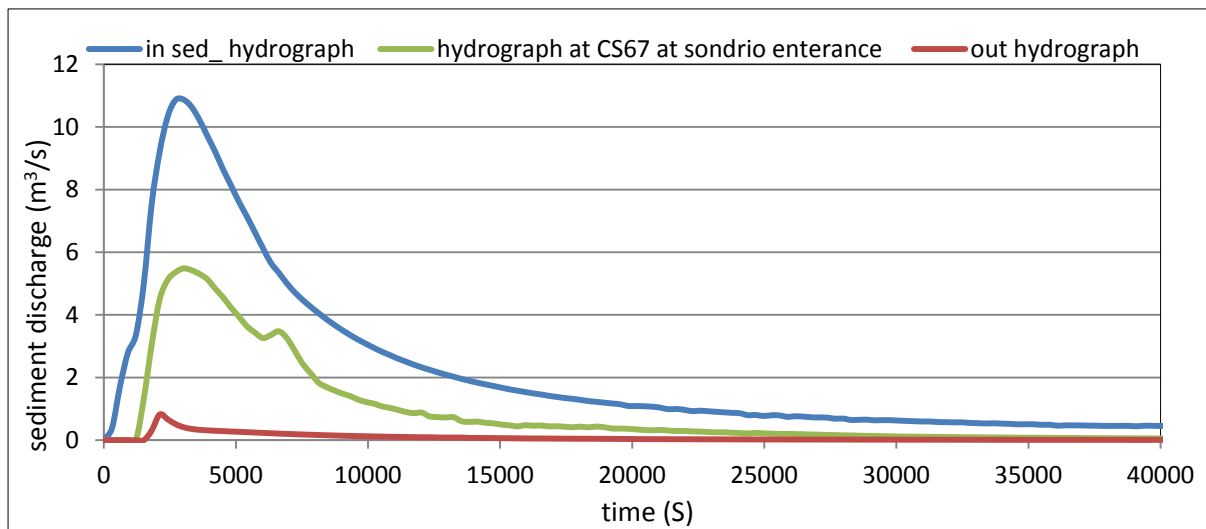


Fig. 6. 50: In, mid and out-flow of sediment hydrographs for scenario 80.

To know the zones of degradation and aggradation, the bed levels are drawn before and after the event in figure 6.51 for 3 models uses 3,4, and 10 diameters respectively, while the diameters used to describe the bed and feeding granulometry are the same described for 1987 event as in table

5.1. As shown, the differences are not clear among the models, so in figure 6.51, the differences only are drawn to be clearer. In addition, the results for 1987 event with 3 diameters included in the figure to compare the morphological evolution of 1987 event with that for the dam breach scenario.

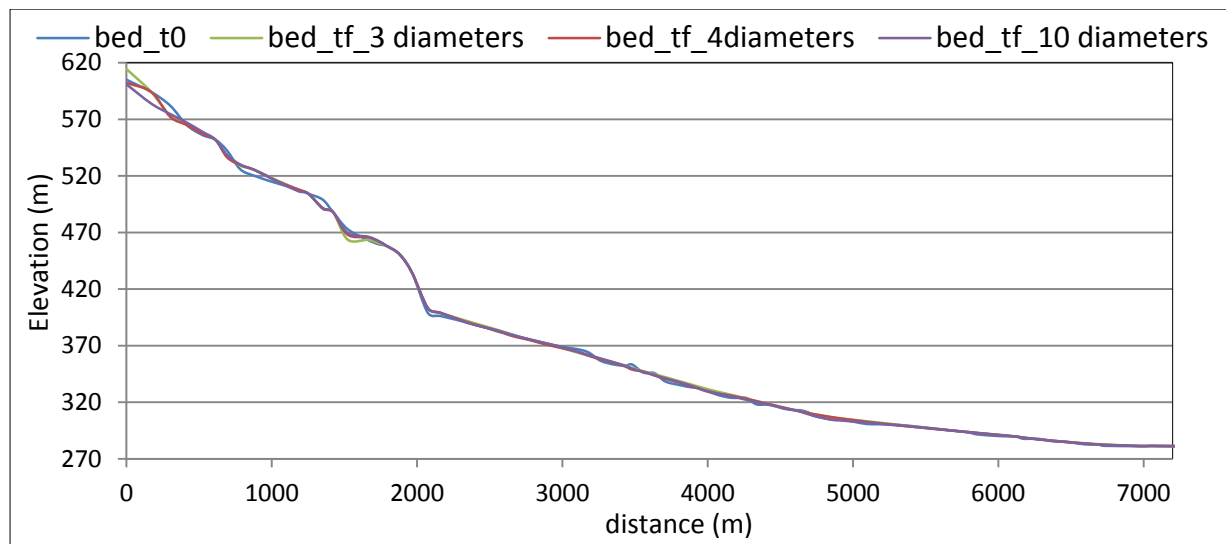


Fig. 6. 51: Bed level before and after the wave for 3,4,and 10 diameters model (tf=216000 s)

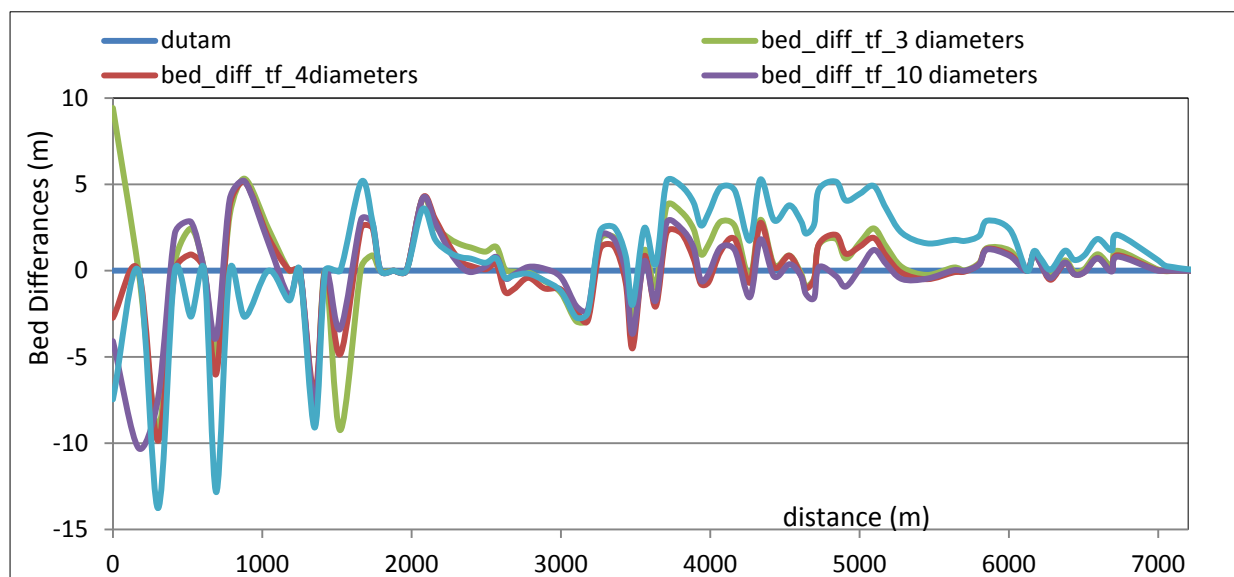


Fig. 6. 52: Bed differences before and after the wave for 3,4,and 10 diameters models and its comparison with 1987 results (3 diameters).

Figure 6.52 show that 3 diameter model gives aggregation at upstream while the other two models give degradation, although of the sediment

feeding from the dam. In Sondrio the behaviour of the three models is similar i.e. the aggradation is the dominant in Sondrio. By comparing the sediment deposition in Sondrio due to 1987 event with scenario 80, it is around twice the deposition due to scenario 80 although the peak discharge is lesser with the same simulation time, but still the sediment deposition must be removed to restore the Mallero capacity. The flood scenario mobilizes more sediment due to relatively high discharges for long time and is able to redistribute the sediments along the reach; the dam-break scenario has huge discharge for very short time, resulting in smaller morphologic evolution, but the very high discharge is however going to imply larger elevation of water and thus inundation of the town. In the end, the even time issue would result to be crucial for the redistribution of sediments

The evolution of bed using model with 3 grain sizes to represent the bed granulometry and the feeding is shown in figure 6.53. At the beginning erosion will occur at upstream then after the peak the aggradation will increase in upstream till reaching 10 m depth, while in downtown the aggradation depths increase with time.

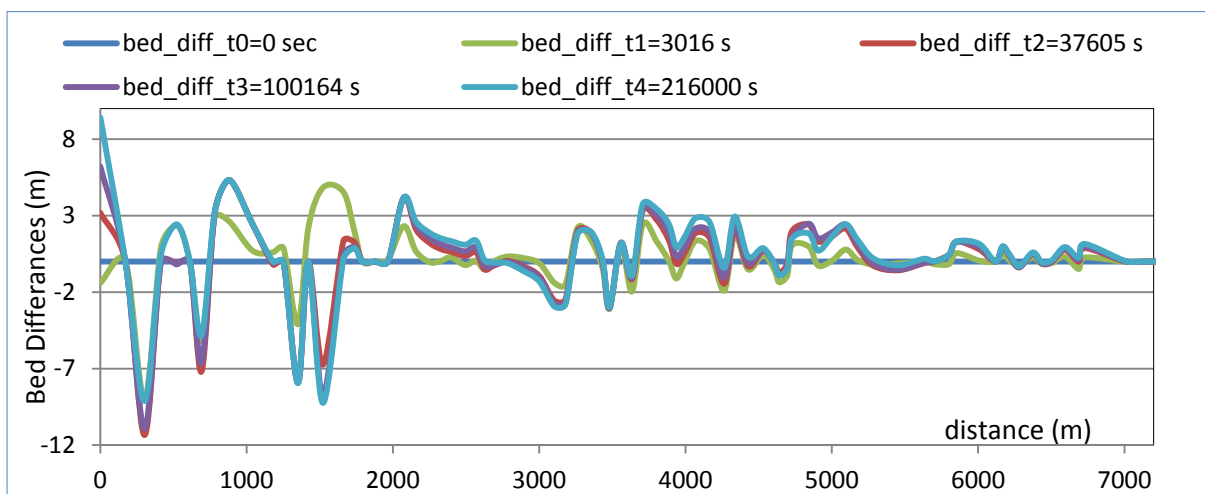


Fig. 6. 53: Bed evolution for scenario 80 using model with 3 grain sizes.

As known, this model composed of 3 grain sizes (table 5.1), so the distribution of the granulometry changes with sorting e.g. the migration of each diameter from the 3 diameters is drawn in the following 3 diagrams.

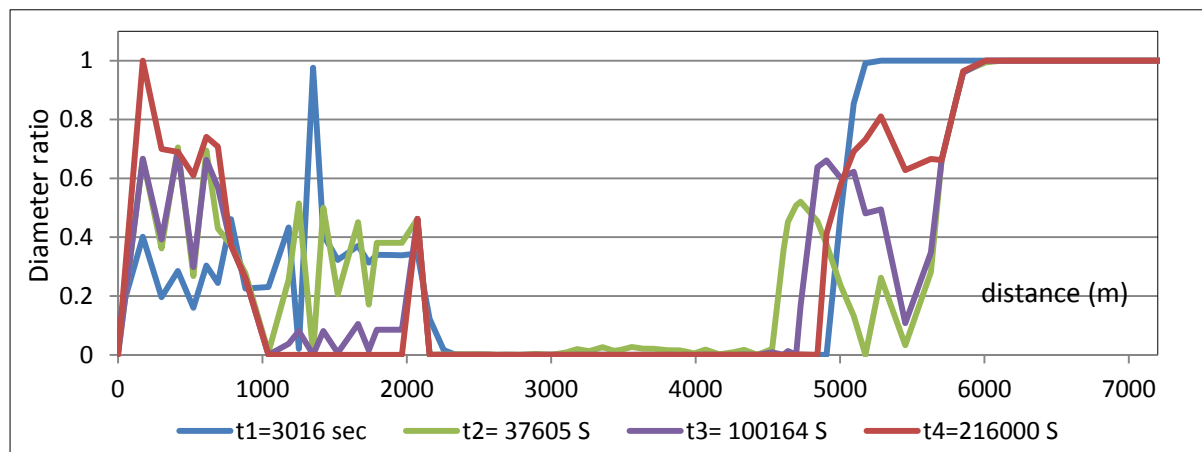


Fig. 6. 54: The migration of the 10 mm diameter after the dam break (3 diameters model).

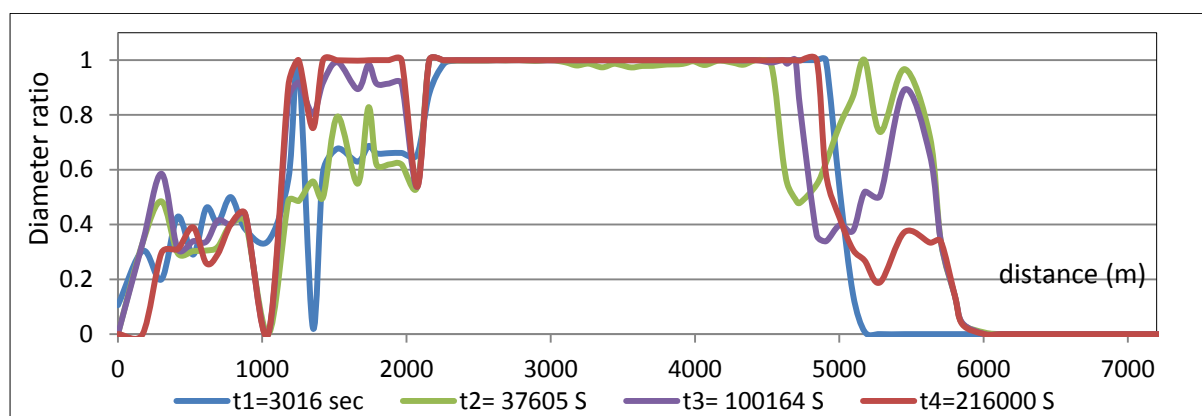


Fig. 6. 55: The migration of the 80 mm diameter after the dam break (3 diameters model).

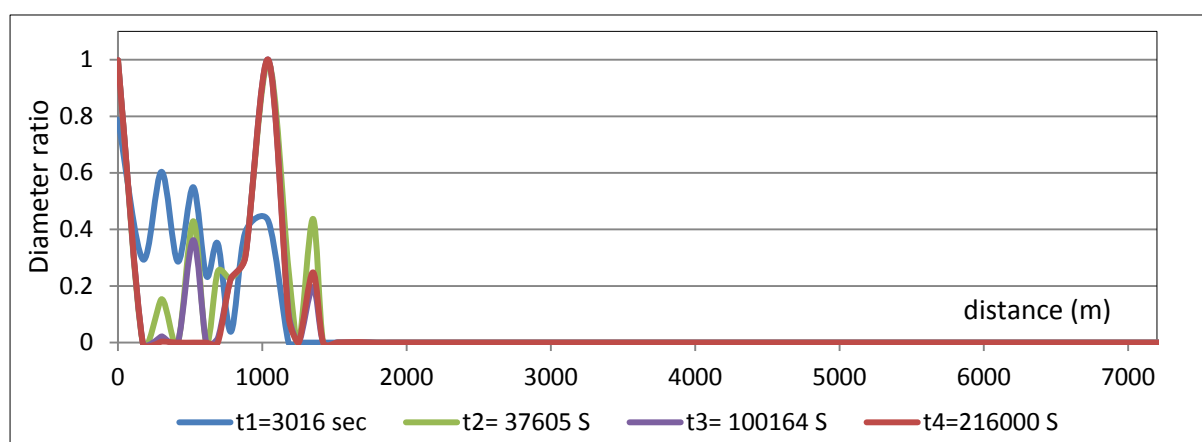


Fig. 6. 56: The migration of the 800 mm diameter after the dam break (3 diameters model).

As shown in figure 6.54; the first 2 km become richer by 10 mm diameter , although this part didn't include this diameter in its bed according table 5.1. Also it became richer by 800mm diameter (figure 6.56). This means that sediment produced by dam breaching will influence only the first 2 km and the smallest diameter distributes in longer distance. The increase in 10 mm and 800 mm ratios with time will reduce 80 mm diameter ratio in the same time.

The question now is: if the dam breaching influence only 2 km, from where the sediment deposited in Sondrio as in figure 6.53? The sedimentation source is the erosion of the bed after the zone of breaching influence till reaching Sondrio. No sediment will arrive from Spriana to Sondrio in this 60 hour event, but it can arrive in future with next floods because the ordinary flow can't urge the deposited sediment behind the dam after breaching to move because the transport capacity is negligible.

Indeed the check dams, built in the Mallerio valley, are very important since it reduce the bed erosion with this type of flood events which, of course, reduces the deposition in Sondrio, so these dams play an important role as structural mitigation measure for flood risk i.e. without this check-dams the bed erosion increases as a sediment source, hence the deposition in the in-town increasing and decreases river capacity.

The previous three figures shows that at 5 km, in which the entrance of Sondrio, 80 mm diameter starts to mix with diameter 10 mm which represent the bed granulometry in Sondrio. So, for around 1 km (5 km to 6 km), the ratio of 10 mm diameter reduces with time while 80 mm diameter ratio increases. This means that this flood wave is able to move 80 mm diameter for around 1km at Sondrio entrance also it able to move 800 mm (0.8m) diameter for 1.5 km behind the dam, which give indication that the

slope has a role in sediment transport. Although 800mm diameter is heavier it moves more than 80 mm diameter because of the bed slope (8% after Spriana and 1% in-town). The movement of boulders that have 800mm diameter gives an indication to how much this wave is risky.

The same behaviour is noted also with model uses 4 diameter to represent the bed granulometry and sediment feeding from the dam breaching. Figure 6.57 shows the bed differences in case of using 4 diameters, while the next 4 figures give the diameters ratios and its evolution with time taking into account that the initial composition of the bed by this diameters is shown in table 5.1.

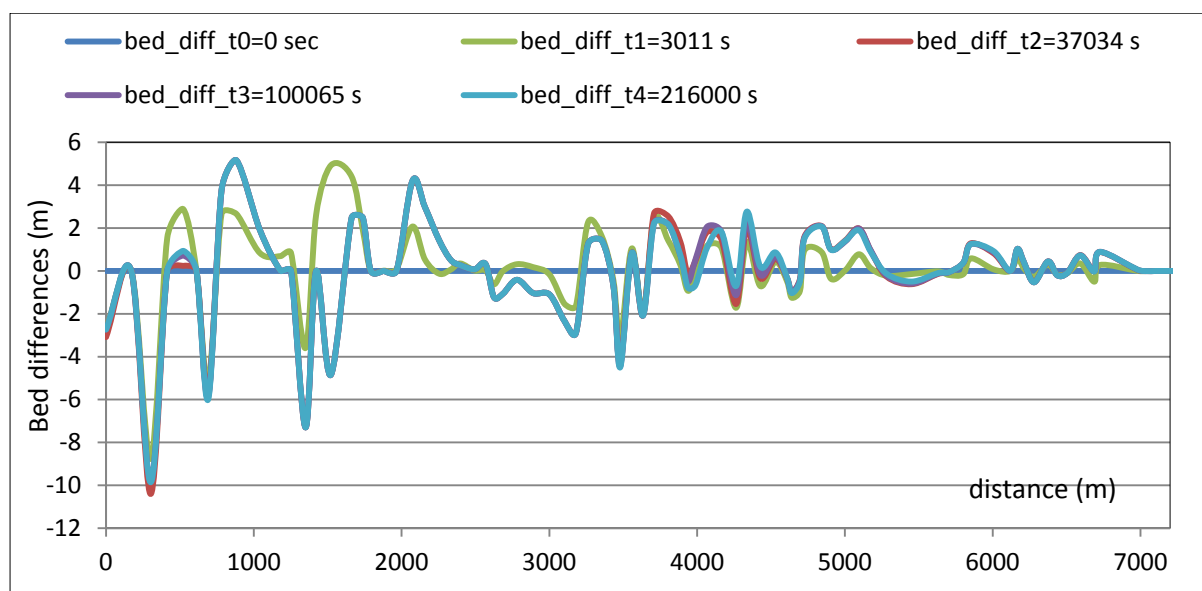


Fig. 6. 57: Bed evolution for scenario 80 using model with 4 grain sizes.

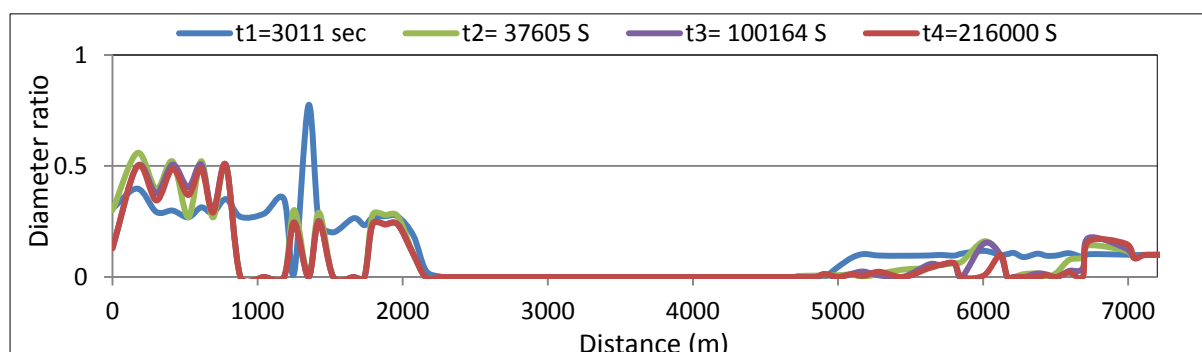


Fig. 6. 58: The migration of the 10 mm diameter after the dam breach (4 diameters model).

The case of Mallero: Integrated scenario for Spriana landslide

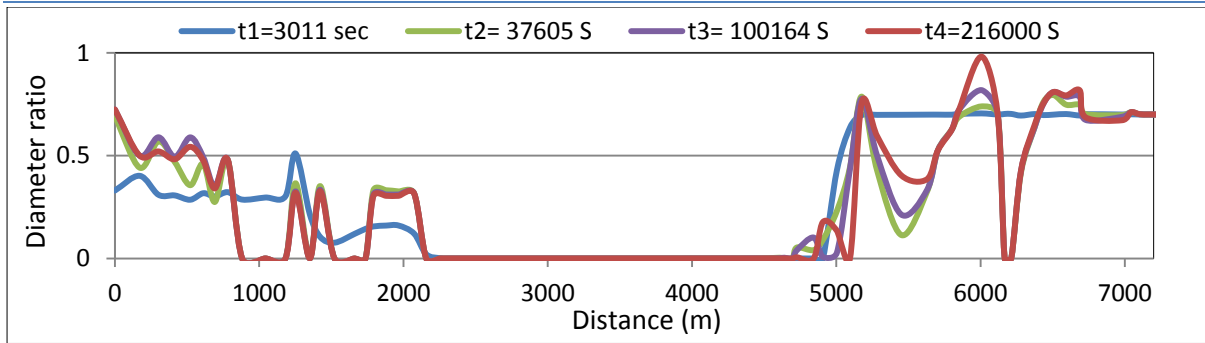


Fig. 6. 59: The migration of the 50 mm diameter after the dam breach (4 diameters model).

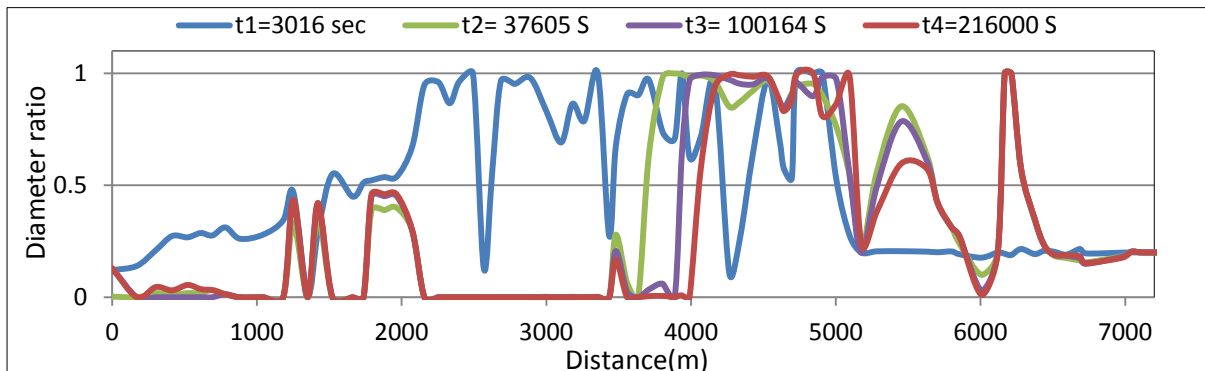


Fig. 6. 60: The migration of the 80 mm diameter after the dam breach (4 diameters model).

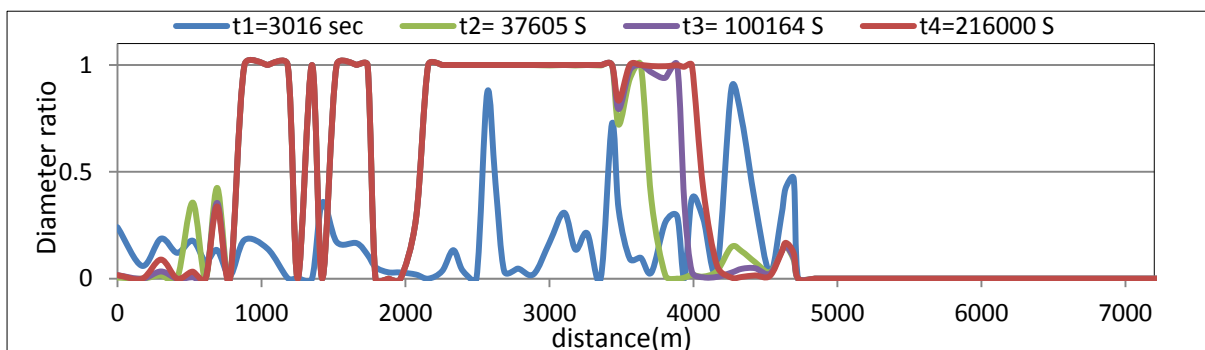


Fig. 6. 61: the propagation of the 800 mm diameter after the dam breach (4 diameters model).

Figure 6.57 shows degradation at upstream although the sediment feeding from breaching. After that; the behaviour, more or less, is the same like model with 3 diameters. The figures (6.58 to 6.61) show that the influence of dam breaching appears only in the first two kilometers which represented by the increasing of 10 mm and 50 mm diameters given by figure 6.58 and 6.59 respectively.

The behaviour in model with 10 diameters is more or less similar to 4 diameters model; the following figure shows the bed evolution in this model.

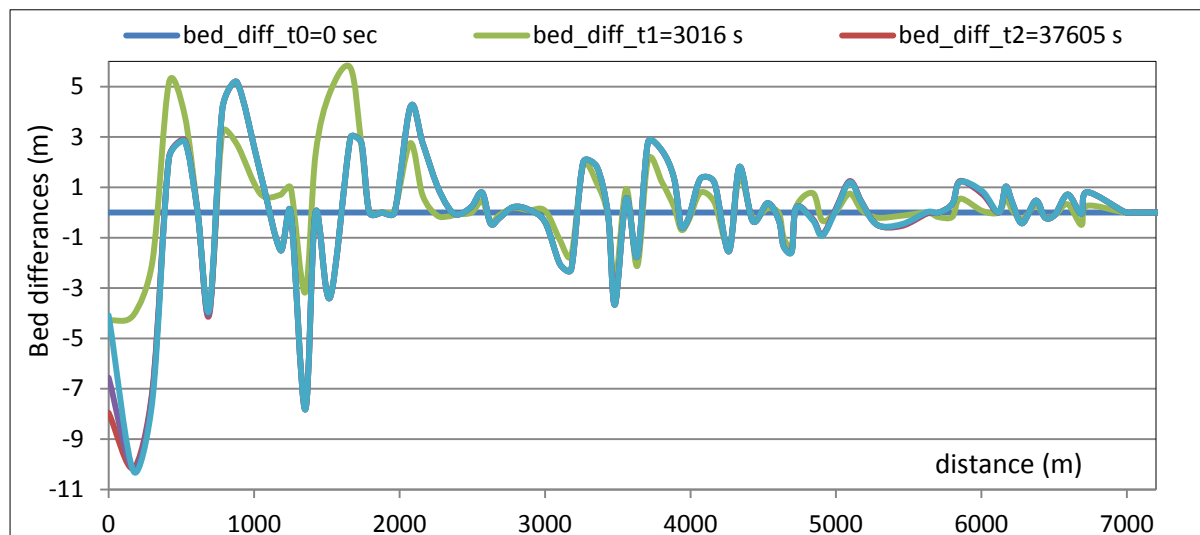


Fig. 6. 62: Bed evolution for scenario 80 using model with 10 grain sizes.

Finally, the dam breaching, from hydraulic point of view, produce catastrophic wave with high velocity which erode the bed and produces huge amount of sediment that deposits in Sondrio and reduces Mallero capacity, but still this reduction of capacity is around half the reduction caused by 1987 event. This means that the capacity will be around 375 m³/s after the dam break. From morphological point of view, the sediment created from breaching will influence from 2 to 2.5 km depend on the composition of the dam material.

6.3 Influence of Morphological evolution on flood risk and emergency cost

For mountain floods (also called flash floods) ,like Sondrio case, usually the slope is very steep, which lead to very fast wave. This wave causes huge damage in case of flooding. Usually, a deterministic scenario, like 1987 flood or the induced flood for the landslide in Spriana, uses to calculate the risk index which is a function of the flood hazard and its consequences. The

flood hazard usually estimated depending on the inundation depth, the water velocity or both. The hazard consequences depend on how many zones and people exposed, also it depends on the vulnerability of the structures, the human and the lifelines e.g. for 1987 event the risk index at any zone outside Mallero valley is zero because the discharge was within the river capacity i.e. no exposure.

As discussed, there are some bridges built in the Mallero valley, the location of these bridges are shown in Fig 4.13 while the water depth at one of these bridges in 1987 event is shown in Fig 6.63 taken from (Molinari, 2011).



Fig. 6. 63: Sondrio during 1987 flood.

These bridges were in risk during 1987 flood because of their exposure to lateral loading due to the flood wave in addition to the scour under the bridge foundations due to high velocity of water within the bridge. This scour (Fig 6.64) can lead to bridge settlement or collapse during the event, so the bridges must be not accessible during the event to save the human and the structure.



Fig. 6. 64: Physical model represents the scour under bridges.

The emergency plan usually built depending on the most probable scenario for the event. It has four phases; monitoring and watching the landslide and/or the induced flood, warning and alert in case of hazardous event, crisis management during the event and transition from emergency to normalcy after the event. The diagram in figure 6.65 shows the scenario corresponding to the Spriana landslide discussed in item 6.2.

The role of estimating the sediment transport appears in the crisis management phase, since all the bridges subject to scour must be inaccessible during the event. Of course the scour will not be the only reason for the inaccessibility but may also be the bridge inundation. The second role appears in the going back to normalcy phase, since it will be needed to restore the river capacity by removing the sediment deposited in Sondrio. Removing this huge amount of sediment will increase the emergency cost so a balance between the cost of removing the sedimentation and constructing structural measures to mitigate the transport capacity must be studied e.g. building more check dams can reduce the bed erosion upstream Sondrio, hence the deposition decreases in Sondrio successively.

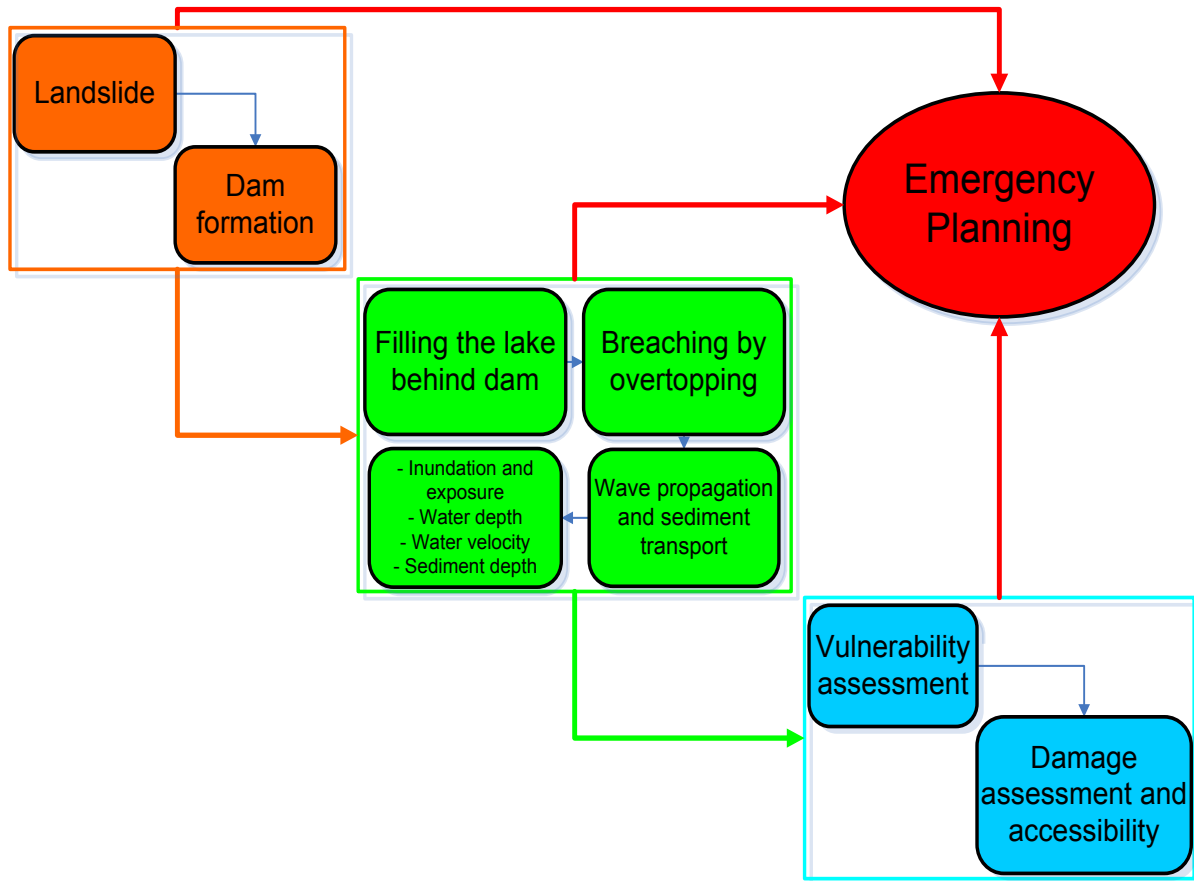


Fig. 6. 65: The scenario for emergency planning corresponding to Spriana landslide.

Indeed collapse of spirant affect the emergency planning not only from morphological point of view but also from inundation point of view. The zones upstream Spriana will be flooded along 2km, so some precautions must be taken to avoid damages there. With the likely scenario of dam (scenario 80), the discharge will be more than the river capacity contrary to 1987 flood, so some structures, human, and lifelines will be exposed to flooding and some roods and all the bridges will not be accessible. A lot of precautions must be taken regarding the ways available in the crisis time for the evacuation and the rescue purposes. With more dam height may be all the city will be inundated which need more circumspect precautions.

6.4 Conclusions and recommendations

After analyzing 1987 flood in chapter 5 and the induced flood for Spriana landslide in this chapter there are some points to summarize:

- Basement software is not able to model the land slide event by reliable manner, so an integrated scenario is built to model the land slide and its effects on the morphological evolution in mallero.
- The collapse of Spriana landslide leads to the creation of an earthen dam which stops the water flow, temporary, in the Mallero and forms a huge lake behind it.
- The expected dam height is 80 m, so behind this dam $1.56 \cdot 10^7 \text{ m}^3$ of water will be restored temporary in a lake behind the created dam.
- The time needed to fill this lake is around 2 days when the feeding discharge is $100 \text{ m}^3/\text{s}$.
- The surface area of this lake, with 80 m dam height, is $5.81 \cdot 10^5 \text{ m}^2$, so this lake will inundate the buildings beside Mallero valley upstream Spriana by 2km (these buildings are recommended to be evacuated once the slide takes place).
- The dam permeability is the most important triggering factor for causing the dam breaching, so more accurate values for permeability are needed by testing.
- The breaching type (overtopping or piping) depends not only on the dam's permeability, but also the feeding discharge and the dam geometry.
- After studying the seepage process through the dam, it is noted that the probability of dam collapse by piping is not likely because of the huge dam width and the shortage in time i.e. there is no sufficient time for completing the breaching process due to piping.

- The overtopping breaching is the most likely cause for the dam break, hence a huge water wave is estimated has a peak flow more than $750 \text{ m}^3/\text{s}$, in case of 80 m dam height .
- The wave will propagates in Mallerio with very fast speed (42 km/h) that takes only 10 minutes to arrive from Spriana to Adda, then some zones are expected to be inundate.
- The dam geometry plays an important role in maximizing or minimizing the wave peak hence the inundation area, so it is recommended, to next studies, to build a model describes the soil distribution (in an attempt to reach to more accurate dam dimensions).
- The sediment generated from the dam breach influence only 2 km downstream the dam.
- The amount of sediment deposited in Sondrio due to breaching of 80m dam is around half of the sediment deposited in 1987 flood although the higher peak.

7 The Millennium Dam

7.1 Introduction

The Grand Ethiopian Renaissance Dam, formerly known as the Millennium Dam and sometimes referred to as Hidase Dam, is an under-construction gravity dam on the Blue Nile River in Ethiopia. It is in the Benishangul-Gumuz region of Ethiopia, about 40 km east of the border with Sudan (Fig 7.1). At 6,000 MW, the dam will be part of the largest hydroelectric power plant in Africa when completed, as well as the 13th or 14th largest in the world. The reservoir at 63 billion cubic meters will be one of the continent's largest. The potential impacts of the dam have been a source of regional controversy. The Government of Egypt, the biggest and most influential consumer of Nile water, protests the dam, so the effects of constructing this dam on the morphological evolution, ecological impact and environmental changes in the Nile River will be discussed in this chapter depending on the analogy with the case of Sondrio discussed in the previous chapters.



Fig 7. 1: Location of the Millennium dam.

7.2 The Nile catchments

The Basin of Nile River, Fig.7. 2, is located between 4° S to 32° N and 23° to 40° E, covering 10.3% of the African continent area. It is the sixth largest basin in the world area encompassing most of the northeastern Africa and incorporating ten countries in total (Burundi, D. R. Congo, Egypt, Eritrea, Ethiopia, Kenya, Rwanda, Sudan, Tanzania and Uganda), with a combined population of about 325 million, about 170 million of them living within the boundaries of the Nile Basin.



Fig 7. 2: Nile River Basin (Ahmed, et al., 2008).

The main branches forming the Nile Basin are; Blue Nile, White Nile and Atbara river systems. The White Nile source is the equatorial lake where it begins as Victoria Nile passing through the Owen Falls Dam in Uganda to Lake Kyoga and then Albert Lake where is known as Albert Nile. Hence it continues into Sudan with the name Bahr El Jebel until it's confluence with Bahr El Ghazal and Sobat rivers near Malakal, and from there on it is known as the White Nile river. The Blue Nile (called Abbay in Ethiopia) and its main tributaries start from the Ethiopian Highlands. The Blue Nile originates from Lake Tana and joins the White Nile at Khartoum (the Capital of Sudan). North of Khartoum at Atbara City, the Atbara River joins the Nile forming the Main Nile River.

The Nile River receives its flows from three main distinct watersheds; the Equatorial Lake Plateau in the south, the Sudd region in the center, and the Ethiopian Highlands in the east (Fig 7.3). From the confluence of Atbara River north of Khartoum to the Mediterranean Sea the Nile receives no effective inflow. On the other hand, although the catchments area of the White Nile is three times the Blue Nile, however, the Blue Nile contribution to the Nile flow is twice that of the White Nile.

The entire Nile Basin area is simply the sum of all the sub-basins mentioned above. Areas in which runoff are diverted to other river basins and arid areas where there is no rain at all are not counted, the entire Nile Basin corresponds to 1,527,500km². However, in the literature the total area of the Nile Basin is estimated as 3,112,369 km², as shown in Table 7.1, which includes areas without rainfall (i.e. with no runoff contribution to the Nile flow).

agreement between Sudan and Egypt was based. However, from Fig. 7.4, the long term average flow of the Nile at AHD is 70.0 billion m³ annually. The latter figure is supposed to cater for Egypt's share in the Nile waters according to the 1959 Agreement i.e. with access of about 4.5 billion m³ in average annually for the last 45 years, considering the share of Egypt is 55.5 billion m³ and 10.0 billion m³ for evaporation annually from AHD reservoir (Nasser Lake).

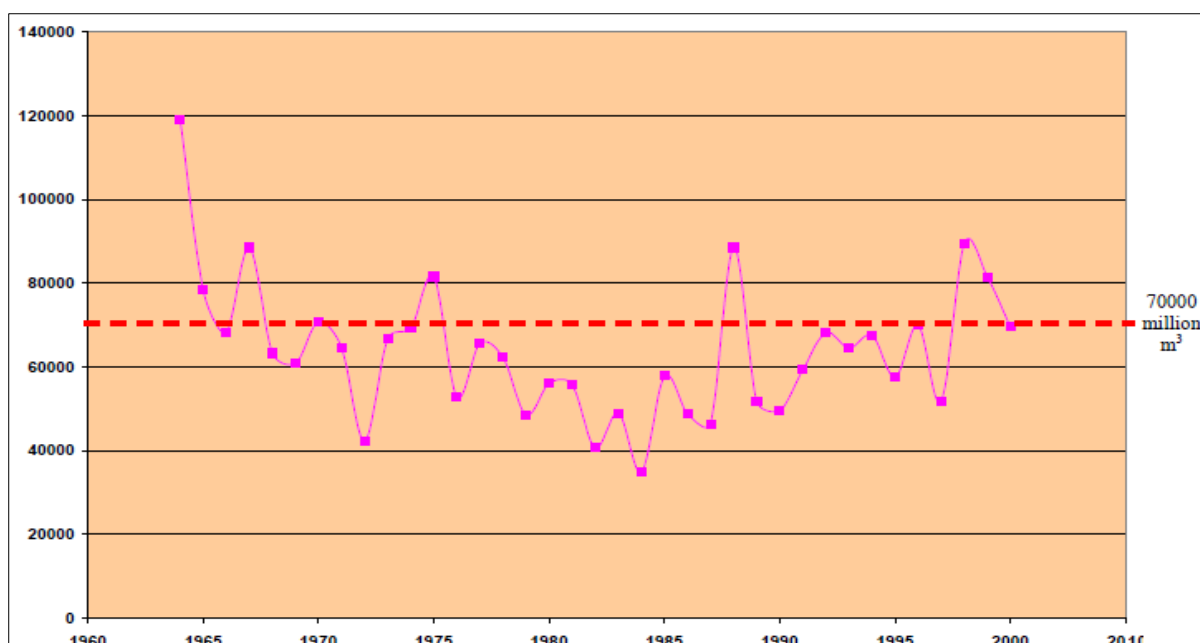


Fig 7. 4: Average flow at Aswan High Dam reservoir.

Fig 7.5 gives the nominal flow hydrographs at AHD of the main Nile and its tributaries, namely, White Nile, Blue Nile and River Atbara. These hydrographs show the average flows over more than 80 years. It is clear that the flows of the White Nile are mild and stable throughout the year and therefore flood flows is not defined. In fact the flood flows of the main Nile downstream Khartoum is solely due to the Blue Nile while the flood flows downstream Atbara town is further supplemented with River Atbara flows as Fig 7.5 reveals.

As shown in Fig 7.5, The White Nile which transports water from the Central Watershed leaves almost all the sediment to be deposited in the Sudd area. The White Nile contributes a relatively constant flow to the Nile River from the

Equatorial lakes through the swamps of the Sudd. This is in strong contrast to the rivers draining the Ethiopian Highlands watersheds (Blue Nile, Atbara and Sobat).

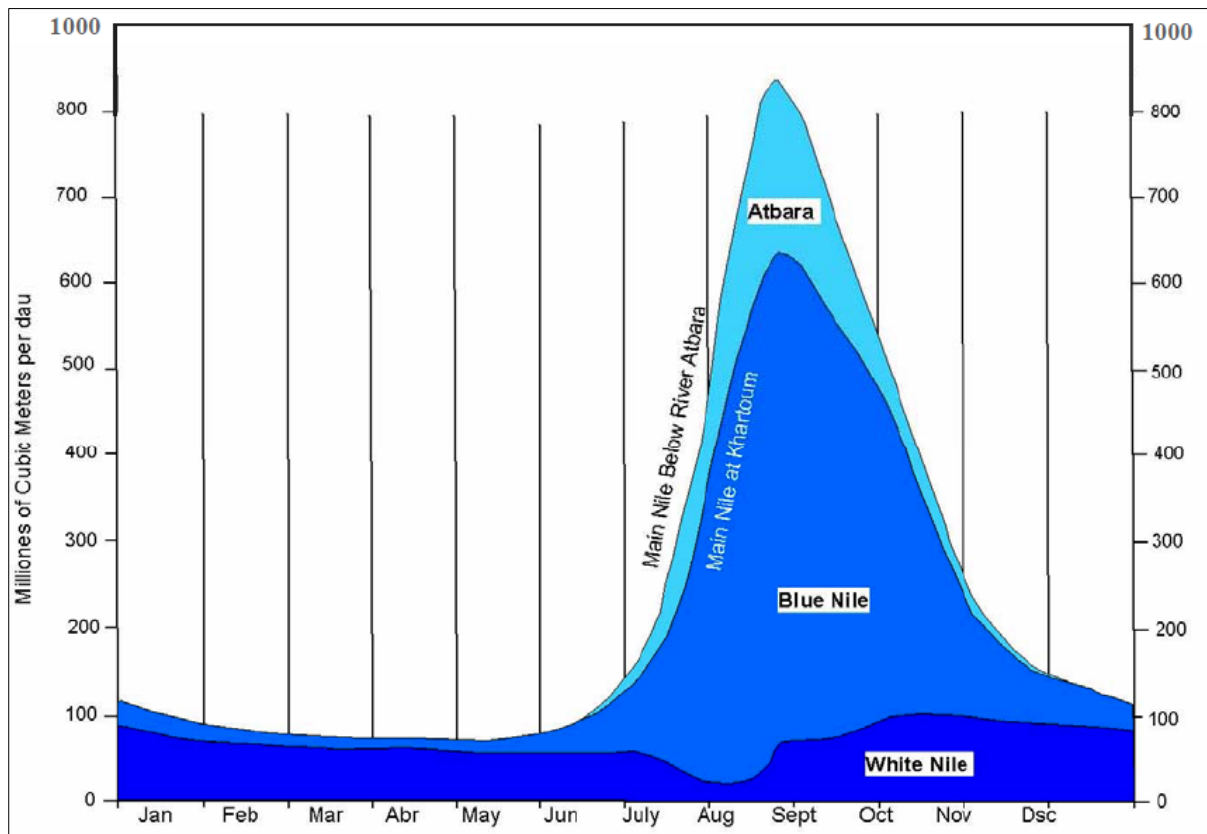


Fig 7.5 : Hydrograph of the Blue Nile, White Nile and Atbara Rivers (Klaassen, et al., 2005).

7.3 Physiography in the Nile Basin

The basin of the Nile, as shown in Fig 7.6, is characterized by the existence of two mountainous plateaus rising some thousands of meters above mean sea level. The Equatorial Plateau in the southern part of the Nile basin, situated between the two branches of the Great Rift, is at a level of 1,000 to 2,000 meters and has peaks of 5,100 and 4,300 meters. This plateau contains Lakes Victoria, George, Edward (Mobutu Sese Seko) and Albert, which slope gently toward the north at an average rate of one meter for every 20 to 50 km of stretch. In contrast the rivers which connect these lakes fall at an average rate of one meter every kilometer or less of length (see the profile in Fig 7.6). The

Comparative study of different scenarios for the morphological evolution in a river stream

Ethiopian Plateau, which forms the eastern part of the basin, has peaks rising to 3,500 meters. North of the Equatorial plateau the basin descends gradually to the Sudan plains where the Nile runs at altitudes lower than 500 m in its northerly direction. About 200 km south of the Egyptian border the river cuts its channel in a narrow trough bounded from each side by the contour line of 200 m ground surface level. Almost 200 km before discharging into the sea (at Cairo), the river bifurcates and it's two branches encompass the Nile Delta (Fig 7.6).

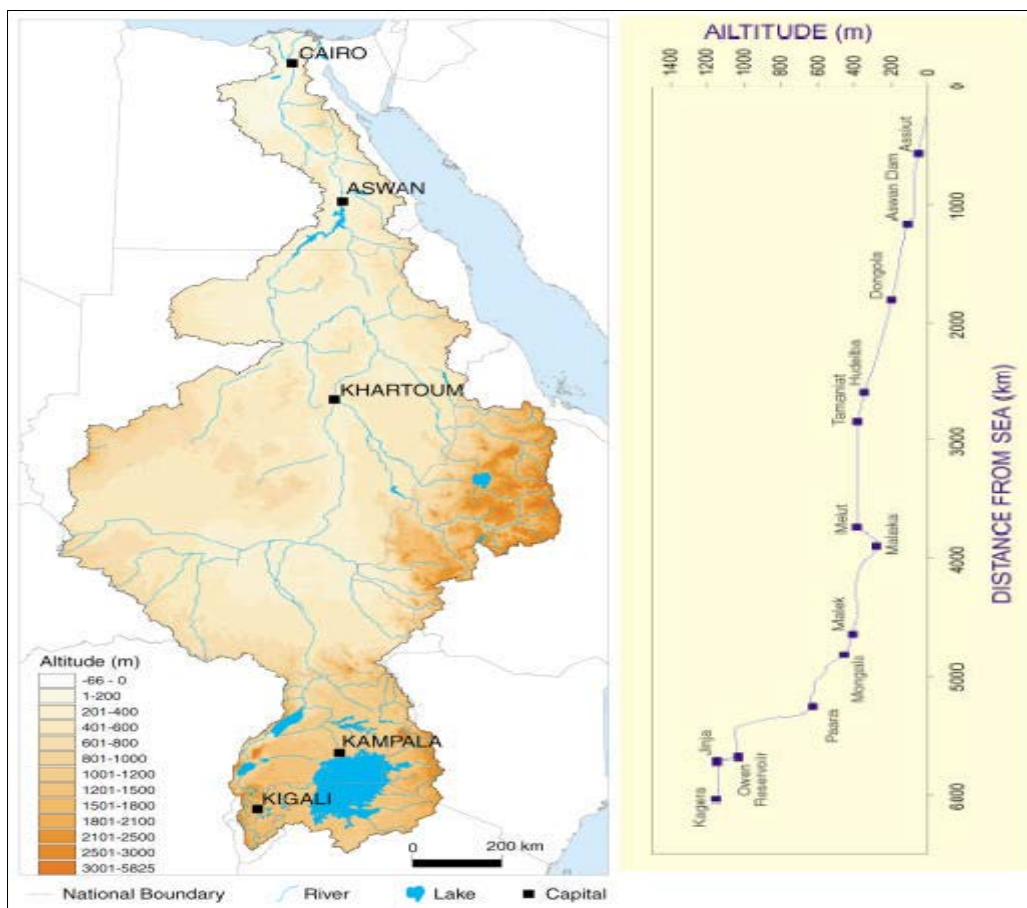


Fig 7. 6: Nile basin topography and profile from the Kagera measure station (Tanzania) to the sea (Karyabwite, 2000).

The Blue Nile and it's tributaries all raise on the Ethiopian Plateau at an elevation of 2,000 to 3,000 meters. The source of the Blue Nile is a small spring at a height of 2,900 m and at about 100 km south of Lake Tana (maximum

length of 78 km, width 67 km and depth 14 m). Most of the Ethiopian Plateau country is hilly with grassy downs, swamps valleys and scattered trees. The high country is cut up by deep ravines or canyons in which the rivers flow. In some places the Blue Nile flows in a channel that is about 1200 m below the level of the country on either side.

7.4 Nile River Sediment

Most of the sediment in the Nile flows from the Ethiopian Highlands through the Blue Nile and Atbara River. Nearly all the sediment (~ 95%) comes from the Blue Nile and Atbara rivers during the flood season (July- Oct.). The White Nile and its tributaries lose most of their sediment load by spilling and deposition over flood plains, lakes and marshlands inside Sudan (this is the reason why it is called, by old Egyptian, the White Nile, since its water is clear).

(Elmonshid, et al., 1997) estimated the sediment load of the Blue Nile at El Diem (the entrance of the river to Sudan) to be 140 million tons per year (this is the reason why they called it the Blue Nile which is the color of the fine sediment in Nile's valley). At the same time their estimation of the sediment load at AHD was 160 million tons taking into consideration the amount of sediment transported by Atbara River, while there is no sediment from the White Nile. This is compared to 150 Million tons for Mississippi river, 250 Million tons for the Colorado River and 1600 - 2000 Million tons for Yellow river in China. On the other hand, there is no reliable means of bed load information in the Nile River, which is believed to be negligible (the soil is finer than that in Sondrio case, so the main load here is suspended). The suspended sediment load in the Nile system is mainly distributed as 30% clay (< 0.002 mm grain size diameter), 40% silt (0.002 – 0.02 mm) and 30% fine sand (0.02 – 0.2 mm). Therefore, the sediment load in the Nile River can be considered in

Comparative study of different scenarios for the morphological evolution in a river stream

general as wash load. Fig. 7.7 compares the average amount of sediment load in different tributaries of the Nile River, while Fig. 7.8 shows the sediment concentration throughout the year at AHD. It is clear that the peak of the sediment concentration in AHD reservoir falls within the period August-September, although the values are small due the fact that most of the sediment settled in the entrance of the reservoir inside Sudan(with a behavior similar to that noted in the synthetic cases in Fig 3.12). In other words, it can be concluded that the AHD has 100% trap efficiency.

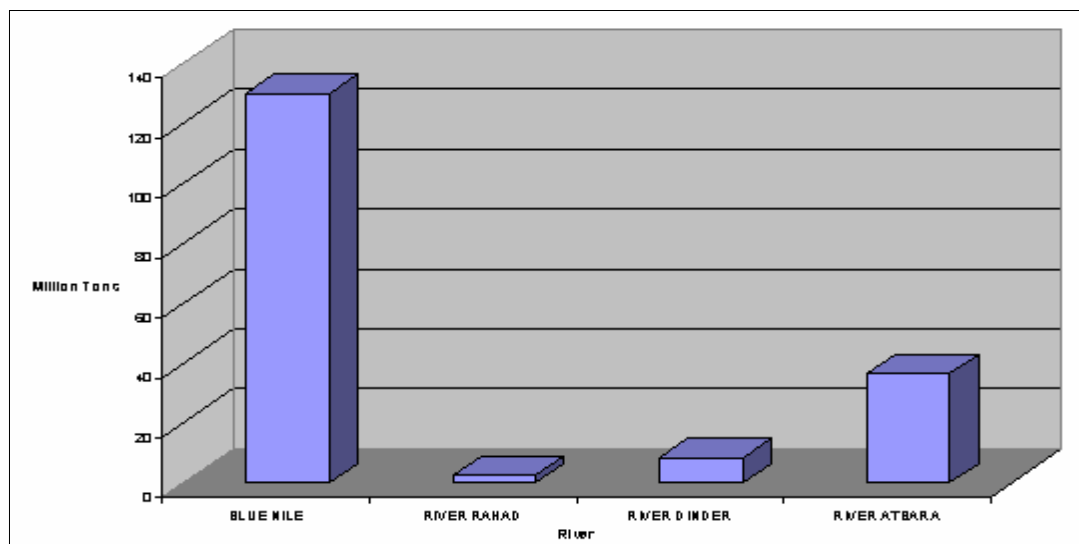


Fig 7. 7 : Sediment load in different tributaries of the Nile river (Ahmed, et al., 2008).

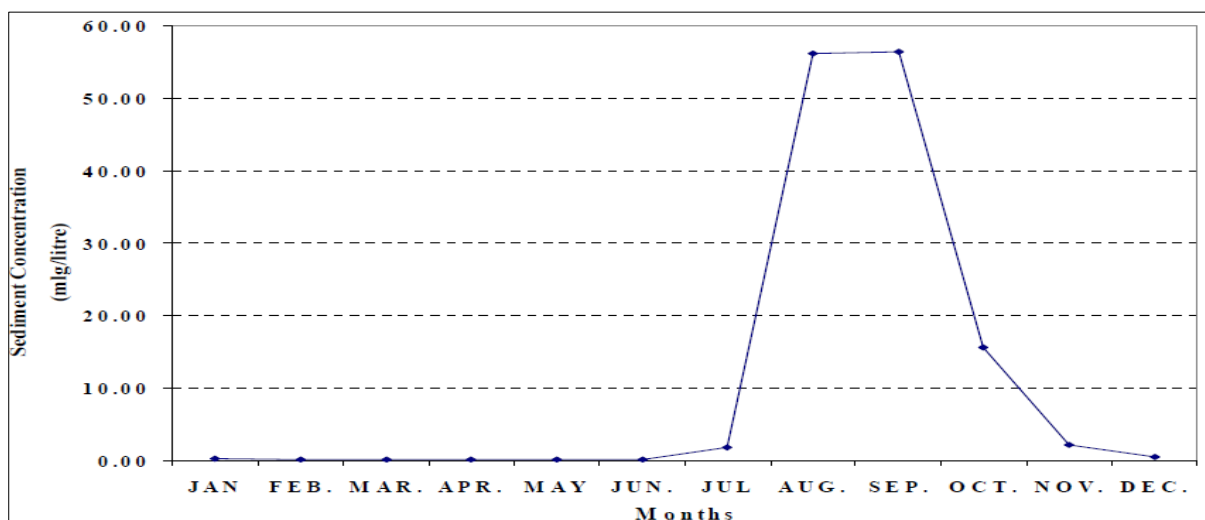


Fig 7. 8: Suspended sediment concentration in AHD reservoir (Ahmed, et al., 2008).

As shown in figure 7.8, sediment starts to increase from the early June until it reaches its peak towards the end of August and beginning of September and hence declines towards the end of the rainy season after October which is the same behavior of the waters

By making comparison between the Blue Nile case and the Mallero case studied from chapter 4 to 5, the main difference between the two cases is that they have different soil (fine sediment in the Blue Nile case in Ethiopian highlands and coarse sediment in the Mallero case in Italian Alps). The sediment transports as suspended load in the Blue Nile case while it transports as a bed load in the Mallero case. The two cases are similar in the topography and the consequences, nevertheless the behavior is totally different. The most interesting here that, the water wave, shown in fig 7.5, and the sediment wave, shown in fig 7.8, are hunted because of the dominance of the suspended load, while there is a delay noted in the Mallero case between the water wave and the sediment wave because of the dominance of the bed load that has a velocity extremely lower than the water velocity.

7.5 The ecological and morphological effects of blue Nile

The Blue Nile is the main contributor to the Nile for both discharge and sediment load. The floods in Sudan (also in Egypt before constructing AHD) usually happen due to the high discharges coming from the Blue Nile in the summer. In addition, there are some morphological effects for the Blue Nile that are summarized in the following.

7.5.1 Bank erosion in the Nile

River bank erosion is one of the most serious problems in river morphology. The process of river bank erosion is a natural process that is unavoidable,

therefore the right protection measures must be selected and designed to provide effective, efficient and durable works after construction. It is a source of sediment in the Nile system especially in the main Nile. Many factors contribute to the bank erosion; one of them is the interaction between the Nile river water levels during the wet and dry seasons and the groundwater table level. This movement of the water levels up and down causes the bank soils to collapse. Moreover, the high velocity of the Nile water near the outer bends creates serious bank erosion and bank sliding. All these contribute significantly to the sediment in the Nile system (fig 7.9). On the other hand, landowners complain of bank erosion and channel shifting, which cause the loss of some parts of their valuable land.



Fig 7. 9: Bank erosion in the main Nile.

7.5.2 Sand encroachment on the Nile River

Natural rivers are exposed to morphological changes due to many factors, which could be internal or external ones. One of the external factors is the sand encroachment. The moving of sands of different sizes (fine and medium) occupies great areas of the banks of the Nile river system particularly in northern Sudan (fig 7.10).



Fig 7. 10: Sand Nile River bank in the Sudan Northern State.

7.5.3 Reservoir sedimentation

Nile tributaries originating from the Ethiopian plateau carry large quantities of sediment estimated at about 160 -180 million tons annually. Most of this sediment is clay and silt carried in suspension during the rainy season. Dam reservoirs built on these tributaries are experiencing alarming loss in capacity due to sedimentation. According to (Ahmed, et al., 2008); in some reservoirs on the Nile, the annual rate of capacity loss may approach 1.0 %.

Sedimentation has serious implications for reservoirs whose primary functions are irrigation, water supply and hydropower. For the former two functions, loss in capacity implies less stored water and for the latter function implies hydropower generation interruption or curtailment.

For example, the AHD was constructed to completely control the Nile waters for the benefit of Egypt and Sudan. AHD reservoir extends for 500 km along the Nile River and covers an area of 6,000 km², of which two-thirds (known as Lake Nasser, 350 km) is in Egypt and one-third (called Lake Nubia, 150 km) is in Sudan. The mean annual discharge before and after the construction of AHD are presented in Fig. 7.11.

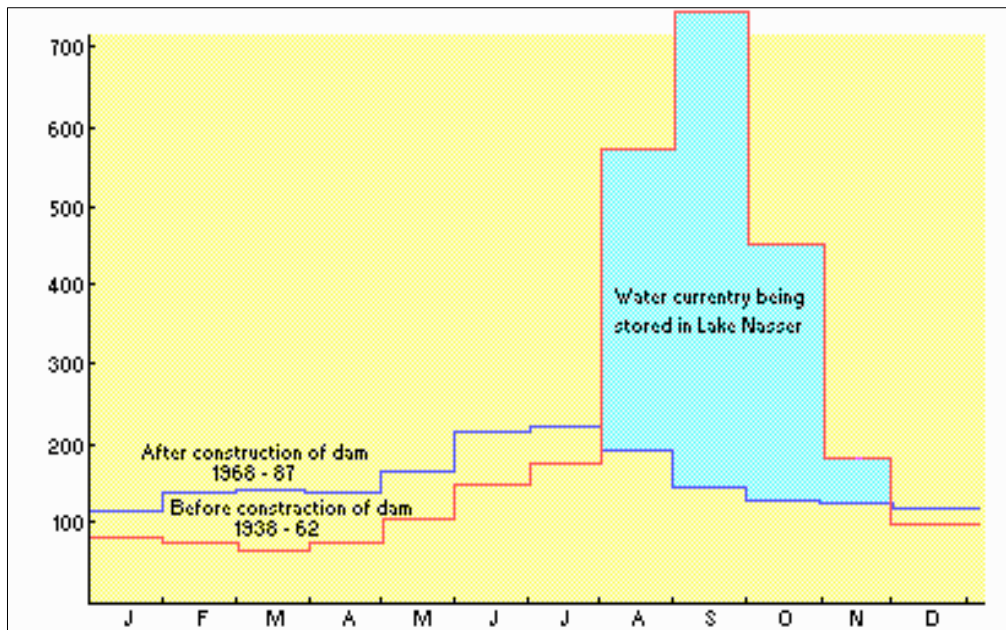


Fig 7. 11: Monthly average discharge (million m³) downstream AHD reservoir before and after construction.

Fig. 7.12 shows the longitudinal profile and suspended sediment distribution along AHD reservoir. The total deposited sediment volume is estimated to be 2.5 billion m³ in the period 1964-1995. This reflects that the average rate of sediment deposition annually is 140 million m³ i.e. the rate of sedimentation is 0.1 %. It has been noticed that almost all the sediment deposition occurs in the Nile reach between 345 km and 430 km south of the dam site.

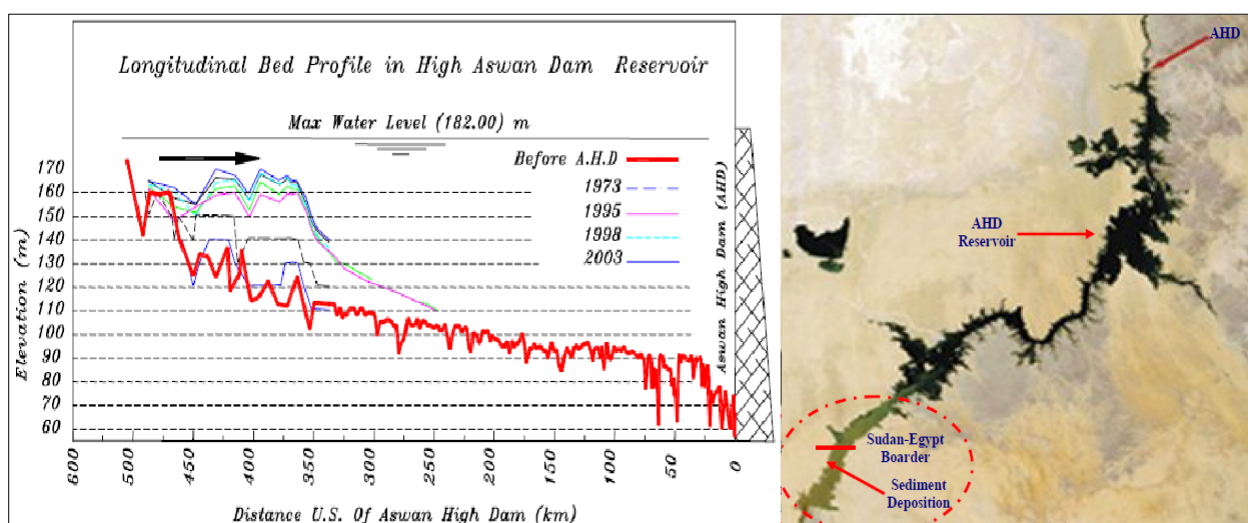


Fig 7. 12: Longitudinal bed profile in AHD reservoir & sediment distribution.

7.6 Statement of the Millennium dam problem

The Nile River has been a source of life for millions over the centuries. Now Ethiopia is diverting water to build a giant dam. Of course, construction of dams on numerous rivers throughout the world must be the greatest achievements of human beings in river development and greatest disturbance to the stream ecology.

The problem that, the Blue Nile contributes to the flow of the main Nile with 65% while Atbara River is contributing with only 16%, that is used mainly by Egypt and Sudan . The two countries say that; the construction of this dam violates a colonial era agreement from 1959, which gave them rights to almost 90 percent of the Nile's waters.

The consequences of the Ethiopia's dam could be very serious for Egypt, which is a dry country (table 7.1), is heavily reliant on the Nile for its water supply. That supply could suffer a loss of between 11 and 19bn cubic meters of water, while the dam is being built.

According to experts, that would cause two million Egyptian families to lose their income. The Grand Ethiopian Renaissance Dam could also lead to a permanent lowering of the water level in Lake Nasser, if floods are stored instead in Ethiopia. This would reduce the current evaporation of more than 10 billion cubic meter per year, but it would also reduce the ability of the Aswan High Dam to produced hydropower to the tune of a 100 MW loss of generating capacity for a 3m reduction of the water level. Hence, the Ethiopian dam could affect Egypt's electricity supply from AHD by 25 to 40 percent, which would leave Upper Egypt in darkness.

Lastly, with a growing population that is expected to hit 150 million by 2050, Egypt will need an extra 21bn cubic meters of water in order to cope with the growth, which makes the dam construction even more serious in the long term.

The dam will be a 170 m tall, 1800 m long gravity-type composed of roller-compacted concrete and will have two power houses, each on either side of the spillway. The left and right power houses will each contain 8 x 350 MW Francis turbine-generators. The dam's reservoir will have a volume of 63×10^9 m³.

Egypt has virtually held monopoly over the Nile waters as per the 1929 colonial treaty with Britain, which gave Egypt veto rights over all upstream projects. In 1959, it signed a deal with Sudan, which allowed both countries 90 percent of the share of the Nile waters. However, recently, Nile basin countries, comprising Ethiopia, Uganda, Rwanda, Tanzania, Kenya and Burundi signed a separate agreement to end Egypt's historical control over the river waters. Once respective parliaments of these countries ratify the agreement, these countries would not be required to seek Egypt's approval before implementing irrigation and hydropower projects on the Nile. Egypt has since been opposing the Entebbe agreement, which calls for redistribution of historical Nile water quotas. Egypt complains that its share of water would drastically reduce, if a dam is constructed. Egypt and Sudan have not ratified the Entebbe Treaty.

7.7 Effects of the Millennium Dam

Building this dam will help Ethiopia to be the first producer and exporter for electricity in Africa. In addition, it will cause some ecological and morphological effects as the following.

7.7.1 Ecological effects

Since the Blue Nile is a highly seasonal river, the dam would reduce flooding downstream of the dam, including on the 40 km stretch within Ethiopia. On the one hand, the reduction of flooding is beneficial since it protects settlements from flood damage. On the other hand, it can be harmful, if flood recession agriculture is practiced in the river valley downstream of the dam since it deprives fields from being watered. The dam could also serve as a bridge across the Blue Nile, complementing a bridge that was under construction in 2009 further upstream.

The International Rivers Organization⁶ reported that: At least 5,110 people will be resettled from the reservoir and downstream area. Villages near the reservoir (home to more than 7,380 people) will also be resettled. This estimate of resettlement is much higher than that made at official presentations, which have indicated that just 800 people will be resettled. Project planning did not involve the participation of affected people. Also they reported that: Ethiopia has been heavily deforested, but the Benishangul-Gumuz region where the dam is being built is one of the few places in the country where remnant forest vegetation still exists. The local community depends heavily on forest resources for their livelihoods (e.g., hunting, gathering of fruits, honey, firewood, medicinal plants, etc). The dam reservoir is expected to flood 1,680 square kilometers, 90% of which is forest. Road construction to the site will also impact forests. In addition they reported that: scientific studies have documented at least 150 indigenous freshwater fish species, with dozens of endemic species, in Ethiopia's portion of the Nile. Fish

⁶ <http://www.internationalrivers.org/resources/about-international-rivers-3679>

consumption by local people is high. The dam is expected to lead to habitat loss and other changes that could lead to a significant change in the fishery.

On the other side, the reservoir volume is about equivalent to the annual flow of the Nile at the Sudanese-Egyptian border (65.5 billion cubic meters). This loss to downstream countries would affect them, temporary, especially Egypt.

7.7.2 Morphological effects

Ethiopia's highlands are one of the most erosion-prone places on earth, so, as discussed in item 1.3, it was the source of the delta formation in Egypt and a very important resource for soil fertility renewal. Hence, sedimentation of the reservoir is a big risk for the dam's power output and lifespan. Indeed, there is no known analysis of the sedimentation risk to the Millennium dam. In addition the climate change could increase sedimentation rates.

On the other side, it will be beneficial for the dams in Sudan and Egypt, since it will increase the useful lifetime of dams in Sudan – such as the Roseires Dam, the Sennar Dam and the Merowe Dam – and of the Aswan High Dam in Egypt. This because the 140 million m³ of sediment transports through the Blue Nile as suspended load each summer and deposits at the entrance of Nasser Lake will silt upstream the Millennium dam.

Ethiopia is a rainy country where the mean precipitation depth is 1125 mm annually (Table 7.1), so they are not building the dam for providing waters. Building this dam will regulate the water flow and prevent the water table changes, hence will mitigate the usual bank erosion in main Nile described in item 7.5.1.

After building this dam, Sudan will not suffer any more from losing the suitable agricultural areas due to the sand encroachment during the flood season, but Ethiopia will suffer from the huge amount of sediment that will deposit behind the dam and can reduce the economic benefit from the construction of the dam.

7.7.3 Effects on the risk management

The Nile is an unending source of sustenance; it provides a crucial role in the development of Egyptian civilization. Silt deposits from the Nile made the surrounding land fertile because the river overflowed its banks annually. On the other hand it was an annual nuisance because of the floods in the summer season, but this problem solved by building the high dam in Aswan at 1970. Still Sudan has been suffering each summer not only from flooding problems but also from the related morphological problems explained above, since they are above the Aswan dam and under the Blue Nile, which is the main source of floods (see fig 7.5). Constructing the Millennium dam will regulate the flow avoiding Sudan not only flooding risk but also it will avoid both Sudan and Ethiopia from the drought risk which sometimes expose them to the risk of famine.

The big issue is the scenario of the Millennium dam-break especially when it is published, by media, that the factor of safety for the dam is 1.5 only which is not suitable for this type of huge dams. There is no study for this scenario, but, based on the analogy with the dam breaching of earthen dam in chapter 6 and by taking into account that the break will produce sudden and huge discharge, this scenario is very risky since it can destroy not only all the cities downstream this dam but also it can destroy the AHD causing catastrophic disaster in Egypt. The slope from the dam to Sudan is extremely steep (as in figure 7.6), so the

dam-break wave will transport without diffusion, while the sediment transport in this case, base in the previous comparison in chapter 6, will be less than the transported during the usual flood.

The dam-break will cause problems for Ethiopia, since they will lose their construction money. So, in case of completing the dam construction, both Sudan and Egypt must prepare a practical and efficient emergency plan hopefully they will escape alive in case of the dam-break.

7.8 Proposal for solving the problem

As shown and expected, constructing this dam has some benefits for all the sides, but also it has extreme risks especially for Sudan and Egypt. So there are two ways; either Egypt with Sudan prevent the completing of these project, even if by force, because it will affect their national security and they have the right to do this according the treaties but this is not preferred, or they accept it under some necessary requirements that must be accepted from the Ethiopian side.

The problem for Egypt is simply summarized in two important points; (1) preserving its historical right in Nile waters especially during filling the dam's reservoir and (2) Egypt with Sudan are guaranteed that the dam is absolutely secure and will be created by a factor of safety of their own consent. Considering these two points the proposal for solving the problem will be in sequent like this:

- The project's blueprints must be accepted by Egyptian specialist team;
- Egyptian engineering team must be involved in the supervising all the construction phases to grantee the dam safety;

- The reservoir must be filled in phases that guarantee the Egyptian rights;
- It can be added to the project costs, Ethiopia bears the expenses of cleaning the White Nile from Herbs and shrubs that cause huge losses of the white river flow. This can recover any loss in the Egyptian allocations;
- Ethiopia must accept the establishment of Egyptian military base in order to contribute in the dam protects.

Considering that Egypt must welcome and contribute the dam construction, also it can be an important partner in this project which will protect the main Nile from the morphological effect and protecting Nasser Lake from the siltation.

Final Conclusions

The study of sediment transport, particularly in mountain areas, is very important for some applications like the risk assessment and mitigation, land-use and planning, settlement areas and the safeguarding of human life. This is the reason why this work is introduced as an extension for the previous studies did by Politecnico di Milano and studying the sediment transports in rivers. The following objectives were aimed in this work:

- Assessing the capabilities and the weak points of three numerical codes (HEC-RAS, Basement and ISIS) simulating the morphological evolution in the rivers, and determining a most suitable code for modelling the phenomenon in both steep and mild channels; Achieving the previous objective by some synthetic test cases, related with (i) the upstream feeding of sediment in mild and steep channels by sediment rates lower or higher than the transport capacity; (ii) lateral sediment feeding at an intermediate section of the channel; (iii) sequent reaches with mobile and fixed beds, with scouring of the bed in the mobile reaches and aggradation to be simulated above hard beds; (iv) presence of significant granulometric variability;
- Numerically modelling the morphological evolution in the Mallero River due to 1987 flood by using different scenarios of bed granulometry;
- Analyzing a second scenario related with occurrence of a landslide in Spriana, with formation and consequent collapse of an earth dam resulting in a dam-break wave;
- Discussing the morphological and ecological effects of constructing the Millennium dam in Ethiopia.

Analysis of code performance

The three programs have been studied and a mini user guide has been introduced for each program. A comparison based on clear-water synthetic cases was introduced among the three programs that proved that the results by the three codes are more or less the same, with a difference only in the treatment of the secondary losses (like bed drop, enlargement and divergence of the channel width). The finite volumes based software (Basement) was more stable and better in the dealing with very steep water waves and with variable spatial discretization in comparison with the finite differences based programs like HEC-RAS and ISIS. It was also noted that the narrow spatial discretization produced accurate result (smooth and identical profiles) reducing the probability of numerical instability.

The capability of modelling the morphological evolution in the river streams was firstly analyzed using a mild channel case with bed slope 2 ‰, uniform discharge, uniform sediment feeding by a feeding ratio k (that is the ratio between the feeding discharge and the transport capacity). The ratio k used in the comparison was 0.5, which was expected to produce degradation at the channel entrance. Basement was able to compute the degradation, but by contrast HEC-RAS and ISIS had problems even for this simple case. The most important results of this stage were the dropping of the two programs (HEC-RAS and ISIS) and completing the analysis using Basement software only. Through the comparison it was noted that, for the bed load calculations, the skin friction must be used in calculating the driving bed shear stress, not the total friction.

Additional synthetic cases simulating specific scenarios have been created for the morphologic evolution. A rectangular channel has been modeled, which

was 10 km long, 50 m width and with a slope of 2 ‰ and 20 ‰ for mild and steep slopes, respectively. A hydrograph with constant flow (the uniform one) was used as the input flow and the channel had a Manning roughness coefficient equal to 0.04.

Regarding the upstream feeding by uniform granulometry, ratios of feeding k ranged from 0 to 3. The values of k lower than 1 showed degradation in upstream, while the feeding by the ratio $k = 1$ showed neither aggradation nor degradation, which can be a proof of the reliability of modelling by Basement, and the value of k more than 1 showed aggradation at the upstream. Of course the length and the depth of either the sediment aggradation or the degradation depend on the feeding ratio k and the sediment diameter.

By testing the differences between the results obtained by using the skin friction instead of the total friction for calculating the driving bed shear stress, the results showed that using the total friction produced more amounts of sediment in case of the aggradation or the degradation. The profile shapes in the two cases are the same, while the depth and the length of the aggradation or the degradation, in case of using the total friction are just amplified by specific values that depend on the feeding ratio k .

In case of feeding by non-uniform granulometry, no rule can be established because of the sediment variability which reflects the complexity of dealing with non-uniform granulometry. The only way for generalizing a rule is to compare the maximum and the minimum sediment size of sediment with the threshold value of the diameter (size at the onset of motion). If all the sizes of sediments are less than the threshold value, the rule for uniform size can be established. If not, the sediments will be sorted keeping the coarser sizes in

their position while, in this case, no rule for degradation or aggradation can be established.

Regarding the point of lateral sediment feeding by uniform granulometry in an intermediate section, the lateral feeding in both mild and steep channel by feeding ratios less than 1 will create a submerged dam if the sediment size is more than the threshold value for the size. If not, the sediment feeding will be totally transported with the flow. Higher values of k , with size less than the threshold value for the size, will definitely create a dam with dimensions depend on the feeding ratio k . The dimension of this dam will be amplified if the feeding size is higher than the threshold value for the sediment size since no sediment will be transported.

In case of feeding by non-uniform granulometry in an intermediate section with values of k less than 1, the dam formation will be expected as long as the feeding has some sizes bigger than the threshold one. While with values of k more than 1 the dam will be formed definitely, with a dimensions depending on the feeding ratio k . Behind the created dam, it is noted a formation of lake with a volume that depends on the dam height and the channel slope. It is also noted that the sediment deposits at the entrance of the formed lake because of the transition from height velocity upstream of the lake to low velocity in the lake zone.

It is noted, through a study of the model sensitivity to the spatial discretization, that the more discretization gives a smoother bed profile, but for the dam height is noted that it is not affected by the spatial discretization. Also the sensitivity of non-uniform granulometry models to the thickness of the active layer is studied, finding that very small values of cvt mean no sediment transportation, while, for limited number of sediment, the cvt has no

effect as long as any logical value more than zero is selected. The effect becomes significant with larger number of sediment sizes because of the increased possibility for sediment sorting.

In case of sequent reaches with mobile and fixed beds, the scouring of the bed in the mobile reaches appeared while was obtained above hard beds. This means that Basement was able to simulate this case. An indication was also obtained of effectiveness of fixing some cross-sections along the stretch of the Mountain Rivers by using for example check dams in the reduction of the bed erosion.

As a general conclusion, the bed erosion is wider and deeper in the case of steep channels than that in mild cases. The transport capacity is also higher than that for mild cases. Once the transition from very steep to mild channel occurs, the sediment deposits and huge amount of sedimentation degrade in the bed.

The Mallero case

The 1987 flood was studied using multiple scenarios for the bed granulometry, the post analysis hydrograph produced by Nash model and a sediment hydrograph proportional to the square root of the water hydrograph. The downstream boundary (confluence point with Adda) was replaced by a 2 km long dummy stretch, while the Meyer-Peter and Müller formula for multiple granulometry was used to calculate the bed load. The comparison of the results with those of (Filippetti, et al., 2012) for the same event showed good agreement. In addition a comparison with some observed measures was done that showed that more reliable results were obtained from the model with less granulometric classes. The sensitivity analysis of the model to the bed

granulometry showed indeed a high sensitivity to the bed granulometry. It is noted also that the results are more reliable as long lag from the boundaries. The model sensitivity to the thickness of the active layer showed that the effect of the cvt appeared when multiple sizes of sediment is used in the bed granulometry which was the same behavior noted in the synthetic cases, while for lower numbers of bed granulometry the effect of cvt was negligible because the sorting effect was limited.

It was noted, by studying the migration of the sediment particles for different scenarios, that the feeding of the sediment would influence only some kilometers downstream of the model entrance depending on the sizes of the granulometry used. Hence, the feeding from the catchments was not the source of the sedimentation noted in Sondrio in 1987, but it was the bed erosion from the last steep part of Mallero at the entrance of Sondrio, as concluded also by (Radice, et al., 2013).

The scenario of the lateral feeding by sediment from Spriana landslide was studied again using Basement. The program was fed by both pulse and distributed sediment feedings corresponding to the volume of the soil likely to generate from the slide, but the modelling results were neither satisfactory nor reliable. For example, the mass balance was checked at the intermediate section where the feeding was, finding that Basement didn't respect the principle of mass conservation with these large values of feedings.

An integrated model for the landslide in Spriana and its consequences was introduced, the model consisting of some sub-models that described together the formation of an earthen dam in the front of Spriana with a lake filling behind this dam. The most likely scenario of the dam height was that of an average height of 80 m, based on previous studies by (Franzetti, 2005), and a

total volume of $20 \times 10^6 \text{ m}^3$ as the volume of the soil produced by the landslide. The volume of the water likely stored behind the dam was estimated at $1.56 \times 10^7 \text{ m}^3$, while the time needed to fill this lake completely from the catchments in upstream is 43.5 hours considering a steady feeding discharge of $100 \text{ m}^3/\text{s}$.

The collapse of the dam due to the seepage effect was studied using wide ranges for the hydraulic conductivity of the dam material. This analysis showed that the piping could hardly be the cause of the collapse, because of the huge width of the dam in addition to the short time of filling the lake. The piping effect could be the dominant cause for the collapse only in case of very low feeding discharges resulting in long filling times.

The breaching of the dam was then investigated by different published breaching models that resulted in producing a huge water wave with a peak estimated by $760 \text{ m}^3/\text{s}$ and 8 hour as a base time. The sensitivity of the breaching models to the dam height showed that duplicating the dam height would increase the peak discharge by around 10 times, while increasing the dam crest width would delay and reduce the peak flow. In addition, increasing the steepness of the dam slopes amplified the peak flow without delaying the peak.

The sediment produced by these breaching models was also estimated; it was noted that the sediment hydrograph peak is around 1.2 % of the water hydrograph peak with the same base time, while the sensitivity analysis of the produced sediment hydrograph to the dam height, the dam slopes and the crest width showed the same sensitivity of the water hydrograph to these effects by keeping the same ratio between the sediment and the water peaks (1.2%).

Finally, the water and the sediment waves produced by the breaching are used to perform the morphological evolution analysis for this scenario by using the Basement software. The wave propagation time from Spriana to Sondrio was estimated by 10 minutes with the water wave translating kinamatically without appreciable diffusion. This translation of the wave would be likely to lead to inundation in Sondrio since the wave peak was more than the river capacity estimated by $690 \text{ m}^3/\text{s}$ as coming in analysis by (Radice, et al., 2013). It was also noted that a higher dam would induce more inundation in Sondrio. The morphology of the river showed that the amount of sediment likely to deposit in Sondrio, using the scenario of 80 m dam, will be around half that produced by 1987 flood. The migration of the sediment particles showed also that the source of the sedimentation will not be the feeding at Spriana but the bed erosion, while the feeding of sediment from the dam breaching at Spriana will influence only some kilometers downstream of the breached dam.

In the case of Mallero it was noted that the river capacity decreased by 77% because of 1987 flood, while it is expected that the Mallero will lose around 35 % or more from its capacity in case of Spriana landslide failure.

The Millennium dam and comparison with the Mallero case

A hypothetical dam breaching was exploited to get a primary estimation for the consequences of the Millennium dam-break in the Ethiopian highlands, taking into account that the break is sudden failure.

It was noted that Lake Nasser loses 0.1% of its capacity annually because of the huge amount of sediment that come each summer hunted to the seasonal floods. This is the reason to recommend taking the influence of the sediment

transport into account during the time line of the emergency planning for the flood risks.

The effect of mountain floods is really risky not only because of the huge water wave that propagates kinematically without diffusion, but also because of the huge amount of sedimentation produced by these floods. The main difference between the two cases is that they have different soil (fine sediment in the Blue Nile case in Ethiopian Highlands and coarse sediment in the Mallero case in Italian Alps). The sediment transports as suspended load in the Blue Nile case while it transports as a bed load in the Mallero case. The two cases are however similar in the consequences, even though the behavior is different.

It was noted from comparison between the two case studies that in case of bed load dominance (as the case of Mallero); the sediment wave is subsequent to the water wave. In the case of suspended load dominance (as the case of blue Nile), the sediment wave is hunted to the water wave i.e. the sediment velocity is the same as the water velocity and this is the reason why the sediment transports all this thousands of kilometers from Ethiopian Highlands to Egypt.

By comparing the influence of the sediment in the Mallero case with its influence in the Blue Nile case, the sediment affects the whole Nile and not only some kilometers from upstream. This is because the water and the sediment waves in the Blue Nile are haunted, because the soil is fine and load is only suspended. That means that the finer sediment is more dangerous because the transport capacity is more and the velocity of the sediment is same as that of water.

List of Symbols

A	flow cross-sectional area (m^2)
B	open channel free-surface width (m)
$C_{\text{Chézy}}$	Chézy coefficient ($\text{m}^{1/2}/\text{s}$)
C	mean volumetric sediment concentration
C	celerity (m/s)
d_s	sediment size (m)
d_{50}	median grain size (m)
F_r	Froude number
g	gravity acceleration (m/s^2)
H	total head (m), dam height
i	integer subscript
K	hydraulic conductivity (m/s) of a soil
k	permeability (m/s) of a soil
k	sediment feeding ratio
$k_{\text{Strickler}}$	Strickler resistance coefficient ($\text{m}^{1/3}/\text{s}$)
k_s	equivalent sand roughness height (m)
L	length (m)
L	crest length (m)
M	total mass (kg)
n	Manning coefficient
P	porosity factor
Q	total volume discharge (m^3/s)
q	discharge per meter width (m^2/s)
q_s	sediment flow rate per unit width (m^2/s)
Re	Reynolds number

Comparative study of different scenarios for the morphological evolution in a river stream

Re^*	shear Reynolds number
R_H	hydraulic radius (m)
S_f	friction slope defined as:
S_o	bed slope
s	relative density of sediment
t	time (s)
u^*	shear velocity (m/s)
V	flow velocity (m/s)
W_o	lake parameter
w_s	settling velocity (m/s)
z	altitude or elevation (m)

Bibliography

- Ahmed A.,A. and Ismail U.,H.** Sediment in the Nile River System [Report] / International Sediment Initiative ; International Hydrological Programme. - Khartoum – Sudan : UNESCO, 2008.
- Ashida K. and Michiue M.** An investigation over river bed degradation downstream of a dam [Conference] // Proceedings 14th Congress of IAHR. - Paris : [s.n.], 1971. - pp. 247-256.
- Bhallamudi S. ,M. and Chaudhry M., H.,** Numerical modeling of aggradation and degradation in alluvial channels [Journal] // Hydraulic Engineering. - [s.l.] : Amer. Soc. Civil Engrs, 1991. - 9 : Vol. 117. - pp. 1145-1164.
- Brunner G. W. and CEIWR-HEC** HEC-RAS:River Analysis System User's Manual,Version 4.1 [Report] : Computer Program Documentation / Hydrologic Engineering Center (HEC) ; Institute for Water Resources. - Davis : US Army Corps of Engineers, 2010.
- Brunner G. W.** HEC-RAS, River Analysis System Hydraulic Reference Manual [Report] / Hydrologic Engineering Center (HEC) ; Institute for Water Resources. - Davis : US ARMY CORPS OF ENGINEERS, 2010.
- Chanson H.** Environmental Hydraulics of Open Channel Flows [Book]. - [s.l.] : Elsevier, 2004.
- Chanson H.** The Hydraulics of Open Channel Flow: An Introduction [Book]. - [s.l.] : Elsevier, 2004. - 2nd.
- Chaudhry M.,H.** Open-Channel Flow [Book]. - [s.l.] : Springer, 2008. - 2nd. - ISBN 978-0-387-30174-7.
- Costa and John E.** Floods from Dam Failures [Report] : Open-File Report / Denver. - Colorado : U.S. Geological Survey, 1985. - pp. 85-560. - 54.
- Crosta G. B., Chen H. and Lee C. F.** Replay of the 1987 Val Pola Landslide, Italian Alps [Journal] // Geomorphology 60. - [s.l.] : EISEVIER, 2004. - pp. 127–146.
- De Vries M.** Considerations about non-steady bedload transport in open channels. - 1965 : Delft Hydraulics.
- Dingman S.,L.** FLUVIAL HYDRAULICS [Book]. - New York : Oxford University Press, 2009. - ISBN 978-0-19-517286-7.
- Elmonshid, ElAwad and Ahmed S.,E.,** Environmental effect of the Blue Nile Sediment on reservoirs and Irrigation Canals [Conference] // Int. 5th Nile 2002 Conf. - Addis Ababa- Ethiopia. : [s.n.], 1997.
- Faeh R., Mueller R. and Rousselot P.** System Manuals of BASEMENT, Version 2.1. [Report] / Laboratory of Hydraulics ; the Swiss Federal Institute of Technology (ETH). - Zurich : ETH Zurich, 2012.
- Filippetti P. and Zoppi A.** EVOLUZIONE MORFOLOGICA DI UN ALVEO MONTANO Strategie di modellazione ed applicazione al caso del torrente Mallero. - 2012.

Comparative study of different scenarios for the morphological evolution in a river stream

- Franzetti S.** Analisi delle procedure di emergenza a fronte di un evento idrogeologico per la città di Sondrio [Report]. - Milan : Politecnico di Milano, 2005.
- Hanson, Cook and Hunt** "Physical modeling of overtopping erosion and breach formation of cohesive embankments [Journal] // ASABE. - 2005. - pp. 1783–1794.
- Hirano M.** On riverbed variation with armoring [Conference].- [s.l.] : Japan Society of Civil Engineering,, 1971. - pp. 55-65.
- ISIS** ISIS [Online] // halcrow.com / ed. Centre Software Support / prod. Centre Software Support. - A CH2M HILL COMPANY, 2012. - 3.6.1 . - <http://www.isisuser.com/learning/default.asp>.
- Jäggi M.** Vorlesung: Flussbau. ETH Abt. II, VIII, und XC. - Zürich : ETH Zürich., 1995.
- Karyabwite D.,R.** Water Sharing in the Nile River Valley [Report]. - Geneva : UNEP/DEWA/GRID, 2000.
- Klaassen G.,J., Osman M.,A. and Ahmed A.,A.** TOWARDS THE IMPROVEMENT OF THE PROTECTION METHODS AGAINST BANK EROSION [Report] / Research Cluster ; River Morphology. - Khartoum, Sudan : Nile Basin Capacity Building Network 'NBCBN', 2005.
- Lyn D.,A. and Altinakar M.** St. venant-Exner Equations for near critical and transcritical flows [Journal]. - [s.l.] : ASCE, 2001. - Vol. 128. - pp. 579-587.
- Macchione F. and Rino A.** Model for Predicting Floods due to Earthen Dam Breaching.II: Comparison with Other Methods and Predictive Use [Journal] // Journal of Hydraulic Engineering. - [s.l.] : ASCE, December 1, 2008. - Vol. 134. - pp. 1697-1707. - ISSN 0733-9429/2008/12-1697–1707/\$25.00..
- Macchione F.** Model for Predicting Floods due to Earthen Dam Breaching.I: Formulation and Evaluation [Journal] // JOURNAL OF HYDRAULIC ENGINEERING. - [s.l.] : ASCE, DECEMBER 1, 2008. - Vol. 134. - pp. 1688-1696. - ISSN 0733-9429/ISSN 0733-9429/.
- Mauri M. and Spagnolatti M.** Modellazione dell'evoluzione morfologica del torrente Mallero durante un evento alluvionale e repercussions sulla città di sondrio. - 2009.
- Molinari D.** FLOOD EARLY WARNING SYSTEMS PERFORMANCE:an approach at the warning chain perspective. - 2011.
- Parker G.** ID SEDIMENT TRANSPORT MORPHODYNAMICS with applications to RIVERS AND TURBIDITY CURRENTS = An e-book by Gary Parker. - 2004.
- Radice A., Rosatti G. and Ballio F.** Management of flood hazard via hydro-morphological river modelling. The case of the Mallero in Italian Alps [Journal]. - Milan : Journal of Flood Risk Management, 2013. - Vol. 6. - pp. 197-209.
- Rubin H. and Atkinson j.** Environmental Fluid Mechanics [Book]. - BASEL : Marcel Dekker, Inc., 2001.
- Van Rijn L.,C.** principles of sediement transport in Rivers, Estuaries and costal seas [Book]. - Delft : AQUA puplications, 1993.

- Wahl T., L.** Prediction of Embankment Dam Breach Parameters:A Literature Review and Needs Assessment [Report] / U.S. Department of the Interior Bureau of Reclamation ; Dam Safety Office. - [s.l.] : Water Resources Research Laboratory, 1998.
- Weiming W.** Earthen Embankment Breaching [Journal] // JOURNAL OF HYDRAULIC ENGINEERING © ASCE. - DECEMBER 2011. - pp. 1549-1564.
- Weiming W.** Simplified Physically Based Model of Earthen Embankment Breaching [Journal] // JOURNAL OF HYDRAULIC ENGINEERING © ASCE. - [s.l.] : ASCE, AUGUST 1, 2013. - Vol. 139. - pp. 837-851. - ISSN 0733-9429/2013/8-837-851/\$25.00..
- Zhixian C, Rodney D and Egashira S.** Coupled and Decoupled Numerical Modeling of Flow and Morphological Evolution in Alluvial Rivers [Journal] // Journal of Hydraulic Engineering. - [s.l.] : ASCE, MARCH 2002. - Vol. 128. - pp. 306-321. - ISSN 0733-9429/2002/3-306-321.